

Analysis and Algorithm

midas **FEA**
Advanced Nonlinear and Detail Analysis Program

CONTENTS

1. Structural Elements

1.1 Overview	1
1.2 Truss Element	9
1.3 Beam Element	14
1.4 Shell Element	29
1.5 Plane Stress Element	55
1.6 Plane Strain Element	66
1.7 Axisymmetric Element	73
1.8 Solid Element	84
1.9 Spring	98
1.10 Rigid Link	102

2. Reinforcement Element

2.1 Introduction	107
2.2 Reinforcement Types	108
2.3 Linear Analysis	114
2.4 Reinforcement in Plane Strain Element	120
2.5 Reinforcement in Axisymmetric Element	125
2.6 Reinforcement in Plane Stress Element	130
2.7 Reinforcement in Solid Element	133
2.8 Reinforcement in Plate Element	139
2.9 Prestress of Reinforcement	144

CONTENTS

3. Interface Element

3.1 Introduction-----	149
3.2 Coordinate System and Relative Displacement-----	151
3.3 Point Interface Element-----	153
3.4 Line Interface Element-----	155
3.5 Surface Interface Element-----	158
3.6 Finite Element Formulation-----	163
3.7 Interface Element Output-----	164

4. Linear Analysis

4.1 Linear Static-----	165
4.2 Linear Static with Nonlinear Elements-----	166

5. Modal Analysis

5.1 Introduction-----	168
5.2 Lanczos Iteration Method-----	173
5.3 Subspace Iteration Method-----	175
5.4 Optional Parameters-----	176

6. Time History Analysis

6.1 Time History Analysis-----	180
6.2 Modal Superposition Method-----	181
6.3 Direct Integration Method-----	183
6.4 Optional Parameters-----	187
6.5 Cautionary Notes-----	189

CONTENTS

7. Response Spectrum

7.1 Response Spectrum Analysis	190
7.2 Spectrum Function	196

8. Linear Buckling Analysis

8.1 Introduction	198
8.2 Geometric Stiffness	201
8.3 Critical Load Factor Extraction	209
8.4 Optimal Parameter	210

9. Load and Boundary

9.1 Constraint Condition of Degrees of Freedom	211
9.2 Skewed (Inclined) Support Condition	214
9.3 Constraint Equation	215
9.4 Nodal Load	218
9.5 Element Pressure Load	219
9.6 Body Force	221
9.7 Prescribed Displacement	222

10. Construction Stage Analysis

10.1 Introduction	223
10.2 Composition of Construction Stages	225
10.3 Time Dependent Material Properties	229

CONTENTS

11. Heat of Hydration

11.1 Introduction	257
11.2 Heat Transfer Analysis	258
11.3 Thermal Stress Analysis	265
11.4 Heat of Hydration Analysis Considering Construction Stages	269
11.5 Results of Heat of Hydration Analysis	270

12. Material Models

12.1 Introduction	271
12.2 Yield Criteria	282

13. Total Strain Crack

13.1 Introduction	301
13.2 Basic Properties	305
13.3 Loading and Unloading	308
13.4 Crack Strain Transformation	311
13.5 Stiffness Matrix	314
13.6 Compression Models	320
13.7 Tension Models	326
13.8 Shear Models	336
13.9 Lateral Influence	337

14. Interface Nonlinear Behaviors Analysis

14.1 Introduction	344
14.2 Discrete Cracking	346
14.3 Crack Dilatancy	352
14.4 Bond Slip	362

CONTENTS

14.5 Coulomb Friction ----- 365

14.6 Combined Cracking-Shearing-Crushing ----- 368

15. Geometric Nonlinear

15.1 Introduction ----- 380

15.2 Truss Element ----- 386

15.3 Plane Stress Element ----- 388

15.4 Plate Element ----- 391

15.5 Plane Strain Element ----- 396

15.6 Axisymmetric Element ----- 397

15.7 Solid Element ----- 400

16. Iteration Method

16.1 Introduction ----- 403

16.2 Initial Stiffness Method ----- 407

16.3 Newton-Raphson Method ----- 408

16.4 Arc-Length Method ----- 411

16.5 Displacement Control ----- 415

16.6 Convergence Criteria ----- 417

16.7 Auto-Switching ----- 419

17. Equation Solver

17.1 Introduction ----- 420

17.2 Direct Method ----- 421

17.3 Iterative Method ----- 425

17.4 Solver Characteristic ----- 427

CONTENTS

18. Contact

18.1 Introduction -----	428
18.2 Contact Search -----	430
18.3 Function -----	435

19. Fatigue

19.1 Introduction -----	437
19.2 Load Cycles -----	438
19.3 Mean Stress Effects -----	441
19.4 Modifying Factors -----	443
19.5 Rainflow-Counting Algorithm -----	449
19.6 Fatigue Analysis Procedure -----	452

20. CFD Analysis (Computational Fluid Dynamic)

20.1 Introduction -----	453
20.2 RANS equation and turbulence model -----	454
20.3 Spatial discretization -----	457
20.4 Steady flow -----	459
20.5 Unsteady flow -----	460
20.6 Numerical stability -----	462
20.7 Computational fluid analysis results -----	463

Chapter 1. Structural Elements

1-1 Overview

The coordinate systems, that are used to define a finite element system of a structure or the analysis results, are the following.

- GCS: global coordinate system
This is a right hand Cartesian coordinate system and the complete model can refer to this system. Capital letters X-Y-Z are used to identify the axes.
- ECS: element coordinate system
This is a right hand Cartesian coordinate system and one or more elements can refer to this system. Lower case letters x-y-z are used to identify the axes..
- Other coordinate systems
Other coordinate systems are the NCS (nodal coordinate system), the OCS (output coordinate system) and the MCS (material coordinate system).

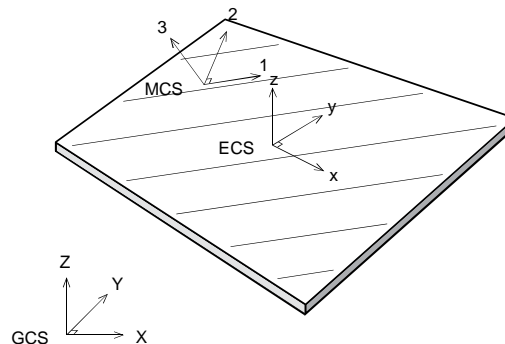


Figure 1-(1) Coordinate Systems

The element library of midas FEA consists of the following element-types:

- Truss Elements
- Beam Elements
- Shell Elements
- Plane Stress Elements
- Plane Strain Elements
- Axisymmetric Elements
- Solid Elements
- Elastic Link/Point Spring/Point Damping/Matrix Spring/Rigid Link Elements

A finite element is defined by the element-type and the numbers of the connecting nodes. Based on the sequence of the node-numbers the ECS is defined. Dependent on the element-type geometrical data and material data must be specified. An overview is given below.

Element-type	Geometrical data	Material Data
Truss Elements	Cross sectional area	Material model
Beam Elements	Cross section definition	Material model
Plane Stress Elements	Thickness	Material model
Shell Elements	Thickness	Material model and MCS
Plane Strain Elements	Thickness	Material model
Axisymmetric Elements	-	Material model
Solid Elements	-	Material model and MCS

The overview of which element-types can be used in a certain type of analysis is given below.

The check '✓' mark indicates that the element is available in the analysis-type.

Element Type	Element Order		Linear Analysis					Nonlinear Analysis		Potential Flow Analysis			
	1 st -order	2 nd -order	Linear Static	Modal	Linear Buckling	Time History	Response Spectrum	Material Nonlinear	Geometric Nonlinear	Heat of Hydration	General Heat Transfer Analysis	Contant Analysis	Fatigue Analysis
Truss	✓		✓	✓	✓	✓	✓	✓	✓	✓	✓		
Beam	✓		✓	✓	✓	✓	✓				✓		
Plane Stress	✓	✓	✓	✓	✓	✓	✓	✓	✓		✓	✓	✓
Shell	✓	✓	✓	✓	✓	✓	✓	✓	✓		✓	✓	✓
Plane Strain	✓	✓	✓	✓		✓	✓	✓	✓		✓		✓
Axisymmetric	✓	✓	✓					✓	✓		✓		✓
Solid	✓	✓	✓	✓	✓	✓	✓	✓	✓	✓	✓	✓	✓

*Note: CFD (Computational Fluid Dynamic) Analysis uses specific shell elements.

The analysis load cases, which can be used for each element type, are listed below.

Element Type	Element Order		Static Load						
	1 st -order	2 nd -order	Body Force	Face Pressure	Edge Pressure	Beam Load	Prestress	Element Temperature	Temperature Gradient
Truss	✓		✓				✓	✓	
Beam	✓		✓			✓	✓	✓	✓
Plane Stress	✓	✓	✓	✓	✓		✓	✓	✓
Shell	✓	✓	✓	✓	✓		✓	✓	
Plane Strain	✓	✓	✓	✓	✓		✓	✓	
Axisymmetric	✓	✓	✓		✓		✓	✓	
Solid	✓	✓	✓	✓			✓	✓	

The analysis types, which can be used for each material type, are listed below.

Material Type	Linear Analysis					Nonlinear Analysis	
	Linear Static	Modal	Linear Buckling	Time History	Response Spectrum	Material Nonlinear	Geometric Nonlinear
Elastic	✓	✓	✓	✓	✓	✓	✓
Multi-Elastic						✓	✓
Rankine						✓	✓
Tresca						✓	✓
Von Mises						✓	✓
Drucker Prager						✓	✓
Mohr Coulomb						✓	✓
Total Strain Crack						✓	✓
User Supplied						✓	✓
Creep/Shrinkage	✓*						

(* Linear construction stage Analysis, Heat of Hydration Analysis)

The following table gives an overview of which material-types can be used in combination with

which element- types.

Material Type	Element Type						
	Truss	Beam	Plane Stress	Shell	Plane Strain	Axysymmetric	Solid
Elastic	✓	✓	✓	✓	✓	✓	✓
Multi-Elastic	✓						
Rankine	✓	✓	✓	✓	✓	✓	✓
Tresca	✓	✓	✓	✓	✓	✓	✓
Von Mises	✓	✓	✓	✓	✓	✓	✓
Drucker Prager	✓	✓	✓	✓	✓	✓	✓
Mohr Clulomb	✓	✓	✓	✓	✓	✓	✓
Total Strain Crack	✓	✓	✓	✓	✓	✓	✓
User Supply	✓	✓	✓	✓	✓	✓	✓
Creep/Shrinkage							✓

The calculated results for static analysis are listed below.

Element Type	Calculated Results			
	Stress	Strain	Element Force	Default Output Coordinate (changeable)
Truss	✓		✓	ECS (no)
Beam			✓	ECS (no)
Plane Stress	✓	✓		ECS (yes)
Shell	✓	✓	✓	ECS (yes)
Plane Strain	✓	✓		GCS (yes)
Axisymmetric	✓	✓		GCS (yes)
Solid	✓	✓		GCS (yes)

In contrary to truss and beam elements the accuracy of results in plane stress, shell, plane strain, axisymmetric and solid elements are strongly affected by the element-size and the element distribution. A finer discretization is required in the following situations.

- Regions of geometric discontinuity (i.e. areas close to sharp corners on the edges or in the vicinity of an opening on the model)
- Regions where applied loadings vary drastically or where concentrated loads are applied
- Regions where the cross section of a beam, the thickness of a shell or the material properties are discontinuous
- Regions where detailed stress/force results are required

Further, the following recommendations are given:

- Size variation between adjacent elements should be kept to less than 1/2.
- If stress results are of interest, 4-noded quadrilateral elements and 8-noded brick elements should be used; instead of 3-Noded triangular elements and 4-noded

tetrahedron elements, higher order elements should be used.

- All the corners of planar elements should be chosen such that the angles are close to 90° for quadrilateral elements and close to 60° for triangular elements. Each corner angle of a quadrilateral element should be within the range of 45° and 135° . For a triangular element, each corner angle should be within the range of 30° and 150° .
- In the case of a quadrilateral element, all the four nodes should be on the same flat plane.
- Where a node is shared between truss, plane stress and solid elements, which have no rotational degrees of freedom, a singular error may occur when no specific measures are taken. Therefore, in such cases, midas FEA automatically assigns rotational degrees of freedom to these nodes.

The element stiffness matrix \mathbf{K}^e is defined in the ECS (element coordinate system) by the following equation.

$$\mathbf{K}^e = \int_{V_e} \mathbf{B}^T \mathbf{D} \mathbf{B} dV \quad (1.1)$$

Here the matrix \mathbf{B} is the strain-displacement-matrix which is based on the shape function \mathbf{N} and its derivatives, and \mathbf{D} is a matrix representing the relation between stress and strain. \mathbf{N} is consisted of the shape function, N_i that defines for the Gauss-point with the natural coordinates, $\xi - \eta - \zeta$ how the position of the Gauss-point can be interpolated from the positions of the nodes of the element.

1-2 Truss Element

1-2-1 Overview

A truss element is a “uniaxial tension-compression 3D line element” defined by two nodes. Truss elements are generally used for modeling space trusses and/or diagonal braces and can be used for both static (linear & nonlinear) and dynamic analyses. A truss element transmits only axial forces and may be combined with tension-only/compression-only functions. The stress and strain tensors of a truss element are expressed as follows:

$$\boldsymbol{\sigma} = \{\sigma_{xx}\}, \quad \boldsymbol{\varepsilon} = \{\varepsilon_{xx}\} \quad (\text{Stress \& strain in axial direction})$$

Since a truss element only has degrees of freedom in the axial direction as shown in Fig. 1-(2), only the ECS x-axis is meaningful. The direction of the ECS axis is defined from Node 1 to Node 2.

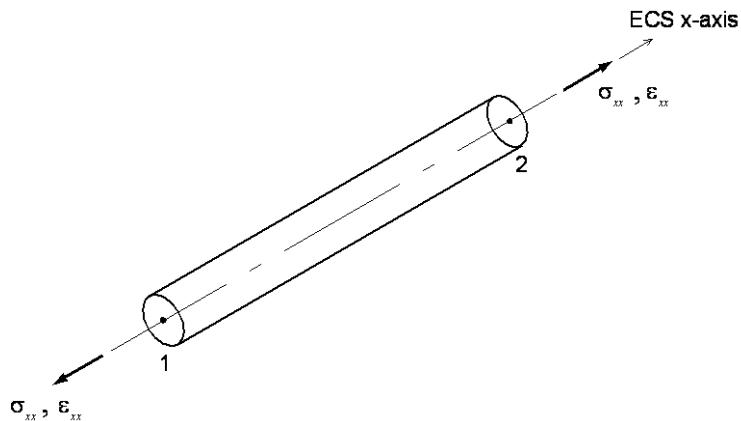


Figure 1-(2) Element Coordinate System and Stress/Strain Convention of Truss Element

1-2-2 Finite Element Formulation

The cross sectional area A is assumed to be constant throughout the entire length L_e of the truss element. The truss element has 2 Gauss-points which are located according to the Gauss-scheme between the 2 nodes. The truss element only has translational displacement degrees of freedom, u , in the ECS x-direction .

$$\mathbf{u}_i = \{u_i\} \quad (1.2)$$

The coordinate x and the translational displacement u can be expressed by the shape functions at the 2 Gauss-points noted below with ξ being the iso-parametric coordinate of the truss element.

$$x = \sum_{i=1}^2 N_i x_i, \quad u = \sum_{i=1}^2 N_i u_i \quad (1.3)$$

$$N_1 = \frac{1-\xi}{2}, \quad N_2 = \frac{1+\xi}{2} \quad (-1 \leq \xi \leq 1) \quad (1.4)$$

The relationship between the nodal displacement and strain can be expressed by the strain-displacement matrix \mathbf{B}_i in the equation (1.5).

$$\boldsymbol{\varepsilon} = \sum_{i=1}^2 \mathbf{B}_i \mathbf{u}_i \quad (1.5)$$

The matrix \mathbf{B}_i is a derivative of the shape function, which is expressed as,

$$\mathbf{B}_i = \left\{ \frac{\partial N_i}{\partial x} \right\} \quad (1.6)$$

Using the matrix \mathbf{B}_i , the element stiffness matrix in ECS, is expressed as,

$$\mathbf{K}_{ij} = \int_{L_e} \mathbf{B}_i^T \mathbf{D} \mathbf{B}_j dL, \quad \mathbf{D} = A \{E\} \quad (1.7)$$

where, A is the cross section of area, L_e is the length of the truss element, \mathbf{D} the stress-strain matrix, and E is the Young's modulus.

The element stiffness matrix of a truss element can be written as follows:

$$\mathbf{K} = \frac{EA}{L_e} \begin{bmatrix} 1 & -1 \\ -1 & 1 \end{bmatrix} \quad (1.8)$$

1-2-3 Loads and Masses

Loads that can be applied to a truss element are body force, prestress, thermal load, etc. The body force is a load, which represents the self weight of an element or the inertia force that acts on an element. A prestress load is used when a tension force needs to be introduced in a truss element as an internal force. A temperature load is used to reflect thermal deformation due to nodal temperature and element temperature loads. The load vectors in the ECS for prestress and temperature loads can be expressed as below.

- Body force

$$\mathbf{F}_i = A \int_{L_e} N_i \begin{Bmatrix} \omega_x \\ \omega_y \\ \omega_z \end{Bmatrix} dL \quad (1.9)$$

where, $\omega_x, \omega_y, \omega_z$ are the weight density vector components

- Prestress load

$$\mathbf{F}_i = - \int_{L_e} \mathbf{B}_i^T P dL \quad (1.10)$$

where, P is the axial prestress force

- Temperature load

$$\mathbf{F}_i = \int_{L_e} \mathbf{B}_i^T EA \alpha \Delta T dL \quad (1.11)$$

where, α is the linear thermal expansion coefficient and ΔT is the temperature change.

The lumped mass and the consistent mass matrices of a truss element only comprise translational displacements in the x, y, z directions and are defined as follows.

- Lumped mass

$$\mathbf{M} = \frac{\rho A L_e}{2} \begin{bmatrix} 1 & & & & & \\ 0 & 1 & & & & \\ 0 & 0 & 1 & & & \\ 0 & 0 & 0 & 1 & & \\ 0 & 0 & 0 & 0 & 1 & \\ 0 & 0 & 0 & 0 & 0 & 1 \end{bmatrix} \quad \text{symm.} \quad (1.12)$$

where ρ is the mass density

- Consistent mass

$$\mathbf{M} = \frac{\rho A L_e}{6} \begin{bmatrix} 2 & & & & & \\ 0 & 2 & & & & \\ 0 & 0 & 2 & & & \\ 1 & 0 & 0 & 2 & & \\ 0 & 1 & 0 & 0 & 2 & \\ 0 & 0 & 1 & 0 & 0 & 2 \end{bmatrix} \quad \text{symm.} \quad (1.13)$$

1-2-4 Element Output

Analysis results for a truss element comprise the element (internal) forces and stresses at Nodes 1 and 2 with reference to the ECS. The calculated element force is the axial force, $N_x (= A\sigma_{xx})$. When the axial force is in tension as shown in Fig. 1-(3), it retains a positive ('+') sign. In general the element forces are equal at two nodes, but they can be different in case of acting self weight load on the element.

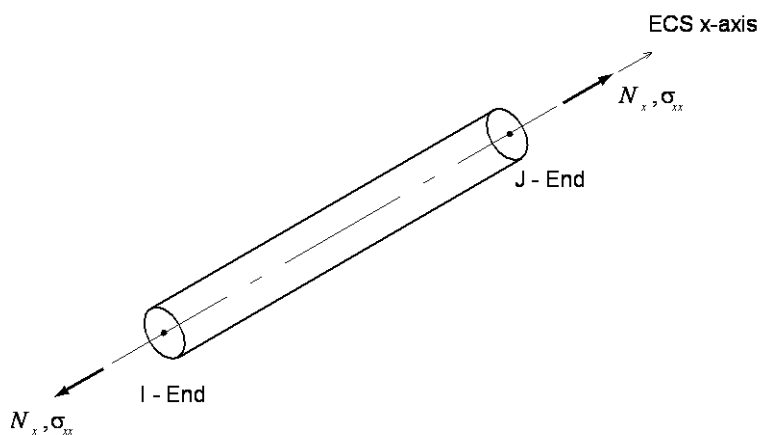


Figure 1-(3) Element Forces/Stresses in Truss Element

1-3 Beam Element

1-3-1 Overview

A beam element is a line element that is defined by two nodes and accounts for elongation, bending, shear and torsion. If bending, shear and torsion are not relevant, then the truss element can be used as alternative to the beam element. Beam elements are generally used to model structures that are relatively long compared to the section dimensions. If the ratio of the section depth to the length is greater than 1/5, the use of shell or solid elements is recommended. This is due to consideration of the effect of shear deformations in beam elements in a very accurate way. The beam element can be used for both static (linear & nonlinear) and dynamic analyses and is capable of accounting for axial deformation, bending, torsion, shear deformation, etc.

Stress, strain and element force are expressed as follows:

$$\boldsymbol{\sigma} = \{\sigma_{xx}\}, \quad \boldsymbol{\varepsilon} = \{\varepsilon_{xx}\} \quad (\text{Stress \& strain in axial direction})$$

$$\mathbf{M} = \begin{Bmatrix} M_y \\ M_z \end{Bmatrix}, \quad \boldsymbol{\kappa} = \begin{Bmatrix} \kappa_y \\ \kappa_z \end{Bmatrix} \quad (\text{Bending moment \& curvature})$$

$$\mathbf{T} = \{M_x\}, \quad \boldsymbol{\phi} = \{\phi_x\} \quad (\text{Torsional moment \& torsion angle})$$

$$\mathbf{Q} = \begin{Bmatrix} Q_y \\ Q_z \end{Bmatrix}, \quad \boldsymbol{\gamma} = \begin{Bmatrix} \gamma_{xy} \\ \gamma_{zx} \end{Bmatrix} \quad (\text{Shear force \& shear strain})$$

The sign convention for beam element forces and stresses is depicted in Fig. 1-(4) and the arrows represent the positive (+) directions. When the user defines the shear area equal to zero, the corresponding shear deformations of the beam element will be ignored.

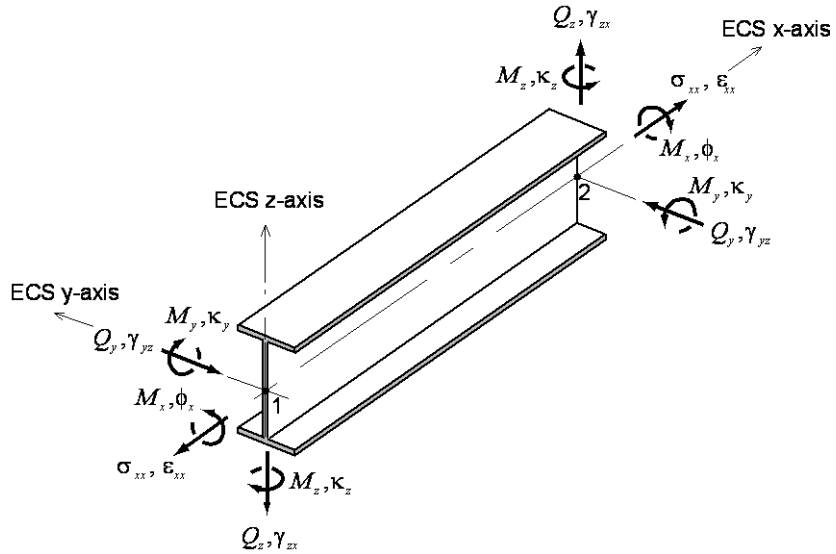


Figure 1-(4) Element Coordinate System and Stress Convention of Beam Element

Beam element forces and stresses are expressed with reference to the ECS. The direction of the ECS x-axis is defined from Node 1 to Node 2. The directions of the ECS y and z-axes are shown in Fig. 1-(4) and defined according to one of the three methods as shown in Fig. 1-(5), (6) & (7). Once the ECS z-axis is defined, the ECS y-axis is automatically defined following the right-hand rule.

Defining ECS using Beta angle

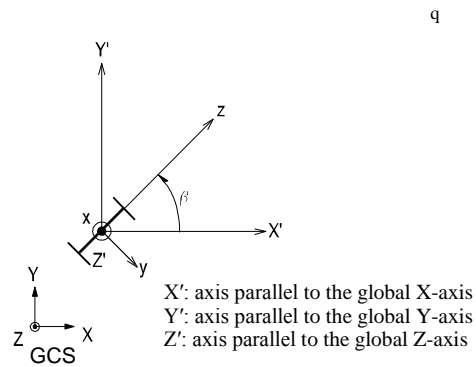
The ECS of the beam element is defined by using the angle β . If the beam is oriented in the vertical direction, i.e. the ECS x-axis for the beam element is parallel with the GCS Z-axis, the beta angle β is defined as the angle between the GCS X-axis and the ECS z-axis (Fig. 1-(5)a). However, if the beam element is not oriented in the vertical direction, the beta angle β is defined as the angle from the GCS Z-axis to the ECS x-z plane (Fig. 1-(5)b).

Defining ECS using a Node

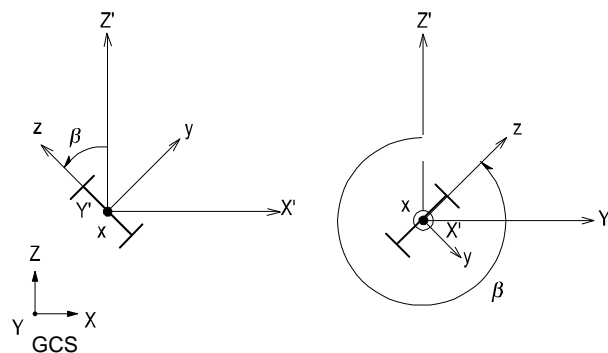
By specifying a node that is not located on the ECS x-axis the local x-z plane is defined as illustrated in Fig. 1-(6).

Defining ECS using a vector

By specifying a vector that is not parallel to the ECS x-axis the local X-Zplane is defined as illustrated in Fig. 1-(7).



(a) Case of vertical members



(b) Case of non-vertical members

Figure 1-(5) Defining ECS using Beta Angle Conventions

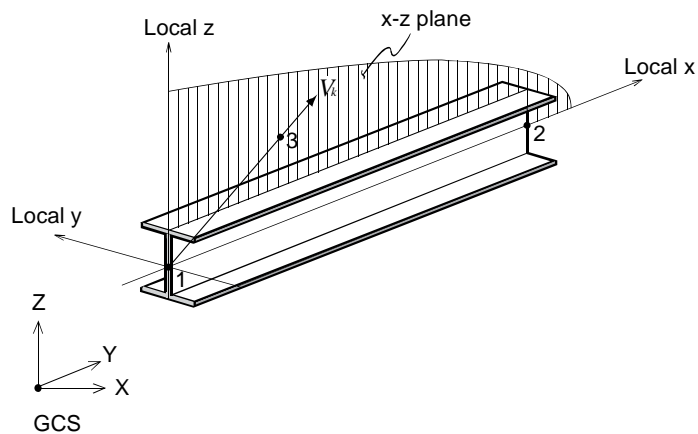


Figure 1-(6) Defining ECS using a Node

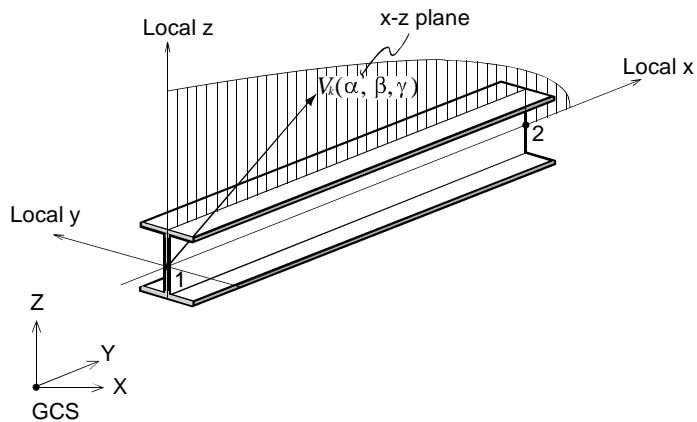


Figure 1-(7) Defining ECS using a K-Vector

1-3-2 Finite Element Formulation

The cross-section shape and dimension of a beam element is assumed to be constant throughout the full length. A beam element has three translational and three rotational degrees of freedom at each node with respect to the ECS. The axial stiffness of a beam element is identical to the axial stiffness of a truss element. In the same way as the axial stiffness the torsional stiffness of the beam element can be calculated. The calculation of bending and shear stiffness is based on the Timoshenko Beam theory or the Euler Beam theory.

The formation of the element stiffness matrix related to the deformation in the axial direction is identical to that for a truss element.

$$\mathbf{u}_i = \{u_i\} \quad (1.14)$$

$$\mathbf{K}_{axial} = \frac{EA}{L_e} \begin{bmatrix} 1 & -1 \\ -1 & 1 \end{bmatrix} \quad (1.15)$$

where, A is the cross section area and L_e is the element length

The torsional stiffness matrix of a beam element is calculated as follows:

$$\mathbf{u}_i = \{\theta_{xi}\} \quad (1.16)$$

$$\mathbf{K}_{torsional} = \frac{GI_x}{L_e} \begin{bmatrix} 1 & -1 \\ -1 & 1 \end{bmatrix} \quad (1.17)$$

where, I_x is the torsional resistance and G is the shear-modulus

Since the shear and bending effects are related to each other, the formulation of these effects to the stiffness matrix will be combined. First, we will explain the shear stiffness, which is based on the Timoshenko Beam theory. The shear and bending deformation in the ECS x-z plane are defined by the translational displacement w in the ECS z-direction and the rotation θ_y around the ECS y-axis.

$$\mathbf{u}_i = \{w_i \quad \theta_{yi}\}^T \quad (1.18)$$

A coordinate x in the element's axial direction and the translational displacement w can be expressed with linear interpolation functions:

$$x = \sum_{i=1}^2 N_i x_i, \quad w = \sum_{i=1}^2 N_i w_i \quad (1.19)$$

However, the rotation around the ECS y-axis is a quadratic interpolation function,

$$\theta_y = \sum_{i=1}^2 N_i \theta_{yi} + P_3 \Delta \theta_{y3} \quad (1.20)$$

$$N_1 = \frac{1-\xi}{2}, \quad N_2 = \frac{1+\xi}{2}, \quad P_3 = 1-\xi^2 \quad (-1 \leq \xi \leq 1) \quad (1.21)$$

In order to calculate the virtual rotation $\Delta \theta_{y3}$ at the mid-point of the element, the following assumptions are made.

- Shear force and bending moment must be in equilibrium.

$$Q_z = -\frac{\partial M_y}{\partial x} \quad (1.22)$$

- The average shear strain $\bar{\gamma}_{zx}$ calculated from the equilibrium equation (1.22) must be equal to the shear strain γ_{zx} calculated from the shape function along the full length of the beam element:

$$\int_{L_e} (\gamma_{zx} - \bar{\gamma}_{zx}) dL = 0 \quad (1.23)$$

Based on the above assumptions, the virtual rotation $\Delta \theta_{y3}$ at the mid-point can be expressed as,

$$\Delta \theta_{y3} = \frac{3}{2L_e(1+\phi_3)} \left[1 \quad -\frac{L_e}{2} \quad -1 \quad -\frac{L_e}{2} \right] \begin{Bmatrix} w_1 \\ \theta_{y1} \\ w_2 \\ \theta_{y2} \end{Bmatrix}, \quad \phi_3 = \frac{12EI_y}{GA_{xz}L_e^2} \quad (1.24)$$

Where A_{xy} is the effective shear area in the z -direction, I_y is the area moment of inertia and G

is the shear modulus.

The matrix \mathbf{B}_{bi} relates the nodal d.o.f.'s to the curvature κ_y :

$$\kappa_y = \sum_{i=1}^2 \mathbf{B}_{bi} \mathbf{u}_i \quad (1.25)$$

$$\mathbf{B}_{bi} = \left\{ \frac{3a_i}{2L_e(1+\phi_3)} \frac{\partial P_3}{\partial x} - \frac{3}{4(1+\phi_3)} \frac{\partial P_3}{\partial x} - \frac{\partial N_i}{\partial x} \right\}, \quad a_1 = -1, \quad a_2 = 1 \quad (1.26)$$

$\bar{\gamma}_{zx}$ is the shear deformation, and the relationship between $\bar{\gamma}_{zx}$ and the nodal displacement can be expressed by the matrix \mathbf{B}_{si} :

$$\bar{\gamma}_{zx} = \sum_{i=1}^2 \mathbf{B}_{si} \mathbf{u}_i \quad (1.27)$$

$$\mathbf{B}_{si} = \left\{ \frac{a_i}{L_e(1+\phi_3)} - \frac{L_e}{2(1+\phi_3)} \right\}, \quad a_1 = -1, \quad a_2 = 1 \quad (1.28)$$

Accordingly, the contribution of shear and bending to the stiffness matrix is:

$$\mathbf{K}_{ij} = \int_{L_e} (\mathbf{B}_{bi}^T \mathbf{D}_b \mathbf{B}_{bj} + \mathbf{B}_{si}^T \mathbf{D}_s \mathbf{B}_{sj}) dL \quad (1.29)$$

$$\mathbf{D}_b = I_y \{E\}, \quad \mathbf{D}_s = A_{xy} \{G\} \quad (1.30)$$

By integrating and rearranging the equation (1.29), the bending and shear stiffness in the ECS x-z plane is defined by the matrix below.

$$\mathbf{K}_{bending} + \mathbf{K}_{shear} = \frac{EI_y}{1+\phi_3} \begin{bmatrix} \frac{12}{L_e^3} & -\frac{6}{L_e^2} & -\frac{12}{L_e^3} & -\frac{6}{L_e^2} \\ & \frac{4}{L_e} \left(1 + \frac{\phi_3}{4}\right) & \frac{6}{L_e^2} & \frac{2}{L_e} \left(1 - \frac{\phi_3}{2}\right) \\ & & \frac{12}{L_e^3} & \frac{6}{L_e^2} \\ \text{Symm.} & & & \frac{4}{L} \left(1 + \frac{\phi_3}{4}\right) \end{bmatrix} \quad (1.31)$$

In the same way the bending and shear stiffness in the ECS x-y plane are calculated.

In order to calculate the stiffness without considering the shear deformation based on the Euler Beam theory, the formulation is based on the following equation, instead of using the equation (1.23), which assumes the presence of shear strain.

$$\int_{L_e} \gamma_{zx} dL = 0 \quad (1.32)$$

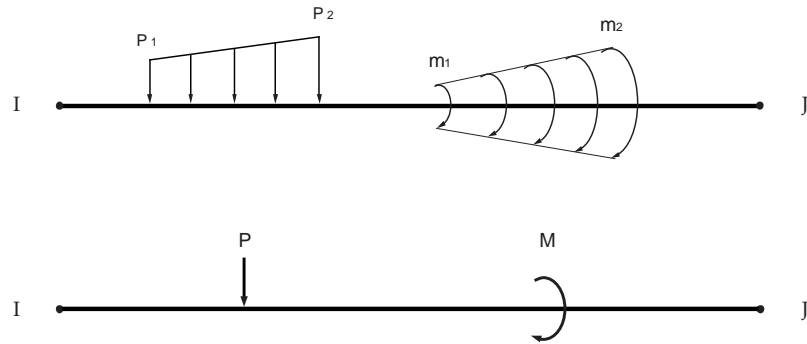
Substituting $\phi_3 = 0$ into the equation (1.31), the pure bending stiffness will be obtained.

1-3-3 Loads and Masses

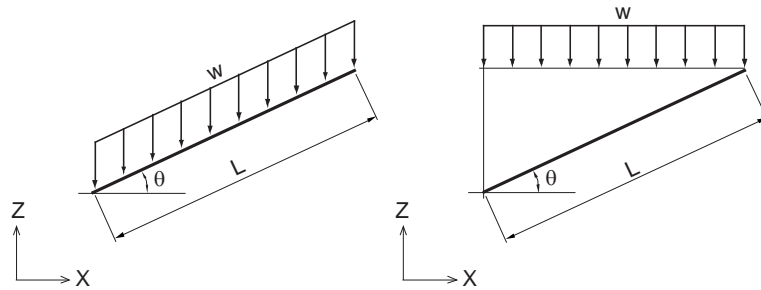
Loads that can be applied to a beam element are the beam load, the body force, the prestress, the thermal load, etc. The body force represents the self weight or the inertia force of an element. The beam load can be a concentrated or distributed load, which works along the length of an element, and can be entered either in the ECS or in the GCS. The prestress load is used when tension deformation needs to be introduced in a beam element by an internal force and is applied along the ECS x-direction. The value of the prestress is equal to the desired value of the stress in the element when both ends of the element are restrained. The temperature loads may cause thermal deformation in longitudinal direction of the beam element and temperature gradient loads may result in bending of the element.

- **Beam load**

A beam load can be a concentrated or distributed load. The loaded zone may be part of the element length and can be specified by the user. In all cases the beam load is automatically converted into equivalent nodal loads. In the calculation of internal forces, beam loads are handled such that the internal forces at I-end, 1/4, 1/2, 3/4 and J-end of an element are exactly calculated. Fig. 1-(8) illustrates the various types of beam loads.



(a) Types of beam loads (concentrated loads & distributed loads)



(b) Distributed loads using the Projection option

Figure 1-(8) Examples of beam loads

- **Body force**

$$\mathbf{F}_i = A \int_{L_e} N_i \begin{Bmatrix} \omega_x \\ \omega_y \\ \omega_z \end{Bmatrix} dL \quad (1-33)$$

where, ω_x , ω_y , ω_z are the weight density vector components

- **Prestress load**

$$\mathbf{F}_i = - \int_{L_e} \mathbf{B}_i^T P dL \quad (1-34)$$

where \mathbf{B}_i is identical to the equivalent matrix of the truss element and P is the axial prestress force

- **Temperature load**

$$\mathbf{F}_i = \int_{L_e} \mathbf{B}_i^T EA\alpha\Delta T dL \quad (1-35)$$

where α is the linear thermal expansion coefficient and ΔT is the temperature change.

The mass of a beam element can be defined as lumped mass or as a consistent mass. The lumped mass of a beam element is composed of translational displacements in the x, y, z directions and similar to the truss-element, has the magnitude of $(\rho AL)/2$ in all directions. The consistent mass of a beam element is accounted for all translational displacements and rotational displacements.

- **Consistent mass**

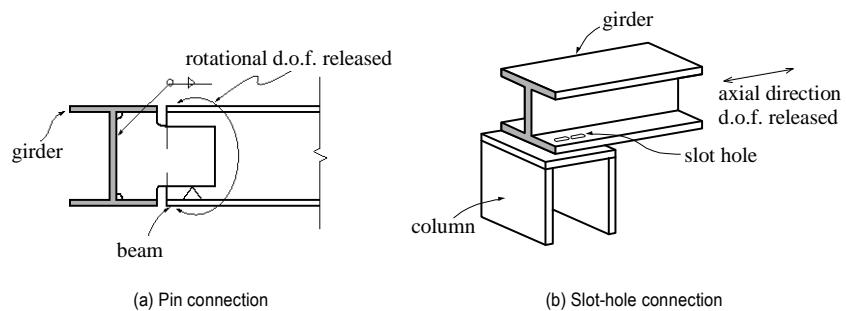
$$\mathbf{M} = \frac{\rho AL_e}{420} \begin{bmatrix} 140 & & & & & & & & & & \\ 0 & 156 & & & & & & & & & \\ 0 & 0 & 156 & & & & & & & & \\ 0 & 0 & 0 & 140 \frac{J}{A} & & & & & & & \\ 0 & 0 & -22L_e & 0 & 4L_e^2 & & & & & & \\ 0 & 22L_e & 0 & 0 & 0 & 4L_e^2 & & & & & \\ 70 & 0 & 0 & 0 & 0 & 0 & 140 & & & & \\ 0 & 54 & 0 & 0 & 0 & 13L_e & 0 & 156 & & & \\ 0 & 0 & 54 & 0 & -13L_e & 0 & 0 & 0 & 156 & & \\ 0 & 0 & 0 & 70 \frac{J}{A} & 0 & 0 & 0 & 0 & 0 & 140 \frac{J}{A} & \\ 0 & 0 & 13L_e & 0 & -3L_e^2 & 0 & 0 & 0 & 22L_e & 0 & 4L_e^2 \\ 0 & -13L_e & 0 & 0 & 0 & -3L_e^2 & 0 & -22L_e & 0 & 0 & 4L_e^2 \end{bmatrix} \quad \text{symm.}$$

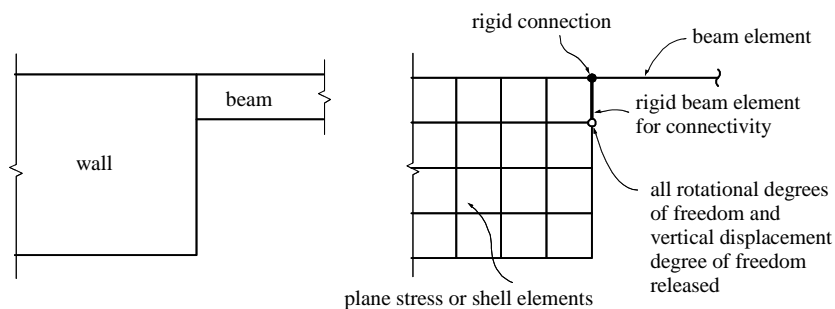
(1-36)

where J is the polar moment of inertia.

1-3-4 Boundary Constraints

In midas FEA End Release and Offset conditions may be applied to beam elements. When members are connected by pins or slotted holes, the Beam End Release option is used as shown in Fig. 1-(9). Beam End Release is applicable to all the degrees of freedom of a beam element. The end release constraints are always specified in the ECS. Caution is required when stiffness in the GCS is to be released. Further, the end release conditions may produce singularities in the system, and therefore, the user is advised take care when applying end release conditions and to ensure that the force-transmission in the system is captured.





(d) Connection of elements with different degrees of freedoms

Figure 1-(9) Examples of Beam End Release Conditions

It is possible to model situations in which the neutral axis of a member does not pass through a node by using Offsets Conditions, without creating additional nodes. There are two types of offsets, the local offset and the global offset.

The “Global Offset” can be defined as the distance vector in the GCS between the ends of two beam elements as illustrated in Fig. 1-(10). The stiffness and loads of an offset beam element are corrected for the offset condition.

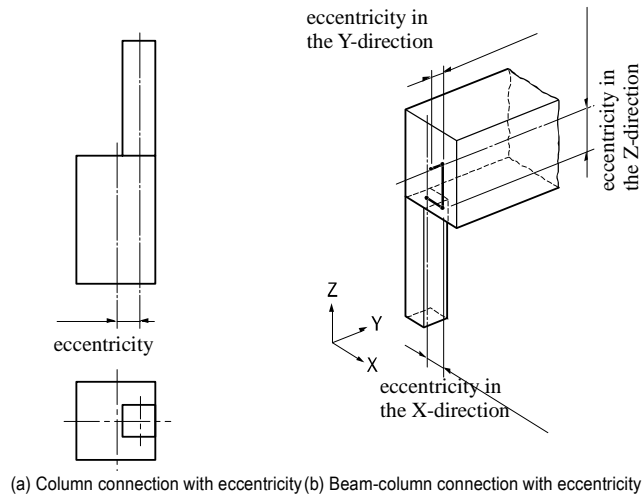


Figure 1-(10) Beam End Global Offset

The “Local Offset” can be defined with reference to the ECS as illustrated in Fig. 1-(11). Midas FEA uses the distance between the end nodes when the axial and torsional stiffnesses of an element with offset are calculated. The effective length of the beam, which the offset has been subtracted, is used for the calculation of the shear and bending stiffnesses.

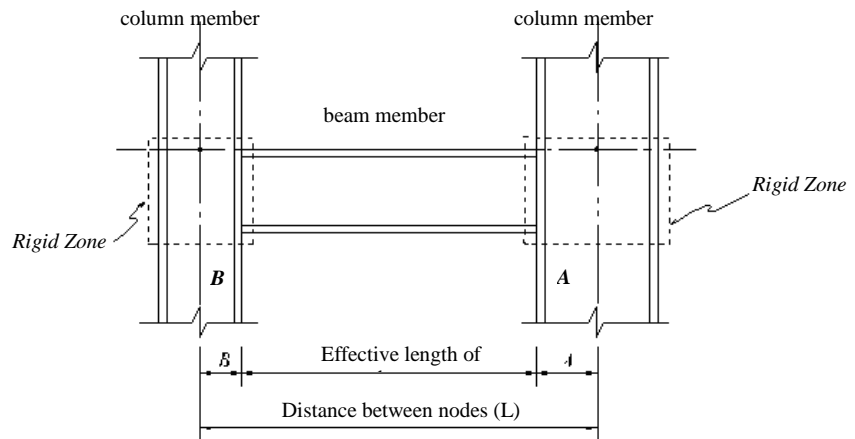
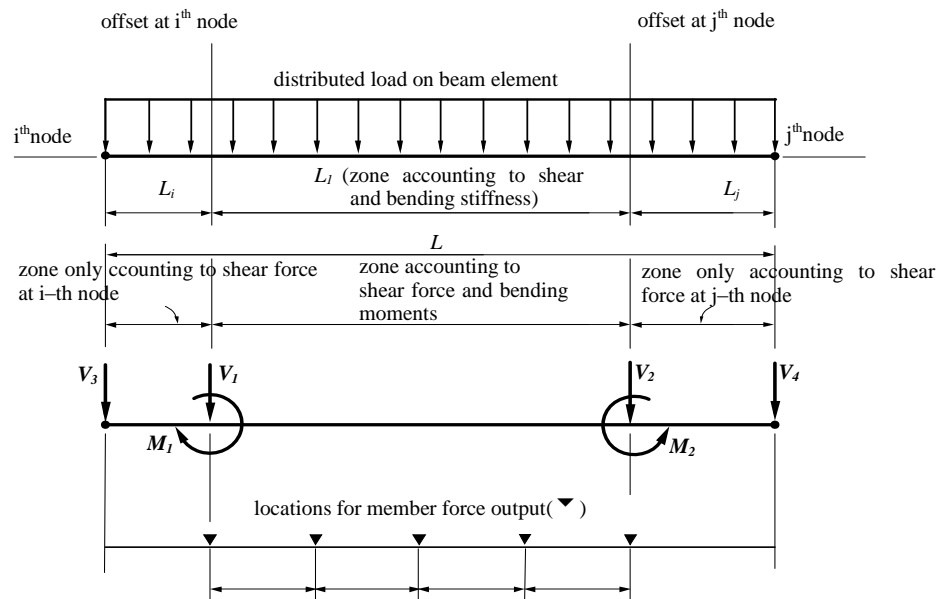


Fig. 1-(12) illustrates the calculation of distributed loads in the situation that “Local Offset” is applied. The distributed load accounting to an offset zone is converted into an equivalent shear force at the corresponding node only where this section does not contribute to the bending moment. At the remaining part the distributed loads are converted into shear forces and moments. The calculation of the body forces is identical to that of distributed loads. The member forces for beam elements are defined at the offset positions.



$L_i = Z_F \times R_i$ “Offset Position” is the location of the force output

$L_j = Z_F \times R_j$ “Offset Position” is the location of the force output

R_i Offset distance at i-th node

R_j Offset distance at j-th node

Z_F Offset Factor

V_1, V_2 shear forces equivalent to distributed load between the offset ends

M_1, M_2 moments equivalent to distributed load between the offset ends

V_3, V_4 shear forces equivalent to distributed load between offset ends and nodal points

Figure 1-(12) Beam load distribution of the force output

1-3-5 Element Output

The member forces for beam elements are produced at 5 locations. The output positions are at I-End, 1/4, 2/4, 3/4 and J-End of the element's length. The arrows in Fig. 1-(13) represent the positive (+) directions.

- Axial force N_x
- Shear force Q_y, Q_z
- Torsional moment M_x
- Bending moment M_y, M_z

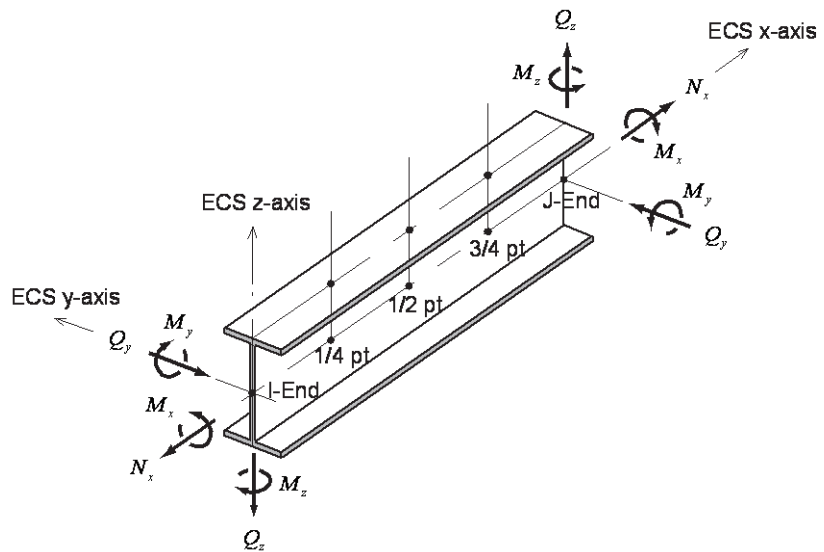


Figure 1-(13) Output Convention of Beam Element

1-4 Shell Element

1-4-1 Overview

There are triangular and rectangular shell elements defined by 3, 4, 6 or 8 nodes. Shell elements can be used for modeling pressure vessels, braced walls, bridge decks, etc. Shell elements can account for in-plane deformation (plane stress) and out-of-plane deformation (bending and shear) and can be used for both static (linear & nonlinear) and dynamic analyses. Stress and strain for defining the deformation of a shell element are expressed as follows:

$$\boldsymbol{\sigma} = \begin{Bmatrix} \sigma_{xx} \\ \sigma_{yy} \\ \sigma_{xy} \end{Bmatrix}, \quad \boldsymbol{\varepsilon} = \begin{Bmatrix} \varepsilon_{xx} \\ \varepsilon_{yy} \\ \gamma_{xy} \end{Bmatrix} \quad (\text{In-plane stress \& strain})$$

$$\mathbf{M} = \begin{Bmatrix} M_{xx} \\ M_{yy} \\ M_{xy} \end{Bmatrix}, \quad \boldsymbol{\kappa} = \begin{Bmatrix} \kappa_{xx} \\ \kappa_{yy} \\ \kappa_{xy} \end{Bmatrix} \quad (\text{Bending moment \& curvature})$$

$$\mathbf{Q} = \begin{Bmatrix} Q_{zx} \\ Q_{yz} \end{Bmatrix}, \quad \boldsymbol{\gamma} = \begin{Bmatrix} \gamma_{zx} \\ \gamma_{yz} \end{Bmatrix} \quad (\text{Shear force \& shear strain})$$

The sign convention for in-plane stress & strain is equal to that for plane stress elements (Fig. 1-(23)) whereas the sign convention for bending moments and shear forces is presented in Fig. 1-(14). The arrows represent the positive (+) directions.

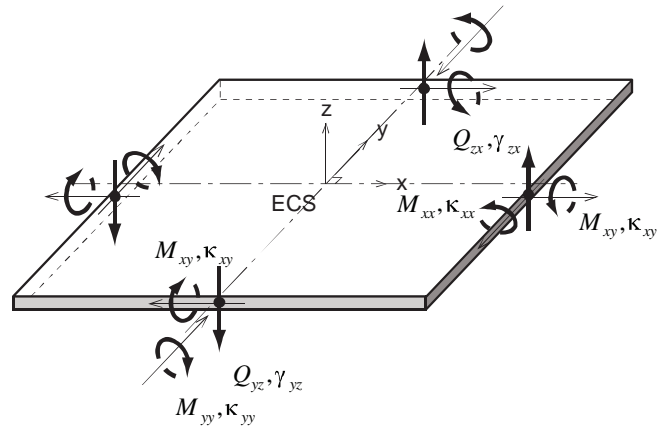
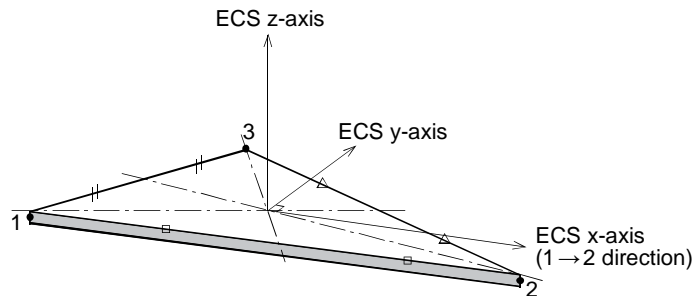


Figure 1-(14) Stress Sign Convention of Shell Element

The ECS is based on x, y & z-axes in the Cartesian coordinate system. The directions of the ECS axes are defined as shown in Fig. 1-(15). In the case of a quadrilateral element, the line connecting the mid point of Node 1 and Node 4 to the mid point of Node 2 and Node 3 defines the direction of the ECS x-axis. For a triangular element, the line parallel to the direction from Node 1 to Node 2 defines the ECS x-axis.



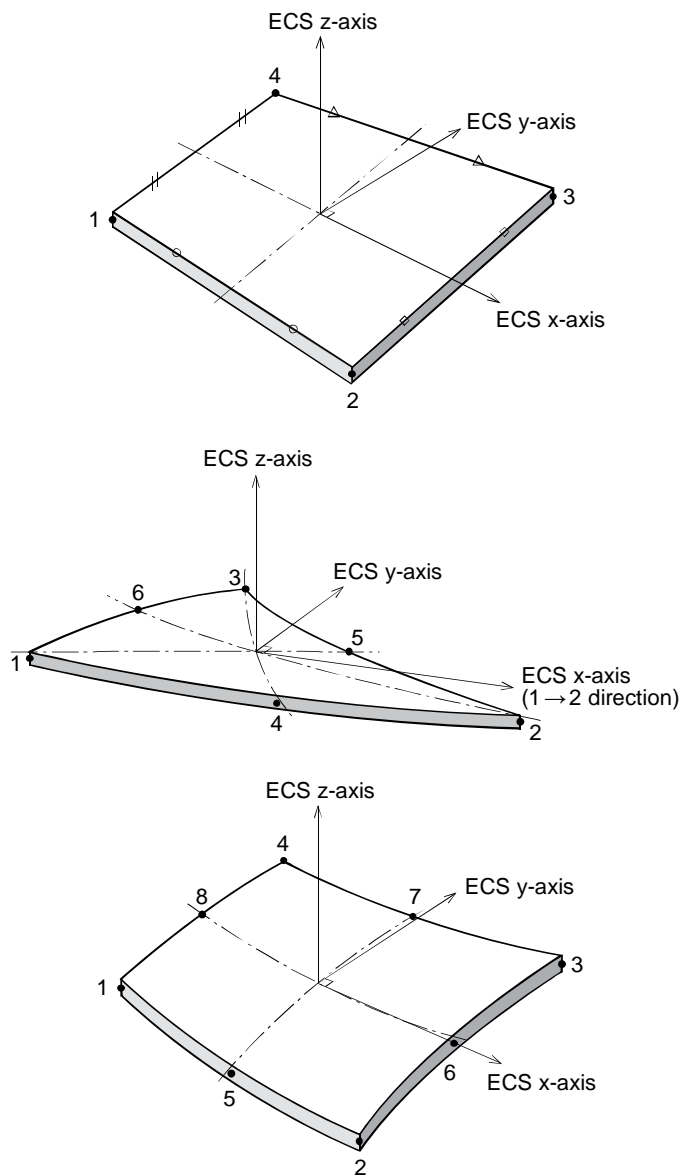
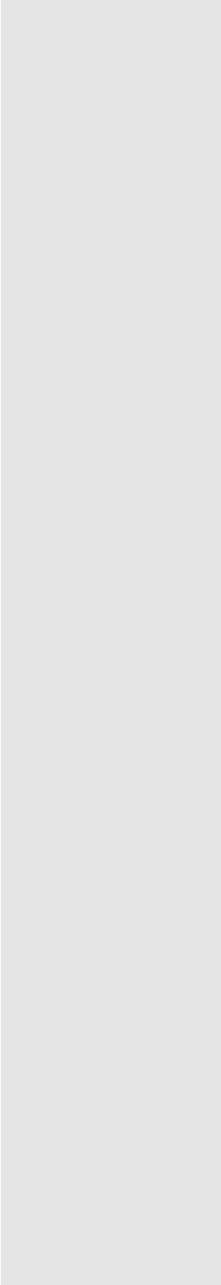


Figure 1-(15) Element Coordinate System of Shell Element



There are two types of shell elements: “Discrete Shell elements” and “Curved shell elements”. The discrete shell elements are available for shapes with 3 or 4 nodes and the curved shell elements for shapes with 6 or 8 nodes... 4-node discrete shell elements generally provide accurate results for the computation of both displacements and stresses. However, 3-node discrete shell elements tend to provide poor results in stresses whereas the calculated displacements are accurate. therefore it is advised not to use 3-node discrete shell elements in model areas where detailed analysis results are required.

1-4-2 Finite Element Formulation

A shell element has three translational degrees of freedom in the ECS x, y and z-directions and two rotational degrees of freedom in the ECS x and y-axes. The discrete shell element separately accounts for in-plane and out-of-plane stiffness effects. Whereas the curved shell element uses the “continuum shell approach”.

(1) Discrete Shell

The following element formulations are used for discrete shell elements:

- In-plane deformation
 - 3-node element
Iso-parametric Element (identical to that of a plane stress element), for which Drilling d.o.f. (rotational d.o.f. about the z-axis) may be activated or not.
 - 4-node element
Iso-parametric Element (identical to that of a plane stress element), for which Drilling d.o.f. (rotational d.o.f. about the z-axis) may be activated or not.
- Out-of-plane deformation
 - 3-node element
DKT¹ (Discrete Kirchhoff triangle) & DKMT² (Discrete Kirchhoff Mindlin triangle)
 - 4-node element
DKQ³ (Discrete Kirchhoff quadrilateral) & DKMQ⁴ (Discrete Kirchhoff Mindlin quadrilateral)

1 J.L. Batoz, K.J. Bathe and L.W. Ho, “A Study of Three-Node Triangular Plate Bending Elements,” International Journal for Numerical Methods in Engineering, Vol. 15, 1771-1812, 1980

2 I. Katili, “A New Discrete Kirchhoff-Mindlin Element Based on Mindlin-Reissner Plate Theory and Assumed Shear Strain Fields – Part I : An Extended DKT Element for Thick-Plate Bending Analysis,” International Journal for Numerical Methods in Engineering, Vol. 36, 1859-1883, 1993

3 J.L. Batoz and M. Ben Tahar, “Evaluation of a New Thin Plate Quadrilateral Element,” International Journal for Numerical Methods in Engineering, Vol. 18, 1655-1678, 1982

4 I. Katili, “A New Discrete Kirchhoff-Mindlin Element Based on Mindlin-Reissner Plate Theory and Assumed Shear Strain Fields-Part II : An Extended DKQ Element for Thick-Plate Bending Analysis,” International Journal for Numerical Methods in Engineering, Vol. 36, 1885-1908, 1993

The “Iso-parametric Element” formulation for the in-plane stiffness is identical to that of the plane stress element and will be explained in section “1.5 Plane Stress Element”. The “Element with Drilling d.o.f.” option activates rotational d.o.f. around the ECS z-axis θ_z in each of the element nodes and these additional rotations contribute to the inplane element displacements u and v .

$$\mathbf{u}_i = \{u_i, v_i, \theta_{zi}\}^T \quad (1.37)$$

For an arbitrary point in an element with N nodes the coordinates x and y and translational displacements u and v can be expressed as follows:

$$x = \sum_{i=1}^N N_i x_i, \quad y = \sum_{i=1}^N N_i y_i \quad (1.38)$$

$$u = \sum_{i=1}^N N_i u_i + \frac{1}{8} \sum_{i=1}^N P_i (y_j - y_i) (\theta_{zj} - \theta_{zi}), \quad v = \sum_{i=1}^N N_i v_i - \frac{1}{8} \sum_{i=1}^N P_i (x_j - x_i) (\theta_{zj} - \theta_{zi})$$

$$i = 1, 2, \dots, N-1, N \quad j = 2, 3, \dots, N, 1 \quad (1.39)$$

where, θ_{zi} represents the drilling d.o.f. at the node, i and the shape function is expressed as follows:

- 3-node element

$$N_1 = 1 - \xi - \eta, \quad N_2 = \xi, \quad N_3 = \eta \quad (1.40.a)$$

$$P_1 = 4\xi(1 - \xi - \eta), \quad P_2 = 4\xi\eta, \quad P_3 = 4\eta(1 - \xi - \eta) \quad (1.40.b)$$

- 4-node element

$$N_1 = \frac{1}{4}(1 - \xi)(1 - \eta), \quad N_2 = \frac{1}{4}(1 + \xi)(1 - \eta), \quad N_3 = \frac{1}{4}(1 + \xi)(1 + \eta),$$

$$N_4 = \frac{1}{4}(1 - \xi)(1 + \eta) \quad (1.41.a)$$

$$P_1 = \frac{1}{2}(1 - \xi^2)(1 - \eta), \quad P_2 = \frac{1}{2}(1 + \xi)(1 - \eta^2), \quad P_3 = \frac{1}{2}(1 - \xi^2)(1 + \eta),$$

$$P_4 = \frac{1}{2}(1 - \xi)(1 - \eta^2) \quad (1.41.b)$$

The relationship between the nodal displacement u and the in-plane strain ε is defined by the matrix \mathbf{B}_i .

$$\varepsilon = \sum_{i=1}^N \mathbf{B}_i u_i \quad (1.42)$$

The matrix \mathbf{B}_i is defined by the differentials of the shape function:

$$\mathbf{B}_i = \begin{bmatrix} \frac{\partial N_i}{\partial x} & 0 & \frac{(y_i - y_k)}{8} \frac{\partial P_k}{\partial x} - \frac{(y_j - y_i)}{8} \frac{\partial P_i}{\partial x} \\ 0 & \frac{\partial N_i}{\partial y} & \frac{(x_k - x_i)}{8} \frac{\partial P_k}{\partial y} - \frac{(x_i - x_j)}{8} \frac{\partial P_i}{\partial y} \\ \frac{\partial N_i}{\partial y} & \frac{\partial N_i}{\partial x} & \frac{(y_i - y_k)}{8} \frac{\partial P_k}{\partial y} - \frac{(y_j - y_i)}{8} \frac{\partial P_i}{\partial y} + \frac{(x_k - x_i)}{8} \frac{\partial P_k}{\partial x} - \frac{(x_i - x_j)}{8} \frac{\partial P_i}{\partial x} \end{bmatrix}$$

$$i = 1, 2, \dots, N-1, N, \quad j = 2, 3, \dots, N, 1, \quad k = N, 1, \dots, N-2, N-1 \quad (1.43)$$

Using the matrix \mathbf{B}_i , the element stiffness matrix for in-plane deformation is defined as follows:

$$\mathbf{K}_{ij}^{(t)} = \int_{A_e} t \mathbf{B}_i^T \mathbf{D} \mathbf{B}_j dA \quad (1.44)$$

where t is the thickness of the shell element and A_e is the element area

The matrix \mathbf{D} represents the relationship between in-plane stress and in-plane strain for isotropic materials:

$$\mathbf{D} = \frac{E}{1-\nu^2} \begin{bmatrix} 1 & \nu & 0 \\ \nu & 1 & 0 \\ 0 & 0 & \frac{1-\nu}{2} \end{bmatrix} \quad (1.45)$$

Where E is the Young's modulus and ν is the Poisson ratio.

When the “Drilling Element” option is activated, the translational displacements perpendicular to the element edges require a third order interpolation as is illustrated in Fig. 1-(16)., which gives more accurate results.

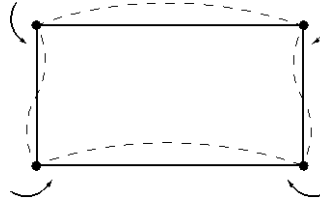


Figure 1-(16) Relation between translations and Drilling DOF

The DKMT (3-node) and DKMQ (4-node) element formulations make use of the method of shear strain assumption. The element considers only three d.o.f at each node, i.e., the translational displacement in the ECS z-direction, w and the rotational displacements about the ECS x and y-axes, θ_x and θ_y .

$$\mathbf{u}_i = \{w_i \quad \theta_{xi} \quad \theta_{yi}\}^T \quad (1.46)$$

For an arbitrary point in an element with N nodes and coordinates x and y the rotational displacements θ_x and θ_y are defined as follows:

$$\theta_x = \sum_{i=1}^N N_i \theta_{xi} + \sum_{i=1}^N P_i S_{ij} \Delta \theta_{ni}, \quad \theta_y = \sum_{i=1}^N N_i \theta_{yi} - \sum_{i=1}^N P_i C_{ij} \Delta \theta_{ni} \quad (1.47)$$

$$C_{ij} = -x_{ij}/L_{ij}, \quad S_{ij} = -y_{ij}/L_{ij}, \quad x_{ij} = x_i - x_j, \quad y_{ij} = y_i - y_j, \quad L_{ij}^2 = x_{ij}^2 + y_{ij}^2$$

$$i = 1, 2, \dots, N-1, N \quad j = 2, 3, \dots, N, 1$$

The shape functions, N_i and P_i are defined by the equations (1.40) and (1.41). When calculating the virtual rotational angle, $\Delta\theta_{ni}$ at the mid point of an edge, we make the following assumptions.

- The equilibrium equations between the shear force and the bending moment should be satisfied for N element edges.

$$Q_s = -M_{ns,s} - M_{ns,n} \quad (1.48)$$

where n is the local coordinate in the direction normal to the edge and s is the local coordinate in the direction tangential to the edge.

- The rotation around the axis perpendicular to the element edge is represented as a quadratic function along the edge, and the rotation around the axis tangential direction to the edge is linear along the edge.

$$\theta_n = (1 - \frac{s}{L_{ij}})\theta_{ni} + \frac{s}{L_{ij}}\theta_{nj} + 4\frac{s}{L_{ij}}(1 - \frac{s}{L_{ij}})\Delta\theta_{ni}, \quad \theta_s = (1 - \frac{s}{L_{ij}})\theta_{si} + \frac{s}{L_{ij}}\theta_{sj}$$

$$i = 1, 2, \dots, N-1, N \quad j = 2, 3, \dots, N, 1 \quad (1.49)$$

- The average shear strain $\bar{\gamma}_{sz}$ which is calculated from the equation (1.48) and the shear strain γ_{sz} which is directly calculated from the shape functions satisfy the following condition:

$$\int_0^{L_{ij}} (\gamma_{sz} - \bar{\gamma}_{sz}) ds = 0 \quad (1.50)$$

Substituting $\Delta\theta_{ni}$ obtained from the above assumptions into the equation (1.47), the rotational displacements θ_x and θ_y can be expressed in terms of \mathbf{u}_i as

$$\theta_x = \sum_{i=1}^N \mathbf{H}_{xi}^T \mathbf{u}_i, \quad \theta_y = \sum_{i=1}^N \mathbf{H}_{yi}^T \mathbf{u}_i \quad (1.51)$$

where, \mathbf{H}_{xi} & \mathbf{H}_{yi} are expressed as follows with respect to $\{w_p, \theta_{xi}, \theta_{yi}\}$

$$\mathbf{H}_{xi} = \begin{Bmatrix} 0 \\ N_i \\ 0 \end{Bmatrix} + \begin{Bmatrix} \frac{3P_k S_{ki}}{2L_{ki}(1+\phi_{ki})} - \frac{3P_i S_{ij}}{2L_{ij}(1+\phi_{ij})} \\ \frac{3P_k S_{ki} y_{ki}}{4L_{ki}(1+\phi_{ki})} + \frac{3P_i S_{ij} y_{ij}}{4L_{ij}(1+\phi_{ij})} \\ -\frac{3P_k S_{ki} x_{ki}}{4L_{ki}(1+\phi_{ki})} - \frac{3P_i S_{ij} x_{ij}}{4L_{ij}(1+\phi_{ij})} \end{Bmatrix} \quad (1.52.a)$$

$$\mathbf{H}_{y,i} = \begin{Bmatrix} 0 \\ 0 \\ N_i \end{Bmatrix} + \begin{Bmatrix} -\frac{3P_k C_{ki}}{2L_{ki}(1+\phi_{ki})} + \frac{3P_i C_{ij}}{2L_{ij}(1+\phi_{ij})} \\ \frac{3P_k C_{ki} y_{ki}}{4L_{ki}(1+\phi_{ki})} - \frac{3P_i C_{ij} y_{ij}}{4L_{ij}(1+\phi_{ij})} \\ \frac{3P_k C_{ki} x_{ki}}{4L_{ki}(1+\phi_{ki})} + \frac{3P_i C_{ij} x_{ij}}{4L_{ij}(1+\phi_{ij})} \end{Bmatrix} \quad (1.52.b)$$

$$\phi_{ij} = \frac{2}{\kappa(1-\nu)} \left(\frac{t^2}{L_{ij}^2} \right) \quad (\text{for an isotropic material})$$

$$i = 1, 2, \dots, N-1, N \quad j = 2, 3, \dots, N, 1 \quad k = N, 1, \dots, N-2, N-1$$

The relationship between the nodal displacement and the curvature κ is by the matrix \mathbf{B}_{bi} :

$$\kappa = \sum_{i=1}^N \mathbf{B}_{bi} \mathbf{u}_i \quad (1.53)$$

$$\mathbf{B}_{bi} = \begin{bmatrix} -\frac{\partial \mathbf{H}_{yi}^T}{\partial x} \\ \frac{\partial \mathbf{H}_{xi}^T}{\partial y} \\ \frac{\partial \mathbf{H}_{xi}^T}{\partial x} - \frac{\partial \mathbf{H}_{yi}^T}{\partial y} \end{bmatrix} \quad (1.54)$$

The shear deformation γ is calculated using $\bar{\gamma}_{sz}$ obtained from the equation (1.50). The relationship between γ and the nodal displacement is defined by the matrix \mathbf{B}_{si} :

$$\gamma = \sum_{i=1}^N \mathbf{B}_{si} \mathbf{u}_i \quad (1.55)$$

- 3-node element

$$\mathbf{B}_{si} = \begin{bmatrix} \left(\frac{S_{jk}}{A_j} N_j - \frac{S_{ki}}{A_i} N_i\right) \frac{\phi_{ij}}{L_{ij}(1+\phi_{ij})} & \left(\frac{S_{ij}}{A_i} N_i - \frac{S_{jk}}{A_k} N_k\right) \frac{\phi_{ki}}{L_{ki}(1+\phi_{ki})} \\ \left(\frac{C_{ki}}{A_i} N_i - \frac{S_{jk}}{A_j} N_j\right) \frac{\phi_{ij}}{L_{ij}(1+\phi_{ij})} & \left(\frac{S}{A_k} N_k - \frac{S}{A_i} N_i\right) \frac{\phi_{ki}}{L_{ki}(1+\phi_{ki})} \end{bmatrix} \begin{bmatrix} 1 & \frac{-y_{ij}}{2} & \frac{x_{ij}}{2} \\ -1 & \frac{-y_{ki}}{2} & \frac{x_{ki}}{2} \end{bmatrix}$$

$$i=1,2,3 \quad j=2,3,1 \quad k=3,1,2, \quad A_i = C_{ij}S_{ki} - C_{ki}S_{ij} \quad (1.56)$$

- 4-node element

$$\mathbf{B}_{si} = \begin{bmatrix} \frac{\partial N_i}{\partial \lambda} \frac{\partial \lambda}{\partial x} \frac{\phi_{ij}}{(1+\phi_{ij})} & \frac{\partial N_k}{\partial \lambda} \frac{\partial \lambda}{\partial x} \frac{\phi_{ki}}{(1+\phi_{ki})} \\ \frac{\partial N_i}{\partial \lambda} \frac{\partial \lambda}{\partial y} \frac{\phi_{ij}}{(1+\phi_{ij})} & \frac{\partial N_k}{\partial \lambda} \frac{\partial \lambda}{\partial y} \frac{\phi_{ki}}{(1+\phi_{ki})} \end{bmatrix} \begin{bmatrix} 1 & \frac{-y_{ij}}{2} & \frac{x_{ij}}{2} \\ -1 & \frac{-y_{ki}}{2} & \frac{x_{ki}}{2} \end{bmatrix} \quad (1.57)$$

$$i=1,2,3,4 \quad j=2,3,4,1 \quad k=4,1,2,3$$

$$\frac{\partial N_i}{\partial \lambda} \frac{\partial \lambda}{\partial x} = \begin{cases} \frac{\partial N_i}{\partial \xi} \frac{\partial \xi}{\partial x} & i=1,3 \\ \frac{\partial N_i}{\partial \eta} \frac{\partial \eta}{\partial x} & i=2,4 \end{cases}, \quad \frac{\partial N_i}{\partial \lambda} \frac{\partial \lambda}{\partial y} = \begin{cases} \frac{\partial N_i}{\partial \xi} \frac{\partial \xi}{\partial y} & i=1,3 \\ \frac{\partial N_i}{\partial \eta} \frac{\partial \eta}{\partial y} & i=2,4 \end{cases} \quad (1.58)$$

Therefore, the element stiffness matrix for bending and shear deformations is defined as follows:

$$\mathbf{K}_{ij}^{(o)} = \int_{A_e} (\mathbf{B}_{bi}^T \mathbf{D} \mathbf{B}_{bj} \frac{t^3}{12} + \mathbf{B}_{si}^T \mathbf{D} \mathbf{B}_{sj} t) dA \quad (1.59)$$

DKT (3-node) and DKQ (4-node) elements ignore shear deformations. For these two elements the discretization as proposed by Kirchhoff-Love is assumed. The element has only three DOF at each node, i.e., the translational displacement in the ECS z-direction, w and the rotational displacements around the ECS x and y-axes, θ_x and θ_y . Within an element the coordinates x and y are defined by the equation (1.38), whereas the rotations θ_x and θ_y are defined using quadratic functions:

$$\theta_x = \sum_{i=1}^N N_i \theta_{xi} + \sum_{i=1}^N N_{i+N} \Delta \theta_{xi}, \quad \theta_y = \sum_{i=1}^N N_i \theta_{yi} + \sum_{i=1}^N N_{i+N} \Delta \theta_{yi} \quad (1.60)$$

- 3-node element

$$N_1 = (1 - \xi - \eta)(1 - 2\xi - 2\eta), \quad N_2 = \xi(2\xi - 1), \quad N_3 = \eta(2\eta - 1)$$

$$N_4 = 4\xi(1 - \xi - \eta), \quad N_5 = 4\xi\eta, \quad N_6 = 4\eta(1 - \xi - \eta) \quad (1.61)$$

- 4-node element

$$N_1 = \frac{1}{4}(1 - \xi)(1 - \eta) - \frac{1}{2}N_5 - \frac{1}{2}N_8, \quad N_2 = \frac{1}{4}(1 + \xi)(1 - \eta) - \frac{1}{2}N_5 - \frac{1}{2}N_6$$

$$N_3 = \frac{1}{4}(1 + \xi)(1 + \eta) - \frac{1}{2}N_6 - \frac{1}{2}N_7, \quad N_4 = \frac{1}{4}(1 - \xi)(1 + \eta) - \frac{1}{2}N_7 - \frac{1}{2}N_8$$

$$N_5 = \frac{1}{2}(1 - \xi^2)(1 - \eta), \quad N_6 = \frac{1}{2}(1 + \xi)(1 - \eta^2)$$

$$N_7 = \frac{1}{2}(1 - \xi^2)(1 + \eta), \quad N_8 = \frac{1}{2}(1 - \xi)(1 - \eta^2) \quad (1.62)$$

With respect to the virtual rotational angles $\Delta\theta_{xi}$ and $\Delta\theta_{yi}$ at the mid-edge point we make following assumptions:

- To each node and mid-edge point the conditions of the Kirchhoff-Love theory are applied.

$$\text{Node: } -\theta_x + \frac{\partial w}{\partial y} = 0, \quad \theta_y + \frac{\partial w}{\partial x} = 0, \quad \text{Mid-edge point: } -\theta_n + \frac{\partial w}{\partial s} = 0 \quad (1.63)$$

- The out of plane deflection w is a cubic function along the element edge, and the rotation θ around the edge is linear along the element edge.

$$\frac{\partial w(L_{ij}/2)}{\partial s} = -\frac{3}{2L_{ij}}w_i - \frac{1}{4}\frac{\partial w(0)}{\partial s} + \frac{3}{2L_{ij}}w_j + \frac{1}{4}\frac{\partial w(L_{ij})}{\partial s} \quad (1.64)$$

$$\Delta\theta_{si} = \frac{1}{2}(\theta_{si} + \theta_{sj}), \quad i = 1, 2, \dots, N-1, N \quad j = 2, 3, \dots, N, 1 \quad (1.65)$$

By substituting $\Delta\theta_{xi}$ and $\Delta\theta_{yi}$ obtained from the above assumptions into the equation (1.60), θ_x and θ_y can be expressed in terms of \mathbf{u}_i :

$$\theta_x = \sum_{i=1}^N \mathbf{H}_{xi}^T \mathbf{u}_i, \quad \theta_y = \sum_{i=1}^N \mathbf{H}_{yi}^T \mathbf{u}_i \quad (1.66)$$

where, \mathbf{H}_{xi} and \mathbf{H}_{yi} are:

$$\mathbf{H}_x = \begin{Bmatrix} -\frac{3}{2}(d_{ij}N_{i+N} - d_{ki}N_{k+N}) \\ N_i - e_{ij}N_{i+N} - e_{ki}N_{k+N} \\ b_{ij}N_{i+N} + b_{ki}N_{k+N} \end{Bmatrix}, \quad \mathbf{H}_{yi} = \begin{Bmatrix} \frac{3}{2}(a_{ij}N_{i+N} - a_{ki}N_{k+N}) \\ b_{ij}N_{i+N} + b_{ki}N_{k+N} \\ N_i - c_{ij}N_{i+N} - c_{ki}N_{k+N} \end{Bmatrix} \quad (1.67)$$

$$i = 1, 2, \dots, N-1, N \quad j = 2, 3, \dots, N, 1 \quad k = N, 1, \dots, N-2, N-1$$

a_{ij} , b_{ij} , c_{ij} , d_{ij} , and e_{ij} are determined by the geometric configuration of the element, which are defined as follows:

$$a_{ij} = -x_{ij}/L_{ij}^2, \quad b_{ij} = \frac{3}{4}x_{ij}y_{ij}/L_{ij}^2, \quad c_{ij} = (\frac{1}{4}x_{ij}^2 - \frac{1}{2}y_{ij}^2)/L_{ij}^2$$

$$d_{ij} = -y_{ij}^2/L_{ij}^2, \quad e_{ij} = (\frac{1}{4}y_{ij}^2 - \frac{1}{2}x_{ij}^2)/L_{ij}^2 \quad (1.68)$$

The relationship between the nodal displacement and the curvature κ is defined by the equation (1.53), and \mathbf{B}_{bi} is defined by the equation (1.54). Since DKT and DKQ elements ignore shear deformations, the element stiffness related to the bending and shearing deformation are defined as follows:

$$\mathbf{K}_j^{(0)} = \int_{A_e} \mathbf{B}_{bi}^T \mathbf{D} \mathbf{B}_{bj} \frac{t^3}{12} dA \quad (1.69)$$

It is possible to define a four-node discrete shell element for which not all the nodes are located on a flat plane. When the above formulation is applied to such an element, the geometric configuration of the element cannot be represented.

In order to resolve this problem, the stiffness correction method proposed by MacNeal⁵ is used. As illustrated in Fig. 1-(17), the stiffness matrix \mathbf{K}_p calculated on the $A-B-C-D$ plane is transformed into the stiffness \mathbf{K} on the actual plane 1-2-3-4, using the transformation matrix \mathbf{S} .

$$\mathbf{K} = \mathbf{S}^T \mathbf{K}_p \mathbf{S} \quad (1.70)$$

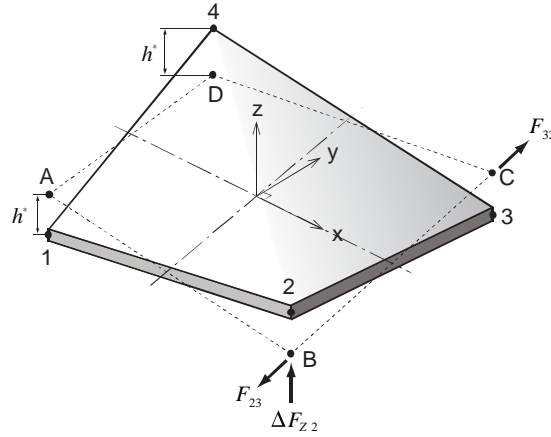


Figure 1-(17) Warped Geometry of 4 Node Flat Shell Element

The transformation matrix \mathbf{S} is used to transform the forces \mathbf{F}_p at nodes ($A-B-C-D$) to the forces \mathbf{F} at nodes (1-2-3-4).

$$\mathbf{F} = \mathbf{S}^T \mathbf{F}_p \quad (1.71)$$

$$\mathbf{F}_p = \{\mathbf{F}_{p1}^T, \mathbf{F}_{p2}^T, \mathbf{F}_{p3}^T, \mathbf{F}_{p4}^T\}^T \quad (1.72)$$

5 R.H. MacNeal, Finite Elements : Their Design and Performance, Marcel Dekker Inc., New York, 1994

$$\mathbf{F}_{Pi} = \{F_x, F_y, F_z, M_x, M_y, M_z\}_{Pi}^T \quad (1.73)$$

The components considered in the calculation of the force transformation matrix are the forces and moments in the out-of-plane directions resulting from the angles formed by the edges of the element ($A - B - C - D$) to the plane ($1 - 2 - 3 - 4$).

$$-\Delta F_{z3} = \Delta F_{z2} = h^* \left(\frac{F_{32}}{L_{23}} - \frac{F_{23}}{L_{23}} \right) \quad (1.74)$$

$$-\Delta M_{z3} = \Delta M_{z2} = h^* \left(\frac{M_{32}}{L_{23}} - \frac{M_{23}}{L_{23}} \right) \quad (1.75)$$

The out-of-plane moment ΔM_{zi} is not directly used in the transformation matrix \mathbf{S}_i .

(2) Curved Shell

The formulation of a Curved Shell Element is based on the “solid shell approach” and therefore no distinction needs to be made between in-plane and out-of-plane stiffness contributions as is the case for discrete shell elements.

Three vectors \mathbf{V}_i defined at each node are shown in Fig. 1-(18). \mathbf{V}_3 is the vector normal to the curved shell surface. \mathbf{V}_1 can be calculated by projecting the element's local x-axis onto the curved surface of the shell. Because the three vectors constitute a right-hand coordinate system \mathbf{V}_2 can be obtained from \mathbf{V}_1 and \mathbf{V}_3 .

$$\mathbf{V}_{1i} = \{l_{1i}, m_{1i}, n_{1i}\}^T, \quad \mathbf{V}_{2i} = \{l_{2i}, m_{2i}, n_{2i}\}^T, \quad \mathbf{V}_{3i} = \{l_{3i}, m_{3i}, n_{3i}\}^T \quad (1.76)$$

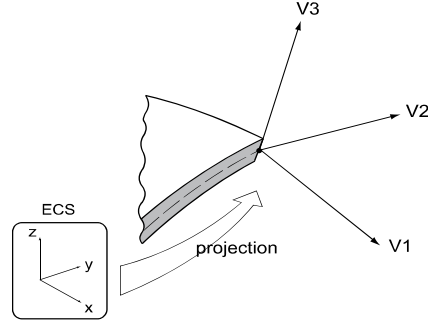


Figure 1-(18) Nodal Coordinate System obtained by projecting ECS

The curved shell element has three translational displacements u , v and w referring to the ECS and two rotations θ_1 and θ_2 around the vectors \mathbf{V}_{1i} and \mathbf{V}_{2i} .

$$\mathbf{u}_i = \{u_i \quad v_i \quad w_i \quad \theta_{1i} \quad \theta_{2i}\}^T \quad (1.77)$$

In an element with N nodes the coordinates x , y and z and displacements u , v and w can be expressed as follows:

$$x = \sum_{i=1}^N N_i(x_i + \zeta \frac{t_i}{2} l_{3i}), \quad y = \sum_{i=1}^N N_i(y_i + \zeta \frac{t_i}{2} m_{3i}), \quad z = \sum_{i=1}^N N_i(z_i + \zeta \frac{t_i}{2} n_{3i}) \quad (1.78)$$

$$\begin{aligned} u &= \sum_{i=1}^N N_i \{u_i + \zeta \frac{t_i}{2} (\mu_{11i} \theta_{1i} + \mu_{12i} \theta_{2i})\} \\ v &= \sum_{i=1}^N N_i \{v_i + \zeta \frac{t_i}{2} (\mu_{21i} \theta_{1i} + \mu_{22i} \theta_{2i})\} \\ w &= \sum_{i=1}^N N_i \{w_i + \zeta \frac{t_i}{2} (\mu_{31i} \theta_{1i} + \mu_{32i} \theta_{2i})\} \end{aligned} \quad (1.79)$$

where t_i is the nodal thickness and $\boldsymbol{\mu}_i$ is the rotation matrix projecting the rotations around the \mathbf{V}_i direction to the ECS.

- 6-node element

$$N_1 = (1 - \xi - \eta)(1 - 2\xi - 2\eta), \quad N_2 = \xi(2\xi - 1), \quad N_3 = \eta(2\eta - 1)$$

$$N_4 = 4\xi(1 - \xi - \eta), \quad N_5 = 4\xi\eta, \quad N_6 = 4\eta(1 - \xi - \eta) \quad (1.80)$$

- 8-node element

$$N_1 = \frac{1}{4}(1 - \xi)(1 - \eta) - \frac{1}{2}N_5 - \frac{1}{2}N_8, \quad N_2 = \frac{1}{4}(1 + \xi)(1 - \eta) - \frac{1}{2}N_5 - \frac{1}{2}N_6$$

$$N_3 = \frac{1}{4}(1 + \xi)(1 + \eta) - \frac{1}{2}N_6 - \frac{1}{2}N_7, \quad N_4 = \frac{1}{4}(1 - \xi)(1 + \eta) - \frac{1}{2}N_7 - \frac{1}{2}N_8$$

$$N_5 = \frac{1}{2}(1 - \xi^2)(1 - \eta), \quad N_6 = \frac{1}{2}(1 + \xi)(1 - \eta^2)$$

$$N_7 = \frac{1}{2}(1 - \xi^2)(1 + \eta), \quad N_8 = \frac{1}{2}(1 - \xi)(1 - \eta^2) \quad (1.81)$$

The matrix \mathbf{B}_i defines the relation between nodal displacements and the strain $\boldsymbol{\varepsilon}_G$,

$$\boldsymbol{\varepsilon}_G = \sum_{i=1}^N \mathbf{B}_i \mathbf{u}_i \quad (1.82)$$

where, the strain $\boldsymbol{\varepsilon}_G$ includes all the components of 3-dimensional strain tensor.

$$\boldsymbol{\varepsilon}_G = \{\varepsilon_{xx}, \varepsilon_{yy}, \varepsilon_{zz}, \gamma_{xy}, \gamma_{yz}, \gamma_{zx}\}^T \quad (1.83)$$

The matrix \mathbf{B}_i is defined as:

$$\mathbf{B}_i = \mathbf{H} \begin{bmatrix} \mathbf{J}^{-1} & \mathbf{0} & \mathbf{0} \\ \mathbf{0} & \mathbf{J}^{-1} & \mathbf{0} \\ \mathbf{0} & \mathbf{0} & \mathbf{J}^{-1} \end{bmatrix} \begin{bmatrix} \frac{\partial N_i}{\partial \xi} & 0 & 0 & -\zeta \frac{t_i}{2} \frac{\partial N_i}{\partial \xi} l_{2,i} & \zeta \frac{t_i}{2} \frac{\partial N_i}{\partial \xi} l_{1,i} \\ \frac{\partial N_i}{\partial \eta} & 0 & 0 & -\zeta \frac{t_i}{2} \frac{\partial N_i}{\partial \eta} l_{2,i} & \zeta \frac{t_i}{2} \frac{\partial N_i}{\partial \eta} l_{1,i} \\ 0 & 0 & 0 & -\frac{t_i}{2} N_i l_{2,i} & \frac{t_i}{2} N_i l_{1,i} \\ 0 & \frac{\partial N_i}{\partial \xi} & 0 & -\zeta \frac{t_i}{2} \frac{\partial N_i}{\partial \xi} m_{2,i} & \zeta \frac{t_i}{2} \frac{\partial N_i}{\partial \xi} m_{1,i} \\ \vdots & \vdots & \vdots & \vdots & \vdots \\ 0 & 0 & 0 & -\frac{t_i}{2} N_i n_{2,i} & \frac{t_i}{2} N_i n_{1,i} \end{bmatrix} \quad (1.84)$$

where \mathbf{H} is the Boolean matrix and \mathbf{J} is the Jacobian matrix.

The strain $\boldsymbol{\varepsilon}_G$ is defined in the ECS which is constant for all points in the element. In order to transfer the strain $\boldsymbol{\varepsilon}_G$ onto the curved surface it must be transformed using the local transformation matrix \mathbf{T} . In a curved shell element every point in the shell element will have its own \mathbf{T} . By using the transformation matrix \mathbf{T} the stiffness matrix can be defined as follows:

$$\mathbf{K}_{ij} = \int_{V_e} \mathbf{B}_i^T \mathbf{T}^T \mathbf{D} \mathbf{T} \mathbf{B}_j dV \quad (1.85)$$

If the drilling d.o.f. is activated, the formulation of the virtual rotational stiffness as proposed by Zienkiewicz and Taylor⁶ is applied.

6 O.C. Zienkiewicz and R.L. Taylor, The Finite Element Method Vol. 2, McGraw-Hill Book Co., London, 1991

1-4-3 Loads and Masses

Loads that can be applied to a shell element are the body force, the pressure load, the edge load, the thermal load, etc. The body force represents the self weight or inertia force of an element, and the pressure load is a distributed load, which acts on the surface of an element. The edge load is a distributed load, which acts along the edges of an element. Both nodal temperature and element temperature loads cause in-plane thermal deformation. Temperature gradient load causes bending of the shell element.

- Body force

$$\mathbf{F}_i = \int_{A_e} t N_i \begin{Bmatrix} \omega_x \\ \omega_y \\ \omega_z \end{Bmatrix} dA \quad (1.87)$$

where ω_x , ω_y , ω_z are the weight density vector components.

- Pressure load

$$\mathbf{F}_i = \int_{A_e} N_i \begin{Bmatrix} P_x \\ P_y \\ P_z \end{Bmatrix} dA \quad (1.88)$$

where P_x , P_y , P_z are the surface pressure load vector components.

- Edge load

$$\mathbf{F}_i = \int_L N_i \begin{Bmatrix} P_x \\ P_y \\ P_z \end{Bmatrix} ds \quad (1.89)$$

where P_x , P_y , P_z are the edge pressure load vector components.

- Temperature load

$$\mathbf{F}_i = \int_{A_e} t \mathbf{B}_i^T \mathbf{D} \begin{Bmatrix} \alpha_x \\ \alpha_y \\ 0 \end{Bmatrix} \Delta T dA \quad (1.90)$$

where α_x, α_y are the linear thermal expansion coefficients in x & y directions, \mathbf{B}_i is the matrix of in-plane deformation and ΔT is the temperature change.

- Temperature gradient load

$$\mathbf{F}_i = \int_{A_e} \frac{t^3}{12} \mathbf{B}_{bi}^T \mathbf{D} \begin{Bmatrix} \alpha_x \\ \alpha_y \\ 0 \end{Bmatrix} \frac{\Delta T_z}{2H_z} dA \quad (1.91)$$

Where $\Delta T_z / H_z$ is temperature gradient over the thickness of the shell element..

The mass of a shell element can be represented by lumped mass or consistent mass and reflects translational displacements in the x, y and z directions only.

- Consistent mass

$$\mathbf{M}_{ij} = \rho t \int_{A_e} N_i N_j dA \quad (1.92)$$

where N_i is the interpolation function identical to that of a plane stress element

- Lumped mass

The total mass ($\rho t A_e$) of the element is distributed to the diagonal terms only. The distribution is done in proportion to the diagonal terms of the consistent mass matrix. The lumped mass matrix is a diagonal matrix.

1-4-4 Shell Thickness / Material / Offset

For a discrete shell element, the thickness of the element can be defined at each node as illustrated in Fig. 1-(19), whereas the thickness of a curved shell element can only be defined at the vertices

of the surface in which the elements are located. Different shell thickness can be specified for in-plane deformation, bending and shear deformation. With the in-plane thickness t , the following values can be defined.

- $12I/t^3$
being the bending stiffness ratio of the actual bending stiffness I and the bending stiffness calculated by the in-plane thickness (default=1.0)
- t_s/t
being the ratio of the actual shear deformation thickness t_s and the in-plane thickness t (default=0.83333)

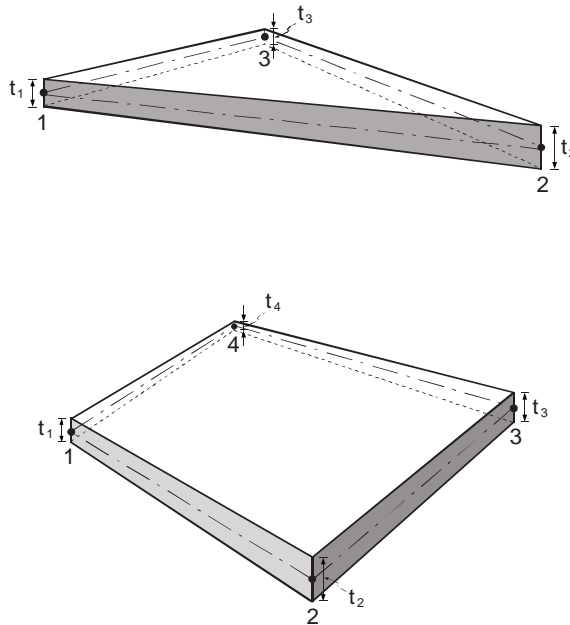


Figure 1-(19) Definition of Nodal Thickness in Shell Element

Material properties of a shell element can be entered for each type of deformation. The mass matrix can be calculated using the thickness and material property corresponding to the in-plane behavior. For an anisotropic material, the MCS (material coordinate system) can be defined such that an axis can be defined in an arbitrary direction. In the case that the MCS is not parallel with the curved surface of a shell element, the MCS x-axis is projected onto the shell element as shown in Fig. 1-(20).

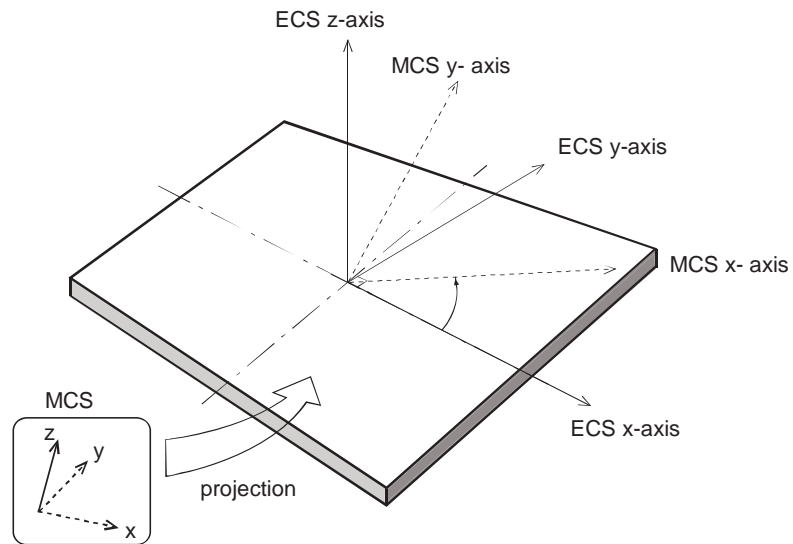


Figure 1-(20) Material Coordinate System and axis projection onto Shell Element

As illustrated in Fig. 1-(21), for shell elements offset distances in nodes can be assigned. The offset represents the distance from the node (reference plane) to the actual location of the element, projected to the ECS z-direction.

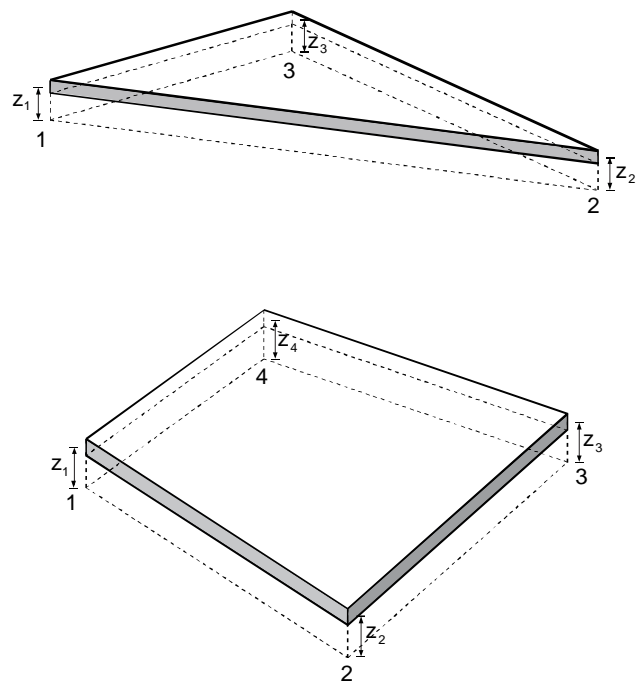


Figure 1-(21) Definition of Offset in Shell Element

1-4-5 Element Output

Analysis results for shell elements are element (internal) forces and stresses/strains at the nodes with reference to the ECS. The analysis results produced in the ECS can be transferred into the GCS or Output Coordinate System. Stresses and strains are calculated at the top end ($z = t/2$) and bottom end ($z = -t/2$) surfaces of the shell element.

The internal forces and stresses/strains calculated for shell elements are listed below.

- Stress components $\sigma_{xx}, \sigma_{yy}, \tau_{xy}$
 - Von-Mises stress $\sqrt{(P_1^2 + P_2^2 - P_1 P_2)}$
 - Maximum shear stress $\sqrt{\left(\frac{\sigma_{xx} - \sigma_{yy}}{2}\right)^2 + \tau_{xy}^2}$
 - Principal stresses P_1, P_2
- $$P_i = \frac{\sigma_{xx} + \sigma_{yy}}{2} \pm \sqrt{\left(\frac{\sigma_{xx} - \sigma_{yy}}{2}\right)^2 + \tau_{xy}^2}$$
- Strain components $\varepsilon_{xx}, \varepsilon_{yy}, \gamma_{xy}$
 - Von-Mises strain $\frac{2}{3} \sqrt{(E_1^2 + E_2^2 - E_1 E_2)}$
 - Volumetric strain $E_1 + E_2$
 - Principal strains E_1, E_2

$$E_i = \frac{\varepsilon_{xx} + \varepsilon_{yy}}{2} \pm \sqrt{\left(\frac{\varepsilon_{xx} - \varepsilon_{yy}}{2}\right)^2 + \frac{\gamma_{xy}^2}{4}}$$

- Membrane forces N_{xx}, N_{yy}, N_{xy}
- Bending moments M_{xx}, M_{yy}, M_{xy}
- Shear forces Q_{yz}, Q_{zx}

The nodal internal forces and stresses/strains are calculated by extrapolation from the results calculated at the integration points (Gauss Points). The integration schemes for shell elements are as follows:

- 3-node triangular element: 3-point Gauss integration in plane and 1 layer of integration points over thickness
- 4-node quadrilateral element: 4-point Gauss integration in plane and 1 layer of integration points over thickness
- 6-node triangular element: 3-point Gauss integration in plane and 2 layers of integration points over thickness
- 8-node quadrilateral element: 4-point Gauss integration in plane and 2 layers of integration points over thickness

The sign convention for stresses and strains is identical to that for a plane stress element. The directions of bending moments and shear forces are shown in Fig. 1-(14). Fig. 1-(22) shows the sign convention for in-plane components among the element forces. The arrows represent the positive (+) directions.

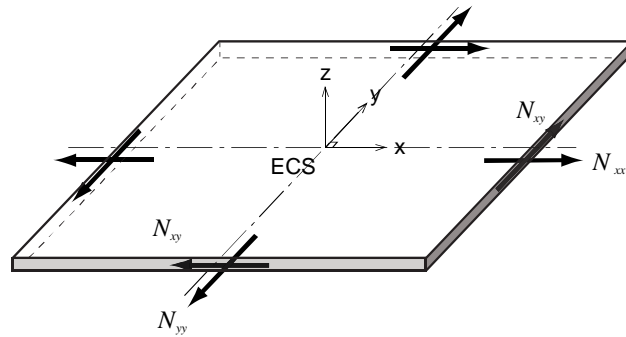


Figure 1-(22) Output Convention for Shell Element

1-5 Plane Stress Element

1-5-1 Overview

There are triangular and quadrilateral plane stress elements with three, four, six or eight nodes. The element is generally used for membranes which have a uniform thickness. It is assumed that no stress components exist in the out-of-plane direction and that the strains in the out-of-plane direction can be obtained on the basis of the Poisson's effects. The plane stress elements can only account for in-plane deformations and may be used for both static (linear & nonlinear) and dynamic analyses. The stress and strain tensors in a plane stress element have 3 components respectively:

$$\boldsymbol{\sigma} = \begin{Bmatrix} \sigma_{xx} \\ \sigma_{yy} \\ \tau_{xy} \end{Bmatrix}, \quad \boldsymbol{\epsilon} = \begin{Bmatrix} \epsilon_{xx} \\ \epsilon_{yy} \\ \gamma_{xy} \end{Bmatrix} \quad (\text{In-plane stress \& strain})$$

Fig. 1-(23) shows the sign convention for stresses and strains, and the arrows represent the positive (+) directions.

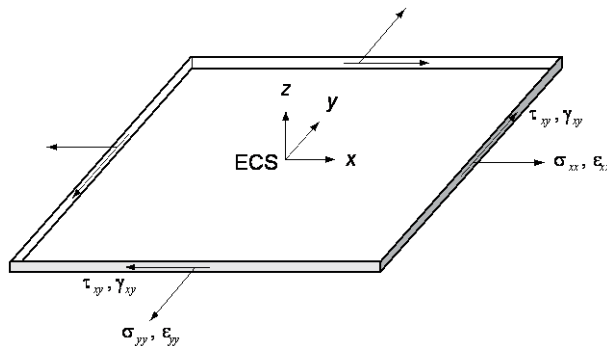
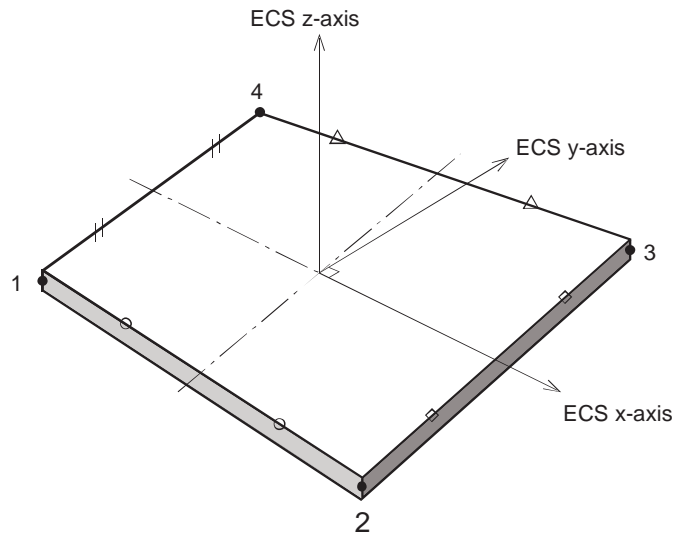
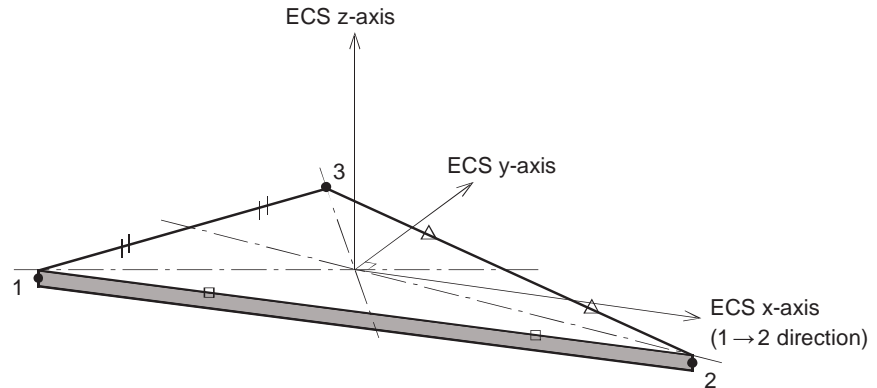


Figure 1-(23) Stress Sign Convention for Plane Stress Element

The ECS is a Cartesian coordinate system. The directions of the ECS axes are defined in Fig. 1-(24). For a triangular element, the line parallel to the direction from N1 to N2 becomes the ECS x-axis. For a quadrilateral element, the line connecting the mid point of N1 and N4 to the mid point of N2 and N3 defines the direction of ECS x-axis.



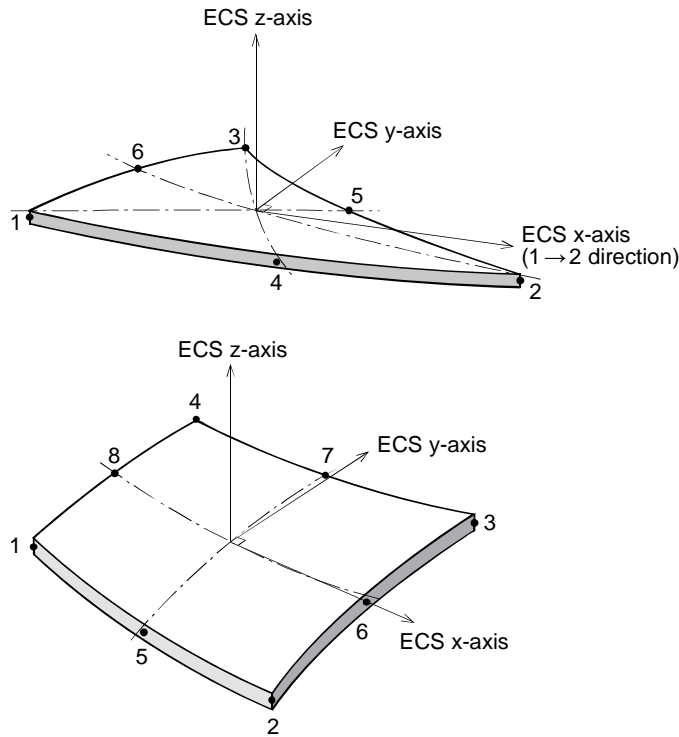


Figure 1-(24) Element Coordinate System for Plane Stress Element

Plane stress elements can have a “Linear Interpolation” or a “Quadratic Interpolation”, depending on the number of nodes. Three-node triangular and four-node quadrilateral plane stress elements are referred to as “Linear Elements”. Six-node triangular and eight-node quadrilateral plane stress elements are referred to as “Quadratic Elements”. Four-node quadrilateral linear elements generally lead to accurate results for the computation of both displacements and stresses, whereas three-node triangular linear elements may give poor stress results and good displacement results. Therefore, it is advised to avoid three-node triangular linear elements in the regions where detailed analysis results are required.

1-5-2 Finite Element Formulation

It is assumed that a plane stress element has a uniform thickness. The plane stress element is an Isoparametric element, and for the four node quadrilateral the Incompatible Mode theory is applied. Each node of the element has two translational displacements u and v in the ECS.

$$\mathbf{u}_i = \{u_i \quad v_i\}^T \quad (1.93)$$

The calculation of the stiffness is identical to all plane stress elements, except for the four node quadrilateral element. Therefore, an explanation on N-node elements will be provided representing all other cases.

In an element the coordinates x and y and translational displacements u and v can be expressed as,

$$x = \sum_{i=1}^N N_i x_i, \quad y = \sum_{i=1}^N N_i y_i, \quad u = \sum_{i=1}^N N_i u_i, \quad v = \sum_{i=1}^N N_i v_i \quad (1.94)$$

- 3 node triangular element

$$N_1 = 1 - \xi - \eta, \quad N_2 = \xi, \quad N_3 = \eta \quad (1.95)$$

- 4 node quadrilateral element

$$N_1 = \frac{1}{4}(1 - \xi)(1 - \eta), \quad N_2 = \frac{1}{4}(1 + \xi)(1 - \eta)$$

$$N_3 = \frac{1}{4}(1 + \xi)(1 + \eta), \quad N_4 = \frac{1}{4}(1 - \xi)(1 + \eta) \quad (1.96)$$

- 6 node triangular element

$$N_1 = (1 - \xi - \eta)(1 - 2\xi - 2\eta), \quad N_2 = \xi(2\xi - 1), \quad N_3 = \eta(2\eta - 1)$$

$$N_4 = 4\xi(1 - \xi - \eta), \quad N_5 = 4\xi\eta, \quad N_6 = 4\eta(1 - \xi - \eta) \quad (1.97)$$

- 8 node quadrilateral element

$$\begin{aligned}
 N_1 &= \frac{1}{4}(1-\xi)(1-\eta) - \frac{1}{2}N_5 - \frac{1}{2}N_8, & N_2 &= \frac{1}{4}(1+\xi)(1-\eta) - \frac{1}{2}N_5 - \frac{1}{2}N_6 \\
 N_3 &= \frac{1}{4}(1+\xi)(1+\eta) - \frac{1}{2}N_6 - \frac{1}{2}N_7, & N_4 &= \frac{1}{4}(1-\xi)(1+\eta) - \frac{1}{2}N_7 - \frac{1}{2}N_8 \\
 N_5 &= \frac{1}{2}(1-\xi^2)(1-\eta), & N_6 &= \frac{1}{2}(1+\xi)(1-\eta^2), & N_7 &= \frac{1}{2}(1-\xi^2)(1+\eta) \\
 N_8 &= \frac{1}{2}(1-\xi)(1-\eta^2)
 \end{aligned} \tag{1.98}$$

The matrix \mathbf{B}_i defines the relation between the nodal displacement \mathbf{u} and the strain $\boldsymbol{\varepsilon}$:

$$\boldsymbol{\varepsilon} = \sum_{i=1}^N \mathbf{B}_i \mathbf{u}_i \tag{1.99}$$

The matrix \mathbf{B}_i can be presented by the differential of the shape function:

$$\mathbf{B}_i = \begin{bmatrix} \frac{\partial N_i}{\partial x} & 0 \\ 0 & \frac{\partial N_i}{\partial y} \\ \frac{\partial N_i}{\partial y} & \frac{\partial N_i}{\partial x} \end{bmatrix} \tag{1.100}$$

Using \mathbf{B}_i , the element stiffness matrix related to in-plane deformation can be arranged as follows:

$$\mathbf{K}_{ij} = t \int_{A_e} \mathbf{B}_i^T \mathbf{D} \mathbf{B}_j dA \tag{1.101}$$

where t is the thickness of the plane stress element and A_e is the element area, and matrix \mathbf{D} represents the stress - strain relation. For an isotropic material the stress – strain relation is expressed as follows:

$$\mathbf{D} = \frac{E}{1-\nu^2} \begin{bmatrix} 1 & \nu & 0 \\ \nu & 1 & 0 \\ 0 & 0 & \frac{1-\nu}{2} \end{bmatrix} \quad (1.102)$$

In linear analysis, a four node quadrilateral element is formulated using incompatible modes. When incompatible modes are used, the element has extra d.o.f. in addition to the nodal displacements.

$$\mathbf{u}_a = \{a_1 \quad b_1 \quad a_2 \quad b_2\}^T \quad (1.103)$$

In that case the coordinates x and y and the translational displacements u and v are:

$$x = \sum_{i=1}^4 N_i x_i, \quad y = \sum_{i=1}^4 N_i y_i, \quad u = \sum_{i=1}^4 N_i u_i + a_1 P_1 + a_2 P_2, \quad v = \sum_{i=1}^4 N_i v_i + b_1 P_1 + b_2 P_2 \quad (1.104)$$

The shape functions representing the incompatible modes are:

$$P_1 = 1 - \xi^2, \quad P_2 = 1 - \eta^2 \quad (1.105)$$

Combining the nodal displacements and the incompatible modes, the strain ϵ is defines as:

$$\epsilon = \sum_{i=1}^4 \mathbf{B}_i \mathbf{u}_i + \mathbf{B}_a \mathbf{u}_a \quad (1.106)$$

The matrix \mathbf{B}_i is presented in the equation (1.106), and the matrix \mathbf{B}_a that relates the incompatible modes to the strain components is defined as:

$$\mathbf{B}_a = \begin{bmatrix} \frac{\partial P_1}{\partial x} & 0 & \frac{\partial P_2}{\partial x} & 0 \\ 0 & \frac{\partial P_1}{\partial y} & 0 & \frac{\partial P_2}{\partial y} \\ \frac{\partial P_1}{\partial y} & \frac{\partial P_1}{\partial x} & \frac{\partial P_2}{\partial y} & \frac{\partial P_2}{\partial x} \end{bmatrix} \quad (1.107)$$

Using the matrices \mathbf{B}_i and \mathbf{B}_a , the element stiffness matrices for in-plane deformation can be

calculated, and four matrices are obtained as follows:

$$\begin{aligned}\mathbf{K}_{ij} &= t \int_{A_e} \mathbf{B}_i^T \mathbf{D} \mathbf{B}_j dA, \quad \mathbf{K}_{ia} = t \int_{A_e} \mathbf{B}_i^T \mathbf{D} \mathbf{B}_a dA \\ \mathbf{K}_{ai} &= t \int_{A_e} \mathbf{B}_a^T \mathbf{D} \mathbf{B}_i dA, \quad \mathbf{K}_{aa} = t \int_{A_e} \mathbf{B}_a^T \mathbf{D} \mathbf{B}_a dA\end{aligned}\quad (1.108)$$

The four stiffness matrices presented in the equation (1.108) have the following relation:

$$\begin{bmatrix} \mathbf{K}_{ij} & \mathbf{K}_{ia} \\ \mathbf{K}_{aj} & \mathbf{K}_{aa} \end{bmatrix} \begin{Bmatrix} \mathbf{u}_j \\ \mathbf{u}_a \end{Bmatrix} = \begin{Bmatrix} \mathbf{F}_i \\ \mathbf{0} \end{Bmatrix}\quad (1.109)$$

The stiffness matrix of the incompatible modes is obtained by static condensation:

$$\mathbf{K}_{ij} = \mathbf{K}_{ij} - \mathbf{K}_{ia} \mathbf{K}_{aa}^{-1} \mathbf{K}_{aj}\quad (1.110)$$

Incompatible modes can account for the bending deformation as shown in Fig. 1-(25) and therefore such elements have a better performance for bending deformations than plane stress elements without incompatible modes..

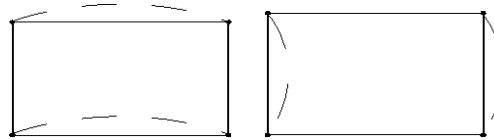


Figure 1-(25) Typical Shapes of Incompatible Mode

1-5-3 Loads and Masses

Loads that can be applied to plane stress elements include are the body force, the pressure load, the edge load, the thermal load, etc. The body force is a load, which represents the self weight or the inertia force of an element. The pressure load is a distributed load, which acts on the surface of an element. The edge load is a distributed load, which acts along the edge of an element. Nodal temperature and element temperature loads cause in-plane thermal deformation.

- Body force

$$\mathbf{F}_i = t \int_{A_e} N_i \begin{Bmatrix} \omega_x \\ \omega_y \\ \omega_z \end{Bmatrix} dA \quad (1.111)$$

where $\omega_x, \omega_y, \omega_z$ are weight density vector components.

- Pressure load

$$\mathbf{F}_i = \int_{A_e} N_i \begin{Bmatrix} P_x \\ P_y \\ 0 \end{Bmatrix} dA \quad (1.112)$$

where P_x, P_y are surface pressure load vector components. Note that the pressure component normal to the elements must be equal to zero for plane stress elements.

- Edge load

$$\mathbf{F}_i = \int_L N_i \begin{Bmatrix} P_x \\ P_y \\ 0 \end{Bmatrix} ds \quad (1.113)$$

where P_x, P_y are edge pressure load vector components. Note that the pressure component normal to the elements must be equal to zero for plane stress elements.

- Temperature load

$$\mathbf{F}_i = t \int_{A_e} \mathbf{B}_i^T \mathbf{D} \begin{Bmatrix} \alpha_x \\ \alpha_y \\ 0 \end{Bmatrix} \Delta T dA \quad (1.114)$$

where α_x, α_y are the linear thermal expansion coefficient in x and y directions

The mass of a plane stress element can be a lumped mass or a consistent mass and reflects translational displacements in the x, y and z directions only.

- Consistent mass

$$\mathbf{M}_{ij} = \rho t \int_{A_e} N_i N_j dA \quad (1.115)$$

- Lumped mass

The total mass ($\rho t A_e$) of the element is distributed to the diagonal terms only in proportion to the diagonal terms of the consistent mass matrix. The lumped mass matrix is a diagonal matrix.

1-5-4 Element Output

Analysis results for plane stress elements include stresses and strains at each node with reference to the ECS. The analysis results calculated in the ECS can be transformed into the GCS or Output Coordinate System. The stresses and strains produced for a plane stress element are as follows:

- Stress components $\sigma_{xx}, \sigma_{yy}, \tau_{xy}$
- Von-Mises stress $\sqrt{(P_1^2 + P_2^2 - P_1 P_2)}$
- Maximum shear stress $\sqrt{\left(\frac{\sigma_{xx} - \sigma_{yy}}{2}\right)^2 + \tau_{xy}^2}$
- Principal stresses P_1, P_2

$$P_i = \frac{\sigma_{xx} + \sigma_{yy}}{2} \pm \sqrt{\left(\frac{\sigma_{xx} - \sigma_{yy}}{2}\right)^2 + \tau_{xy}^2}$$
- Strain components $\varepsilon_{xx}, \varepsilon_{yy}, \gamma_{xy}$
- Von-Mises strain $\frac{2}{3} \sqrt{(E_1^2 + E_2^2 - E_1 E_2)}$
- Volumetric strain $E_1 + E_2$
- Principal strains E_1, E_2 and $E_3 = \varepsilon_{zz}$

$$E_i = \frac{\varepsilon_{xx} + \varepsilon_{yy}}{2} \pm \sqrt{\left(\frac{\varepsilon_{xx} - \varepsilon_{yy}}{2}\right)^2 + \frac{\gamma_{xy}^2}{4}}$$

Stress and strain results in the nodes are extrapolated from the calculated results at integration points (Gauss Points). The integration points for a plane stress element are as follows:

- 3 node triangular element: 1-point Gauss integration
- 4 node quadrilateral element: 4-point Gauss integration
- 6 node triangular element: 3-point Gauss integration
- 8 node quadrilateral element: 9-point Gauss integration

Plane stress elements have only one layer of integration points over the thickness.

Fig. 1-(23) shows the sign convention for stresses and strains.

1-6 Plane Strain Element

1-6-1 Overview

There are triangular and quadrilateral plane strain elements with three, four, six or eight nodes. The plane strain element can be used to model a long structure, having a uniform cross section along its entire length, such as dams and tunnels. No strain is assumed in the thickness direction, and the stress component in the thickness direction can be obtained through the Poisson's effect. The plane strain element is capable of accounting for in-plane stresses only and can be used for both static (linear & nonlinear) and dynamic analyses. The stresses and strains defining the deformation of a plane strain element are expressed as follows:

$$\boldsymbol{\sigma} = \begin{Bmatrix} \sigma_{xx} \\ \sigma_{yy} \\ \tau_{xy} \end{Bmatrix}, \quad \boldsymbol{\epsilon} = \begin{Bmatrix} \epsilon_{xx} \\ \epsilon_{yy} \\ \gamma_{xy} \end{Bmatrix} \quad (\text{In-plane stress \& strain})$$

Fig. 1-(26) shows the sign convention for stresses and strains and the arrows represent the positive (+) directions.

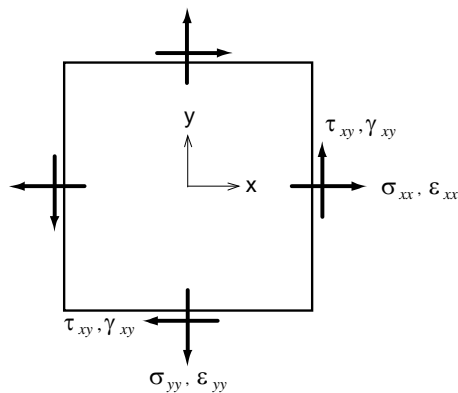
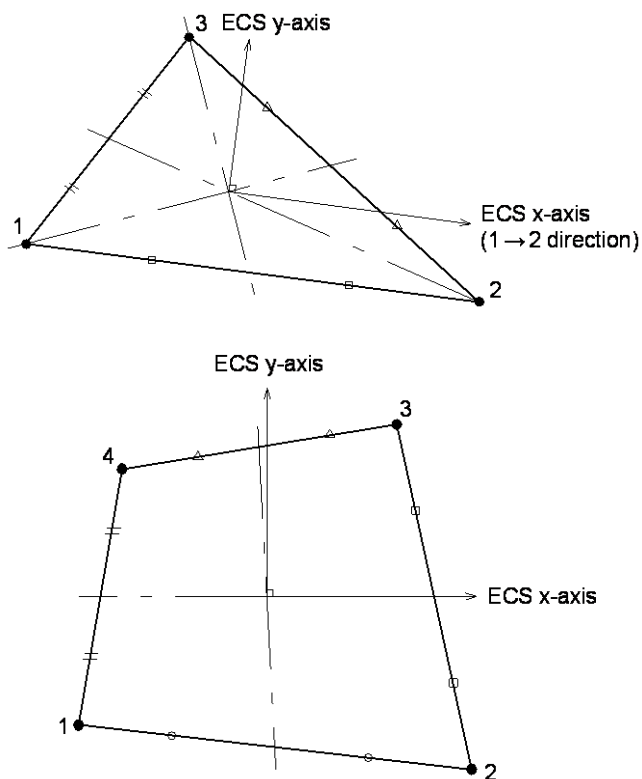


Figure 1-(26) Stress Sign Convention for Plane Strain Element

The directions of the ECS axes are defined in Fig. 1-(27). For a triangular element, the ECS x-axis is parallel to the direction from Node 1 to Node 2. In the case of a quadrilateral element, the line connecting the mid point of Node 1 and Node 4 to the mid point of N2 and N3 is the direction of ECS x-axis.



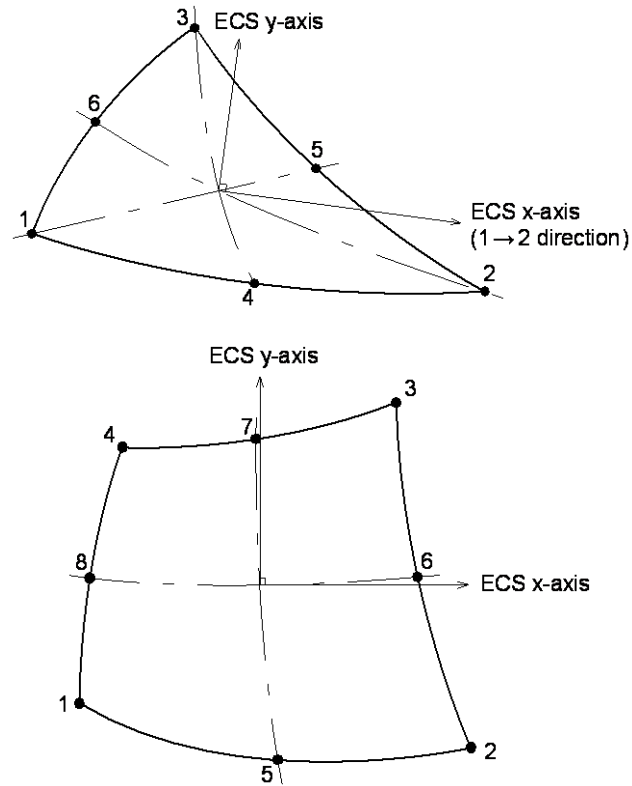


Figure 1-(27) Element Coordinate System for Plane Strain Element

There are plane strain elements with “Linear Interpolation” and with “Quadratic Interpolation”. Three-node triangular and four-node quadrilateral elements are “Linear Elements”. Six-node triangular and eight-node quadrilateral elements are “Quadratic Elements”. Four-node quadrilateral elements generally lead to accurate displacement and stress results, whereas three-node triangular elements tend to produce poor accuracy of stresses while the displacement results are good. Therefore, it is advised not to use three-node triangular elements in the regions where detailed analysis results are required. The plane strain element does not have strain in the out-of-plane direction but it has the stress component σ_{zz} in that direction.

1-6-2 Finite Element Formulation

The plane strain element is formulated according to the Isoparametric Formulation, and the Incompatible Mode theory is used for the four node quadrilateral element. The standard isoparametric plane strain formulation procedure is identical to the formulation for the plane stress element, which is explained in section “1.5 Plane Stress Element”.

For an isotropic material, the stress-strain relationship for the plane strain element is expressed as,

$$\mathbf{D} = \frac{E(1-\nu)}{(1+\nu)(1-2\nu)} \begin{bmatrix} 1 & \frac{\nu}{1-\nu} & 0 \\ \frac{\nu}{1-\nu} & 1 & 0 \\ 0 & 0 & \frac{1-2\nu}{2(1-\nu)} \end{bmatrix} \quad (1.116)$$

The displacement d.o.f.'s are defined in the plane of the element, but an additional stress-component σ_{zz} exists in the direction of the thickness. For an isotropic material, the stress in the thickness direction can be calculated as follows:

$$\sigma_{zz} = \nu(\sigma_{xx} + \sigma_{yy}) \quad (1.117)$$

In midas FEA the user is required to define a thickness for plane strain elements. This parameter is only used to calculate the nodal forces from the typical forces per unit length which are characteristic for plane strain elements. In order to be able to connect e.g. plane strain elements such as beams, forces need to be calculated to check the equilibrium.

1-6-3 Loads and Masses

Loads that can be applied to a plane strain element are the body force, the edge load, the thermal load, etc. The body force is the self weight or the inertia force of an element. The edge load is a distributed load acting along the edge of an element. Nodal temperature and element temperature loads are available for thermal expansion effects. The body force, edge load and thermal load are identical to that for the plane stress element.

The mass of a plane strain element can be represented by lumped mass or consistent mass and comprises translational displacements in the x and y directions only.

- Consistent mass

$$\mathbf{M}_{ij} = \rho t \int_{A_e} N_i N_j dA \quad (1.118)$$

- Lumped mass

The total mass ($\rho t A_e$) of the element is distributed to the diagonal terms only in proportion to the diagonal terms of the consistent mass matrix. The lumped mass matrix is a diagonal matrix.

1-6-4 Element Output

Analysis results for plane strain elements include stresses and strains at each node. Analysis using plane strain elements is carried out in the GCS $X-Y$, $Y-Z$ or $X-Z$ plane, and accordingly, the stress and strain results are produced in the GCS. The analysis results produced in the GCS can be converted into the ECS or to the Output Coordinate System.

When the analysis is carried out in the $X-Y$ plane, the stresses and strains produced for the element are as follows:

- Stress components $\sigma_{xx}, \sigma_{yy}, \sigma_{zz}, \tau_{xy}$
 - Von-Mises stress $\sqrt{(P_1^2 + P_2^2 + P_3^2 - P_1P_2 - P_2P_3 - P_3P_1)}$
 - Mean stress $\frac{P_1 + P_2 + P_3}{3}$
 - Maximum shear stress $\frac{\max(|P_1 - P_2|, |P_2 - P_3|, |P_3 - P_1|)}{2}$
 - Principal stresses P_1, P_2, P_3
- $$P_i = \frac{\sigma_{xx} + \sigma_{yy}}{2} \pm \sqrt{\left(\frac{\sigma_{xx} - \sigma_{yy}}{2}\right)^2 + \tau_{xy}^2} \text{ and } \sigma_{zz} \text{ are denoted as}$$
- P_1, P_2 and P_3 in a descending order.
- Strain components $\varepsilon_{xx}, \varepsilon_{yy}, \gamma_{xy}$
 - Von-Mises strain $\sqrt{(E_1^2 + E_2^2 + E_3^2 - E_1E_2 - E_2E_3 - E_3E_1)}$

- Volumetric strain $E_1 + E_2 + E_3$
- Principal strains E_1, E_2, E_3

$$E_i = \frac{\varepsilon_{xx} + \varepsilon_{yy}}{2} \pm \sqrt{\left(\frac{\varepsilon_{xx} - \varepsilon_{yy}}{2}\right)^2 + \frac{\gamma_{xy}^2}{4}} \quad \text{and } 0 \text{ (zero) are denoted as}$$

E_1, E_2 and E_3 in a descending order.

The integration points for a plane strain element are as follows:

- 3 node triangular element: 1-point Gauss integration
- 4 node quadrilateral element: 4-point Gauss integration
- 6 node triangular element: 3-point Gauss integration
- 8 node quadrilateral element: 9-point Gauss integration

Plane strain elements have only 1 layer of integration points.

Fig. 1-(28) shows the sign convention for stresses and strains, and the arrows represent the positive (+) directions.

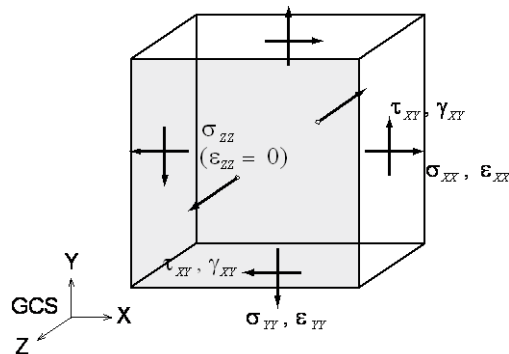


Figure 1-(28) Output Sign Convention for Plane Strain Element

1-7 Axisymmetric Element

1-7-1 Overview

Axisymmetric elements can be used for modeling a structure with an axial symmetry with respect to the geometry, material properties and loading conditions, such as a deep well, a circular foundation, a circular tunnel, etc. The element cannot be used in connection with any other types of elements and can be used for both static (linear/nonlinear) and dynamic analyses. Because this element is formulated on the basis of its axisymmetric properties, it is assumed that circumferential shear strains and circumferential shear stresses do not exist. The stresses and strains of an axisymmetric element are defined as follows:

$$\boldsymbol{\sigma} = \begin{Bmatrix} \sigma_{xx} \\ \sigma_{yy} \\ \sigma_{zz} \\ \tau_{xy} \end{Bmatrix}, \quad \boldsymbol{\varepsilon} = \begin{Bmatrix} \varepsilon_{xx} \\ \varepsilon_{yy} \\ \varepsilon_{zz} \\ \gamma_{xy} \end{Bmatrix} \quad (\text{In-plane sectional stress/strain \& circumferential stress/strain})$$

Fig. 1-(29) shows the sign convention for stresses and strains and the arrows represent the positive (+) directions.

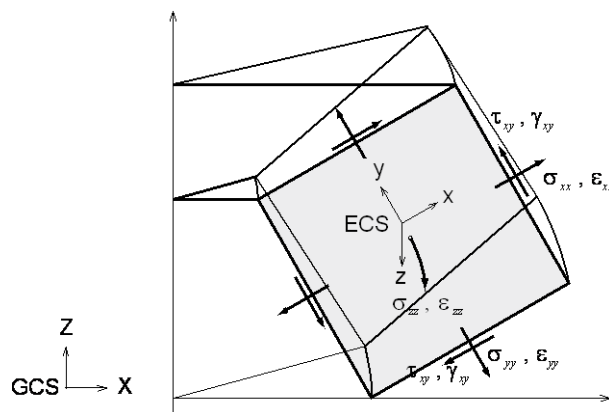
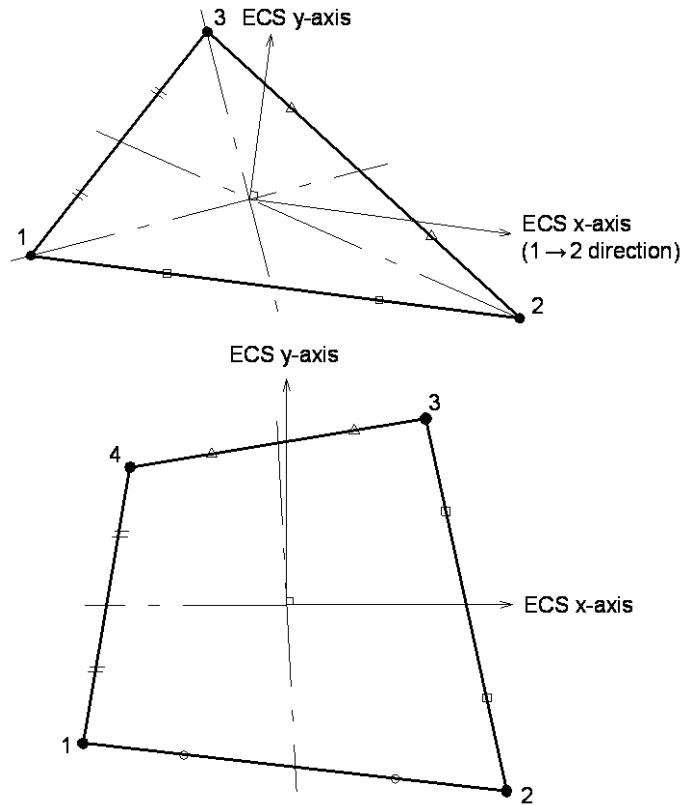


Figure 1-(29) Sign Convention for Axisymmetric Element

The directions of the ECS axes are defined in Fig. 1-(30). For a triangular element, the ECS x-axis is parallel to the direction from Node 1 to Node 2. In the case of a quadrilateral element, ECS x-axis is defined by the line connecting the mid point of Node 1 and Node 4 to the mid point of Node 2 and Node 3.



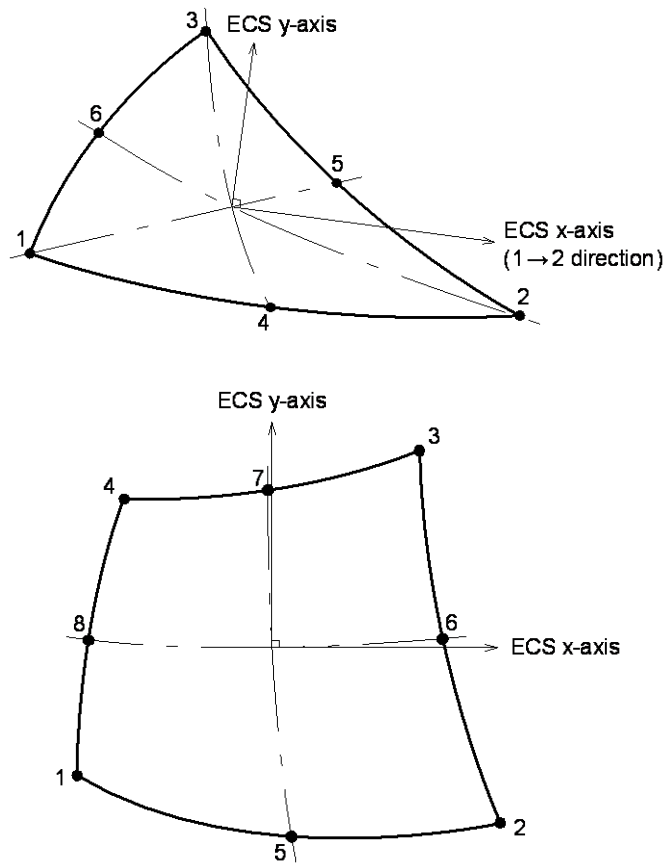


Figure 1-(30) Element Coordinate System for Axisymmetric element

The GCS Z-axis is always the axis of rotation and the elements must be defined in the global X-Z plane. By default, the width of the element is automatically preset to a unit width (1.0radian) as illustrated in Fig. 1-(31).

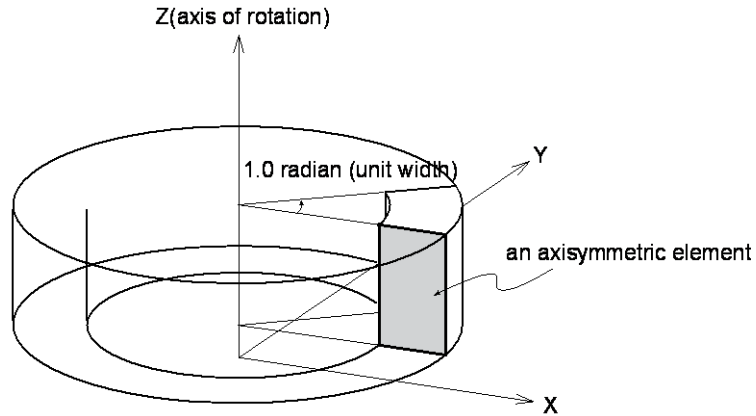


Figure 1-(31) Unit width of an axisymmetric element

There are axisymmetric elements with a “Linear Interpolation” and with a “Quadratic Interpolation”. Three-node triangular and four-node quadrilateral elements are “Linear Elements”. Six-node triangular and eight-node quadrilateral elements are “Quadratic Elements”. Please note that axisymmetric elements have a stress and strain component in the circumferential direction.

1-7-2 Finite Element Formulation

Axisymmetric elements are defined as regular isoparametric elements without incompatible modes. At each node of the element there are two translational displacements u and v in the ECS x and y-directions.

$$\mathbf{u}_i = \{u_i \quad v_i\}^T \quad (1.119)$$

For all axisymmetric elements the stiffness is defined in the same way. Therefore, the generalized number of nodes (N) is assumed in the following formulation of axisymmetric elements.

In the element the coordinates x and y and translational displacements u and v can be expressed as follows:

$$x = \sum_{i=1}^N N_i x_i, \quad y = \sum_{i=1}^N N_i y_i, \quad u = \sum_{i=1}^N N_i u_i, \quad v = \sum_{i=1}^N N_i v_i \quad (1.120)$$

- 3 node triangular element

$$N_1 = 1 - \xi - \eta, \quad N_2 = \xi, \quad N_3 = \eta \quad (1.121)$$

- 4 node quadrilateral element

$$N_1 = \frac{1}{4}(1 - \xi)(1 - \eta), \quad N_2 = \frac{1}{4}(1 + \xi)(1 - \eta),$$

$$N_3 = \frac{1}{4}(1 + \xi)(1 + \eta), \quad N_4 = \frac{1}{4}(1 - \xi)(1 + \eta) \quad (1.122)$$

- 6 node triangular element

$$N_1 = (1 - \xi - \eta)(1 - 2\xi - 2\eta), \quad N_2 = \xi(2\xi - 1), \quad N_3 = \eta(2\eta - 1)$$

$$N_4 = 4\xi(1 - \xi - \eta), \quad N_5 = 4\xi\eta, \quad N_6 = 4\eta(1 - \xi - \eta) \quad (1.123)$$

- 8 node quadrilateral element

$$\begin{aligned}
 N_1 &= \frac{1}{4}(1-\xi)(1-\eta) - \frac{1}{2}N_5 - \frac{1}{2}N_8, \quad N_2 = \frac{1}{4}(1+\xi)(1-\eta) - \frac{1}{2}N_5 - \frac{1}{2}N_6 \\
 N_3 &= \frac{1}{4}(1+\xi)(1+\eta) - \frac{1}{2}N_6 - \frac{1}{2}N_7, \quad N_4 = \frac{1}{4}(1-\xi)(1+\eta) - \frac{1}{2}N_7 - \frac{1}{2}N_8 \\
 N_5 &= \frac{1}{2}(1-\xi^2)(1-\eta), \quad N_6 = \frac{1}{2}(1+\xi)(1-\eta^2), \quad N_7 = \frac{1}{2}(1-\xi^2)(1+\eta) \\
 N_8 &= \frac{1}{2}(1-\xi)(1-\eta^2)
 \end{aligned} \tag{1.124}$$

The matrix \mathbf{B}_i defines the relationship between the nodal displacements and the strain tensor $\boldsymbol{\varepsilon}$:

$$\boldsymbol{\varepsilon} = \sum_{i=1}^N \mathbf{B}_i \mathbf{u}_i \tag{1.125}$$

The matrix \mathbf{B}_i is defined by the differentials of the shape function:

$$\mathbf{B}_i = \begin{bmatrix} \frac{\partial N_i}{\partial x} & 0 \\ 0 & \frac{\partial N_i}{\partial y} \\ \alpha \frac{N_i}{X} & \beta \frac{N_i}{X} \\ \frac{\partial N_i}{\partial y} & \frac{\partial N_i}{\partial x} \end{bmatrix} \tag{1.126}$$

$$\text{where, } \alpha = \vec{x} \bullet \vec{X} \text{ and } \beta = \vec{y} \bullet \vec{X}$$

The inproduct of the ECS x coordinate and the GCS X coordinate represents the distance of the point to the GCS Z -axis. This distance is called the radius.

Using the matrix \mathbf{B}_i , the element stiffness matrix related is defined as,

$$\mathbf{K}_{ij} = \int_{A_e} \chi \mathbf{B}_i^T \mathbf{D} \mathbf{B}_j dA \quad (1.127)$$

For an isotropic material, the stress-strain relationship for an axisymmetric element is expressed as,

$$\mathbf{D} = \frac{E(1-\nu)}{(1+\nu)(1-2\nu)} \begin{bmatrix} 1 & \frac{\nu}{1-\nu} & \frac{\nu}{1-\nu} & 0 \\ \frac{\nu}{1-\nu} & 1 & \frac{\nu}{1-\nu} & 0 \\ \frac{\nu}{1-\nu} & \frac{\nu}{1-\nu} & 1 & 0 \\ 0 & 0 & 0 & \frac{1-2\nu}{2(1-\nu)} \end{bmatrix} \quad (1.128)$$

1-7-3 Loads

The following loads can be applied to an axisymmetric element: body force, edge load, thermal load, etc. The body force represents the self weight or inertia force of an element, and the edge load is a distributed load, which acts along the edges of an element. The pressure load and edge load are applied to the normal direction to the edge of an element. Nodal temperature and element temperature loads cause thermal deformation. Please note that the edge load acting on an axisymmetric element is defined as force per unit circumference and be aware that when nodal loads are specified, the nodal loads are considered to have been integrated over the full circumference ($2\pi r$).

- Body force

$$\mathbf{F}_i = \int_{A_e} XN_i \begin{Bmatrix} \omega_x \\ \omega_y \\ \omega_z \end{Bmatrix} dA \quad (1.129)$$

where $\omega_x, \omega_y, \omega_z$ are weight density vector components.

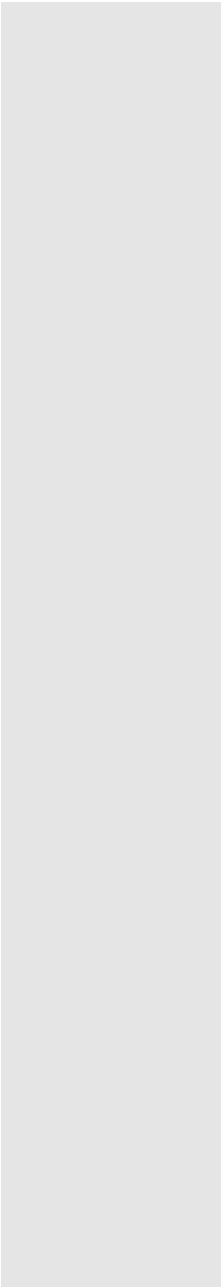
- Edge load

$$\mathbf{F}_i = \int_L XN_i \begin{Bmatrix} P_x \\ P_y \\ P_z \end{Bmatrix} ds \quad (1.130)$$

where P_x, P_y, P_z are edge load vector components. For axisymmetric elements the P_y component must be equal to zero.

- Temperature load

$$\mathbf{F}_i = \int_{A_e} X\mathbf{B}_i^T \mathbf{D} \begin{Bmatrix} \alpha_x \\ \alpha_y \\ \alpha_z \\ 0 \end{Bmatrix} \Delta T dA \quad (1.131)$$



where $\alpha_x, \alpha_y, \alpha_z$ are the linear thermal expansion coefficients in x, y and z directions.

1-7-4 Element Output

Analysis results for axisymmetric elements are stresses and strains at each node of the element. The symmetry axis for axisymmetric elements is the GCS Z-axis and the element can only deform in the $X - Z$ plane. Therefore, stress and strain results are produced in the GCS. The analysis results produced in the GCS can be converted into the ECS or the Output Coordinate System. Stresses and strains produced for the element are as follows:

- Stress components $\sigma_{xx}, \sigma_{yy}, \sigma_{zz}, \tau_{zx}$
 - Von-Mises stress $\sqrt{(P_1^2 + P_2^2 + P_3^2 - P_1P_2 - P_2P_3 - P_3P_1)}$
 - Mean stress $\frac{P_1 + P_2 + P_3}{3}$
 - Maximum shear stress $\frac{\max(|P_1 - P_2|, |P_2 - P_3|, |P_3 - P_1|)}{2}$
 - Principal stresses P_1, P_2, P_3
- $$P_i = \frac{\sigma_{xx} + \sigma_{zz}}{2} \pm \sqrt{\left(\frac{\sigma_{xx} - \sigma_{zz}}{2}\right)^2 + \tau_{zx}^2} \text{ and } \sigma_{yy} \text{ are denoted as } P_1, P_2$$
- and P_3 in a descending order.
- Strain components $\epsilon_{xx}, \epsilon_{yy}, \epsilon_{zz}, \gamma_{zx}$
 - Von-Mises strain $\frac{2}{3} \sqrt{(E_1^2 + E_2^2 + E_3^2 - E_1E_2 - E_2E_3 - E_3E_1)}$
 - Volumetric strain $E_1 + E_2 + E_3$

- Principal strains E_1, E_2, E_3

$$E_i = \frac{\varepsilon_{xx} + \varepsilon_{zz}}{2} \pm \sqrt{\left(\frac{\varepsilon_{xx} - \varepsilon_{zz}}{2}\right)^2 + \frac{\gamma_{zx}^2}{4}} \quad \text{and} \quad \varepsilon_{yy} \quad \text{are denoted as} \quad E_1, E_2$$

and E_3 in a descending order.

The stress and strain results at nodes are extrapolated from the integration points. The integration points for an axisymmetric element are as follows:

- 3-node triangular element: 1-point Gauss integration
- 4-node quadrilateral element: 4-point Gauss integration
- 6-node triangular element: 3-point Gauss integration
- 8-node quadrilateral element: 9-point Gauss integration

Fig. 1-(32) shows the sign convention for stresses and strains and the arrows represent the positive (+) directions.

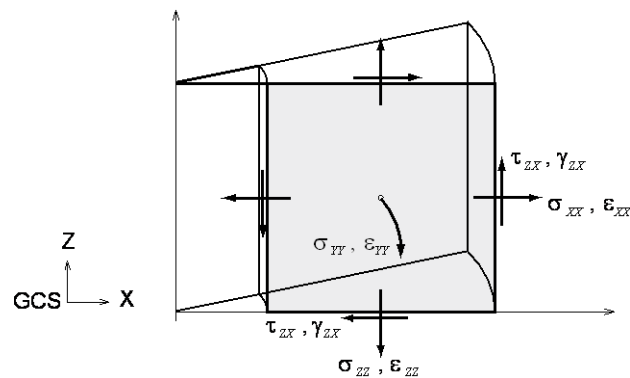


Figure 1-(32) Output Convention of Axisymmetric Element

1-8 Solid Element

1-8-1 Overview

Solid elements are generally used to model voluminous structures such as concrete foundations, car engines, thick walls, rubbers, etc. A solid element may be a tetrahedron, pentahedron or hexahedron. The solid element can be used for both static (linear & nonlinear) and dynamic analyses. The solid element has the following stress and strain tensors:

$$\boldsymbol{\sigma} = \begin{Bmatrix} \sigma_{xx} \\ \sigma_{yy} \\ \sigma_{zz} \\ \tau_{xy} \\ \tau_{yz} \\ \tau_{zx} \end{Bmatrix}, \quad \boldsymbol{\epsilon} = \begin{Bmatrix} \epsilon_{xx} \\ \epsilon_{yy} \\ \epsilon_{zz} \\ \gamma_{xy} \\ \gamma_{yz} \\ \gamma_{zx} \end{Bmatrix} \quad (\text{Stress \& strain})$$

The sign convention for stresses and strains is shown in Fig. 1-(33) and the arrows represent the positive (+) directions.

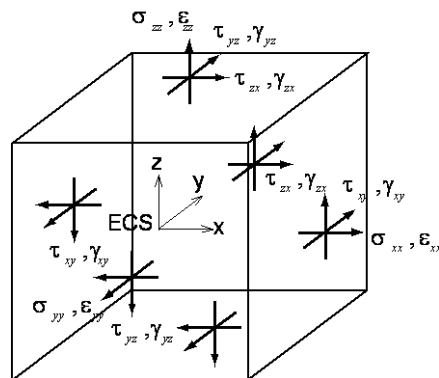


Figure 1-(33) Stress Sign Convention for Solid Element

The directions of the ECS axes are defined in Fig. 1-(34). In the case of a hexahedron, the line connecting the mid point of Node 1 and Node 4 to the mid point of Node 2 and Node 3 defines the direction of the ECS x-axis. For a tetrahedron or pentahedron, the line parallel to the direction from Node 1 to Node 2 is the ECS x-axis.

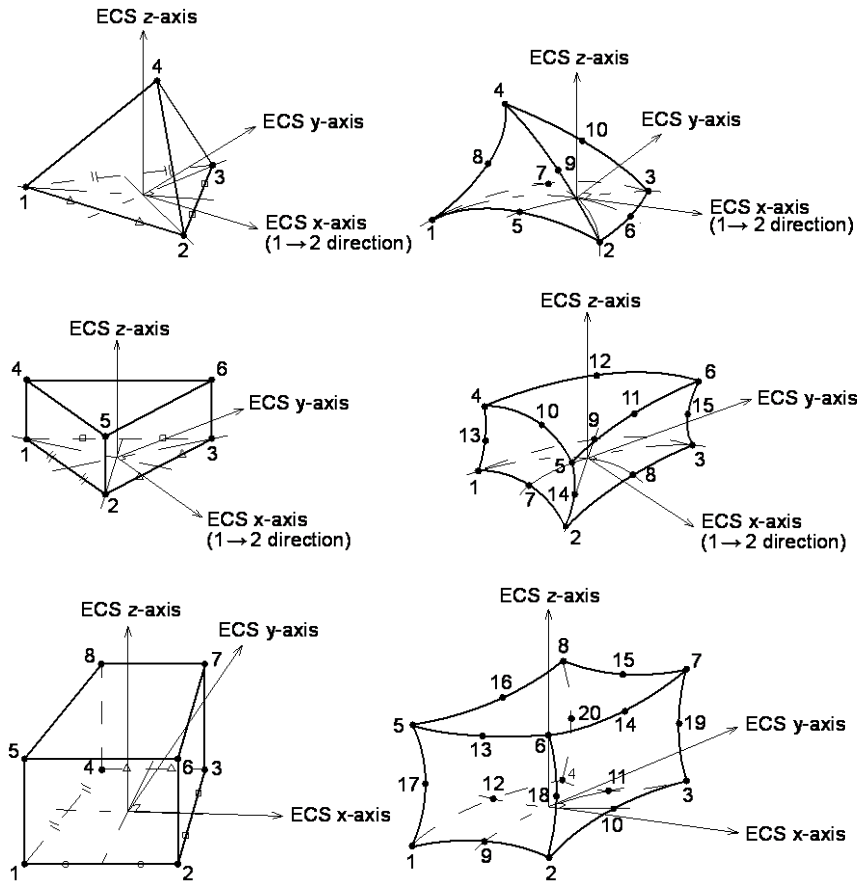
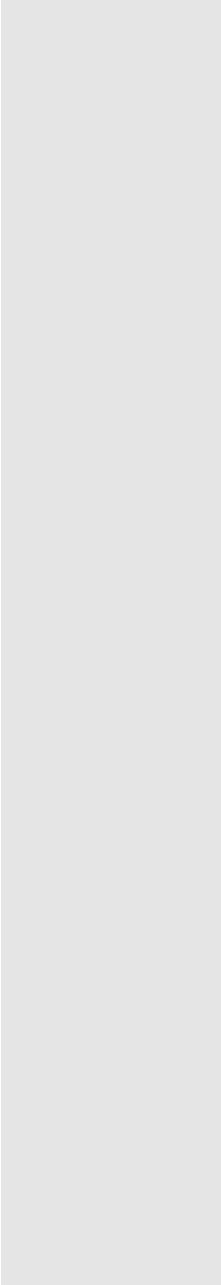


Figure 1-(34) Element Coordinate System for Solid Element

The solid element has a linear or a quadratic shape function. 8-node hexahedron, 6-node



pentahedron and 4-node tetrahedron are “Linear” elements. 20-node hexahedron, 15-node pentahedron and 10-node tetrahedron are “Quadratic” elements. Linear hexahedron elements generally lead to more accurate stress and strain results than linear tetrahedron and linear pentahedron. Therefore, it is advised to use linear hexahedron elements or quadratic elements in the model parts where detailed analysis results are required.

1-8-2 Finite Element Formulation

The solid element is formulated as an isoparametric element, and the Incompatible Modes theory is used for 8-node hexahedron and 6-node pentahedron. Solid elements only have translational displacements u , v and w in the ECS x , y and z directions in each node.

$$\mathbf{u}_i = \{u_i \quad v_i \quad w_i\}^T \quad (1.132)$$

For all solid elements the calculation of the stiffness is identical, except for elements with incompatible modes. In this paragraph N indicates the number of nodes of the element.

In the element the coordinates x , y and z and displacements u , v and w can be expressed as follows:

$$\begin{aligned} x &= \sum_{i=1}^N N_i x_i, \quad y = \sum_{i=1}^N N_i y_i, \quad z = \sum_{i=1}^N N_i z_i \\ u &= \sum_{i=1}^N N_i u_i, \quad v = \sum_{i=1}^N N_i v_i, \quad w = \sum_{i=1}^N N_i w_i \end{aligned} \quad (1.133)$$

- 4-node tetrahedron

$$N_1 = 1 - \xi - \eta - \zeta, \quad N_2 = \xi, \quad N_3 = \eta, \quad N_4 = \zeta \quad (1.134)$$

- 6-node pentahedron

$$\begin{aligned} N_1 &= \frac{\lambda}{2}(1 - \zeta), \quad N_2 = \frac{\xi}{2}(1 - \zeta), \quad N_3 = \frac{\eta}{2}(1 - \zeta), \quad N_4 = \frac{\lambda}{2}(1 + \zeta) \\ N_5 &= \frac{\xi}{2}(1 + \zeta), \quad N_6 = \frac{\eta}{2}(1 + \zeta) \end{aligned} \quad (1.135)$$

$$\lambda = 1 - \xi - \eta$$

- 8-node hexahedron

$$N_1 = \frac{1}{8}(1-\xi)(1-\eta)(1-\zeta), \quad N_2 = \frac{1}{8}(1+\xi)(1-\eta)(1-\zeta)$$

$$N_3 = \frac{1}{8}(1+\xi)(1+\eta)(1-\zeta), \quad N_4 = \frac{1}{8}(1-\xi)(1+\eta)(1-\zeta)$$

$$N_5 = \frac{1}{8}(1-\xi)(1-\eta)(1+\zeta), \quad N_6 = \frac{1}{8}(1+\xi)(1-\eta)(1+\zeta)$$

$$N_7 = \frac{1}{8}(1+\xi)(1+\eta)(1+\zeta), \quad N_8 = \frac{1}{8}(1-\xi)(1+\eta)(1+\zeta) \quad (1.136)$$

- 10-node tetrahedron

$$N_1 = -\lambda(1-2\lambda), \quad N_2 = -\xi(1-2\xi), \quad N_3 = -\eta(1-2\eta), \quad N_4 = -\zeta(1-2\zeta)$$

$$N_5 = 4\xi\lambda, \quad N_6 = 4\xi\eta, \quad N_7 = 4\eta\lambda, \quad N_8 = 4\zeta\lambda, \quad N_9 = 4\xi\zeta, \quad N_{10} = 4\eta\zeta \quad (1.137)$$

$$\lambda = 1 - \xi - \eta - \zeta$$

- 15-node pentahedron

$$N_1 = \frac{\lambda}{2}(1-2\lambda)\zeta(1-\zeta), \quad N_2 = \frac{\xi}{2}(1-2\xi)\zeta(1-\zeta), \quad N_3 = \frac{\eta}{2}(1-2\eta)\zeta(1-\zeta)$$

$$N_4 = -\frac{\lambda}{2}(1-2\lambda)\zeta(1+\zeta), \quad N_5 = -\frac{\xi}{2}(1-2\xi)\zeta(1+\zeta)$$

$$N_6 = -\frac{\eta}{2}(1-2\eta)\zeta(1+\zeta)$$

$$N_7 = -2\xi\lambda\zeta(1-\zeta), \quad N_8 = -2\xi\eta\zeta(1-\zeta)$$

$$N_9 = -2\eta\lambda\zeta(1-\zeta), \quad N_{10} = 2\xi\lambda\zeta(1+\zeta)$$

$$N_{11} = 2\xi\eta\zeta(1+\zeta), \quad N_{12} = 2\eta\lambda\zeta(1+\zeta), \quad N_{13} = (1-\xi-\eta)(1-\zeta^2)$$

$$N_{14} = \xi(1-\zeta^2), \quad N_{15} = \eta(1-\zeta^2) \quad (1.138)$$

$$\lambda = 1 - \xi - \eta$$

- 20-node hexahedron

$$N_1 = \frac{1}{8}(1-\xi)(1-\eta)(1-\zeta)(-2-\xi-\eta-\zeta)$$

$$N_2 = \frac{1}{8}(1+\xi)(1-\eta)(1-\zeta)(-2+\xi-\eta-\zeta)$$

$$N_3 = \frac{1}{8}(1+\xi)(1+\eta)(1-\zeta)(-2+\xi+\eta-\zeta)$$

$$N_4 = \frac{1}{8}(1-\xi)(1+\eta)(1-\zeta)(-2+\xi+\eta-\zeta)$$

$$N_5 = \frac{1}{8}(1-\xi)(1-\eta)(1+\zeta)(-2-\xi-\eta+\zeta)$$

$$N_6 = \frac{1}{8}(1+\xi)(1-\eta)(1+\zeta)(-2+\xi-\eta+\zeta)$$

$$N_7 = \frac{1}{8}(1+\xi)(1+\eta)(1+\zeta)(-2+\xi+\eta+\zeta)$$

$$N_8 = \frac{1}{8}(1-\xi)(1+\eta)(1+\zeta)(-2-\xi+\eta+\zeta)$$

$$N_9 = \frac{1}{4}(1-\eta)(1-\zeta)(1-\xi^2), \quad N_{10} = \frac{1}{4}(1+\xi)(1-\zeta)(1-\eta^2)$$

$$N_{11} = \frac{1}{4}(1+\eta)(1-\zeta)(1-\xi^2)$$

$$\begin{aligned}
N_{12} &= \frac{1}{4}(1-\xi)(1-\zeta)(1-\eta^2), \quad N_{13} = \frac{1}{4}(1-\eta)(1+\zeta)(1-\xi^2) \\
N_{14} &= \frac{1}{4}(1+\xi)(1+\zeta)(1-\eta^2) \\
N_{15} &= \frac{1}{4}(1-\eta)(1+\zeta)(1-\xi^2), \quad N_{16} = \frac{1}{4}(1+\xi)(1-\zeta)(1-\eta^2) \\
N_{17} &= \frac{1}{4}(1-\xi)(1-\eta)(1-\zeta^2) \\
N_{18} &= \frac{1}{4}(1+\xi)(1-\eta)(1-\zeta^2), \quad N_{19} = \frac{1}{4}(1+\xi)(1+\eta)(1-\zeta^2) \\
N_{20} &= \frac{1}{4}(1-\xi)(1+\eta)(1-\zeta^2)
\end{aligned} \tag{1.139}$$

The matrix \mathbf{B}_i defines the relation between the nodal displacements \mathbf{u} and the strain tensor $\boldsymbol{\varepsilon}$:

$$\boldsymbol{\varepsilon} = \sum_{i=1}^N \mathbf{B}_i \mathbf{u}_i \tag{1.140}$$

The matrix \mathbf{B}_i is defined by the differentials of the shape function:

$$\mathbf{B}_i = \begin{bmatrix} \frac{\partial N_i}{\partial x} & 0 & 0 \\ 0 & \frac{\partial N_i}{\partial y} & 0 \\ 0 & 0 & \frac{\partial N_i}{\partial z} \\ \frac{\partial N_i}{\partial y} & \frac{\partial N_i}{\partial x} & 0 \\ 0 & \frac{\partial N_i}{\partial z} & \frac{\partial N_i}{\partial y} \\ \frac{\partial N_i}{\partial z} & 0 & \frac{\partial N_i}{\partial x} \end{bmatrix} \tag{1.141}$$

Using the matrix \mathbf{B}_i , the element stiffness matrix \mathbf{k} can be defined:

$$\mathbf{K}_{ij} = \int_{V_e} \mathbf{B}_i^T \mathbf{D} \mathbf{B}_j dV \quad (1.142)$$

where V_e is the element volume

The matrix \mathbf{D} represents the relationship between the stress and the strain tensor. For isotropic materials, \mathbf{D} is:

$$\mathbf{D} = \frac{E}{(1+\nu)(1-2\nu)} \begin{bmatrix} 1-\nu & \nu & \nu & 0 & 0 & 0 \\ \nu & 1-\nu & \nu & 0 & 0 & 0 \\ \nu & \nu & 1-\nu & 0 & 0 & 0 \\ 0 & 0 & 0 & \frac{1-2\nu}{2} & 0 & 0 \\ 0 & 0 & 0 & 0 & \frac{1-2\nu}{2} & 0 \\ 0 & 0 & 0 & 0 & 0 & \frac{1-2\nu}{2} \end{bmatrix} \quad (1.143)$$

Where E is the Young's modulus and ν is the Poisson ratio. Orthotropic materials can be defined in the Material Coordinate System MCS.

In the case of linear analysis, incompatible modes are applied in the stiffness definition of the 6-node pentahedron and the 8-node hexahedron. Elements with incompatible modes have extra d.o.f.'s in addition to the nodal displacements. The incompatible modes for solid elements are similar to plane stress elements. Therefore in this paragraph only the incompatible mode shapes and some matrices are outlined.

- 6-node pentahedron

$$\mathbf{u}_a = \{a_1 \quad b_1 \quad c_1\}^T \quad (1.144)$$

$$u = \sum_{i=1}^6 N_i u_i + a_1 P_1, \quad v = \sum_{i=1}^6 N_i v_i + b_1 P_1, \quad w = \sum_{i=1}^6 N_i w_i + c_1 P_1 \quad (1.145)$$

$$P_1 = 1 - \zeta^2 \quad (1.146)$$

$$\mathbf{B}_a = \begin{bmatrix} \frac{\partial P_1}{\partial x} & 0 & 0 \\ 0 & \frac{\partial P_1}{\partial y} & 0 \\ 0 & 0 & \frac{\partial P_1}{\partial z} \\ \frac{\partial P_1}{\partial y} & \frac{\partial P_1}{\partial x} & 0 \\ 0 & \frac{\partial P_1}{\partial z} & \frac{\partial P_1}{\partial y} \\ \frac{\partial P_1}{\partial z} & 0 & \frac{\partial P_1}{\partial x} \end{bmatrix} \quad (1.147)$$

- 8-node hexahedron

$$\mathbf{u}_a = \{a_1 \quad b_1 \quad c_1 \quad a_2 \quad b_2 \quad c_2 \quad a_3 \quad b_3 \quad c_3\}^T \quad (1.148)$$

$$u = \sum_{i=1}^8 N_i u_i + a_1 P_1 + a_2 P_2 + a_3 P_3 \quad , \quad v = \sum_{i=1}^8 N_i v_i + b_1 P_1 + b_2 P_2 + b_3 P_3$$

$$w = \sum_{i=1}^8 N_i w_i + c_1 P_1 + c_2 P_2 + c_3 P_3 \quad (1.149)$$

$$P_1 = 1 - \xi^2, \quad P_2 = 1 - \eta^2, \quad P_3 = 1 - \zeta^2 \quad (1.150)$$

$$\mathbf{B}_a = \begin{bmatrix} \frac{\partial P_1}{\partial x} & 0 & 0 & \frac{\partial P_2}{\partial x} & 0 & 0 & \frac{\partial P_3}{\partial x} & 0 & 0 \\ 0 & \frac{\partial P_1}{\partial y} & 0 & 0 & \frac{\partial P_2}{\partial y} & 0 & 0 & \frac{\partial P_3}{\partial y} & 0 \\ 0 & 0 & \frac{\partial P_1}{\partial z} & 0 & 0 & \frac{\partial P_2}{\partial z} & 0 & 0 & \frac{\partial P_3}{\partial z} \\ \frac{\partial P_1}{\partial y} & \frac{\partial P_1}{\partial x} & 0 & \frac{\partial P_2}{\partial y} & \frac{\partial P_2}{\partial x} & 0 & \frac{\partial P_3}{\partial y} & \frac{\partial P_3}{\partial x} & 0 \\ 0 & \frac{\partial P_1}{\partial z} & \frac{\partial P_1}{\partial y} & 0 & \frac{\partial P_2}{\partial z} & \frac{\partial P_2}{\partial y} & 0 & \frac{\partial P_3}{\partial z} & \frac{\partial P_3}{\partial y} \\ \frac{\partial P_1}{\partial z} & 0 & \frac{\partial P_1}{\partial x} & \frac{\partial P_2}{\partial z} & 0 & \frac{\partial P_2}{\partial x} & \frac{\partial P_3}{\partial z} & 0 & \frac{\partial P_3}{\partial x} \end{bmatrix} \quad (1.151)$$

1-8-3 Loads and Masses

The following loads can be applied to solid elements: the body force, the pressure load, the thermal load, etc. The body force represents the self weight or inertia force on an element, and the pressure load is a distributed load, which acts on the surface of an element. The types of temperature loads include nodal temperature and element temperature loads may be applied.

- Body force

$$\mathbf{F}_i = \int_{V_e} N_i \begin{Bmatrix} \omega_x \\ \omega_y \\ \omega_z \end{Bmatrix} dV \quad (1.152)$$

where $\omega_x, \omega_y, \omega_z$ are the weight density vector components.

- Pressure load

$$\mathbf{F}_i = \int_{A_e} N_i \begin{Bmatrix} P_x \\ P_y \\ P_z \end{Bmatrix} dA \quad (1.153)$$

where P_x, P_y, P_z are the pressure load vector components.

- Temperature load

$$\mathbf{F}_i = \int_{V_e} \mathbf{B}_i^T \mathbf{D} \begin{Bmatrix} \alpha_x \\ \alpha_y \\ \alpha_z \end{Bmatrix} \Delta T dV \quad (1.154)$$

where $\alpha_x, \alpha_y, \alpha_z$ are the linear thermal expansion coefficients in x, y and z directions

The mass of a solid element can be represented by lumped mass or consistent mass and reflects translational displacements in the x, y and z directions only.

- Consistent mass

$$\mathbf{M}_{ij} = \rho \int_{V_e} N_i N_j dV \quad (1.155)$$

- Lumped mass

The total mass (ρV_e) of the element is only distributed to the diagonal terms in proportion to the diagonal terms of the consistent mass matrix. The lumped mass matrix is a diagonal matrix.

1-8-4 Element Output

The analysis results for a solid element include stresses and strains in the nodes of an element with reference to the GCS. The analysis results produced in the GCS can be converted into the ECS or Output Coordinate System. The stresses and strains produced for a solid element are as follows:

- Stress components $\sigma_{xx}, \sigma_{yy}, \sigma_{zz}, \tau_{xy}, \tau_{yz}, \tau_{zx}$
- Von-Mises stress $\frac{2}{3} \sqrt{(E_1^2 + E_2^2 + E_3^2 - E_1 E_2 - E_2 E_3 - E_3 E_1)}$
- Mean stress $\frac{P_1 + P_2 + P_3}{3}$
- Maximum shear stress $\frac{\max(|P_1 - P_2|, |P_2 - P_3|, |P_3 - P_1|)}{2}$
- Principal stresses P_1, P_2, P_3

The solutions of $\det \begin{bmatrix} \sigma_{xx} - P_i & \tau_{xy} & \tau_{zx} \\ \tau_{xy} & \sigma_{yy} - P_i & \tau_{yz} \\ \tau_{zx} & \tau_{yz} & \sigma_{zz} - P_i \end{bmatrix} = 0$ are denoted as P_1, P_2

and P_3 in a descending order.

- Strain components $\varepsilon_{xx}, \varepsilon_{yy}, \varepsilon_{zz}, \gamma_{xy}, \gamma_{yz}, \gamma_{zx}$
- Von-Mises strain $\sqrt{(E_1^2 + E_2^2 + E_3^2 - E_1 E_2 - E_2 E_3 - E_3 E_1)}$
- Volumetric strain $E_1 + E_2 + E_3$

- Principal strains E_1, E_2, E_3

The solutions of $\det \begin{bmatrix} \varepsilon_{xx} - E_i & \gamma_{xy}/2 & \gamma_{zx}/2 \\ \gamma_{xy}/2 & \varepsilon_{yy} - E_i & \gamma_{yz}/2 \\ \gamma_{zx}/2 & \gamma_{yz}/2 & \varepsilon_{zz} - E_i \end{bmatrix} = 0$ are denoted as E_1, E_2 and E_3 in a

descending order.

For calculation of the strains and stresses at the nodes, the results calculated at the integration points (Gauss Points) are extrapolated. The integration points for a solid element are as follows:

- 4-node tetrahedron: 1-point Gauss integration
- 6-node pentahedron: 6-point Gauss integration
- 8-node hexahedron: 8-point Gauss integration
- 10-node tetrahedron: 4-point Gauss integration
- 15-node pentahedron: 9-point Gauss integration
- 20-node hexahedron: 27-point Gauss integration

Fig. 1-(35) shows the sign convention for stresses and strains, and the arrows represent the positive (+) directions.

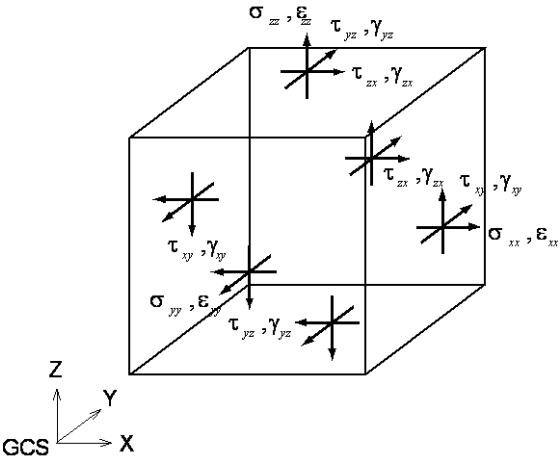


Figure 1-(35) Output Sign Convention for Solid Element

1-9 Spring

1-9-1 Elastic Link

An elastic link connects two nodes and its stiffness is defined by the user. The elastic link only accounts for the stiffness which has to be defined by the user in the ECS. Fig. 1-(39) presents the directions of the ECS axes. An elastic link may be assigned as tension-only or compression-only. An elastic link is composed of three translational and three rotational stiffnesses. The translational and rotational stiffnesses of an elastic link element are expressed in terms of unit force per unit length and unit moment per unit radian respectively.

Examples for elastic link elements are elastic bearings of a bridge structure, connecting the bridge deck and the piers. Compression-only elastic link elements can be used to model soil boundary conditions. The rigid link option connects two nodes with an “infinite” stiffness.

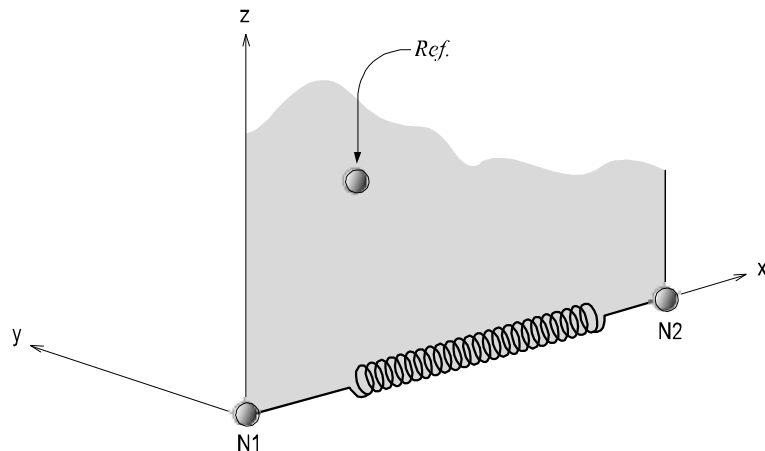


Figure 1-(39) Element Coordinate System of Elastic Link

1-9-2 Point Spring/Damping

Point springs are used to define the elastic stiffness of adjoining structures or ground support conditions. They are also used to prevent singular errors from occurring at the connecting nodes of elements with limited degrees of freedom, such as truss, plane stress, etc.

Point spring at a node can be expressed in six degrees of freedom: three translational and three rotational components with respect to the GCS. The translational and rotational spring stiffnesses are defined in unit force per unit length and unit moment per unit radian respectively. When using point springs for modelling sub-soil for foundation supports, the spring stiffness can be calculated as the product of Young's modulus of subsoil and the effective areas of the corresponding node divided by the effective deformation of the soil in depth.

Point damping defines a damping spring at a node. The point damping can be mainly used to model viscous damping boundary conditions of soils and is defined as six degrees of freedom: three translational and three rotational components, per node. Due to the characteristics of damping, the point damping can only be used in dynamic analyses and not in linear analysis.

Point spring and point damping specified at a node, in general, follows the GCS unless an NCS is specified, in which case they are defined relative to the NCS.

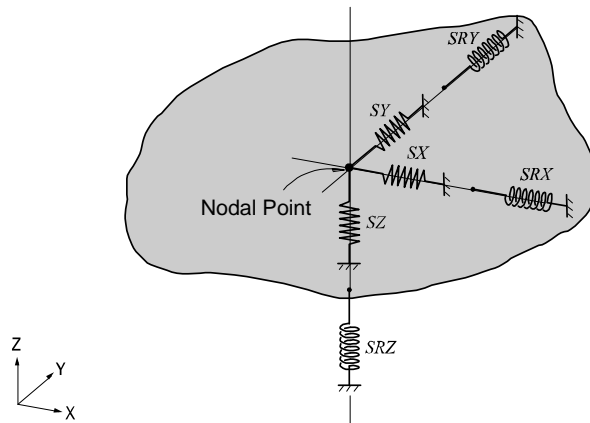


Figure 1-(40) Element Coordinate System of Point Spring/Damping

1-9-3 Matrix Spring

The stiffnesses in different directions of a point spring are independent of each other. Matrix Springs are introduced to couple displacements or rotations in one direction to forces and moments in another direction. An example of an application of a matrix spring is the coupling of a rotation to translations.

Matrix spring stiffnesses can be defined by the user, but attention should be given to the condition that the matrix must be positive definite. Because the matrix must be symmetric only the upper triangular matrix can be specified.

In general matrix springs follows the GCS unless an NCS is specified, in which case it is defined relative to the NCS.

1-10 Rigid Link

The rigid link function constrains geometric relative displacements or rotations between 2 or more nodes of a structure. A geometric constraint prescribes that one degree of freedom of a particular node is defined by one or more degrees of freedom of one or more nodes. The reference nodes are called the master nodes, and the subordinated node is called the slave node. The geometric relationships for the eccentric bending condition of the master node and slave node are expressed by the equation (1.156).

$$\begin{aligned}
 U_{Xs} &= U_{Xm} + R_{Ym}\Delta Z - R_{Zm}\Delta Y \\
 U_{Ys} &= U_{Ym} + R_{Zm}\Delta X - R_{Xm}\Delta Z \\
 U_{Zs} &= U_{Zm} + R_{Xm}\Delta Y - R_{Ym}\Delta X \\
 R_{Xs} &= R_{Xm} \\
 R_{Ys} &= R_{Ym} \\
 R_{Zs} &= R_{Zm} \\
 \Delta X &= X_m - X_s \\
 \Delta Y &= Y_m - Y_s \\
 \Delta Z &= Z_m - Z_s
 \end{aligned} \tag{1.156}$$

- | | |
|--------------------------------|--|
| U_{Xs} , U_{Ys} , U_{Zs} | : Translations of slave node in the GCS X, Y and Z directions |
| U_{Xm} , U_{Ym} , U_{Zm} | : Translations of master node in the GCS X, Y and Z directions |
| R_{Xs} , R_{Ys} , R_{Zs} | : Rotations of slave node in the GCS X, Y and Z directions |
| R_{Xm} , R_{Ym} , R_{Zm} | : Rotations of master node in the GCS X, Y and Z directions |
| X_s , Y_s , Z_s | : Global coordinates of slave node |
| X_m , Y_m , Z_m | : Global coordinates of master node |

A rigid link may be applied to a model part which is assumed to be rigid. It also can be used in the case of a stiffened plate for an eccentric connection of plate and stiffener.

Fig. 1-(41) illustrates a rigid plane connection applied to a floor (diaphragm). When a building is subjected to a lateral load, the relative horizontal deformation in the floor plane is generally negligible compared to that in columns, walls and bracings. This rigid diaphragm behavior of the floor can be prescribed by constraining all the relative in-plane displacements to be equal. The movements consist of two in-plane translational displacements and one rotational displacement about the perpendicular direction to the plane.

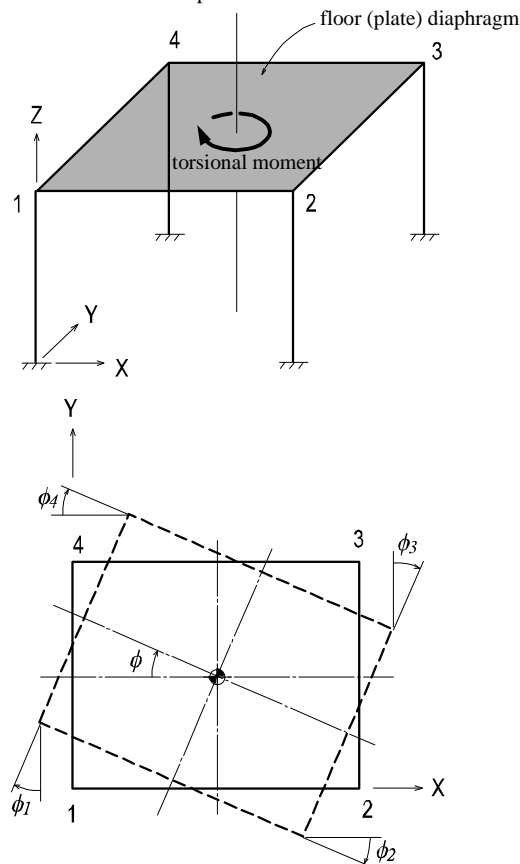
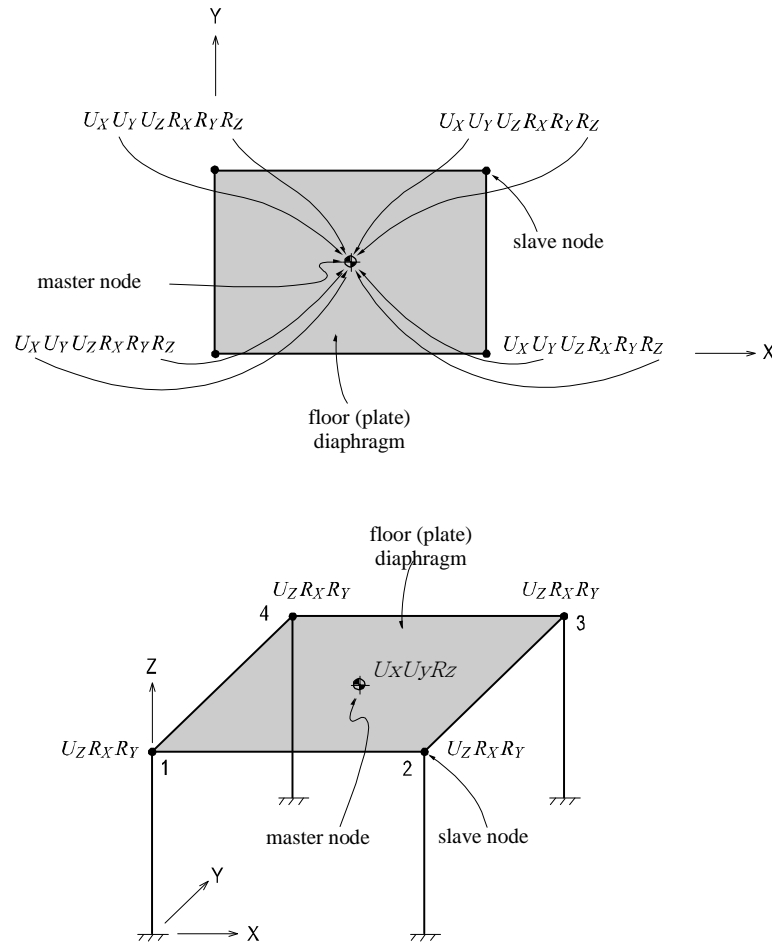
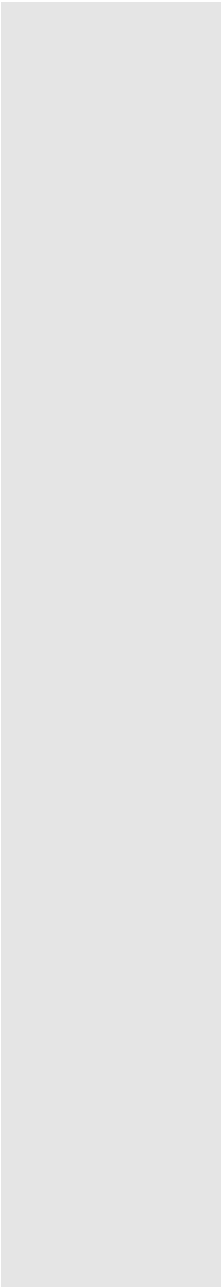


Figure 1-(41) A floor (plate) diaphragm subjected to a torsional moment about a vertical axis

When a floor structure, as illustrated in Fig. 1-(41), is subjected to a torsional moment around the vertical direction and the in-plane stiffness of the floor is significantly greater than the stiffness of the columns, the entire floor will be rotated by ϕ , where, $\phi_1 = \phi_2 = \phi_3 = \phi_4 = \phi$. Accordingly, the four degrees of freedom can be reduced to a single degree of freedom.

Fig. 1-(42) shows a process in which a total of 24 (6×4) degrees of freedom are reduced to 15 d.o.f. within the floor plane, based on the assumption that the floor shape is rigid when rotating.

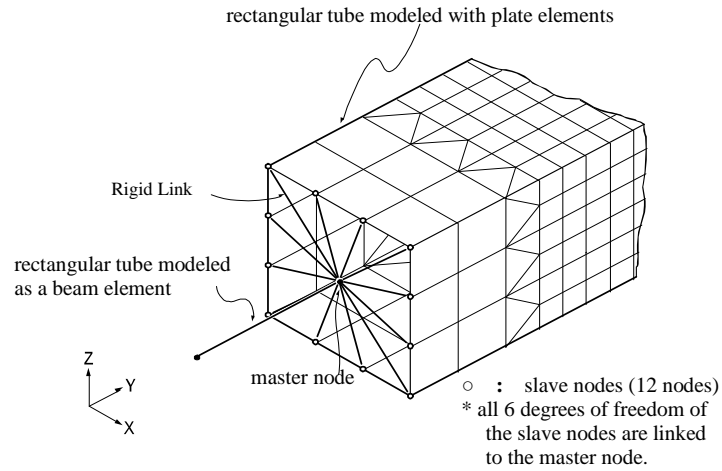




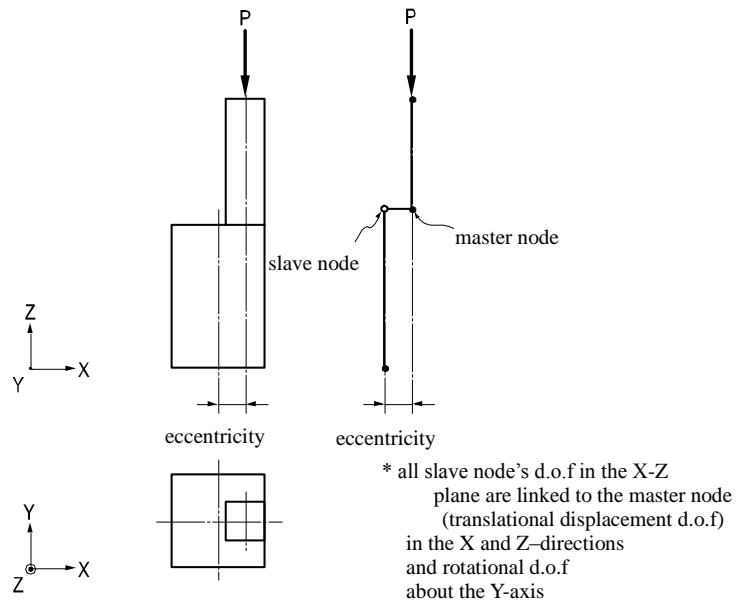
UX	:	displacement in the X-direction at the corresponding node
UY	:	displacement in the Y-direction at the corresponding node
UZ	:	displacement in the Z-direction at the corresponding node
RX	:	rotation around the X-axis at the corresponding node
RY	:	rotation around the Y-axis at the corresponding node
RZ	:	rotation around the Z-axis at the corresponding node

Figure 1-(42) Reduction of d.o.f for floor diaphragm of significant in-plane stiffness

Fig. 1-(43) shows a rigid body connection and a rigid plane connection. Fig. 1-(43) (a) illustrates the application of a rigid link using a rigid body connection. In the region where detail results are required the rectangular tube is modeled with shell elements, and the tube is represented by beam elements where no detailed results are required. Fig. 1-(43) (b) shows an application of a rigid plane connection for a column offset in a two-dimensional plane. Whenever the rigid link is used in a plane, geometric constraints must be assigned to two translational displacement components and one rotational component around the axis perpendicular to the plane. When a rigid link is used for all directional components, as shown in Fig. 1-(43) (a), geometric constraints must be assigned to all six degrees of freedom.



(a) A tube modeled using a beam element and shell elements, and connected by Rigid Body Connection



(b) Eccentricity of an offset-column linked by Rigid Plane Connection

Figure 1-(43) Application examples of Rigid Links

Chapter 2. Embedded Reinforcements

2-1 Introduction

Rather than defining reinforcements with distinct finite elements, the concept of embedded reinforcements can be used. In this concept the stiffness of the reinforcements is added to the stiffness of the continuum elements in which the reinforcements are located. The continuum elements in which reinforcement is embedded are called mother elements. The following should be noted for using embedded reinforcements.

- The user defines the reinforcement location and the software may calculate the intersections of reinforcement position with the mother elements.
- Reinforcement does not have separate degrees of freedom.
- Reinforcement and their mother elements are assumed to be perfectly bonded.
- Reinforcement's strains are obtained from the displacements of its mother elements.

There are two types of embedded reinforcement elements, Bar and Grid. The input information required to define a reinforcement consists of location data, shape information and material properties. The location information comprises the location points of the reinforcement. There are two ways of defining the reinforcement. In the global definition the reinforcement consists of one or more sections, and each section is defined by a number of location points. The software calculates the intersections of each section and the mother elements, resulting in reinforcement segments. The reinforcements segments constitute together the reinforcement. A reinforcement segment never crosses the boundaries of a mother element. In the local definition the reinforcement is consisting of 1 section and this section equal to 1 segment. The shape information of the reinforcement depends on the type of the reinforcement and the type of the mother elements, which is explained in the following paragraphs.

When relative displacements between the concrete and steel reinforcement are relevant, the embedded reinforcement concept cannot be used and the reinforcement must be modeled with

truss elements having its own nodes and being connected by interface elements to the concrete elements. In such situations the interface elements will exhibit nonlinear failure behavior.

2-2 Reinforcement Types

2-2-1 Bar Reinforcement

The bar reinforcement can be represented by the line or a point, dependent on the type of mother element:

- Line: for solid, plate, shell & plane stress elements
- Point: for plane strain & axisymmetric elements

The bar reinforcement for the different element types will be explained in the following paragraphs.

In midas FEA the location information defines lines and points. A bar may be divided into sections. The following properties are required for a bar reinforcement:

- Material property
- Cross-section
- Pre-stress and post-tensioning

An embedded reinforcement to which a pre-stress is assigned is called a tendon.

Fig. 2-(1) shows the 2 possible bar sections. Bar sections can be defined by a straight 2-node line and second order 3-node curve.



Figure 2-(1) Bar sections with location points

In the global reinforcement definition preprocessing phase the bar sections are automatically divided into segments matching with the elements which the reinforcement is embedded. Bar reinforcement segments retain the properties of the related bar section.

The order (linear or quadratic interpolation) of the segments is equal to the corresponding bar sections which they have been calculated. If a bar section is defined by 2-nodes, the bar segments derived from it also retain 2-node location points each. Similarly, if a higher order bar section is defined by 3-nodes, each of the related bar segments also has 3-node location points. The shapes of divided bar reinforcement segments can be checked in the post-processing.

In the local reinforcement definition the user directly defines the bar segment in an individual mother element in such a way that a reinforcement segment never crosses the boundaries of the mother element. In this case the bar segment input will be without a separate division process.

The stiffness of the divided bar reinforcement segments will be added to the stiffness of the corresponding mother elements. In bar reinforcement segments, 2 integration points are used for the line type and 1 integration point is used for the point type reinforcement. The locations of the integration points are automatically calculated. Fig 2-(2) (a) shows two bar segments with their location points and for every segment 2 integration points have been defined. Fig 2-(2) (b) shows a stress component σ_{xx} and the strain component ε_{xx} at integration point. The stress is oriented in the tangential direction of the reinforcement segment at the location of the integration point.

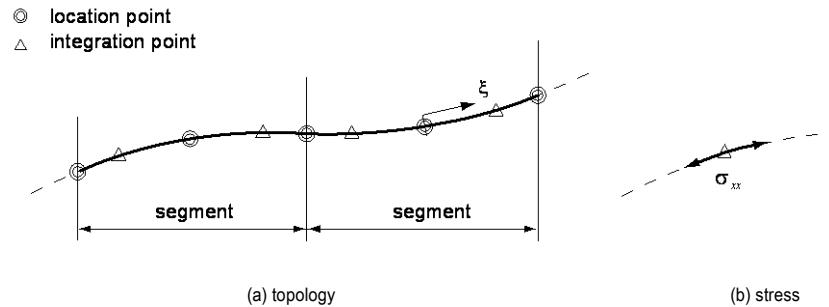


Figure 2-(2) Bar reinforcement segments

2-2-2 Grid Reinforcement

Grid reinforcement can be defined as a plane or as a line. In its turn the plane shape grid can be composed of triangular and quadrilateral shapes. The shape of the grid reinforcement is dependent on the type of the mother element.

- Plane: for solid, plate, shell & plane stress elements
- Line: for plane strain & axisymmetric elements

The grid reinforcement is explained in the following sections for the respective element types.

In midas FEA, the shape of the grid reinforcement is defined by location points and the reinforcement is divided into grid reinforcement sections. The properties of the grid sections are equal to the properties of the corresponding grid reinforcement. The grid reinforcement has the following properties:

- Material Property (Isotropic/Orthotropic)
- Reinforcement Axes
- Equivalent Thickness (Isotropic/Orthotropic)
- Prestress and post-tensioning

There are 4 types of reinforcement grid sections. A quadrilateral grid section can be defined by 4 or 8 nodes as shown in Fig 2-(3), and a triangular grid section can be defined by 3 or 6 nodes as shown in Fig 2-(4).

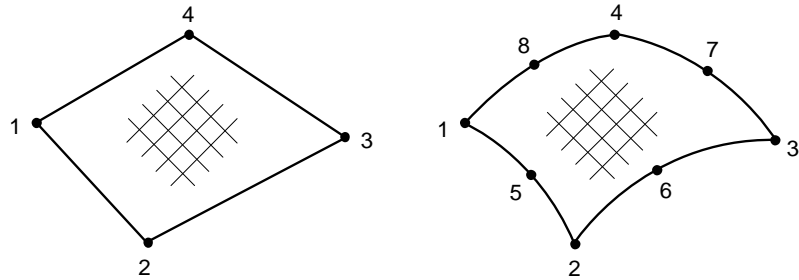


Figure 2-(3) GRID contour of quadrilateral sections with nodes

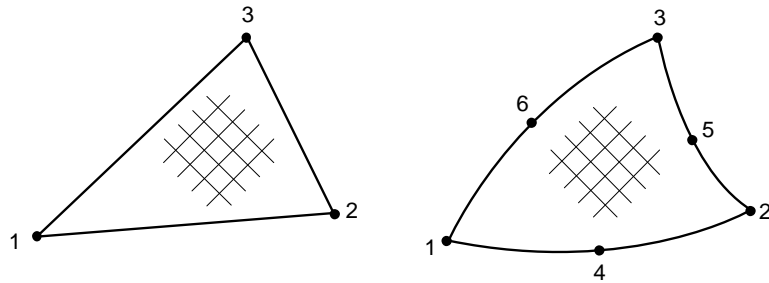


Figure 2-(4) GRID contour of triangular sections with nodes

During the preprocessing the grid sections are subdivided into particles which are located in the mother elements, such that a grid section is divided into grid reinforcement segments matching to the shape of the mother elements. Grid sections are divided into triangular grid reinforcement segments.

If the user wishes to use the local reinforcement definition the grid segments must be defined one-to-one with the grid sections and match to the shapes of the mother elements. In this case, the grid sections input will be used as grid segments without a separate division process. Plane grid reinforcements which are divided in the preprocessing will result into triangular shaped segments. Although when the user directly inputs the grid reinforcement segments, the user is free to input both triangular and quadrilateral shapes of grid segments.

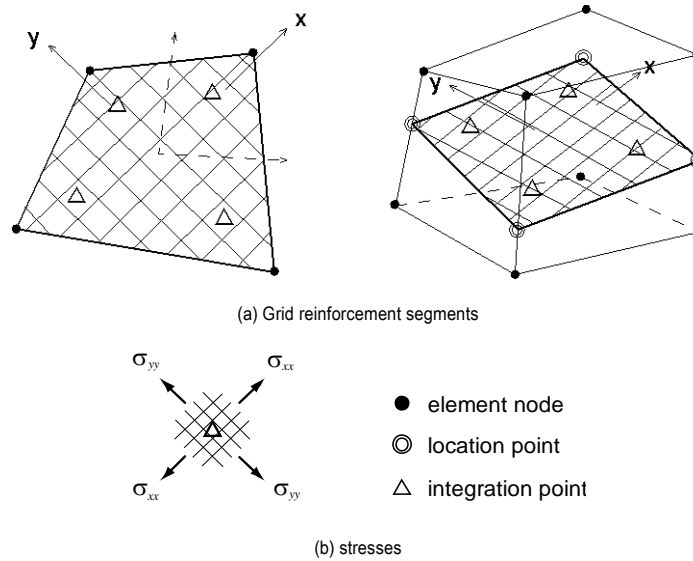


Figure 2-(5) Reinforcement grid

Quadrilateral grid reinforcement segments have 4 integration points, triangular grid reinforcement segments with 3 nodes have one integration point, triangular grid reinforcement segments with 6 nodes have 3 integration points and line shape grid reinforcement segments have 2 integration points. Fig 2-(5) (a) shows the quadrilateral grid segment in a solid element with the location points and integration points of the grid segment. The locations of integration points in the grid segments are automatically calculated.

For grid reinforcement, the local \hat{x} axes can be defined by the user. The local axes, \hat{x} and \hat{y} are orthogonal to each other, and the strains (ε_{xx} and ε_{yy}) and stresses (σ_{xx} and σ_{yy}) at the integration points are oriented in the \hat{x} and \hat{y} directions respectively.

A grid reinforcement has local axes in the \hat{x} and \hat{y} directions, and the stiffness only exists in these directions. A reinforcement grid cannot carry shear-stresses. Different equivalent thickness values may be specified for each axis.

2-3 Finite Element Formulation

The position of a reinforcement can be defined by the positions of the location points of its segments. A reinforcement segment consists of n location points, and each point is defined by the coordinates X_{re}^i , Y_{re}^i and Z_{re}^i . The location points of the reinforcement segment can be arranged in a matrix as Eq. (2.1). The superscripts refer to the location points.

$$\mathbf{X}_{re} = \begin{Bmatrix} X_{re}^1 & X_{re}^2 & \cdots & X_{re}^n \\ Y_{re}^1 & Y_{re}^2 & \cdots & Y_{re}^n \\ Z_{re}^1 & Z_{re}^2 & \cdots & Z_{re}^n \end{Bmatrix} \quad (2.1)$$

The shape function of reinforcement can be expressed as Eq. (2.2).

$$\mathbf{N} = \{N_1 \quad N_2 \quad \cdots \quad N_n\} \quad (2.2)$$

The general form of shape function N_i ($i = 1, 2, \dots, n$) depends on the order of the reinforcement segment and is defined as follows:

Shape function of a 2-node line bar reinforcement segment

$$N_1(\xi) = \frac{1}{2}(1 - \xi), \quad N_2(\xi) = \frac{1}{2}(1 + \xi) \quad (2.3)$$

Shape function of a 3-node line bar reinforcement segment

$$N_1(\xi) = -\frac{1}{2}(1 - \xi)\xi, \quad N_2(\xi) = \frac{1}{2}(1 + \xi)\xi, \quad N_3(\xi) = (1 - \xi^2) \quad (2.4)$$

Shape function of a 4-node quadrilateral grid reinforcement segment

$$\begin{aligned} N_1(\xi, \eta) &= \frac{1}{4}(1 - \xi)(1 - \eta), \quad N_2(\xi, \eta) = \frac{1}{4}(1 + \xi)(1 - \eta), \\ N_3(\xi, \eta) &= \frac{1}{4}(1 + \xi)(1 + \eta), \quad N_4(\xi, \eta) = \frac{1}{4}(1 - \xi)(1 + \eta) \end{aligned} \quad (2.5)$$

Shape function of an 8-node quadrilateral grid reinforcement segment

$$\begin{aligned}
 N_1(\xi, \eta) &= \frac{1}{4}(1-\xi)(1-\eta) - \frac{1}{2}N_5 - \frac{1}{2}N_8, \\
 N_2(\xi, \eta) &= \frac{1}{4}(1+\xi)(1-\eta) - \frac{1}{2}N_5 - \frac{1}{2}N_6, \\
 N_3(\xi, \eta) &= \frac{1}{4}(1+\xi)(1+\eta) - \frac{1}{2}N_6 - \frac{1}{2}N_7, \\
 N_4(\xi, \eta) &= \frac{1}{4}(1-\xi)(1+\eta) - \frac{1}{2}N_7 - \frac{1}{2}N_8, \\
 N_5(\xi, \eta) &= \frac{1}{2}(1-\xi^2)(1-\eta), \\
 N_6(\xi, \eta) &= \frac{1}{2}(1+\xi)(1-\eta^2), \\
 N_7(\xi, \eta) &= \frac{1}{2}(1-\xi^2)(1+\eta), \\
 N_8(\xi, \eta) &= \frac{1}{2}(1-\xi)(1-\eta^2)
 \end{aligned} \tag{2.6}$$

Shape function of 3-node triangular grid reinforcement segment

$$\begin{aligned}
 N_1(\xi, \eta) &= 1 - \xi - \eta, \\
 N_2(\xi, \eta) &= \xi, \\
 N_3(\xi, \eta) &= \eta
 \end{aligned} \tag{2.7}$$

Shape function of 6-node triangular grid reinforcement segment

$$N_1(\xi, \eta) = \frac{1}{4}(1-\xi)(1-\eta) - \frac{1}{2}N_5 - \frac{1}{2}N_8$$

$$N_2(\xi, \eta) = \frac{1}{4}(1 + \xi)(1 - \eta) - \frac{1}{2}N_5 - \frac{1}{2}N_6 \quad (2.8)$$

$$N_3(\xi, \eta) = \frac{1}{4}(1 + \xi)(1 + \eta) - \frac{1}{2}N_6 - \frac{1}{2}N_7$$

$$N_4(\xi, \eta) = \frac{1}{4}(1 - \xi)(1 + \eta) - \frac{1}{2}N_7 - \frac{1}{2}N_8$$

$$N_5(\xi, \eta) = \frac{1}{2}(1 - \xi^2)(1 - \eta)$$

$$N_6(\xi, \eta) = \frac{1}{2}(1 + \xi)(1 - \eta^2)$$

$$N_7(\xi, \eta) = \frac{1}{2}(1 - \xi^2)(1 + \eta)$$

$$N_8(\xi, \eta) = \frac{1}{2}(1 - \xi)(1 - \eta^2)$$

If the j^{th} integration point of reinforcement segment,

$$\mathbf{N}(j)\mathbf{X}_{re} \quad (2.9)$$

represents the coordinates of this integration point associated with the reinforcement segment. Since the reinforcement segment is located within the mother element, the integration point is also located within the mother element.

An isoparametric mapping technique is used for each element used in midas FEA. For each integration points on a reinforcement segment, the isoparametric coordinates with respect to the mother element are calculated.

The isoparametric coordinates of the j^{th} integration point of a reinforcement segment in a 3D element can be written as:

$$\mathbf{G}_j(\xi, \eta, \varsigma) \quad (2.10)$$

The isoparametric coordinates of the j^{th} integration point of a reinforcement segment in a 2D element can be written as:

$$\mathbf{G}_j(\xi, \eta) \quad (2.11)$$

$\hat{\mathbf{B}}_{\text{Rein.}}$ in Eq. (2.12) represents the strain-displacement matrix for the reinforcement strain in the j^{th} integration point of a reinforcement section as a function of the displacements of the nodes of the mother element.

$$\hat{\mathbf{B}}_{\text{Rein.}}^j = \mathbf{B}_{\text{mother}}(\mathbf{G}_j) \quad (2.12)$$

The strain-displacement matrix of the reinforcement uses the element coordinate system of the mother element. The stiffness of the reinforcement is expressed in the reinforcement coordinate system. Accordingly, $\hat{\mathbf{B}}_{\text{Rein.}}$ needs to be rotated from the element local coordinate system into the local coordinate axes of the reinforcement.

If the mother element is a 3D element, the strain in the local coordinate system of the mother element can be transformed into the strain in the local coordinate system of the reinforcement as follows:

$$\mathbf{T} \begin{Bmatrix} \varepsilon_{xx} \\ \varepsilon_{yy} \\ \vdots \\ \varepsilon_{zz} \end{Bmatrix} = \begin{Bmatrix} \varepsilon_{\bar{x}\bar{x}} \\ \varepsilon_{\bar{y}\bar{y}} \end{Bmatrix} \quad (2.13)$$

Here, \mathbf{T} is a matrix, which projects and rotates the strain tensor of the mother element into the strain tensor of the reinforcement segment. The same transformation can be applied to the \mathbf{B} matrix.

$$\mathbf{B}_{\text{Rein.}}^j = \mathbf{T} \hat{\mathbf{B}}_{\text{Rein.}}^j \quad (2.14)$$

The stress-strain matrix in the reinforcement can be expressed as follows:

For a reinforcement bar,

$$\mathbf{D} = \mathbf{E}_{xx} A_e \quad (2.15)$$

where, A is the cross section of the bar reinforcement.

For an isotropic reinforcement grid,

$$\mathbf{D} = \begin{bmatrix} \mathbf{E}_{xx} t_{xx} & 0 \\ 0 & \mathbf{E}_{xx} t_{xx} \end{bmatrix}. \quad (2.16)$$

For an orthotropic reinforcement grid,

$$\mathbf{D} = \begin{bmatrix} \mathbf{E}_{xx} t_{xx} & 0 \\ 0 & \mathbf{E}_{yy} t_{yy} \end{bmatrix} \quad (2.17)$$

where, \mathbf{E}_{xx} is the Young's modulus in the \hat{x} axis direction of the local coordinate of the reinforcement. t_{xx} and t_{yy} represent the thicknesses in the \hat{x} and \hat{y} directions in the local coordinate system of the reinforcement segment respectively.

The stresses in the local coordinate of the reinforcement can be obtained as follows:

$$\begin{Bmatrix} \sigma_{xx} \\ \sigma_{yy} \end{Bmatrix} = \mathbf{D} \begin{Bmatrix} \varepsilon_{xx} \\ \varepsilon_{yy} \end{Bmatrix} \quad (2.18)$$

The contribution of the reinforcement segment to the element stiffness matrix is:

$$\int_V \mathbf{B}_{Rein}^T \mathbf{D} \mathbf{B}_{Rein} dV = \mathbf{K}_{rein} \quad (2.19)$$

and the contribution of the reinforcement segment to the element internal force vector is.

$$\int_V \mathbf{B}_{Rein}^T \boldsymbol{\sigma} dV = \mathbf{F}_{rein} \quad (2.20)$$

where $\boldsymbol{\sigma}$ is the stress tensor at the reinforcement integration point as defined in (2.18).

When we substitute the integrals in the Eq. (2.19) and Eq. (2.20) by numerical integrations, the contribution of a reinforcement segment to the element stiffness matrix and the element internal force vector can be expressed as:

$$\sum_{j=1}^{Nip} \mathbf{B}_{Rein}^j{}^T \mathbf{D} \mathbf{B}_{Rein}^j \det \mathbf{J}^j \quad (2.21)$$

$$\sum_{j=1}^{Nip} \mathbf{B}_{Rein}^j{}^T \boldsymbol{\sigma} \det \mathbf{J}^j \quad (2.22)$$

where, Nip represents the number of integration points at the reinforcement segment.

2-4 Reinforcement in Plane Strain Element

2-4-1 Bar in Plane Strain Element

In a plane strain element the bar reinforcement can be inserted as a point shape as illustrated in Fig. 2-(6).

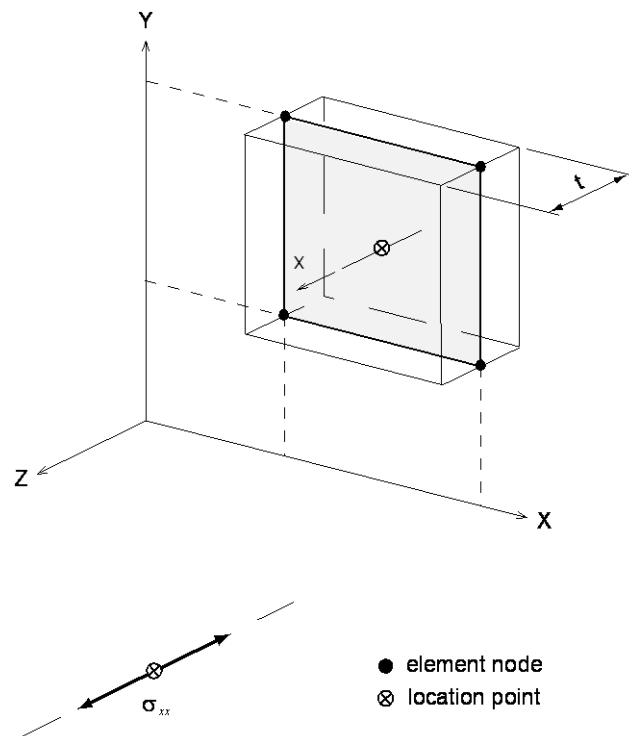


Figure 2-(6) BAR in plane strain element

In a plane strain element the bar reinforcement is defined by a single location point and therefore

a division of the bar into sections or particles is not necessary.

Fig. 2-(7) (a) shows a bar reinforcement inserted into a higher order plane strain element. Fig. 2-(7) (b) shows a number of BAR reinforcements inserted into plane strain elements 1, 2, 3 and 4.

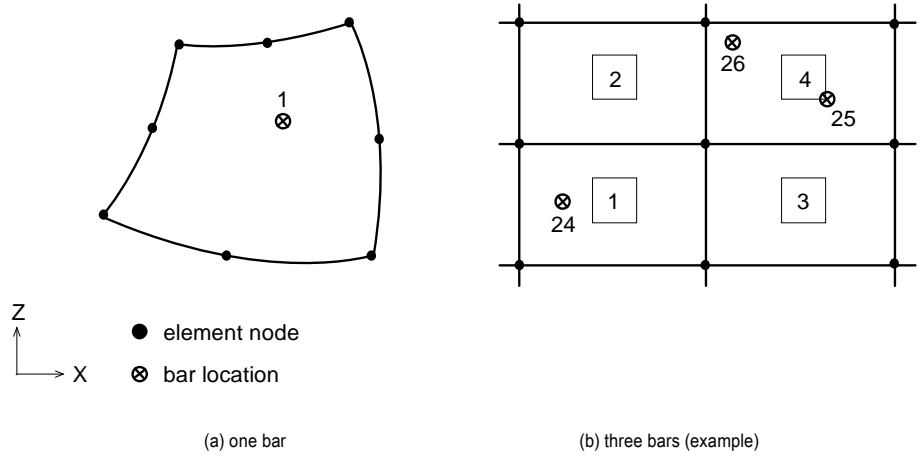


Figure 2-(7) Bar location points in plane strain elements

A bar reinforcement in a plane strain elements has a single strain component, ϵ_{xx} and a single stress component, σ_{xx} in the axial direction..

2-4-2 Grid in Plane Strain Element

In a plane strain element a reinforcement grid can be inserted as a 2 or 3 points line. Note that the definition of a grid reinforcement for plane strain elements differs from that for plane stress elements. Because plane strain elements are used for structures with an infinite thickness, the grid is expanded in a perpendicular direction to the element.

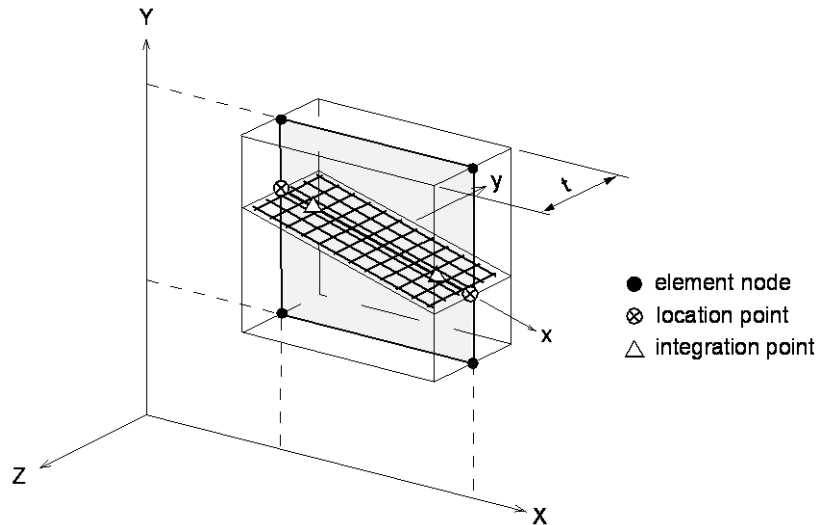


Figure 2-(8) Grid segment in plane strain element

Numerical integration is performed along the line of the grid reinforcement. A grid reinforcement inserted into plane strain elements has two strain components, ε_{xx} and ε_{yy} and two stress components, σ_{xx} and σ_{yy} . In plane strain elements the x-axis of grid reinforcement is by default defined as the tangential direction of the line shape. In contrary to other element types, the x-axis of grid reinforcement in a plane strain element cannot be defined in a different direction than the default direction. For a grid reinforcement in a plane strain element different thicknesses and Young's moduli may be specified in the x-axis and y-axis directions.

In plane strain elements a grid reinforcement is defined as a line, which is subsequently divided into sections by the Auto-mesh function. And the sections are divided into reinforcement segments which are one-to-one related to individual plane strain elements. The shapes of reinforcement sections are defined by the location points and shape functions of the lines. Fig. 2-(9) shows the grid sections of plane strain elements, which can be input in midas FEA. The fish bone like shape represents that the line is extruded to a plane in the plane strain elements.

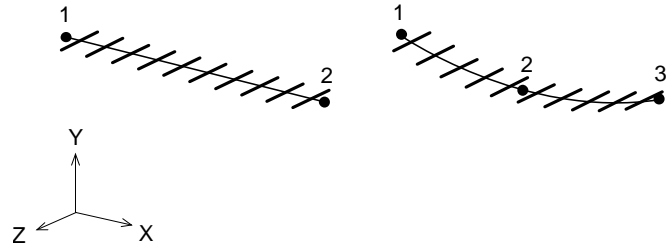


Figure 2-(9) Grid sections with reinforcement nodes

Fig. 2-(10) shows how a grid reinforcement is divided into section 1 and section 2. Section 1 is a higher order section, and section 2 is a lower order section. For each section the intersection points with the boundaries of the plane strain elements are calculated and by this operation the sections are divided into segments which each of them matches to 1 element. The location points are defined at the intersections with elements. For the higher order sections also location points are defined in the middle of each segment.

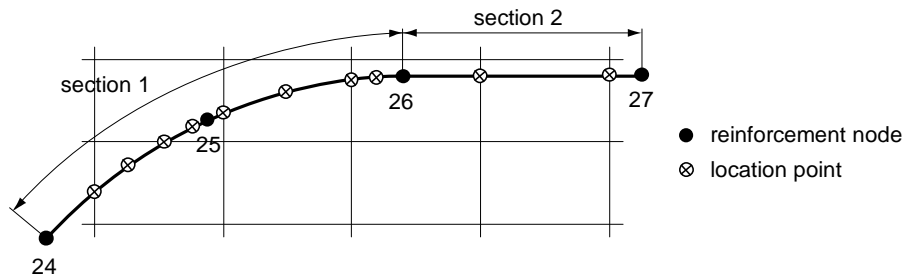


Figure 2-(10) GRID sections in plane strain elements

In case of local reinforcement definitions the sections are defined as segments. That means each section is defined such that it does not cross the element boundaries. In that case a section can be directly connected to one element.

Fig. 2-(11) shows the two possible reinforcement sections for a grid in a plane strain element.

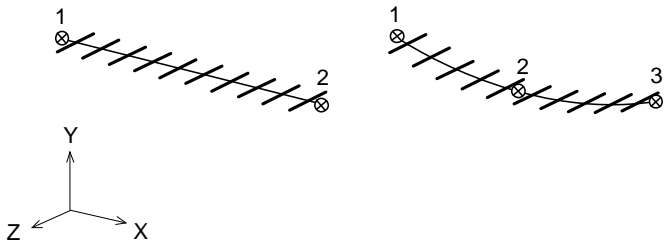


Figure 2-(11) Grid segments with location points in plane strain elements

Fig. 2-(12) shows how the 2 sections in Fig. 2-(10) are defined in segments which each have their location points.

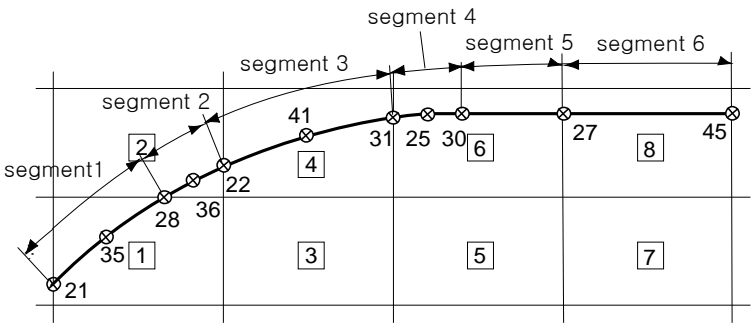


Figure 2-(12) Grid segments in plane strain elements

2-5 Reinforcement in Axisymmetric Element

2-5-1 Bar in Axisymmetric Element

In axisymmetric elements a bar reinforcement can be inserted by defining a single point location as illustrated in Fig. 2-(13).

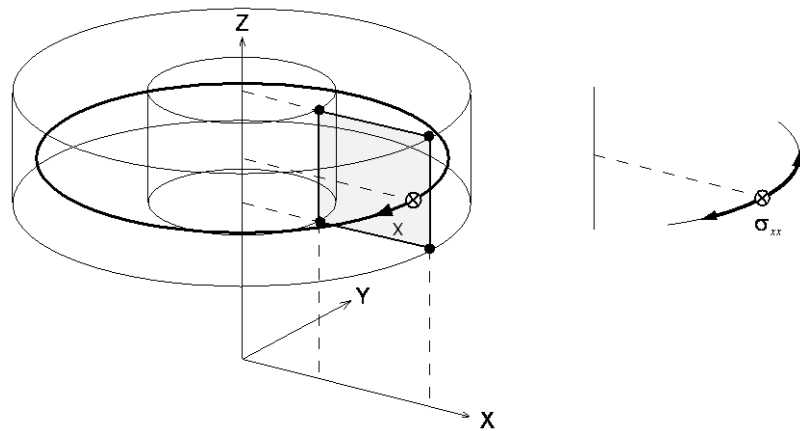


Figure 2-(13) BAR in axisymmetric element

A bar reinforcement in an axisymmetric element is oriented in the circumferential direction and has a constant cross section. The bar reinforcement cannot be divided into sections..

Fig. 2-(14) (a) shows a bar reinforcement inserted into a higher order axisymmetric element. Fig. 2-(14) (b) shows a number of BAR reinforcements inserted into axisymmetric elements 1, 2, 3 and 4.

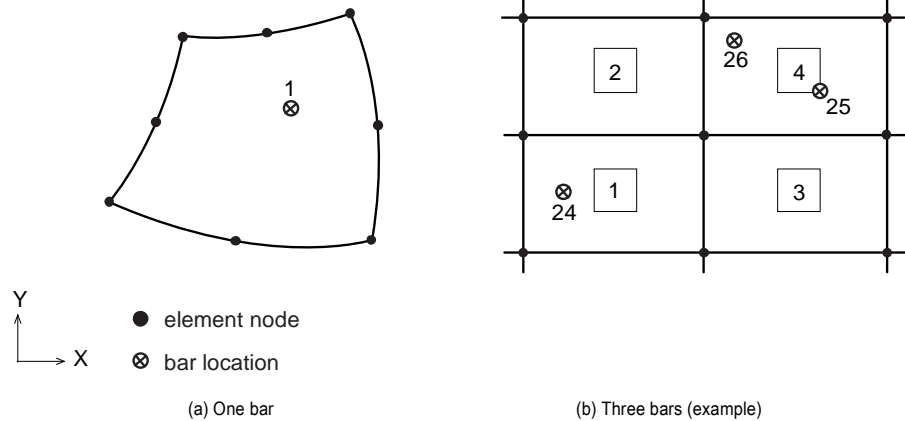


Figure 2-(14) Bar location points in axisymmetric elements

A bar reinforcement in an axisymmetric element has a single strain component, ε_{xx} and a single stress component, σ_{xx} . The strain in the bar reinforcement is related to the displacements in the nodes of the mother element.

2-5-2 Grid in Axisymmetric Element

In every type of axisymmetric element grid reinforcement can be inserted and grids can be defined by 2 or 3 points. The definition of grid reinforcement in axisymmetric elements is similar to grid reinforcement in plane strain elements. Axisymmetric elements are symmetric around the GCS Z-axis. Fig. 2-15 shows a grid reinforcement embedded in an axisymmetric element and both the element and the grid are rotated in the circumferential direction.

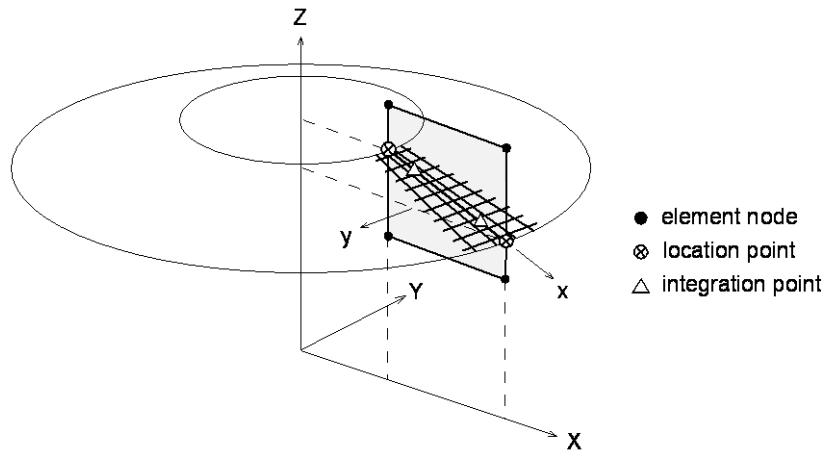


Figure 2-(15) Grid section in axisymmetric element

Numerical integration is performed along the line of the grid reinforcement. At each integration point of the grid reinforcement segment in an axisymmetric element two strain components, ε_{xx} and ε_{yy} and two stress components, σ_{xx} and σ_{yy} are defined. The x-axis of a grid reinforcement in an axisymmetric element is by default set to the direction tangential to the line of the grid section in the plane of the element which is always defined in the GCS XZ-plane in midas FEA. In contrary to other element types, the x-axis of a grid reinforcement in an axisymmetric element cannot be defined in a different direction than the default direction..

A grid reinforcement in axisymmetric elements is defined by a line geometry which is subsequently divided into reinforcement sections by the Auto-mesh function. The divided reinforcement sections are defined by location points. The grid sections as displayed in Fig. 2-(16) can be defined for axisymmetric elements.

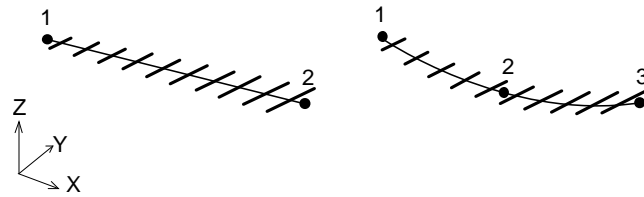


Figure 2-(16) Grid sections with nodes in axisymmetric elements

Fig. 2-(17) illustrates how a grid reinforcement can be composed of section 1 and section 2. In this figure section 1 is a higher order line, and section 2 is a lower order line. For each section the intersection points with the boundaries of the axisymmetric elements are calculated and by this operation the sections are divided into segments which each matches to 1 element. At the intersections location points are defined. For the higher order sections also location points are defined in the middle of each segment.

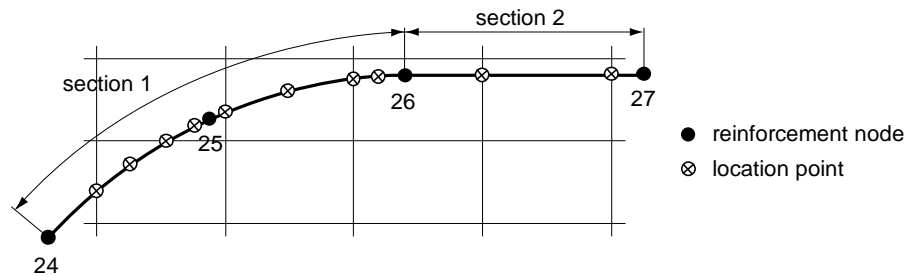


Figure 2-(17) Grid sections in axisymmetric elements

In case of local reinforcement definitions the sections are defined as segments. That means each section is defined such that it does not cross the element boundaries. In that case a section can be directly connected to 1 element.

Fig. 2-(18) shows the 2 possible reinforcement sections for a grid in an axisymmetric element.

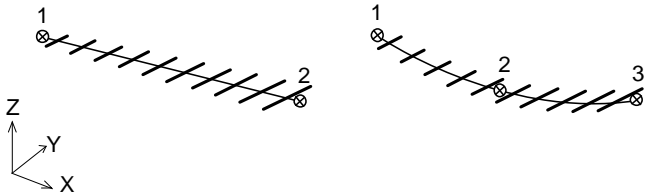


Figure 2-(18) Grid segments with location points in axisymmetric elements

Fig. 2-(19) shows the 2 sections in Fig. 2-(17) are defined in segments which each have their location points.

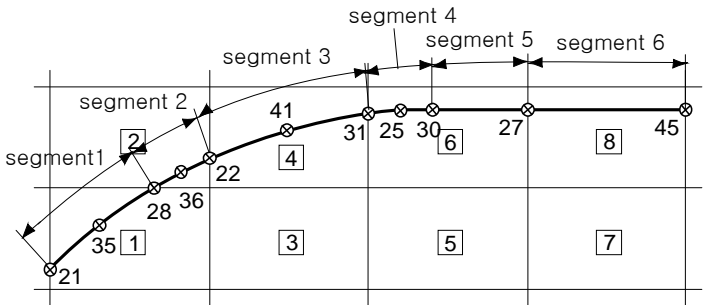


Figure 2-(19) Grid segments in Axisymmetric Elements

2-6 Reinforcement in Plane Stress Element

2-6-1 BAR in Plane Stress Element

In all plane stress element types bar reinforcement can be defined by 2 nodes or 3 nodes line sections. Fig. 2-(20) shows a line consisting of 2 sections, section 1 and section 2, which each are split into reinforcement segments such that a segment never crosses an edge of the mother element. Section 1 is a 3-noded higher line, and Section 2 is a 2-noded lower order line. The higher order section is divided into 3-point segments. Similarly the lower order section is divided into 2-point segments. The position of each segment is defined by location points.

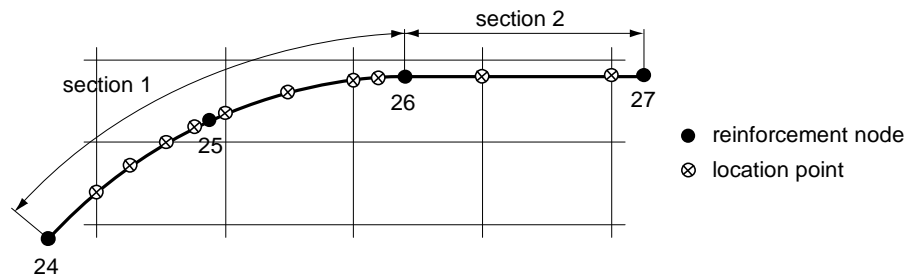


Figure 2-(20) Bar sections in plane stress elements

Fig. 2-(21) shows the mother elements and the bar reinforcement segments. The bar segment defined by the location points 28, 36 and 22 is located in the plane stress element No. 2. Since the section number 1 is a higher order line, the segment related to this section is also a higher order line. The segment defined by Location points 30 and 27 is a lower line because it is related to the section number 2 which is a lower order line.

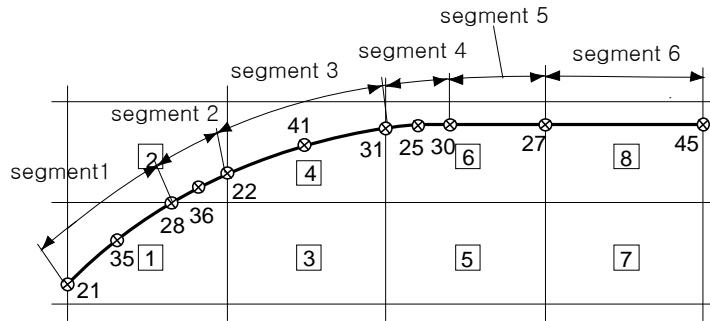


Figure 2-(21) Bar segments in plane stress elements

Fig. 2-(22) shows a bar reinforcement segment in an 8-node quadrilateral plane stress element. Each line segment has 2 integration points.

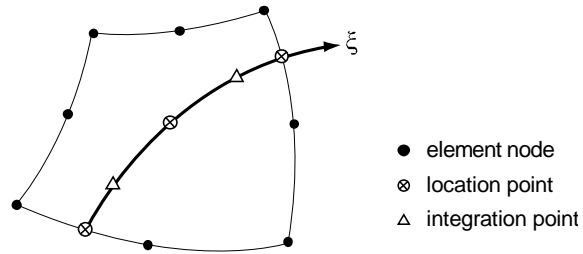


Figure 2-(22) Bar segment in plane stress element with integration points

The required properties for a bar reinforcement in plane stress elements consist of the cross section of the reinforcement bar and the Young's modulus..

2-6-2 Grid in Plane Stress Element

In all types of plane stress elements in midas FEA grid reinforcement can be inserted. The grid reinforcement sections can be defined by 3, 4, 6 or 8 points. The method of defining a grid reinforcement for plane stress elements is identical to that for bar reinforcement. In a plane stress

element a grid reinforcement always covers the full surface of the element.

The grid reinforcement will only be applied to those plane stress elements, which are fully covered by a grid reinforcement section.

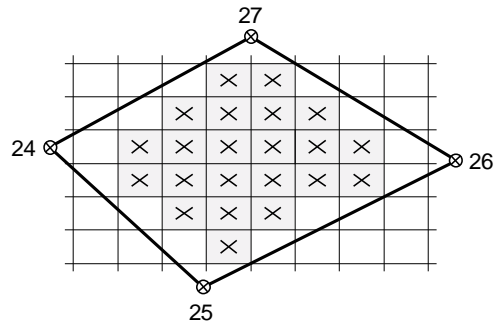


Figure 2-(23) Grid sections in plane stress elements

As shown in Fig. 2-(23), a quadrilateral grid reinforcement section is defined by the location point 24, 27, 25 and 26. The regular grid in the background is a mesh consisting of plane stress elements. Only the surfaces of the plane stress elements which are marked with an X will be covered by a grid reinforcement.

2-7 Reinforcement in Solid Element

2-7-1 Bar in Solid Element

In all solid element types bar reinforcement can be inserted by 2 or 3 nodes lines. A bar reinforcement may consist of one or more reinforcement sections. The user defines reinforcement sections, and in the pre-processing phase the intersections of the bar sections and the mother elements are calculated. Each section is divided into one or more reinforcement segments that are located in one mother element. In midas FEA a reinforcement bar can be defined by a geometrical line and by using the auto-mesh function the line can be divided into the reinforcement sections. The location of each reinforcement section is defined by 2 or 3 reinforcement nodes. The location of a reinforcement segment is defined by the location points. The location point coordinates are used to calculate the contribution of the bar-segment to the stiffness and internal forces of the mother element.

Fig. 2-(24) shows a bar reinforcement that consists of 2 reinforcement sections. The first section is defined by the reinforcement nodes 16, 27 and 28 and the section is defined by the reinforcement nodes 28 and 29. The first section is a higher order line, while the second section is a lower order line. The user can define the sections using the Auto-mesh function.

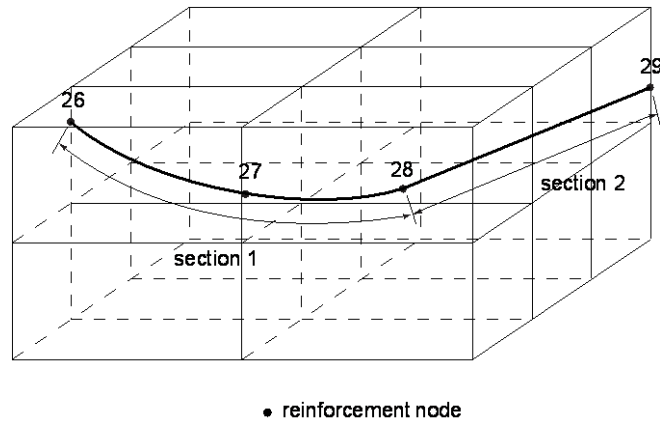


Figure 2-(24) Bar sections in solid elements

In Fig. 2-(25) the same mesh of solid elements and the same bar reinforcement are shown as in Fig. 2-(24), but now the bar reinforcement has been split into reinforcement segments. The section number 1 crosses the elements number 2 and 4 and therefore has been split into 2 segments. The section number 2 intersects the elements 4, 8 and 12 and therefore has to be split into 3 segments. Each segment of section 1 has 3 location points, because this is a higher order section and each segment of section 2 has 2 location points because this is a lower order section.

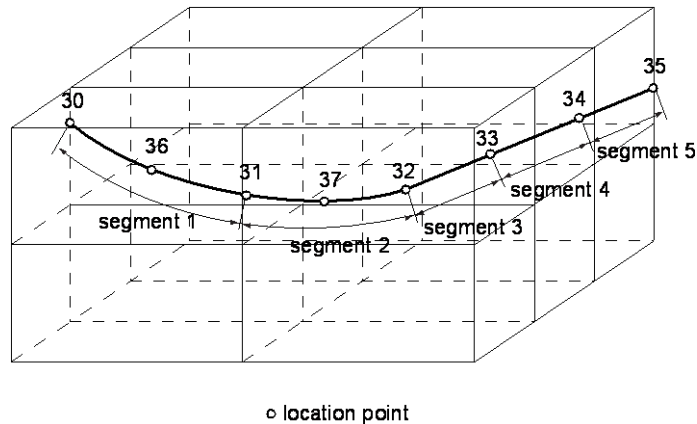


Figure 2-(25) Bar location points in solid elements

Fig. 2-(26) shows a bar reinforcement segment in a 20-node hexahedron solid element. Each line segment, both 2 nodes and 3 nodes types, has 2 integration points. The local x direction of the stress σ_{xx} and strain ϵ_{xx} at the integration points is tangential to the bar.

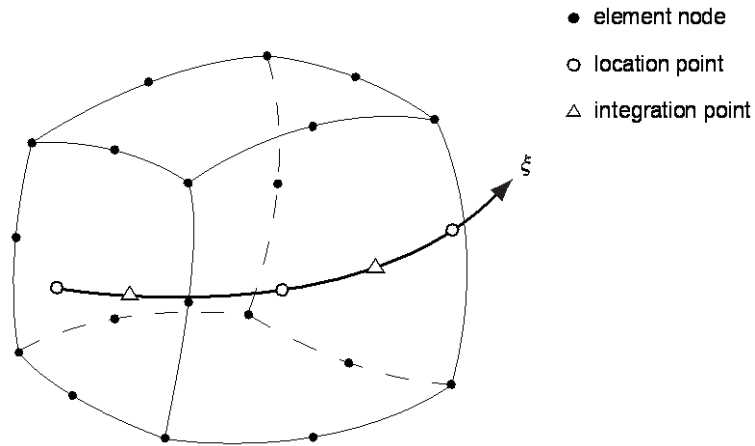
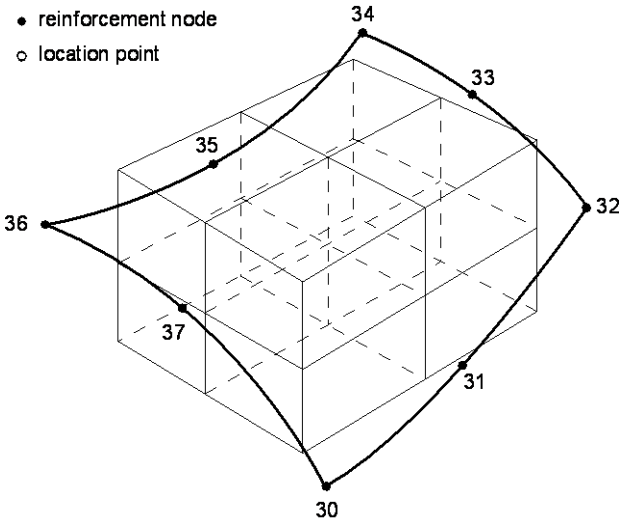


Figure 2-(26) BAR location points in solid element

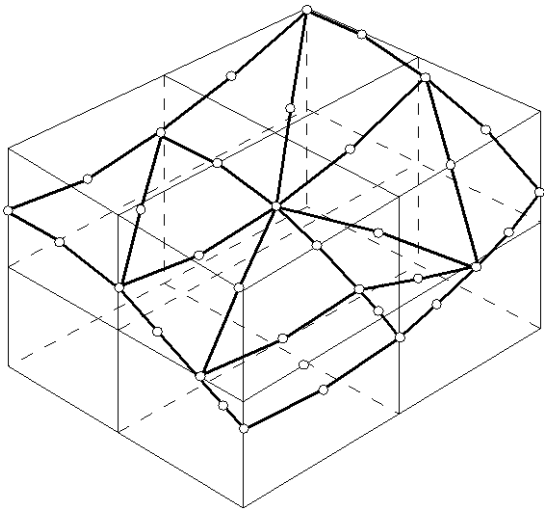
2-7-2 Grid in Solid Element

In all types of solid elements in midas FEA a grid reinforcement can be defined as 3 or 6-noded triangular grid or as 4 or 8-noded quadrilateral grid. A grid reinforcement is defined in a similar way as the bar reinforcement. A geometrical surface is defined as reference for the reinforcement grid. The grid reinforcement is divided into reinforcement sections using the Auto-mesh function. In the preprocessing phase the reinforcement sections are subsequently divided into grid reinforcement segments, which are defined such that each segment is always positioned within one single mother elements.

When a grid reinforcement is defined into solid elements, we can check whether the position of the grid is located inside the mother elements. If the grid reinforcement is not fully located within the mother elements, an error is logged and the program terminates the execution.



(a) Input a grid reinforcement into solid elements



(b) Generated location points of the grid segments

Figure 2-(27) Grid sections in solid elements

Fig. 2-(27) shows a mesh of solid elements and a quadrilateral, which is defined by the reinforcement nodes 30, 31, 32, 33, 34, 35, 36 and 37 for the definition of a grid reinforcement segment. In the preprocessing the grid segment is divided into triangular grid segments as shown in Fig. 2-(27) (b).

The user may also directly input the desired reinforcement segments without going through the division process in the preprocessing. In such a case, the user needs to define grid reinforcement sections corresponding to the target elements, thereby using the reinforcement sections as reinforcement segments.

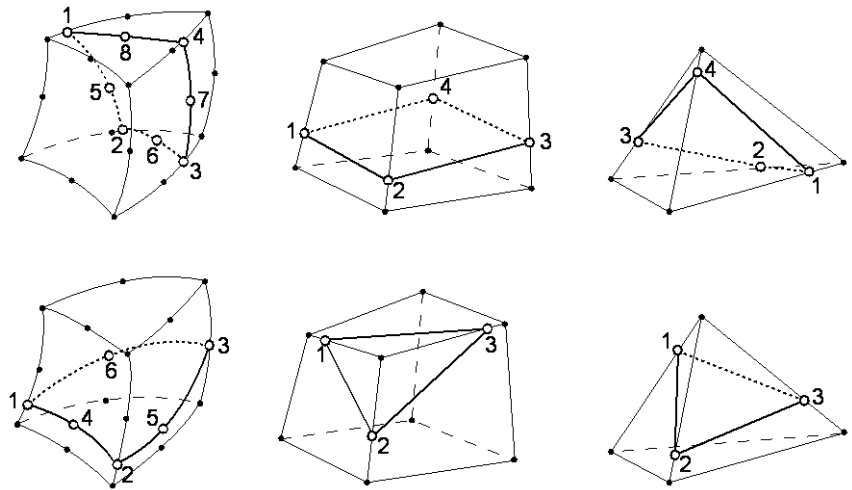


Figure 2-(28) Grid segments in solid elements

Fig. 2-(28) shows the possible combinations of grid reinforcement segments that may be coupled directly into elements. If reinforcement segments are created using the preprocessing, only triangular segments will be created. However, the user is free to input directly any type of segments.

In Fig. 2-(29) a grid reinforcement segment is located in a solid element and the x and y in the figure represent the local axes of the grid reinforcement segment.

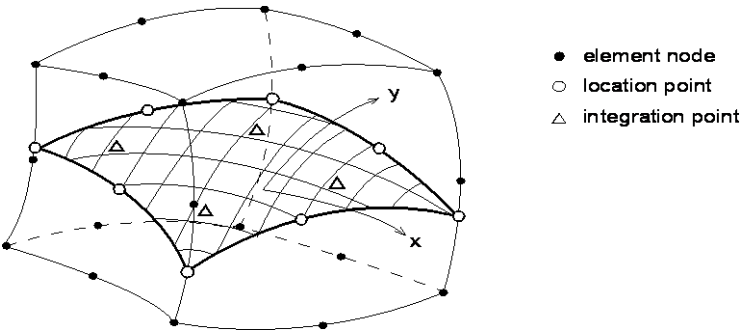


Figure 2-(29) Grid segment in a solid element

2-8 Reinforcement in Plate Element

2-8-1 Bar in Plate Element

In a curved or discrete plate elements a bar reinforcement section can be defined by a straight line with 2 points or a curved line with 3 points. The position of a bar reinforcement section is defined by reinforcement nodes. In the preprocessing phase the reinforcement section is split into bar-segments, which of them is positioned within 1 shell element. The position of a bar reinforcement segment is defined by location points.

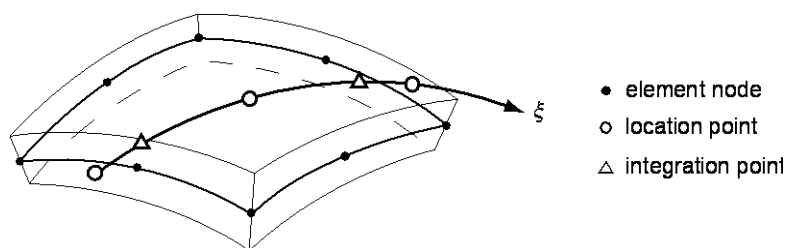


Figure 2-(30) Bar location points in plate element

In Fig. 2-(30) a Bar reinforcement segment inserted in a curved shell element is shown. The bar reinforcement segment is defined by 3 location points, and each bar segment has two integration points which are automatically calculated.

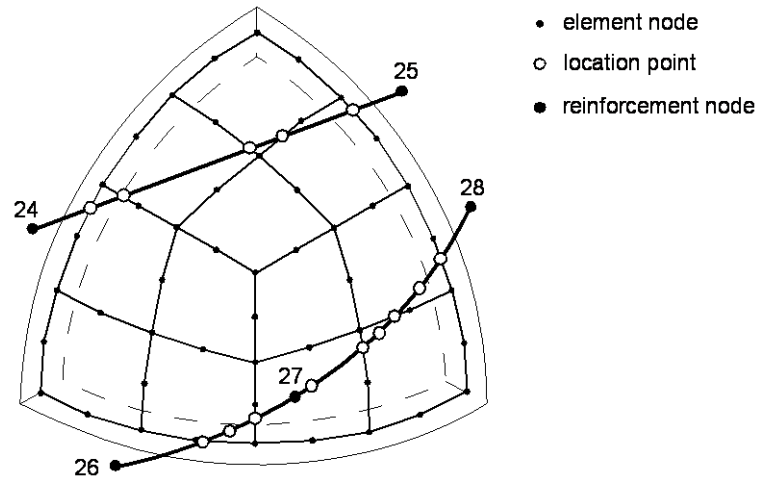


Figure 2-(31) Bar sections in mesh of curved plate elements

The user can input a bar reinforcement by defining a line in a 3-dimensional space. Fig. 2-(31) shows two bar sections that the first section is a straight line defined by nodes 24 and 25 and the second section is a curved line defined by the nodes 26, 27 and 28. These sections are intersected by the element boundaries and at the intersection points of the bar sections and element boundaries location points are generated. Each segment, split from sections, corresponds to one plate element. On the curved segments all location points are generated in the middle of each segment so that the curved shape of the section is transferred to the respective segment.

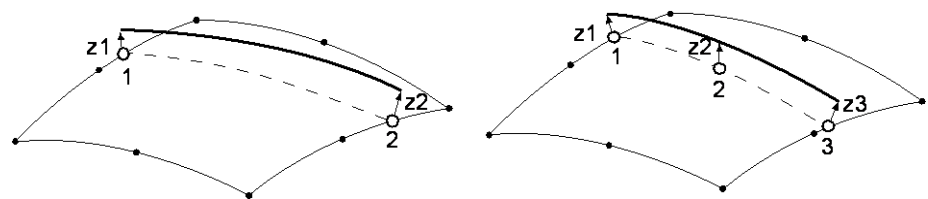


Figure 2-(32) Eccentricities for Bar location points in curved plate elements

Each location point is defined in the neutral plane of the respective plate element. In addition, the local-z coordinate in the ECS is kept for each location point. Figure 2-(32) illustrates the local z-coordinates of the location points of the bar segment as $z1$, $z2$ and $z3$. The local-z coordinate indicates the distance from the neutral plane of the plate element to the actual location of the reinforcement location point. The local-z coordinate is automatically calculated in the preprocessing when the bar segment is split into segments.

2-8-2 Grid in Plate Element

In a curved or discrete plate element a grid_reinforcement section can be defined as 3 or 6-noded triangular grid or as 4 or 8-noded quadrilateral grid.

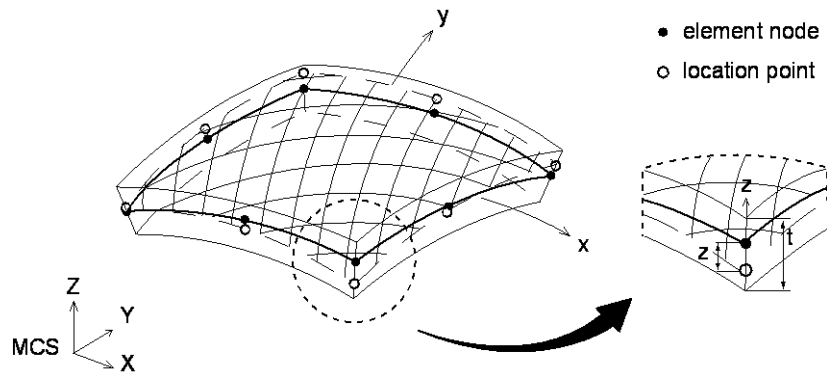


Figure 2-(33) Grid location points in curved plate element

In Fig. 2-(33) a grid reinforcement segment in a curved shell element is shown. For a grid reinforcement in a shell element two material models, isotropic linear elastic and orthotropic linear elastic, can be used. The orientation of the bars in the reinforcement grid is defined by the material axes as shown in Fig. 2-(33). The MCS, x and y axes are always orthogonal. In case of an orthotropic reinforcement grid, different thicknesses and modulus of elasticity in x and y direction of the Grid are defined.

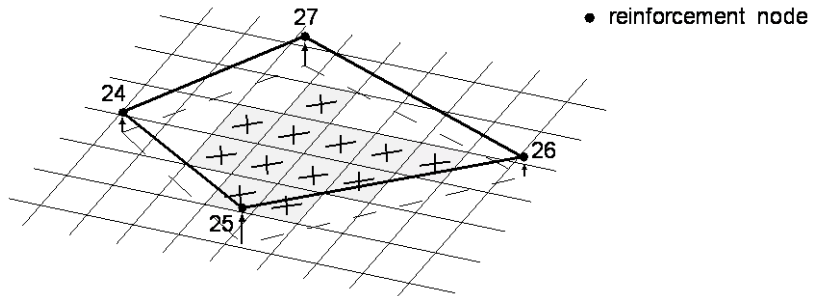


Figure 2-(34) Grid section in curved plate elements

In Fig. 2-(34) a quadrilateral grid reinforcement is defined by the reinforcement nodes 24, 25, 26 and 27. The Grid sections can be defined as a 3 or 6-noded triangle or a 4 or 8-noded quadrilateral. In Fig.2-(34) the grid section is divided into grid reinforcement segments such that only those elements that are fully covered by the grid section will contain a grid reinforcement segment. These plate elements are highlighted with gray shadow.

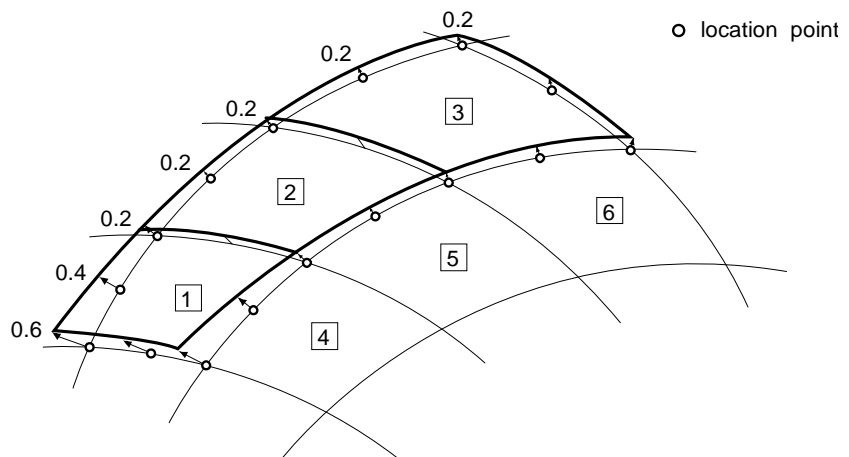
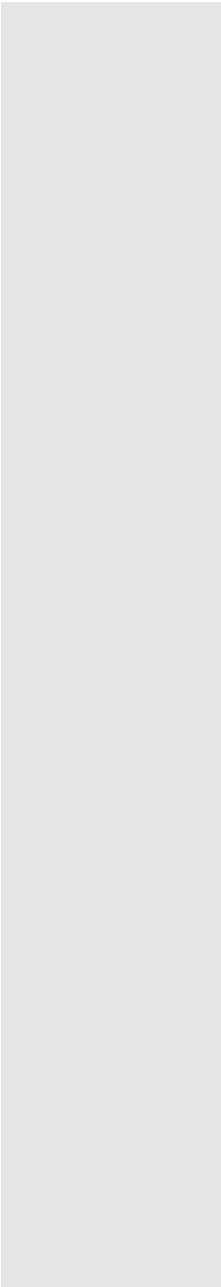


Figure 2-(35) Eccentricities for Grid in curved plate elements



Grid reinforcement segments are defined by the location points in the neutral plane of the plate elements. In addition to that a local-z component in ECS for each location point is calculated. This local-z coordinate is identical to that explained previously in Bar reinforcement. The element numbers 2 and 3 in Fig. 2-(35) retain equal local-z coordinates in all location points. The local z coordinates of the location points in element number 1 varies from 0.2-0.6.

2-9 Prestress of Reinforcement

2-9-1 Overview

Two types of Bar reinforcement exist, reinforcement and tendon. The reinforcement type is used for reinforcement in structures, and the tendon type is used to represent tendons to which prestress is applied. Two types of prestress can be applied to a tendon. One is the uniform prestress type in which a constant value of the prestress is applied to the entire tendon, and the other is the post-tension type, which accounts for prestress losses due to friction, etc.

2-9-2 Uniform Prestress Reinforcement

For uniform prestress reinforcement, different prestress values can be applied to each axis of the grid, and a single prestress can be applied to the bar.

2-9-3 Post-tensioned Reinforcement

(1) Loss of Prestress

Tendon prestress forces are generally introduced to tendons by jacking forces at each end of the tendon, whereas the prestress forces applied to the tendons are reduced by prestress losses, which are caused by several factors.

Tendons placed in curvature induce prestress losses due to the curvature effect, which is referred to as friction loss due to curvature. Apart from this, prestress losses due to the wobble effect exist. Even after the tendons are tensioned and friction losses take place, movement of the anchorage device induces tension losses.

Midas FEA finds such tension losses through modeling the tendons and concrete.

(2) Friction Losses

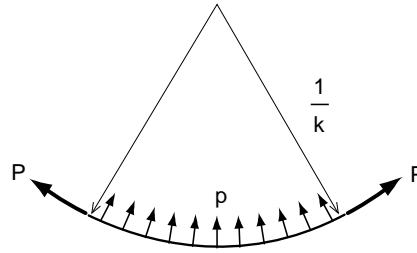


Figure 2-(36) Pressure exerted onto concrete by curved tendon

Prestress losses take place due to friction between the tendons and the surrounding sheathing. The friction is classified into the curvature friction due to the curvature of tendons and the wobble friction due to the length effect.

The curvature friction can be obtained as follows. The geometry of a tendon in a curved profile can be expressed in $x(r)$ with respect to the coordinate axis, r in the axial direction of the tendon. If an external force, P is applied to each end of the tendon, the following pressure, p is induced by the curvature.

$$p = \kappa P \quad (2.23)$$

where, κ represents the curvature, which is calculated as

$$\kappa = \left| \frac{\partial^2 x}{\partial r^2} \right| \quad (2.24)$$

The prestress loss due to the pressure, p per unit length can be found using the frictional coefficient, μ (/radian).

$$\frac{\partial P}{\partial r} = \mu P \quad (2.25)$$

In order to reflect the wobble (friction) effect, which stems from imperfect linear alignment of the sheathing, a fictitious curvature, ϕ_1 is introduced, which is referred to as the wobble parameter. The reduction in prestress forces due to curvature can be expressed as:

$$\frac{\partial P}{\partial r} = -\mu \phi_1 P \quad (2.26)$$

Prestress loss at a particular location can be obtained by integration in the axial direction starting from the anchorage where the prestressing is applied.

$$\Delta P = \int \frac{\partial P}{\partial r} dr \quad (2.27)$$

If the tendon has uniform curvature, κ , and the prestressing force at the anchorage is P_0 , the prestress force at the location, Δr length away from the starting point is obtained as follows:

$$P(\Delta r) = P_0 e^{-(\kappa + \phi_1) \Delta r} \quad (2.28)$$

Eq. (2.28) can be written as

$$P(\Delta r) = P_0 e^{-\mu \Delta \phi} \quad (2.29)$$

where, $\Delta \phi$ represents the rotation angle between the vector in the axial direction at the starting point and the tangential vector at the location Δr away.

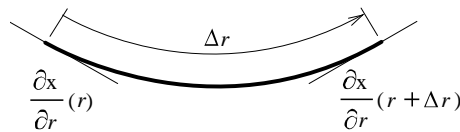


Figure 2-(37) Angular rotation of tendon curvature

$\Delta\phi$ used in Eq. (2.29) is as follows:

$$\Delta\phi = \Delta r(\phi_1 + \kappa) = \Delta r\phi_1 + \left| \Delta \frac{\partial x}{\partial r} \right| \quad (2.30)$$

Midas FEA finds the prestress forces, which reflect the losses using the jacking force at the anchorage, P_0 and the tendon properties, at each integration point of reinforcement.

(3) Slippage of Anchorage Device

Tendons are anchored by wedging at the anchorages. When the tendons are tensioned and released, inward slippage at the wedges takes place thus allowing the tendons to release slightly. If we assume that the length of this slippage is Δl , tension losses in the tendons in the vicinity of the anchorages take place. If we also assume that Δx is the length affected by the loss in prestress due to the penetration (slippage), we can derive an equilibrium equation.

$$\int_{\Delta x} \Delta P(r) dr = \Delta l EA \quad (2.31)$$

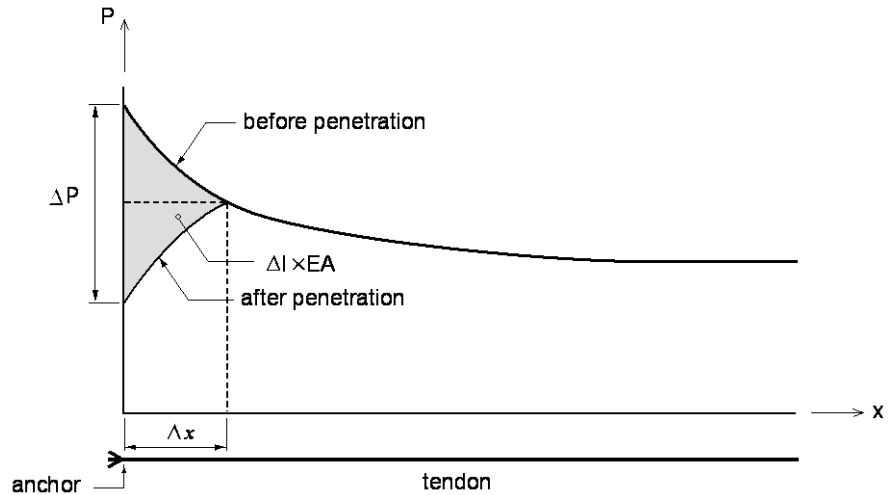


Figure 2-(38) Loss of prestress in anchored tendon

And the tendon prestress force is found, which satisfies Eq. (2.32) starting from the anchorage.

$$\int_L \Delta P(x) dr \geq \Delta IEA \quad (2.32)$$

The integration of Eq. (2.32) is performed by the trapezoidal rule. And the integration points, which satisfy the condition of Eq. (2.32), are found first. If the point satisfying the condition of Eq. (2.32) does not lie within the tendon, the process of calculating the tension loss in the tendon is not performed properly. If the tendon is prestressed from both ends simultaneously, the tendon stress is calculated in two steps reflecting the effect of tension losses at each end separately. Prestress losses are also individually calculated at each end at this time. Fig. 4 shows the prestress losses due to penetration (slippage) at the anchorages at both ends.

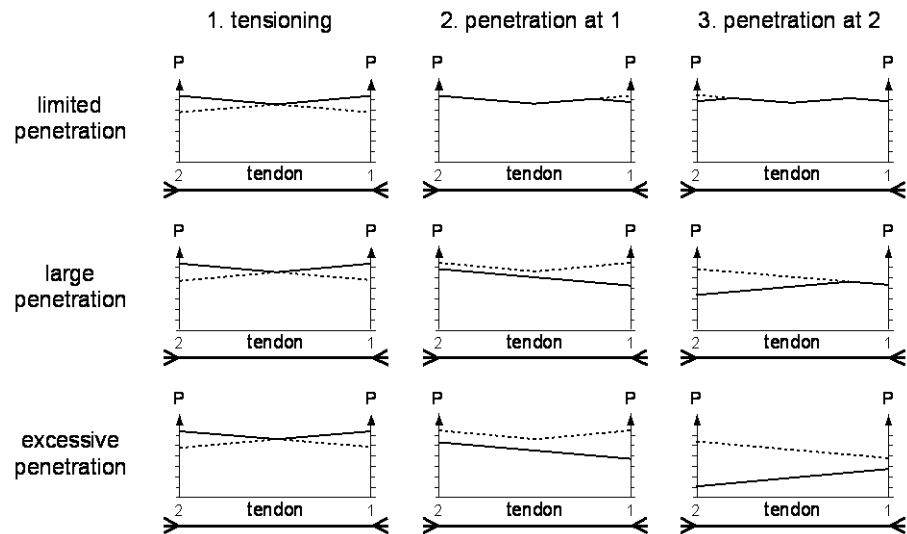


Figure 2-(39) Loss of prestress due to penetration of anchorages

Prestress forces resulting from jacking at the anchorage positions 1 and 2 in Fig. 2-(39) are calculated separately. The prestress forces at this time do not reflect the losses due to anchorage penetration. Once the prestress force distributions are obtained while reflecting the prestress losses due to the penetration of anchorages at each end separately, the two prestress force distributions are combined.

Chapter 3. Interface Elements

3-1 Introduction

Interface elements are used to model discrete cracks in materials or relative movements at the boundaries of model parts. Interface elements for instance can be used to account for discrete-cracking of concrete, bond-slip at the bonding face of a steel reinforcement bar and concrete and failure of mortar in a masonry wall.

Interface elements are defined by using the general finite element formulation, whereas the thickness of the elements is assumed to be zero. In order to define an interface element with zero-thickness from numerical analysis point of view, a penalty stiffness is assigned for the interface element. If the penalty stiffness is too high it might cause numerical problems and when the penalty stiffness is too low the interface may yield with undesired relative displacements from both sides of the interface element. The user should pay attention to a proper definition of the penalty stiffness. It is advised to choose the penalty stiffness as $\mathbf{k} = 1000 * \mathbf{E} * \mathbf{d}$, with \mathbf{E} being the highest Young's modulus of used in the finite element model and \mathbf{d} being a representative element size. The relationship between the relative displacement $\Delta \mathbf{u}$ and the traction \mathbf{t} is defined by equation (3.1).

$$\mathbf{t} = \mathbf{D} \cdot \Delta \mathbf{u} \quad (3.1)$$

\mathbf{t} , \mathbf{D} and $\Delta \mathbf{u}$ in a two-dimensional element are expressed in Eq. (3.2). The relative displacement and traction at one integration point on an interface are shown in Fig. 3-(1).

$$\mathbf{t} = \begin{Bmatrix} t_n \\ t_t \end{Bmatrix}, \quad \mathbf{D} = \begin{bmatrix} k_n & 0 \\ 0 & k_t \end{bmatrix}, \quad \Delta \mathbf{u} = \begin{Bmatrix} \Delta u_n \\ \Delta u_t \end{Bmatrix} \quad (3.2)$$

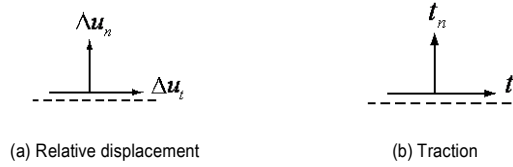


Figure 3-(1) Relative displacement and traction in 2-D

In a three-dimensional case, the same components are given by Eq. (3.3) and shown in Fig. 3-(2).

$$\mathbf{t} = \begin{Bmatrix} t_n \\ t_s \\ t_t \end{Bmatrix}, \mathbf{D} = \begin{bmatrix} k_n & 0 & 0 \\ 0 & k_s & 0 \\ 0 & 0 & k_t \end{bmatrix}, \Delta \mathbf{u} = \begin{Bmatrix} \Delta u_n \\ \Delta u_s \\ \Delta u_t \end{Bmatrix} \quad (3.3)$$

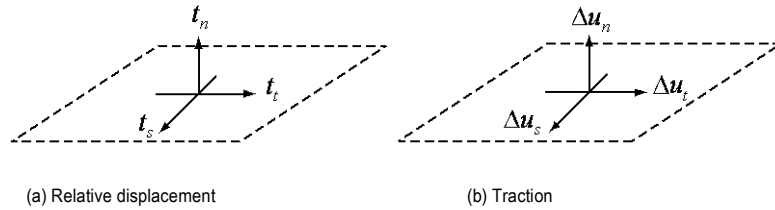


Figure 3-(2) Relative displacement and traction in 3-D

The dotted lines represent the interface surface. t_n denotes the normal traction and t_s and t_t denote the tangential tractions. Δu_n denotes the normal relative displacement and Δu_s and Δu_t denote the tangential relative displacements. Please note that in the linear constitutive equations (3.2) and (3.3) the relations between relative displacements and traction for each of the directions are fully uncoupled i.e. the normal traction does not have any influence on the stiffness in the tangential direction.

3-2 Coordinate System and Relative Displacement

The relative displacement vector $\Delta \mathbf{u}$ at an integration point of an interface element is computed by using the displacements of the nodes of the element at the top and the bottom faces. For this, the displacements at the top nodes of the interface element are given by:

$$\mathbf{u}_i^{top} = \{u_i^{top} \quad v_i^{top} \quad w_i^{top}\}^T \quad (3.4)$$

The translational displacements u , v and w and the coordinates x , y and z within the element are expressed as:

$$\begin{aligned} x^{top} &= \sum_{i=1}^N N_i^{top} x_i^{top}, \quad y^{top} = \sum_{i=1}^N N_i^{top} y_i^{top}, \quad z^{top} = \sum_{i=1}^N N_i^{top} z_i^{top} \\ u^{top} &= \sum_{i=1}^N N_i^{top} u_i^{top}, \quad v^{top} = \sum_{i=1}^N N_i^{top} v_i^{top}, \quad w^{top} = \sum_{i=1}^N N_i^{top} w_i^{top} \end{aligned} \quad (3.5)$$

The displacements and coordinates at the bottom of the interface element can be expressed in the same way. The Eq. (3.6) and (3.7) are identical to Eq. (3.4) and (3.5) except that the superscript “top” is replaced with “bot”.

$$\mathbf{u}_i^{bot} = \{u_i^{bot} \quad v_i^{bot} \quad w_i^{bot}\}^T \quad (3.6)$$

$$\begin{aligned} x^{bot} &= \sum_{i=1}^N N_i^{bot} x_i^{bot}, \quad y^{bot} = \sum_{i=1}^N N_i^{bot} y_i^{bot}, \quad z^{bot} = \sum_{i=1}^N N_i^{bot} z_i^{bot} \\ u^{bot} &= \sum_{i=1}^N N_i^{bot} u_i^{bot}, \quad v^{bot} = \sum_{i=1}^N N_i^{bot} v_i^{bot}, \quad w^{bot} = \sum_{i=1}^N N_i^{bot} w_i^{bot} \end{aligned} \quad (3.7)$$

The nodal displacements are defined in the element local coordinate system ECS. However, the relative displacements and tractions at the integration points are defined in the normal and

tangential directions of the interface element. In addition, the constitutive relation of the interface is defined in this system. Since interface elements do not transmit rotational stiffness, only the relative displacements in ECS are used to calculate the relative displacements as illustrated in Eq. (3.8).

$$\Delta \mathbf{u} = \mathbf{u}^{top} - \mathbf{u}^{bot} \quad (3.8)$$

where,

$$\mathbf{u}^{top} = \{u_n^{top} \quad u_s^{top} \quad u_t^{top}\}^T$$

$$\mathbf{u}^{bot} = \{u_n^{bot} \quad u_s^{bot} \quad u_t^{bot}\}^T$$

The following condition applies to all interface elements in FEA due to equality in number of nodes at each side of the element.

$$\mathbf{N}^{bot} = \mathbf{N}^{top}.$$

The matrix B which is used to calculate the relative displacements in the integration points from the displacements in the nodes.

$$\Delta \mathbf{u} = \mathbf{B} \mathbf{u} \quad (3.9)$$

where,

$$\mathbf{B} = [\mathbf{N}^{bot} \quad \mathbf{N}^{top}]$$

$$\mathbf{u} = \{\mathbf{u}^{bot} \quad \mathbf{u}^{top}\}^T$$

3-3 Point Interface Element

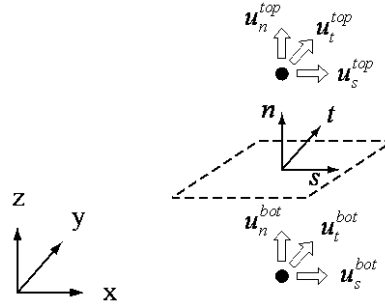


Figure 3-(3) Point interface element

A point interface element is defined by the top and bottom nodes and the element axes at the boundary surface as shown in Fig. 3-(3). Since the top and bottom nodes of the element can be defined at the same position, the user must directly assign the element axes of the boundary surface. Fig. 3-(3) shows the two nodes separately for the sake of clarity in explanation. The user should be aware that the interface element axes are determined by the user-defined element x-axis. That is, the normal n and tangential directions t and s of the axes of the interface element are determined by the x, y and z axes of the element respectively. The element local x axis is assigned in the direction from the bottom node to the top node.

In general the global coordinates of a point in an element are defined by using the shape function (N_i) as follows:

$$\begin{aligned} x^{bot} &= N_1^{bot} \cdot x_1^{bot} \\ x^{top} &= N_2^{top} \cdot x_2^{top} \end{aligned} \quad (3.10)$$

The total displacements at a point are defined by the isoparametric shape function as follows:

$$\begin{aligned} u^{bot} &= N_1^{bot} \cdot u_1^{bot} \\ u^{top} &= N_2^{top} \cdot u_2^{top} \end{aligned} \quad (3.11)$$

For a point interface element the isoparametric shape function is defined as one.

$$N_1^{bot} = N_2^{top} = 1 \quad (3.12)$$

The relative displacement-element displacement matrix can be thus expressed as:

$$\mathbf{B} = \begin{bmatrix} -N_1^{bot} & 0 & 0 & N_2^{top} & 0 & 0 \end{bmatrix} \quad (3.13)$$

3-4 Line Interface Element

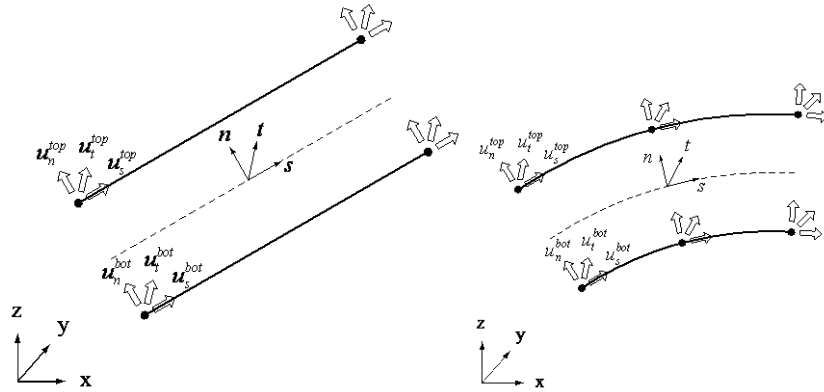


Figure 3-(4) Line interface element

Midas FEA provides line interface elements with lower order and higher order interpolation functions as shown in Fig. 3-(4). The line interface elements can be used to connect plane elements as well as to connect plane elements and line elements.

The stiffness matrix \mathbf{D} is identical to Eq. (3.2).

The global coordinate of a point in a line interface element is defined by using the shape function as follows:

$$x^{bot} = N_1^{bot} \cdot x_1^{bot} + N_2^{bot} \cdot x_2^{bot} (+N_5^{bot} \cdot x_5^{bot})$$

$$x^{top} = N_3^{top} \cdot x_3^{top} + N_4^{top} \cdot x_4^{top} (+N_6^{top} \cdot x_6^{top})$$

$$\begin{aligned}
 y^{bot} &= N_1^{bot} \cdot y_1^{bot} + N_2^{bot} \cdot y_2^{bot} (+N_5^{bot} \cdot y_5^{bot}) \\
 y^{top} &= N_3^{top} \cdot y_3^{top} + N_4^{top} \cdot y_4^{top} (+N_6^{top} \cdot y_6^{top})
 \end{aligned} \tag{3.14}$$

where, the coordinates in the parentheses represent the higher order element.

The total displacements at a point is given by

$$\begin{aligned}
 u^{bot} &= N_1^{bot} \cdot u_1^{bot} + N_2^{bot} \cdot u_2^{bot} (+N_5^{bot} \cdot u_5^{bot}) \\
 u^{top} &= N_3^{top} \cdot u_3^{top} + N_4^{top} \cdot u_4^{top} (+N_6^{top} \cdot u_6^{top}) \\
 v^{bot} &= N_1^{bot} \cdot v_1^{bot} + N_2^{bot} \cdot v_2^{bot} (+N_5^{bot} \cdot v_5^{bot}) \\
 v^{top} &= N_3^{top} \cdot v_3^{top} + N_4^{top} \cdot v_4^{top} (+N_6^{top} \cdot v_6^{top})
 \end{aligned} \tag{3.15}$$

The isoparametric shape function for a lower order line interface element is defined by

$$\begin{aligned}
 N_1^{bot}(\xi) &= N_3^{top}(\xi) = \frac{1}{2}(1 - \xi), \\
 N_2^{bot}(\xi) &= N_4^{top}(\xi) = \frac{1}{2}(1 + \xi)
 \end{aligned} \tag{3.16}$$

and eq. (3.17) is expressed for the higher order element.

$$\begin{aligned}
 N_1^{bot}(\xi) &= N_3^{top}(\xi) = -\frac{1}{2}(1 - \xi)\xi, \\
 N_2^{bot}(\xi) &= N_4^{top}(\xi) = \frac{1}{2}(1 + \xi)\xi, \\
 N_5^{bot}(\xi) &= N_6^{top}(\xi) = (1 - \xi^2)
 \end{aligned} \tag{3.17}$$

(5 and 6 nodes represent the higher order elements of 2-D line interface elements.)

The relative displacement-element displacement matrix **B** can be expressed considering the difference between the normal-tangential direction and the element coordination system.

3-5 Surface Interface Element

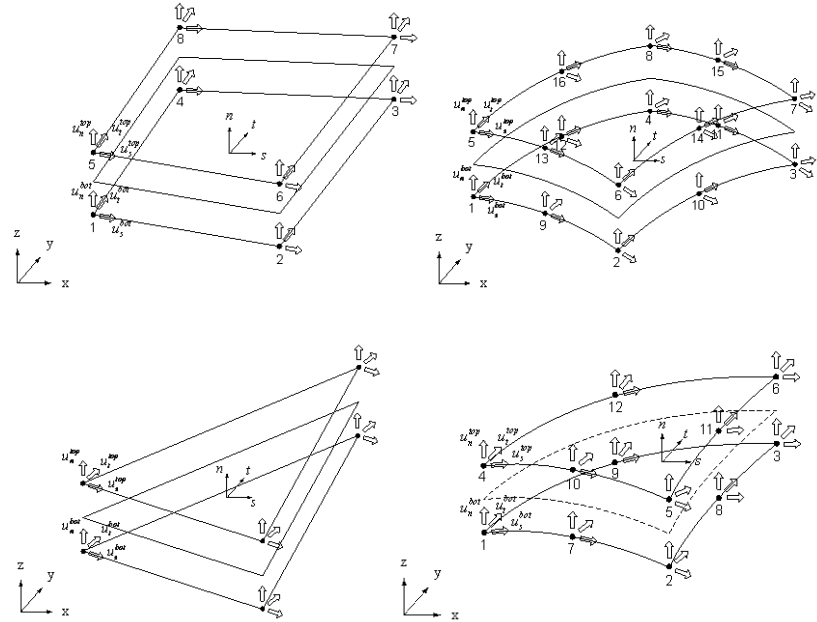


Figure 3-5) Surface interface element

Midas FEA provides surface interface elements, which are lower and higher order triangular and quadrilateral elements as shown in Fig. 3-5). The surface interface elements are used to analyze the interface behavior between solid elements or between shell and solid elements.

The global coordinates of an arbitrary point in a quadrilateral interface element are defined by the shape function as expressed in Eq. (3.18)

$$x^{bot} = N_1^{bot} \cdot x_1^{bot} + N_2^{bot} \cdot x_2^{bot} + N_3^{bot} \cdot x_3^{bot} + N_4^{bot} \cdot x_4^{bot} \\ (+ N_9^{bot} \cdot x_9^{bot} + N_{10}^{bot} \cdot x_{10}^{bot} + N_{11}^{bot} \cdot x_{11}^{bot} + N_{12}^{bot} \cdot x_{12}^{bot})$$

$$\begin{aligned}
x^{top} &= N_5^{top} \cdot x_5^{top} + N_6^{top} \cdot x_6^{top} + N_7^{top} \cdot x_7^{top} + N_8^{top} \cdot x_8^{top} \\
&\quad (+N_{13}^{top} \cdot x_{13}^{top} + N_{14}^{top} \cdot x_{14}^{top} + N_{15}^{top} \cdot x_{15}^{top} + N_{16}^{top} \cdot x_{16}^{top}) \\
y^{bot} &= N_1^{bot} \cdot y_1^{bot} + N_2^{bot} \cdot y_2^{bot} + N_3^{bot} \cdot y_3^{bot} + N_4^{bot} \cdot y_4^{bot} \\
&\quad (+N_9^{bot} \cdot y_9^{bot} + N_{10}^{bot} \cdot y_{10}^{bot} + N_{11}^{bot} \cdot y_{11}^{bot} + N_{12}^{bot} \cdot y_{12}^{bot}) \\
y^{top} &= N_5^{top} \cdot y_5^{top} + N_6^{top} \cdot y_6^{top} + N_7^{top} \cdot y_7^{top} + N_8^{top} \cdot y_8^{top} \\
&\quad (+N_{13}^{top} \cdot y_{13}^{top} + N_{14}^{top} \cdot y_{14}^{top} + N_{15}^{top} \cdot y_{15}^{top} + N_{16}^{top} \cdot y_{16}^{top}) \\
z^{bot} &= N_1^{bot} \cdot z_1^{bot} + N_2^{bot} \cdot z_2^{bot} + N_3^{bot} \cdot z_3^{bot} + N_4^{bot} \cdot z_4^{bot} \\
&\quad (+N_9^{bot} \cdot z_9^{bot} + N_{10}^{bot} \cdot z_{10}^{bot} + N_{11}^{bot} \cdot z_{11}^{bot} + N_{12}^{bot} \cdot z_{12}^{bot}) \\
z^{top} &= N_5^{top} \cdot z_5^{top} + N_6^{top} \cdot z_6^{top} + N_7^{top} \cdot z_7^{top} + N_8^{top} \cdot z_8^{top} \\
&\quad (+N_{13}^{top} \cdot z_{13}^{top} + N_{14}^{top} \cdot z_{14}^{top} + N_{15}^{top} \cdot z_{15}^{top} + N_{16}^{top} \cdot z_{16}^{top})
\end{aligned} \tag{3.18}$$

The total displacements of an arbitrary point in a quadrilateral element are defined by using the isoparametric shape function as expressed in Eq. (3.19)

$$\begin{aligned}
u^{bot} &= N_1^{bot} \cdot u_1^{bot} + N_2^{bot} \cdot u_2^{bot} + N_3^{bot} \cdot u_3^{bot} + N_4^{bot} \cdot u_4^{bot} \\
&\quad (+N_9^{bot} \cdot u_9^{bot} + N_{10}^{bot} \cdot u_{10}^{bot} + N_{11}^{bot} \cdot u_{11}^{bot} + N_{12}^{bot} \cdot u_{12}^{bot}) \\
u^{top} &= N_5^{top} \cdot u_5^{top} + N_6^{top} \cdot u_6^{top} + N_7^{top} \cdot u_7^{top} + N_8^{top} \cdot u_8^{top} \\
&\quad (+N_{13}^{top} \cdot u_{13}^{top} + N_{14}^{top} \cdot u_{14}^{top} + N_{15}^{top} \cdot u_{15}^{top} + N_{16}^{top} \cdot u_{16}^{top}) \\
v^{bot} &= N_1^{bot} \cdot v_1^{bot} + N_2^{bot} \cdot v_2^{bot} + N_3^{bot} \cdot v_3^{bot} + N_4^{bot} \cdot v_4^{bot} \\
&\quad (+N_9^{bot} \cdot v_9^{bot} + N_{10}^{bot} \cdot v_{10}^{bot} + N_{11}^{bot} \cdot v_{11}^{bot} + N_{12}^{bot} \cdot v_{12}^{bot}) \\
v^{top} &= N_5^{top} \cdot v_5^{top} + N_6^{top} \cdot v_6^{top} + N_7^{top} \cdot v_7^{top} + N_8^{top} \cdot v_8^{top} \\
&\quad (+N_{13}^{top} \cdot v_{13}^{top} + N_{14}^{top} \cdot v_{14}^{top} + N_{15}^{top} \cdot v_{15}^{top} + N_{16}^{top} \cdot v_{16}^{top}) \\
w^{bot} &= N_1^{bot} \cdot w_1^{bot} + N_2^{bot} \cdot w_2^{bot} + N_3^{bot} \cdot w_3^{bot} + N_4^{bot} \cdot w_4^{bot} \\
&\quad (+N_9^{bot} \cdot w_9^{bot} + N_{10}^{bot} \cdot w_{10}^{bot} + N_{11}^{bot} \cdot w_{11}^{bot} + N_{12}^{bot} \cdot w_{12}^{bot}) \\
w^{top} &= N_5^{top} \cdot w_5^{top} + N_6^{top} \cdot w_6^{top} + N_7^{top} \cdot w_7^{top} + N_8^{top} \cdot w_8^{top} \\
&\quad (+N_{13}^{top} \cdot w_{13}^{top} + N_{14}^{top} \cdot w_{14}^{top} + N_{15}^{top} \cdot w_{15}^{top} + N_{16}^{top} \cdot w_{16}^{top})
\end{aligned} \tag{3.19}$$

The isoparametric shape function of a 3-dimensional surface interface element is defined by the equations below.

The shape function of an 8-node interface element

$$\begin{aligned}
 N_1^{bot}(\xi, \eta) &= N_5^{top}(\xi, \eta) = \frac{1}{4}(1-\xi)(1-\eta), \\
 N_2^{bot}(\xi, \eta) &= N_6^{top}(\xi, \eta) = \frac{1}{4}(1+\xi)(1-\eta), \\
 N_3^{bot}(\xi, \eta) &= N_7^{top}(\xi, \eta) = \frac{1}{4}(1+\xi)(1+\eta), \\
 N_4^{bot}(\xi, \eta) &= N_8^{top}(\xi, \eta) = \frac{1}{4}(1-\xi)(1+\eta)
 \end{aligned} \tag{3.20}$$

The shape function of a 16-node interface element

$$\begin{aligned}
 N_1^{bot}(\xi, \eta) &= N_5^{top}(\xi, \eta) = \frac{1}{4}(1-\xi)(1-\eta)(-\xi-\eta-1), \\
 N_2^{bot}(\xi, \eta) &= N_6^{top}(\xi, \eta) = \frac{1}{4}(1+\xi)(1-\eta)(\xi-\eta-1) \\
 N_3^{bot}(\xi, \eta) &= N_7^{top}(\xi, \eta) = \frac{1}{4}(1+\xi)(1+\eta)(\xi+\eta-1) \\
 N_4^{bot}(\xi, \eta) &= N_8^{top}(\xi, \eta) = \frac{1}{4}(1-\xi)(1+\eta)(-\xi+\eta-1) \\
 N_9^{bot}(\xi, \eta) &= N_{13}^{top}(\xi, \eta) = \frac{1}{2}(1-\xi^2)(1-\eta), \\
 N_{10}^{bot}(\xi, \eta) &= N_{14}^{top}(\xi, \eta) = \frac{1}{2}(1+\xi)(1-\eta^2), \\
 N_{11}^{bot}(\xi, \eta) &= N_{15}^{top}(\xi, \eta) = \frac{1}{2}(1-\xi^2)(1+\eta),
 \end{aligned}$$

$$N_{12}^{bot}(\xi, \eta) = N_{16}^{top}(\xi, \eta) = \frac{1}{2}(1-\xi)(1-\eta^2) \quad (3.21)$$

The shape function of a 6-node triangular interface element

$$N_1^{bot}(\xi, \eta) = N_4^{top}(\xi, \eta) = 1 - \xi - \eta,$$

$$N_2^{bot}(\xi, \eta) = N_5^{top}(\xi, \eta) = \xi,$$

$$N_3^{bot}(\xi, \eta) = N_6^{top}(\xi, \eta) = \eta \quad (3.22)$$

The shape function of a 12-node triangular interface element

$$N_1^{bot}(\xi, \eta) = N_4^{top}(\xi, \eta) = (1 - 2\xi - 2\eta)(1 - \xi - \eta)$$

$$N_2^{bot}(\xi, \eta) = N_5^{top}(\xi, \eta) = (2\xi - 1)\xi$$

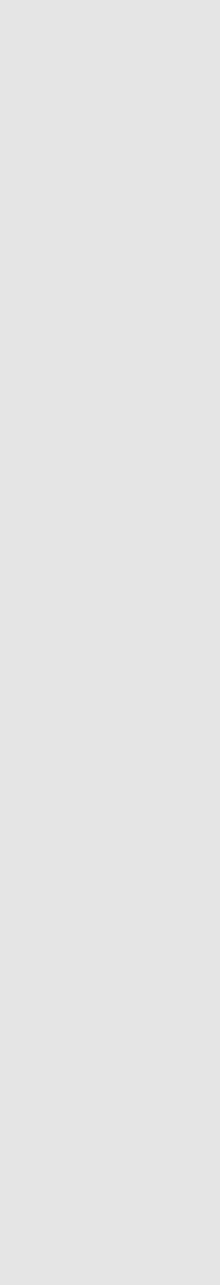
$$N_3^{bot}(\xi, \eta) = N_6^{top}(\xi, \eta) = (2\eta - 1)\eta$$

$$N_7^{bot}(\xi, \eta) = N_{10}^{top}(\xi, \eta) = 4(1 - \xi - \eta)\xi$$

$$N_8^{bot}(\xi, \eta) = N_{11}^{top}(\xi, \eta) = 4\xi\eta$$

$$N_9^{bot}(\xi, \eta) = N_{12}^{top}(\xi, \eta) = 4\eta(1 - \xi - \eta) \quad (3.23)$$

The integration points are located in the mid-plane between the top and bottom faces. Since the Newton-Cotes scheme is used for integration, the integration points are located on the nodal positions.



The relative displacement-element and displacement matrix of the surface interface element is identical to matrix **B** which is expanded from 2 dimensional.

3-6 Finite Element Formulation

The tractions in the local coordinate system are derived from the relative displacements in the local coordinate system $\Delta \mathbf{u}_x$, $\Delta \mathbf{u}_y$ and $\Delta \mathbf{u}_z$ of the interface element and the stiffness matrix \mathbf{D} .

$$\begin{Bmatrix} \mathbf{t}_x \\ \mathbf{t}_y \\ \mathbf{t}_z \end{Bmatrix} = \mathbf{D} \begin{Bmatrix} \Delta \mathbf{u}_x \\ \Delta \mathbf{u}_y \\ \Delta \mathbf{u}_z \end{Bmatrix} \quad (3.24)$$

The stiffness matrix can be obtained by variation of the strain energy equation for the interface element and is given by

$$\mathbf{K}_{inter} = \int_{\Gamma} \mathbf{B}_{inter}^T \mathbf{D} \mathbf{B}_{inter} d\Gamma \quad (3.25)$$

And the internal force is given by

$$\mathbf{F}_{inter} = \int_{\Gamma} \mathbf{B}_{inter}^T \mathbf{t} d\Gamma \quad (3.26)$$

Expanding Eq. (3.26) into a numerical integration expression, the following equation of the stiffness matrix of the interface element is obtained:

$$\mathbf{K}_{inter} = \sum_{j=1}^{Nip} \mathbf{B}_{inter}^j{}^T \mathbf{D} \mathbf{B}_{inter}^j \det \mathbf{J}^j \quad (3.27)$$

where, Nip is the number of integration points for the interface element.

3-7 Interface Element Output

Tractions and relative displacements are produced as the analysis results of interface elements. The sign convention follows the local element coordinate system. The tractions and relative displacements are defined in the nodes of the elements such that corresponding nodes at both sides have equal result values. The types of output for tractions and relative displacements for the interface elements are as follows:

- Traction components t_x, t_y, t_z
- Relative displacement components $\Delta u_x, \Delta u_y, \Delta u_z$

Since tractions and displacements at a node are calculated from the Newton-Cotes Integration method, the results at the integration points are shared at the nodes. The integration points of the interface elements are given by:

- 1+1-node point element: 1 point Newton-Cotes integration
- 2+2-node line element: 2 point Newton-Cotes integration
- 3+3-node line element: 3 point Newton-Cotes integration
- 3+3-node triangular element: 3 point Newton-Cotes integration
- 4+4-node quadrilateral element: 4 point Newton-Cotes integration
- 6+6-node triangular element: 6 point Newton-Cotes integration
- 8+8-node quadrilateral element: 8 point Newton-Cotes integration

Chapter 4. Linear Analysis

4-1 Linear Static

The basic equation for linear static analysis is represented by (4.1). The structural stiffness matrix **K**, the load vector **p** and the displacement vector **u** are defined in the global coordinate system (GCS). Users are advised to assign sufficient constraints and/or supports for the structural model to avoid any rigid body motion and singular errors.

$$\mathbf{Ku} = \mathbf{p} \quad (4.1)$$

where,

K : Stiffness matrix of structure in GCS

u : Displacement vector in GCS

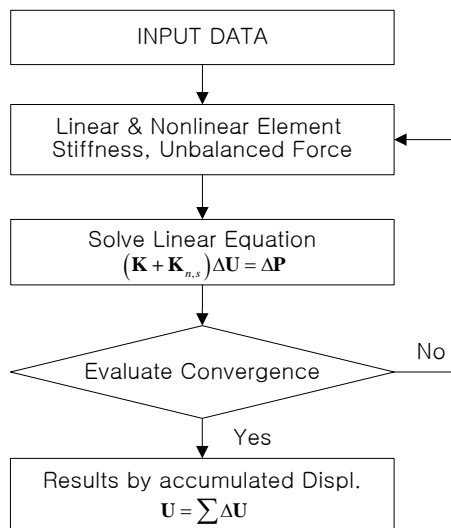
p : Load vector in GCS

4-2 Linear Static with Nonlinear Elements

MIDAS offers truss and elastic link elements with compression only and tension only characteristics. For these nonlinear elements the actual values of the stiffness matrix are dependent on the calculated stress in the truss or elastic link element. For a tension only element the stiffness matrix will be set to zero when a compressive stress is found in the nonlinear element, while for a compression only element the stiffness will be set to zero when a tensile stress is found in the nonlinear element. In case a linear static analysis is performed on a model that includes these nonlinear elements, an iterative procedure is applied for making the stiffness and stresses in these nonlinear elements in agreement with each other, as illustrated in the diagram below.

The linear and nonlinear element stiffness matrices are calculated together with the unbalance between stresses in the model and the external applied loading forces. This linear set of equations is solved, resulting in a change of displacements. The total stresses in the nonlinear elements are calculated and evaluated. If the stresses in the nonlinear elements are in agreement with the actual nonlinear element stiffness matrices, then the result will be accepted, otherwise the respective element stiffness will be adapted and a new displacement change will be calculated and corresponding total stresses will be evaluated.

Please note that the results from an analysis including nonlinear elements, is in principle a nonlinear solution and may therefore not be linearly combined with results from other load cases. In such case the full load combination must be included in the external load-vector before calculating the displacements and stresses/forces.



where,

\mathbf{K} : Stiffness of linear members

\mathbf{K}_{nl} : Stiffness of nonlinear members

$\Delta\mathbf{U}, \mathbf{U}$: Incremental and accumulated displacements due to unbalanced forces

$\Delta\mathbf{P}$: Unbalanced forces (external-internal)

Chapter 5. Modal Analysis

5-1 Introduction

Eigenvalue analysis for analyzing the dynamic behavior of structures is also referred to as “free vibration analysis”. For a system without damping and with no excitation, the motion equation is the 2nd order linear differential equation (5.1).

$$\mathbf{M}\ddot{\mathbf{u}}(t) + \mathbf{K}\mathbf{u}(t) = \mathbf{0} \quad (5.1)$$

where,

\mathbf{K} : Stiffness matrix of structure

\mathbf{M} : Mass matrix of structure

$\mathbf{u}(t)$: Displacement vector of structure

$\ddot{\mathbf{u}}(t)$: Acceleration vector of structure

If the displacement vector \mathbf{u} is assumed to be a linear combination of mode-shape-vectors, defined by the mode shape matrix Φ , and the combination factors for the selected modes are defined by a vector of time-functions $\mathbf{Y}(t)$, we can replace the displacement vector $\mathbf{u} = \Phi\mathbf{Y}(t)$. By substituting the expression for \mathbf{u} in equation (5.1) the following equation is obtained:

$$\mathbf{M}\Phi\ddot{\mathbf{Y}} + \mathbf{K}\Phi\mathbf{Y} = \mathbf{0} \quad (5.2)$$

The time function, $\mathbf{Y}(t)$ is defined as.

$$\mathbf{Y}(t) = \{y_1(t) \quad \cdots \quad y_m(t) \quad \cdots \quad y_n(t)\}^T \quad (5.3)$$

where n is the total number of degrees of freedom in the system.

When we assume that the combination factors $y_m(t)$ are harmonic functions in time

$$y_m(t) : \cos(\omega_m t + \beta_m)$$

The second derivative $\ddot{y}_m(t)$ with time of the harmonic function can be written as inverse multiplication with a constant factor $\lambda_m = \omega_m^2$ of the original function $y_m(t)$:

$$\ddot{y}_m(t) = -\lambda_m y_m(t) \quad (5.3.1)$$

Subsequently we can use this assumption to transform the equation (5.3) into,

$$(-\mathbf{M}\Phi\Lambda + \mathbf{K}\Phi)\mathbf{Y} = \mathbf{0} \quad (5.4)$$

where the matrices Λ and Φ are formulated as below.

$$\Lambda = \begin{bmatrix} \lambda_1 & & & \\ & \ddots & & \\ & & \lambda_m & \\ & & & \ddots \\ & & & & \lambda_n \end{bmatrix}, \quad \lambda_m = \omega_m^2 \quad (5.5)$$

$$\Phi = [\phi_1 \quad \cdots \quad \phi_m \quad \cdots \quad \phi_n] \quad (5.6)$$

The equation (5.4) must be valid for every harmonic function, that means for every $y_m(t)$, it can be transformed into.

$$\mathbf{K}\phi_m - \lambda_m \mathbf{M}\phi_m = 0 \quad (5.7)$$

Equation (5.7) is an eigenvalue problem, which must satisfy the condition of equation (5.8) and from this condition the free vibration modes can be calculated.

$$|\mathbf{K} - \lambda_m \mathbf{M}| = 0 \quad (5.8)$$

Equation (5.8) has n number of solutions (eigenvalues) $\lambda_1, \lambda_2, \dots, \lambda_n$ that satisfy the condition (5.8) and equal to the number of degrees of freedom of the finite element model. Usually the eigenvalues are ordered such that λ_1 is the smallest eigenvalue. For each eigenvalue, λ_m a corresponding eigen mode, ϕ_m exists. Since the mass matrix, \mathbf{M} and the stiffness matrix, \mathbf{K} in

equation (5.7) are symmetrical, the eigenvalue, λ_m and the eigen mode, ϕ_m are real numbers. Because the mass matrix is positive definite, and the stiffness matrix is positive semi-definite $\lambda_m \geq 0$. As such the circular frequency, ω_m under the condition of undamped free vibration is a real number.

A structure vibrates in the eigen mode shapes of ϕ_m without external excitation, and the velocities are circular frequencies, ω_m (radian/time). The velocities of a structure are expressed in terms of natural frequencies, f_m (cycle/time) or natural periods, T_m (time/cycle). The relationship between ω_m , f_m and T_m is given below.

$$T_m = \frac{1}{f_m}, \quad f_m = \frac{\omega_m}{2\pi} \quad (5.9)$$

Generally the eigenvalue, λ_m represents the ratio of the strain energy to the kinetic energy for the m -th mode shape, and the modes are referred to as 1st mode, 2nd mode, ..., n -th mode from the smallest ratio onward. Fig. 5-(1) shows the free vibration modes of a cantilever from the 1st to 3rd mode.

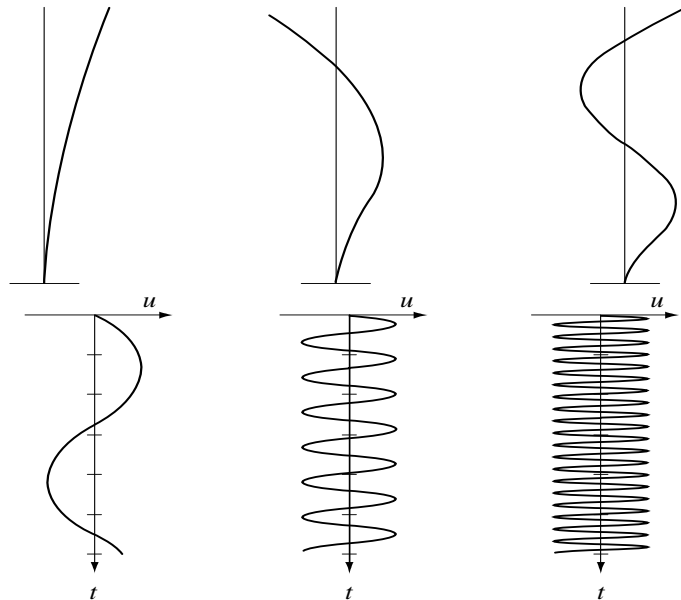


Figure 5-(1) Vibration of a Cantilever

MIDAS calculates indices of the dynamic properties of a structure such as modal participation factors, effective modal masses and modal direction factors. The values of the directional modal participation factors are calculation by equation (5.10), which are used for response spectrum analysis or time history analysis of a structure subjected to seismic loads.

$$\Gamma_{mX} = \frac{\phi_m^T \mathbf{M} \mathbf{1}_X}{\phi_m^T \mathbf{M} \phi_m}, \quad \Gamma_{mY} = \frac{\phi_m^T \mathbf{M} \mathbf{1}_Y}{\phi_m^T \mathbf{M} \phi_m}, \quad \Gamma_{mZ} = \frac{\phi_m^T \mathbf{M} \mathbf{1}_Z}{\phi_m^T \mathbf{M} \phi_m} \quad (5.10)$$

$$\Gamma_{mRX} = \frac{\phi_m^T \mathbf{M} \mathbf{1}_{RX}}{\phi_m^T \mathbf{M} \phi_m}, \quad \Gamma_{mRY} = \frac{\phi_m^T \mathbf{M} \mathbf{1}_{RY}}{\phi_m^T \mathbf{M} \phi_m}, \quad \Gamma_{mRZ} = \frac{\phi_m^T \mathbf{M} \mathbf{1}_{RZ}}{\phi_m^T \mathbf{M} \phi_m}$$

where,

$\Gamma_{mX}, \Gamma_{mY}, \Gamma_{mZ}$: Modal participation factors in the GCS X, Y and Z translations for the m -th mode
$\Gamma_{mRX}, \Gamma_{mRY}, \Gamma_{mRZ}$: Modal participation factors in the GCS X, Y and Z rotations for the m -th mode
$\mathbf{1}_X, \mathbf{1}_Y, \mathbf{1}_Z$: Directional vectors, which retain unit values only for the translations in the X, Y and Z directions
$\mathbf{1}_{RX}, \mathbf{1}_{RY}, \mathbf{1}_{RZ}$: Directional vectors, which retain unit values only for the rotations in the respective X, Y and Z directions
ϕ_m	: m^{th} mode shape

The directional values of the modal participation masses for each mode are calculated according to equation (5.11). Since the calculation includes the signs (positive or negative) of the modes, the values can be 0 depending on the mode shapes. The sum of the directional participation masses for all the modes is equal to the total mass of the structure in each corresponding direction. General seismic design codes require that the sum of the modal participation masses included in the analysis of a structure in each direction be at least 90% of the total mass. This is intended to include most of the major modes, which influence the analysis results.

$$\begin{aligned}
 M_{mX}^* &= \frac{[\phi_m^T \mathbf{M} \mathbf{1}_X]^2}{\phi_m^T \mathbf{M} \phi_m}, \quad M_{mY}^* = \frac{[\phi_m^T \mathbf{M} \mathbf{1}_Y]^2}{\phi_m^T \mathbf{M} \phi_m}, \quad M_{mZ}^* = \frac{[\phi_m^T \mathbf{M} \mathbf{1}_Z]^2}{\phi_m^T \mathbf{M} \phi_m} \\
 M_{mRX}^* &= \frac{[\phi_m^T \mathbf{M} \mathbf{1}_{RX}]^2}{\phi_m^T \mathbf{M} \phi_m}, \quad M_{mRY}^* = \frac{[\phi_m^T \mathbf{M} \mathbf{1}_{RY}]^2}{\phi_m^T \mathbf{M} \phi_m}, \quad M_{mRZ}^* = \frac{[\phi_m^T \mathbf{M} \mathbf{1}_{RZ}]^2}{\phi_m^T \mathbf{M} \phi_m}
 \end{aligned}
 \tag{5.11}$$

where,

$M_{mX}^*, M_{mY}^*, M_{mZ}^*$: Modal participation masses in the GCS X, Y and Z translations for the m -th mode
$M_{mRX}^*, M_{mRY}^*, M_{mRZ}^*$: Modal participation masses in the GCS X, Y and Z rotations for the m -th mode

The directional coefficient for each mode represents the ratio of the directional participation mass to the total participation mass for the corresponding mode.

MIDAS uses the Lanczos and subspace iteration methods which are suitable for analyzing large systems of eigenvalue problems such as equation (5.7) .

5-2 Lanczos Iteration Method

The Lanczos iteration method finds approximate eigenvalues using a tri-diagonal matrix, \mathbf{T}_k , which can be found by defining the Krylov subspace $span\{\mathbf{V}_1, \mathbf{V}_2, \dots, \mathbf{V}_k\}$. In order to effectively apply the Lanczos iteration method to the free vibration eigenvalue problem as expressed in equation (5.7), the eigenvalue, λ_m must be replaced by $\lambda_m = \sigma + 1/\theta_m$. This is referred to as a shift-invert technique. σ is the expected first eigenvalue. The Lanczos iteration calculation process applying the shift-invert technique is described in below.

- Assume an initial value \mathbf{V}_1 for the block vector in case of first iterative calculation.
- Multiply the mass matrix $\mathbf{U}_k = \mathbf{M}\mathbf{V}_k$
- Solve linear simultaneous equations $(\mathbf{K} - \sigma\mathbf{M})\mathbf{W}_k = \mathbf{U}_k$
- Orthogonalize \mathbf{W}_k $\mathbf{W}_k^* = \mathbf{W}_k - \mathbf{V}_{k-1}\mathbf{B}_{k-1}^T$
- Calculate matrix \mathbf{C}_k $\mathbf{C}_k = \mathbf{V}_k\mathbf{M}\mathbf{W}_k^*$
- Orthogonalize \mathbf{W}_k^* $\mathbf{W}_k^{**} = \mathbf{W}_k^* - \mathbf{V}_k\mathbf{C}_k$
- Normalize the block vector $\mathbf{W}_k^{**} = \mathbf{V}_{k+1}\mathbf{B}_k$

MIDAS uses the block vector, \mathbf{V}_k for effectively calculating eigenvalues. This is referred to as the Block Lanczos method. The block tri-diagonal matrix, \mathbf{T}_k , which takes place in the process of iterative calculations above, is as follows:

$$\mathbf{T}_k = \begin{bmatrix} \mathbf{C}_1 & \mathbf{B}_1^T & & & \\ \mathbf{B}_1 & \mathbf{C}_2 & \ddots & & \\ & \ddots & \ddots & \ddots & \\ & & \ddots & \mathbf{C}_{k-1} & \mathbf{B}_{k-1}^T \\ & & & \mathbf{B}_{k-1}^T & \mathbf{C}_k \end{bmatrix} \quad (5.12)$$

If \mathbf{T}_k is used to solve the eigenvalue problem, $\mathbf{T}_k \psi_m^* = \theta_m^* \psi_m^*$, λ_m^* can be obtained using $\lambda_m^* = \sigma + 1/\theta_m^*$. λ_m^* is an approximate value of the original eigenvalue problem of Eq. (5.7). If N_b is defined to be the block size of \mathbf{V}_k , the size of \mathbf{T}_k increases to as much as N_b and λ_m^* converges to λ_m , as the number of iterations increases in the process of iterative calculations. The approximate value, ϕ_m^* of the eigenmode, ϕ_m can be obtained by the equation below, which converges with λ_m^* .

$$\phi_m^* = [\mathbf{V}_1 \quad \mathbf{V}_2 \quad \mathbf{V}_3 \quad \dots \quad \mathbf{V}_k] \psi_m^* \quad (5.13)$$

The convergence criterion for eigenvalues and eigenmodes calculated from the Lanczos iteration method is noted below.

$$\frac{\|\mathbf{K}\phi_m^* - \lambda_m^* \mathbf{M}\phi_m^*\|}{\|\mathbf{K}\|} \leq \varepsilon \quad (5.14)$$

Where, $\|\cdot\|$ means 2-norm. MIDAS uses $\varepsilon = 2.22 \times 10^{-16}$.

5-3 Subspace Iteration Method

The Subspace method searches for a set of N_s orthogonal vectors \mathbf{X}_k that expand over the subspace E_k that is defined by the eigen modes $[\phi_1 \ \phi_2 \ \dots \ \phi_{N_s}]$. For large systems the number of N_s is much smaller than the number of degrees of freedom in the finite element model. The iterative process of calculating the set of vectors \mathbf{X}_k is explained below.

- Assume a first set of N_s vectors \mathbf{X}_1 and call this \mathbf{X}_k
- Calculate vector \mathbf{Y}_k with length N_s by solving linear set of equations $\mathbf{K}\mathbf{Y}_k = \mathbf{M}\mathbf{X}_k$
- Calculate the projection of stiffness in E_k $\mathbf{K}_{k+1} = \mathbf{Y}_k^T \mathbf{K} \mathbf{Y}_k$
- Calculate the projection of mass E_k $\mathbf{M}_{k+1} = \mathbf{Y}_k^T \mathbf{M} \mathbf{Y}_k$
- Solve projected eigenvalue problem of size N_s $\mathbf{K}_{k+1} \mathbf{Q}_{k+1} = \mathbf{M}_{k+1} \mathbf{Q}_{k+1} \mathbf{\Lambda}_{k+1}$ by using classical eigenvalue solution techniques

$$\mathbf{Q}_{k+1} = [\psi_1^* \ \psi_2^* \ \dots \ \psi_{N_s}^*] \quad \mathbf{\Lambda}_{k+1} = \begin{bmatrix} \lambda_1^* & & & \\ & \lambda_2^* & & \\ & & \ddots & \\ & & & \lambda_{N_s}^* \end{bmatrix}$$

Calculating \mathbf{X}_{k+1} by $\mathbf{X}_{k+1} = \mathbf{Y}_k \mathbf{Q}_{k+1}$ and repeating these steps until λ_m^* and \mathbf{X}_k , individually converge to N_s eigenvalues and N_s eigen modes of the system

$$\lambda_m^* \rightarrow \lambda_m, \quad \mathbf{X}_k \rightarrow [\phi_1 \ \phi_2 \ \dots \ \phi_{N_s}] \quad (5.15)$$

If \mathbf{X}_k is composed of N_s vectors, the sizes of \mathbf{K}_k and \mathbf{M}_k are $N_s \times N_s$, irrespective of the number of iterations in the process of iterative calculations. The convergence of eigenvalues calculated by the subspace iteration method is evaluated by the change of λ_m^* .

$$\left\| \frac{\lambda_m^{(k+1)} - \lambda_m^{(k)}}{\lambda_m^{(k+1)}} \right\| \leq \varepsilon \quad (5.16)$$

5-4 Optional Parameters

5-4-1 Mass Matrix

Two types of mass matrices can be used in an eigenvalue analysis, which are the consistent mass matrix and the lumped mass matrix. When the consistent mass matrix is applied, this generally results in higher eigenvalues compared to the theoretical values. Whereas using the lumped mass matrix results in smaller eigenvalues. It is known that using the consistent mass matrix results in better convergence than using the lumped mass matrix depending on the number of elements. The drawback however is that the consistent mass matrix requires more calculations and memory (see figure 5-(2)).

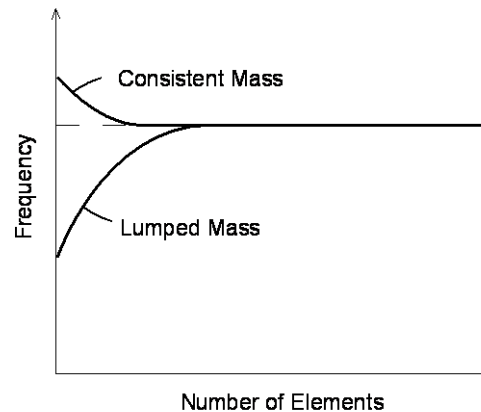


Figure 5-(2) Lumped Mass vs Consistent Mass

5-4-2 Parameters for Lanczos Iteration

When calculating eigen frequencies using the Lanczos iteration method in MIDAS two

frequencies, f_1 and f_2 can be specified by the user for defining the range of interest of eigen frequencies. The range of interest of frequencies is used in the calculation to define the expected eigenvalues to $\sigma = (2\pi f_1)^2$ by the shift-invert technique. Fig. 5-(3) shows the range and sequence of calculating eigenvalues for combinations of f_1 and f_2 . If N_f is defined as the number of eigenvalues to be calculated, the number of each calculated eigenvalues is determined based on f_1 and f_2 as,

- If $f_1 = f_2$: The N_f frequencies closest to f_1 are calculated.
- If $f_1 < f_2$: The N_f frequencies closest to f_1 within the range, $[f_1, f_2]$ are calculated.
- If $f_1 > f_2$: The N_f frequencies closest to f_2 within the range, $[f_1, f_2]$ are calculated.

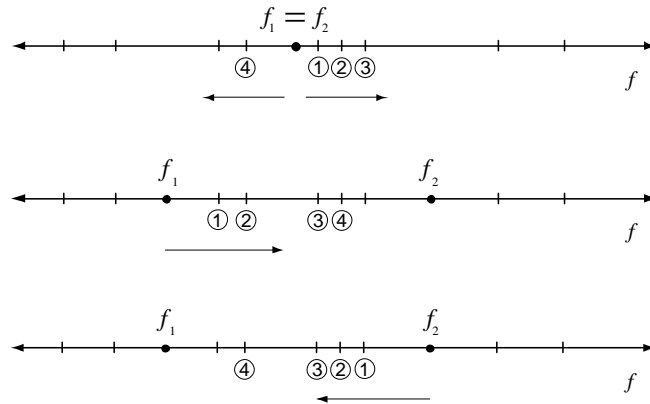


Figure 5-(3) Eigenvalue Searching Direction

The default values of f_1 and f_2 , in the range of interest are $f_1 = f_2 = 0$.

(1) Sturm Sequence Check

When eigenvalues are calculated using an iteration method, there is a possibility that higher eigenvalues are found before the lower eigenvalues. MIDAS provides functionality, which

prevents that frequencies are skipped. When applying the Lanczos iteration method the vector \mathbf{W}_k is calculated by solving the following set of equations:

$$(\mathbf{K} - \sigma \mathbf{M})\mathbf{W}_k = \mathbf{U}_k \quad (5.17)$$

In order to solve the equations, the matrix is decomposed by the matrices $\mathbf{L}\mathbf{D}\mathbf{L}^T$ and the number of negative values in the diagonal terms in the matrix, \mathbf{D} is calculated. The number represents the number of eigenvalues, λ_n that are smaller than σ . For example, if $\sigma = \lambda_{N_f} + \delta$ and the matrix is decomposed, we can find eigenvalues that are smaller than $\lambda_{N_f} + \delta$. If the number of eigenvalues smaller than $\lambda_{N_f} + \delta$ is greater than N_f , the process of the Lanczos iteration continues until all the omitted eigenvalues are converged. At this point, δ should satisfy the relationship below.

$$\lambda_{N_f} < \lambda_{N_f} + \delta < \lambda_{N_f+1} \quad (5.18)$$

This condition to δ is called the Sturm-sequence check. When MIDAS performs a Sturm sequence check, the size of the Lanczos block vector, \mathbf{V}_k is set to $N_b = 7$ to speed up the calculations. For limiting the computational effort MIDAS also provides an option to skip the Sturm sequence check.

(2) Rigid Body Mode

When a free-vibration analysis of a structure with insufficient boundary conditions is performed, \mathbf{K} will be a singular matrix and the calculations cannot be progressed with $\sigma = 0$. In such a case, the shift-invert technique is applied with a negative value for σ . In this case the calculated eigenvalues will include a 0 for every rigid mode. MIDAS predicts the expected first mode frequency, $\bar{\lambda}_1$ using the diagonal terms of the matrices \mathbf{K} and \mathbf{M} and sets $\sigma = -\bar{\lambda}_1$.

5-4-3 Parameters for Subspace Iteration

The subspace iteration method in MIDAS allows the user to set the size, N_s of the subspace, \mathbf{X}_k , the number of maximum iterations, N_I and the convergence criterion, ε in Eq. (5.16). The actual size of subspace, N_s used for the calculations is as follows:

$$N_s = \max\{N_{s_0}, \min(2N_f, N_f + 8)\} \quad (5.19)$$

Where, N_{s_0} is the user input N_s value.

The default value for the maximum number of iterations is $N_I = 30$. The default value for the convergence criterion is $\varepsilon = 1.0 \times 10^{-6}$.

Chapter 6. Time History Analysis

6-1 Time History Analysis

When a structure is subjected to a dynamic load, the behavior is described by the dynamic motion equation given by (6.1).

$$\mathbf{M}\ddot{\mathbf{u}}(t) + \mathbf{C}\dot{\mathbf{u}}(t) + \mathbf{K}\mathbf{u}(t) = \mathbf{F}(t) \quad (6.1)$$

where,

M	: Mass matrix
C	: Damping matrix
K	: Stiffness matrix
F(t)	: Dynamic load vector
u(t) , $\dot{\mathbf{u}}(t)$ & $\ddot{\mathbf{u}}(t)$: Displacement, Velocity & Acceleration vector

In case there is no external excitation $\mathbf{F}(t) = \mathbf{0}$ and the damping matrix $\mathbf{C} = \mathbf{0}$, the equation (6.1) will reduce to the free vibration equation (5.1).

However, if $\mathbf{F}(t)$ is an external force (or external displacement, velocity, acceleration, etc.), which varies with time, the equation (6.1) becomes a forced vibration analysis problem. For this type of problems MIDAS provides a modal superposition method as well as a direct integration method.

6-2 Modal Superposition Method

The modal superposition method makes use of the orthogonality of eigen modes and decomposes the equation (6.1) into independent mode equations. This method assumes that the damping matrix is composed of a linear combination of the mass matrix and the stiffness matrix. The displacement vector is obtained by a linear combination of a selected number n of orthogonal eigen modes as expressed in equation (6.2).

$$\mathbf{u}(t) = \Phi \mathbf{Y}(t) = \sum_{i=1}^n \phi_i Y_i(t) \quad (6.2)$$

By substituting equation (6.2) into equation (6.1), we get

$$\mathbf{M} \Phi \ddot{\mathbf{Y}}(t) + \mathbf{C} \Phi \dot{\mathbf{Y}}(t) + \mathbf{K} \Phi \mathbf{Y}(t) = \mathbf{F}(t) \quad (6.3)$$

Multiplying equation (6.3) by ϕ_m^T (m -th mode shape), the equation (6.4) is obtained.

$$\phi_m^T \mathbf{M} \Phi \ddot{\mathbf{Y}}(t) + \phi_m^T \mathbf{C} \Phi \dot{\mathbf{Y}}(t) + \phi_m^T \mathbf{K} \Phi \mathbf{Y}(t) = \phi_m^T \mathbf{F}(t) \quad (6.4)$$

The mass and stiffness matrices can be orthogonalized to eigen modes as,

$$\begin{aligned} \phi_i^T \mathbf{M} \phi_j &= m_{ij} \delta_{ij} \\ \phi_i^T \mathbf{K} \phi_j &= k_{ij} \delta_{ij} \end{aligned} \quad (6.5)$$

where, δ_{ij} : Krönecker Delta ($i = j$; $\delta_{ij} = 1$, $i \neq j$; $\delta_{ij} = 0$)

Using the above orthogonality, the dynamic motion equation (6.3) can be decomposed into n independent equations.

$$\phi_m^T \mathbf{M} \Phi \ddot{\mathbf{Y}}(t) + \phi_m^T \mathbf{C} \Phi \dot{\mathbf{Y}}(t) + \phi_m^T \mathbf{K} \Phi \mathbf{Y}(t) = \phi_m^T \mathbf{F}(t) \quad (m = 1, 2, \dots, n) \quad (6.6)$$

The above n independent decomposed equations thus become dynamic motion equations for a single degree of freedom in a general coordinate system.

Subsequently we rearrange equation (6.6)

$$\ddot{Y}_m(t) + 2\xi_m \omega_m \dot{Y}_m(t) + \omega_m^2 Y_m(t) = \frac{\phi_m^T F(t)}{\phi_m^T M \phi_m} \quad (6.7)$$

where,

$$2\xi_m \omega_m = \frac{\phi_m^T C \phi_m}{\phi_m^T M \phi_m}$$

$$\omega_m^2 = \frac{\phi_m^T K \phi_m}{\phi_m^T M \phi_m}$$

ξ_m : m^{th} mode damping ratio

ω_m : m^{th} mode natural frequency

$q_m(t), \dot{q}_m(t) \& \ddot{q}_m(t)$: m^{th} mode general displacement, velocity and acceleration

Displacement response in the general coordinate system is obtained by equation (6.8).

$$q_m(t) = e^{-\xi_m \omega_m t} \left[q_m(0) \cos \omega_{Dm} t + \frac{\xi_m \omega_m q_m(0) + \dot{q}_m(0)}{\omega_{Dm}} \sin \omega_{Dm} t \right] \\ + \frac{1}{m_m \omega_{Dm}} \int_0^t P_m(\tau) e^{-\xi_m \omega_m (t-\tau)} \sin \omega_{Dm} (t-\tau) d\tau \quad (6.8)$$

where, $\omega_{Dm} = \omega_m \sqrt{1 - \xi_m^2}$

The displacement response of a structure is obtained by substituting the general displacement of each mode, which is obtained by the single degree of freedom equation (6.8), into the system equation (6.2). The accuracy of the displacement response in the modal superposition method depends on the selected modes used for analysis. The modal superposition method is most widely used by structural analysis programs, and it is effective in linear dynamic analyses of large structures. However, this method cannot be used for nonlinear dynamic analysis; nor can it be used in case damping devices are included and their properties cannot be assumed on the basis of a linear combination of stiffness and mass.

6-3 Direct Integration Method

Using the direct integration method is one in which the total analysis time range is sub-divided into a number of finite time steps, and numerical integration of the dynamic equilibrium equation is performed at each time step. This method can be applied to systems reflecting nonlinearity of stiffness and/or damping. Since the direct integration method evaluates the dynamic motion equation at every time step, the analysis time increases with the number of time steps.

A variety of methods can be applied for numerical integration. MIDAS uses the average acceleration method of the Newmark- β method in which the acceleration $\ddot{\mathbf{u}}(t)$ in the time range $t_i < t < t_{i+1}$ is assumed to be constant at the average of $\ddot{\mathbf{u}}_i$ and $\ddot{\mathbf{u}}_{i+1}$ in Eq. (6.9).

$$\ddot{\mathbf{u}}(t) = \frac{\ddot{\mathbf{u}}_i + \ddot{\mathbf{u}}_{i+1}}{2} = \text{const.} \quad (6.9)$$

Consequently, the velocity and displacement at $t = t_{i+1}$ are expressed as,

$$\dot{\mathbf{u}}_{i+1} = \dot{\mathbf{u}}_i + \frac{\ddot{\mathbf{u}}_i + \ddot{\mathbf{u}}_{i+1}}{2} \Delta t \quad (6.10)$$

$$\mathbf{u}_{i+1} = \mathbf{u}_i + \dot{\mathbf{u}}_i \Delta t + \frac{\ddot{\mathbf{u}}_i + \ddot{\mathbf{u}}_{i+1}}{4} \Delta t^2 \quad (6.11)$$

Expressing the equations (6.10) and (6.11) with the integration variables of the Newmark- β method,

$$\dot{\mathbf{u}}_{i+1} = \dot{\mathbf{u}}_i + (1 - \gamma) \Delta t \ddot{\mathbf{u}}_i + \gamma \Delta t \ddot{\mathbf{u}}_{i+1} \quad (6.12)$$

$$\mathbf{u}_{i+1} = \mathbf{u}_i + \Delta t \dot{\mathbf{u}}_i + \left(\frac{1}{2} - \beta \right) \Delta t^2 \ddot{\mathbf{u}}_i + \beta \Delta t^2 \ddot{\mathbf{u}}_{i+1} \quad (6.13)$$

where, $\beta = 0.25$, $\gamma = 0.5$.

Rearranging the equation (6.13) gives the following expression for the acceleration at the end of the time-step,

$$\ddot{\mathbf{u}}_{i+1} = \frac{1}{\beta \Delta t^2} \left\{ \mathbf{u}_{i+1} - \mathbf{u}_i - \Delta t \dot{\mathbf{u}}_i - \left(\frac{1}{2} - \beta \right) \Delta t^2 \ddot{\mathbf{u}}_i \right\} \quad (6.14)$$

Substituting equation (6.14) into equation (6.12) and rearranging it, gives the following expression for the velocity at the end of the time-step,

$$\dot{\mathbf{u}}_{i+1} = \frac{\gamma}{\beta \Delta t} \mathbf{u}_{i+1} - \frac{\gamma}{\beta \Delta t} \mathbf{u}_i + \left(1 - \frac{\gamma}{\beta} \right) \dot{\mathbf{u}}_i + \left(1 - \frac{\gamma}{2\beta} \right) \Delta t \ddot{\mathbf{u}}_i \quad (6.15)$$

The equations (6.14) and (6.15) are substituted into the dynamic motion equation, which is rearranged for the displacement response \mathbf{u}_{i+1} at the end of the increment as follows:

$$\begin{aligned} & \left(\frac{1}{\beta \Delta t^2} \mathbf{M} + \frac{\gamma}{\beta \Delta t} \mathbf{C} + \mathbf{K} \right) \mathbf{u}_{i+1} \\ &= \mathbf{F} + \mathbf{M} \left\{ \frac{1}{\beta \Delta t^2} \mathbf{u}_i + \frac{1}{\beta \Delta t} \dot{\mathbf{u}}_i + \left(\frac{1}{2\beta} - 1 \right) \ddot{\mathbf{u}}_i \right\} + \mathbf{C} \left\{ \frac{\gamma}{\beta \Delta t} \mathbf{u}_i + \left(\frac{\gamma}{\beta} - 1 \right) \dot{\mathbf{u}}_i + \left(\frac{\gamma}{2\beta} - 1 \right) \Delta t \ddot{\mathbf{u}}_i \right\} \end{aligned} \quad (6.16)$$

Substituting the displacement \mathbf{u}_{i+1} at the time t_{i+1} as defined in equation (6.16) into equations (6.14) and (6.15), the velocity and acceleration at the end of the increment as function of status at the beginning of the increment only can be obtained.

Rayleigh damping expressed in equation (6.17) is used for damping in the direct integration

method.

$$\text{Rayleigh Damping: } \mathbf{C} = a_0 \mathbf{M} + a_1 \mathbf{K} \quad (6.17)$$

where, a_0 & a_1 : Proportional constants for mass and stiffness for damping calculation

By substituting the equation (6.17) into equation (6.16), the dynamic motion equation is expressed as,

$$\begin{aligned} & \left\{ \left(\frac{1}{\beta \Delta t^2} + \frac{a_1 \gamma}{\beta \Delta t} \right) \mathbf{M} + \left(\frac{a_2 \gamma}{\beta \Delta t} + 1 \right) \mathbf{K} \right\} \mathbf{u}_{i+1} \\ & = \mathbf{F} + \mathbf{M} \left\{ \frac{1}{\beta \Delta t^2} \mathbf{u}_i + \frac{1}{\beta \Delta t} \dot{\mathbf{u}}_i + \left(\frac{1}{2\beta} - 1 \right) \ddot{\mathbf{u}}_i + a_1 \bar{\mathbf{D}} \right\} + a_2 \mathbf{K} \bar{\mathbf{D}} \end{aligned} \quad (6.18)$$

$$\text{where, } \bar{\mathbf{D}} = \frac{\gamma}{\beta \Delta t} \mathbf{u}_i + \left(\frac{\gamma}{\beta} - 1 \right) \dot{\mathbf{u}}_i + \left(\frac{\gamma}{2\beta} - 1 \right) \Delta t \ddot{\mathbf{u}}_i$$

The solutions for the dynamic motion equation that are found through time history analysis are the relative displacement $\mathbf{u}(t)$, the relative velocity $\dot{\mathbf{u}}(t)$ and the relative acceleration $\ddot{\mathbf{u}}(t)$. When a structure is subjected to dynamic loads such as ground acceleration, the absolute response of the structure is obtained by adding the relative response and the ground response as expressed in equation (6.19).

$$\ddot{\mathbf{u}}_{g,i+1} + \ddot{\mathbf{u}}_{i+1} : \text{Absolute acceleration}$$

$$\dot{\mathbf{u}}_{g,i+1} + \dot{\mathbf{u}}_{i+1} : \text{Absolute velocity} \quad (6.19)$$

$$\mathbf{u}_{g,i+1} + \mathbf{u}_{i+1} : \text{Absolute displacement}$$

where, $\ddot{\mathbf{u}}_{g,i+1}$, $\dot{\mathbf{u}}_{g,i+1}$ & $\mathbf{u}_{g,i+1}$ are ground acceleration, velocity & displacement respectively.

In MIDAS, ground velocity and displacement due to ground acceleration are calculated by using the linear acceleration method (equation 6.20), which are applied to calculating the absolute response in the modal superposition and direct integration methods.

$$\begin{aligned}\dot{\mathbf{u}}_{g,i+1} &= \dot{\mathbf{u}}_{g,i} + \Delta t \ddot{\mathbf{u}}_{g,i} + \frac{1}{2} \frac{\ddot{\mathbf{u}}_{g,i+1} - \ddot{\mathbf{u}}_{g,i}}{\Delta t} \Delta t^2 \\ \mathbf{u}_{g,i+1} &= \mathbf{u}_{g,i} + \Delta t \dot{\mathbf{u}}_{g,i} + \frac{1}{2} \Delta t^2 \ddot{\mathbf{u}}_{g,i} + \frac{1}{6} \frac{\ddot{\mathbf{u}}_{g,i+1} - \ddot{\mathbf{u}}_{g,i}}{\Delta t} \Delta t^3\end{aligned}\quad (6.20)$$

6-4 Damping

In MIDAS, the following damping methods are used depending on the method of dynamic analysis.

Selection of damping for time history analysis by response spectrum and modal superposition:

- Modal
- Mass & Stiffness Proportional (Rayleigh damping)

Selection of damping for time history analysis by direct integration:

- Mass & Stiffness Proportional (Rayleigh damping)

6-4-1 Rayleigh Damping

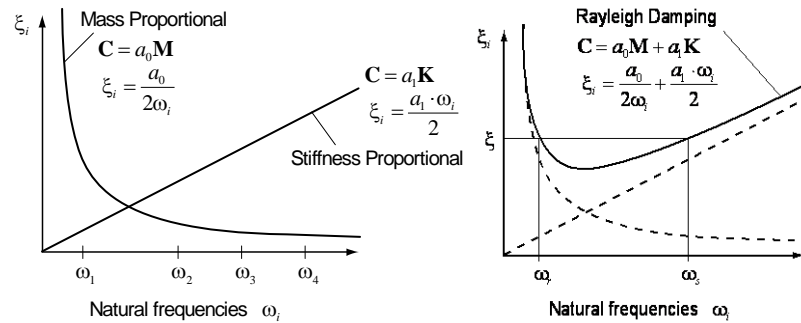
The damping matrix in Rayleigh Damping is composed of the linear combination of the mass matrix and the stiffness matrix of a structure as shown in Fig. (6-1b). If the damping integer ξ_r and the natural frequency ω_r for the r^{th} mode and the damping integer ξ_s and the natural frequency ω_s for the s^{th} mode are given, the Rayleigh damping matrix is expressed below. Notice that the r^{th} and s^{th} modes represent the two main modes of the structure.

$$\mathbf{C} = a_0 \mathbf{M} + a_1 \mathbf{K} \quad (6.21)$$

$$\xi_i = \frac{1}{2} \left(\frac{a_0}{\omega_i} + a_1 \cdot \omega_i \right) \quad (6.22)$$

where,

$$a_0 = \frac{2 \cdot \omega_r \cdot \omega_s (\xi_r \cdot \omega_s - \xi_s \cdot \omega_r)}{(\omega_s^2 - \omega_r^2)}, \quad a_1 = \frac{2 (\xi_s \cdot \omega_s - \xi_r \cdot \omega_r)}{(\omega_s^2 - \omega_r^2)}$$



(a) Mass Proportional Damping and

(b) Rayleigh Damping

Stiffness Proportional Damping

Figure 6-1) Variation of modal damping ratios with natural frequency

6-4-2 Modal Damping

For modal damping, the user directly defines the damping ratio for each mode. Modal damping can be used for time history analysis, by response spectrum analysis and the modal superposition method. When the response spectrum analysis and modal superposition method are used, the kinematic equation of the structure is decomposed by modes to which the modal damping ratios defined by the user are applied.

6-5 Cautionary notes

The accuracy of analysis depends greatly on the time interval used in analysis. Improper time interval may result in inaccurate solutions. In particular, the size of the time interval is closely related to the maximum frequency of movement of the structure. In general, one-tenth of the highest modal period under consideration is a reasonable value for the time interval. In addition, the time interval should be smaller than that of the applied load. A dynamic load needs to sufficiently depict the change in the total loads. MIDAS linearly interpolates the excitation loads.

Chapter 7. Response Spectrum

7-1 Response Spectrum Analysis

Response spectrum analyses are generally carried out for seismic designs using the design spectra defined in design standards. Response spectrum analysis assumes the response of a multi-degree-of-freedom (MDOF) system as a combination of multiple single-degree-of-freedom (SDOF) systems. A response spectrum defines the peak values of responses corresponding to and varying with natural periods (or frequencies) of vibration that have been prepared through a numerical integration process. Displacements, velocities and accelerations form the basis of a spectrum. To predict the peak design response values, the maximum response for each mode is obtained first and then combined by an appropriate method.

Equation (7.1) shows the dynamic motion equation for a structure subjected to a ground motion used in a response spectrum analysis.

$$\mathbf{M}[\ddot{\mathbf{u}}(t) + \mathbf{r}\ddot{u}_g(t)] + \mathbf{C}\dot{\mathbf{u}}(t) + \mathbf{K}\mathbf{u}(t) = \mathbf{0} \quad (7.1)$$

$$\mathbf{M}\ddot{\mathbf{u}}(t) + \mathbf{C}\dot{\mathbf{u}}(t) + \mathbf{K}\mathbf{u}(t) = -\mathbf{M}\mathbf{r}\ddot{u}_g(t)$$

where,

M	: Mass matrix
C	: Damping matrix
K	: Stiffness matrix
r	: Directional vector of ground acceleration
$\ddot{u}_g(t)$: Time history of ground acceleration
$\mathbf{u}(t)$, $\dot{\mathbf{u}}(t)$ & $\ddot{\mathbf{u}}(t)$: Relative displacement, velocity and acceleration

If the displacement, $\mathbf{u}(t)$ is expressed in terms of a combination of modal displacements using the eigen mode shapes Φ , obtained from undamped, free vibration analysis, equation (7.2) is

applicable.

$$\mathbf{u}(t) = \Phi \mathbf{y}(t) \quad (7.2)$$

Now we substitute equation (7.2) into equation (7.1) and multiply both sides by Φ^T , resulting in

$$\Phi^T \mathbf{M} \Phi \ddot{\mathbf{y}}(t) + \Phi^T \mathbf{C} \Phi \dot{\mathbf{y}}(t) + \Phi^T \mathbf{K} \Phi \mathbf{y}(t) = -\Phi^T \mathbf{M} \mathbf{r} \ddot{u}_g(t) \quad (7.3)$$

The relationship below is found due to orthogonality of the eigen modes.

$$\phi_i (\mathbf{M} \text{ or } \mathbf{C} \text{ or } \mathbf{K}) \phi_j = 0 \quad (i \neq j) \quad (7.4)$$

Accordingly, if the dimensionless eigen mode shape ($\Phi^T \mathbf{M} \Phi = 1$) for mass is applied to equation (7.3), we obtain the independent simultaneous differential equations for each mode.

$$\begin{bmatrix} 1 & & & \\ & \ddots & & \\ & & 1 & \\ & & & \ddots \\ & & & & 1 \end{bmatrix} \ddot{\mathbf{y}}(t) + \begin{bmatrix} 2\zeta_1 \omega_1 & & & \\ & \ddots & & \\ & & 2\zeta_m \omega_m & \\ & & & \ddots \\ & & & & 2\zeta_n \omega_n \end{bmatrix} \dot{\mathbf{y}}(t) + \begin{bmatrix} \omega_1^2 & & & \\ & \ddots & & \\ & & \omega_m^2 & \\ & & & \ddots \\ & & & & \omega_n^2 \end{bmatrix} \mathbf{y}(t) = -\Phi^T \mathbf{M} \mathbf{r} \ddot{u}_g(t) \quad (7.5)$$

And rearranging the expression for the m -th mode in equation (7.5) results in.

$$\ddot{y}_m(t) + 2\zeta_m \omega_m \dot{y}_m(t) + \omega_m^2 y_m(t) = -\Gamma_m \ddot{u}_g(t) \quad (7.6)$$

$$\Gamma_m = \phi_m^T \mathbf{M} \mathbf{r}$$

The modal participation factor, Γ_m in equation (7.6) is defined by the multiplication of the dimensionless mode shape for mass ϕ_m , the mass matrix \mathbf{M} and the directional vector of ground acceleration \mathbf{r} . The directional vector of ground acceleration contains unit value only for the degree of freedom in the direction of ground acceleration and all other components are equal to zero. The solution to the dynamic equilibrium equation of a structure under ground acceleration

action is obtained by solving the n equations of (7.6) and then combining them in the same way as equation (7.7).

$$\mathbf{u}(t) = \Phi \mathbf{y}(t), \quad \dot{\mathbf{u}}(t) = \Phi \dot{\mathbf{y}}(t), \quad \ddot{\mathbf{u}}(t) = \Phi \ddot{\mathbf{y}}(t) \quad (7.7)$$

The concept of the dynamic equilibrium equation subjected to a ground acceleration action in response spectrum analysis follows the equations (7.1) to (7.7). In response spectrum analysis, spectrum functions are used to obtain the results for each mode rather than defining the seismic acceleration as a specific function. Generally, the spectrum function means the maximum value for each period in equation (7.5). The spectrum function is defined in various design codes and specifications, which consider the probabilities of seismic accelerations, characteristics of regions and importance of structures. The solutions to a single d.o.f system corresponding to the m -th mode like equation (7.6) are found by multiplying the displacement, velocity and acceleration obtained from the spectrum function by the corresponding modal participation factors as equation (7.8).

$$S_{dm} = \frac{S_{am}}{\omega_m^2}, \quad S_{vm} = \frac{S_{am}}{\omega_m} \quad (7.8)$$

$$y_m = \Gamma_m S_{dm}, \quad \dot{y}_m = \Gamma_m S_{vm}, \quad \ddot{y}_m = \Gamma_m S_{am}$$

The results for each mode are calculated by multiplying the results of equation (7.7) by the mode shapes as in equation (7.9).

$$\mathbf{u}_m = \phi_m \Gamma_m S_{dm}, \quad \dot{\mathbf{u}}_m = \phi_m \Gamma_m S_{vm}, \quad \ddot{\mathbf{u}}_m = \phi_m \Gamma_m S_{am} \quad (7.9)$$

where,

S_{dm}	: Spectral displacement of m^{th} mode
S_{vm}	: Spectral velocity for of m^{th} mode
S_{am}	: Spectral acceleration of m^{th} mode

Since the analysis results for each mode pertain to only the maximum values, it is not possible to perform linear combinations as done in time history analysis. Therefore, the final results of a

response spectrum analysis are obtained by a modal combination of the analysis results for each mode in equation (7.9).

MIDAS enables us to analyze response spectrum in any direction on the X-Y plane and in the Z-direction in the global coordinate system. The user can choose one of the 3 methods for modal combination, which are ABS (**A**bsolute **S**um), SRSS (**S**quare **R**oot of the **S**um of the **S**quares) and CQC (**C**omplete **Q**uadratic **C**ombination) methods.

ABS (**A**bsolute **S**um)

$$R_{\max} = |R_1| + |R_2| + \cdots + |R_n| \quad (7.10)$$

SRSS (**S**quare **R**oot of the **S**um of the **S**quares)

$$R_{\max} = \left[R_1^2 + R_2^2 + \cdots + R_n^2 \right]^{1/2} \quad (7.11)$$

CQC (**C**omplete **Q**uadratic **C**ombination)

$$R_{\max} = \left[\sum_{i=1}^N \sum_{j=1}^N R_i \rho_{ij} R_j \right]^{1/2} \quad (7.12)$$

$$\rho_{ij} = \frac{8\sqrt{\xi_i \xi_j} (\xi_i + r_{ij} \xi_m) r_{ij}^{3/2}}{(1 - r_{ij}^2)^2 + 4\xi_i \xi_j r_{ij} (1 + r_{ij}^2) + 4(\xi_i^2 + \xi_j^2) r_{ij}^2}$$

$$\rho_{ij} = \frac{8\xi^2 (1 + r_{ij}) r_{ij}^{3/2}}{(1 - r_{ij}^2)^2 + 4\xi^2 r_{ij} (1 + r_{ij}^2)} \quad (\xi_i = \xi_j = \xi)$$

$$r_{ij} = \frac{\omega_i}{\omega_j} \quad \omega_j > \omega_i$$

$$0 \leq \rho_{ij} \leq 1 \quad \rho_{ij} = 1 \quad (i = j)$$

where,

R_{\max}	: Peak response
R_i	: Peak response (spectrum value) of i^{th} mode
r_{ij}	: Eigenvalue ratio of j^{th} mode to i^{th} mode
ω_i, ω_j	: Eigenvalues of i^{th} and j^{th} modes
ξ_i, ξ_j	: Damping ratios of i^{th} and j^{th} modes

In equation (7.12), when $i = j$, then $\rho_{ij} = 1$ regardless of the damping ratio (ξ_i, ξ_j). If the damping ratio becomes zero (0), both CQC and SRSS methods produce identical results. The ABS method produces the largest combination values among the three methods. The SRSS method has been widely used in the past, but it tends to overestimate or underestimate the combination results in the cases where the values of natural frequencies are close to one another. As a result, the use of the CQC method is increasing recently as it accounts for probabilistic inter-relations between the modes.

Example

If we now compare the natural frequencies and displacements for each mode for a structure having 3 DOF's with a damping ratio of 0.05, the results from the applications of SRSS and CQC are as follows:

Natural frequencies

$$\omega_1 = 0.46, \quad \omega_2 = 0.52, \quad \omega_3 = 1.42$$

Response spectrum value for each mode: D_{ij} (displacement component of i -th degree of freedom for j -th mode)

$$[D_{ij}] = \begin{bmatrix} 0.036 & 0.012 & 0.019 \\ -0.012 & 0.044 & -0.005 \\ 0.049 & 0.002 & -0.017 \end{bmatrix}$$

SRSS method results

$$R_{\max} = \left[R_1^2 + R_2^2 + R_3^2 \right]^{1/2} = \begin{bmatrix} 0.042 \\ 0.046 \\ 0.052 \end{bmatrix}$$

CQC method results

$$\rho_{12} = \rho_{21} = 0.3985$$

$$\rho_{13} = \rho_{31} = 0.0061$$

$$\rho_{23} = \rho_{32} = 0.0080$$

$$R_{\max} = \left[R_1^2 + R_2^2 + R_3^2 + 2\rho_{12}R_1R_2 + 2\rho_{13}R_1R_3 + 2\rho_{23}R_2R_3 \right]^{1/2} = \begin{bmatrix} 0.046 \\ 0.041 \\ 0.053 \end{bmatrix}$$

Comparing the two sets of displacements for each degree of freedom, we note that the SRSS method underestimates the magnitude for the first degree of freedom but overestimates the value for the second degree of freedom relative to those obtained by CQC. Thus, the SRSS method should be used with care when natural frequencies are close to one another.

7-2 Spectrum Function

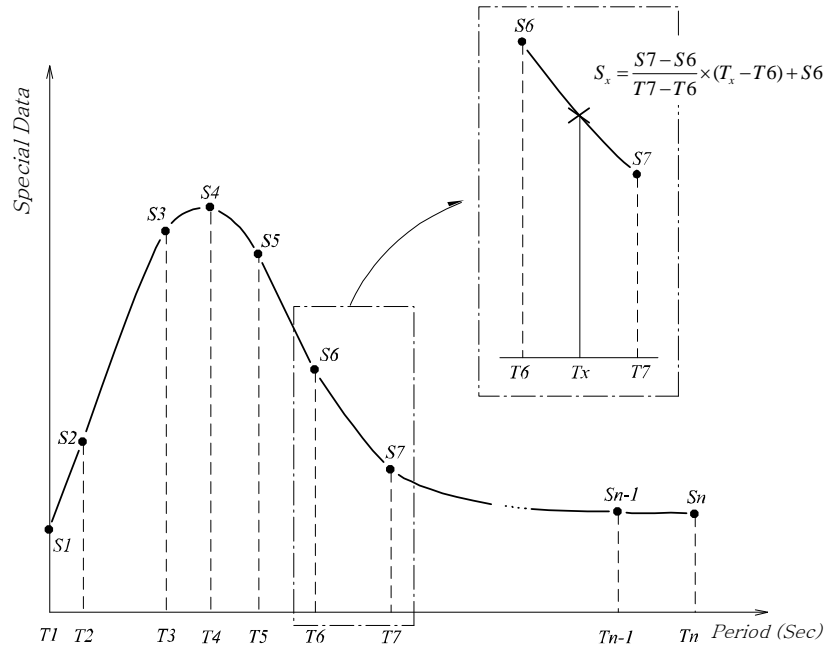


Figure 7-(1) Response spectrum curve and linear interpolation of spectral data

In response spectrum analysis, results for each mode are calculated by using spectrum functions. Generally, the spectrum functions are composed of the maximum values of time history analysis results obtained from equation (7.6). Once the damping ratio ξ and the seismic acceleration varying with time $\ddot{u}_g(t)$ are defined, solutions to equation (7.6) can be found according to the natural periods of the structure. Fig. 7-(1) shows how the spectrum functions are determined using a plot of the results of displacement, velocity and acceleration vertically against the periods of the

structure horizontally. Spectrum functions used in response spectrum analysis are generally provided by various design codes. MIDAS generates spectrum functions used in seismic analysis according to a selected design codes by simply entering the dynamic factor, foundation factor, zoning factor, importance factor, response modification factor, etc. Since linear or log scale interpolation is used to determine spectrum values corresponding to the natural periods of the structure, it is recommended that the data in the region of rapid changes be closely defined. And the range of the spectrum function must cover the range of the maximum and minimum periods calculated from the eigenvalue analysis. MIDAS uses the maximum or minimum value of the spectrum function if the periods of eigenvalue analysis exceed the range of the inputted range of the spectrum function.

Chapter 8. Linear Buckling Analysis

8-1 Introduction

Linear buckling analysis is used to determine critical load factors of a structure and the corresponding buckling mode shapes. For linear buckling analysis, the equilibrium equation for a structure considering its geometric stiffness due to stresses is as follows:

$$\mathbf{K}\mathbf{u} + \bar{\mathbf{K}}_G\mathbf{u} = \bar{\mathbf{p}} \quad (8.1)$$

where,

- \mathbf{K} : Elastic stiffness matrix
- $\bar{\mathbf{K}}_G$: Geometric stiffness matrix due to stresses
- \mathbf{u} : Total displacement of the structure
- $\bar{\mathbf{p}}$: Loads acting on the structure

In linear analysis, stresses in a structure are proportional to loads, and the geometric stiffness matrix is proportional to the stresses. Therefore, if we assume that the load, $\bar{\mathbf{p}}$ is proportional to a reference load, \mathbf{p} , the geometric stiffness, $\bar{\mathbf{K}}_G$ can be expressed as,

$$\bar{\mathbf{K}}_G = \alpha \mathbf{K}_G \quad (8.2)$$

$$\bar{\mathbf{p}} = \alpha \mathbf{p} \quad (8.3)$$

where,

- \mathbf{p} : Reference load
- \mathbf{K}_G : Geometric stiffness matrix corresponding to the reference load
- α : Load factor

Substituting the equations (8.2) and (8.3) into equation (8.1), we obtain,

$$\mathbf{K}\mathbf{u} + \alpha \mathbf{K}_G\mathbf{u} = \alpha \mathbf{p} \quad (8.4)$$

The equilibrium state as in equation (8.4) can be either stable or unstable depending on the magnitude of the load factor, α . In order to assess its stability, the perturbation, $\delta \mathbf{u}$ is added to \mathbf{u} at an equilibrium state.

$$\mathbf{K}(\mathbf{u} + \delta \mathbf{u}) + \alpha \mathbf{K}_G(\mathbf{u} + \delta \mathbf{u}) = \alpha \mathbf{p} \quad (8.5)$$

The non-perturbation terms in equation (8.5) are eliminated using the equilibrium equation (8.4), and then we obtain an eigenvalue problem as follows:

$$(\mathbf{K} + \alpha \mathbf{K}_G) \delta \mathbf{u} = \mathbf{0} \quad (8.6)$$

At this point, the stability of the equilibrium state can be assessed by the following matrix equation:

$$|\mathbf{K} + \alpha \mathbf{K}_G| > 0 \quad : \text{Stable status}$$

$$|\mathbf{K} + \alpha \mathbf{K}_G| \leq 0 \quad : \text{Unstable status}$$

So the eigenvalue, α , which satisfies equation (8.6), can be referred to as the critical load factor at which instability of the equilibrium begins. And the corresponding eigen mode, $\phi (= \delta \mathbf{u})$ represents the buckling shape of the structure. The critical load causing buckling in the structure can be expressed as $\alpha \mathbf{p}$ considering the critical load factor and the reference load. Fig. 8-(1) shows a column subjected to a compression load in its equilibrium state and the buckling shape due to the critical load.

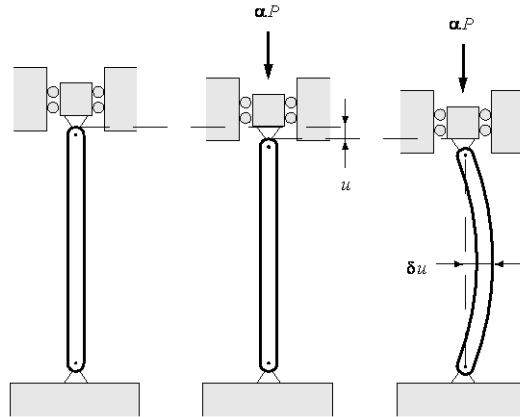


Figure 8-(1) Buckling of Column under Compression

In linear buckling analysis, the geometric stiffness matrix, \mathbf{K}_G needs to be set up and the eigenvalue problem of equation (8.6) must be solved. MIDAS calculates the geometric stiffness making use of the linear stresses or internal forces in elements and calculates the eigenvalue problem by the Lanczos iteration method.

8-2 Geometric Stiffness

The elements for which MIDAS considers geometric stiffness due to stresses are Truss, Beam, Plane Stress, Plate and Solid elements.

It is cautioned that buckling analysis requires of existing of elements in the model for which a geometric stiffness can be considered.

The general form of a geometric element stiffness matrix is as follows:

$$\mathbf{K}_G^e = \int \mathbf{G}^T \mathbf{S} \mathbf{G} dV \quad (8.7)$$

where, \mathbf{S} represents the stresses or internal element forces, and \mathbf{G} represents the matrix defining the relationship of nodal displacements and displacement derivatives.

8-2-1 Truss Element

Only the translational displacements in the transverse (y and z) directions in the element coordinate system are considered when the geometric stiffness of a truss element is calculated.

$$\mathbf{u}_i = \{v_i \quad w_i\}^T \quad (8.8)$$

$$v = \sum_{i=1}^2 N_i v_i, \quad w = \sum_{i=1}^2 N_i w_i \quad (8.9)$$

where,

N_i : 2-node linear shape function

For the formation of \mathbf{S} , only the axial stress, σ_{xx} is considered.

$$\mathbf{S} = \begin{bmatrix} \sigma_{xx} & 0 \\ 0 & \sigma_{xx} \end{bmatrix} \quad (8.10)$$

The relationship of nodal displacement and displacement derivative function, \mathbf{G}_i is expressed as

$$\mathbf{G}_i = \begin{bmatrix} \frac{\partial N_i}{\partial x} & 0 \\ 0 & \frac{\partial N_i}{\partial x} \end{bmatrix} \quad (8.11)$$

The geometric stiffness of a truss element can be expressed using the matrix \mathbf{G}_i .

$$\mathbf{K}_{Gij} = A \int_{L_e} \mathbf{G}_i^T \mathbf{S} \mathbf{G}_j dL \quad (8.12)$$

where,

A : Section area

L_e : Element length

By rearranging Eq. (8.12), the element stiffness matrix of a truss element can be calculated as follows:

$$\mathbf{K}_G = \frac{N_x}{L_e} \begin{bmatrix} 1 & 0 & -1 & 0 \\ 0 & 1 & 0 & -1 \\ -1 & 0 & 1 & 0 \\ 0 & -1 & 0 & 1 \end{bmatrix} \quad (8.13)$$

where,

N_x : Axial force

8-2-2 Beam Element

Since the geometric stiffness of a beam element in linear buckling analysis only considers axial force, N_x , the calculation process is similar to that for a truss element. In a beam element, the translational displacements in the transverse directions can be expressed as nodal d.o.f, which reflects rotations.

$$\mathbf{u}_i = \{v_i \quad w_i \quad \theta_{yi} \quad \theta_{zi}\}^T \quad (8.14)$$

$$v = \sum_{i=1}^2 (H_{0i}v_i + H_{1i}\theta_{zi}), \quad w = \sum_{i=1}^2 (H_{0i}w_i - H_{1i}\theta_{yi}) \quad (8.15)$$

H_{0i} and H_{1i} are Hermite cubic shape functions.

$$H_{01} = 1 - 3\xi^2 + 2\xi^3, \quad H_{02} = 3\xi^2 - 2\xi^3, \quad H_{11} = L_e(\xi - 2\xi^2 + \xi^3),$$

$$H_{02} = L_e(-x^2 + x^3)$$

where,

$$\xi : 0 \leq \xi \leq 1$$

L_e : Element length

Thus, the relationship of nodal displacement and displacement derivative function, \mathbf{G}_i , is noted as,

$$\mathbf{G}_i = \begin{bmatrix} \frac{\partial H_{0i}}{\partial x} & 0 & 0 & \frac{\partial H_{1i}}{\partial x} \\ 0 & \frac{\partial H_{0i}}{\partial x} & -\frac{\partial H_{1i}}{\partial x} & 0 \end{bmatrix} \quad (8.16)$$

Since the matrix, \mathbf{S} is identical to that for a truss element, the geometric stiffness matrix of a beam element can be calculated as follows:

$$\mathbf{K}_G = N_x \begin{bmatrix} \frac{6}{5L_e} & & & & & & & \\ 0 & \frac{6}{5L_e} & & & & & & \\ & & \frac{1}{10} & \frac{2L_e}{15} & & & & \\ & & 0 & 0 & \frac{2L_e}{15} & & & \\ -\frac{6}{15L_e} & 0 & 0 & -\frac{1}{10} & \frac{6}{5L_e} & & & \\ & -\frac{6}{15L_e} & \frac{1}{10} & 0 & 0 & \frac{6}{5L_e} & & \\ 0 & -\frac{1}{10} & -\frac{L_e}{30} & 0 & 0 & \frac{1}{10} & \frac{2L_e}{15} & \\ \frac{1}{10} & 0 & 0 & -\frac{L_e}{30} & -\frac{1}{10} & 0 & 0 & \frac{2L_e}{15} \end{bmatrix} \quad \text{symm.}$$

(8..17)

The calculation for the geometric stiffness of a beam element is performed while considering shear forces, bending moments and torsion moments. MIDAS uses various buckling types (lateral-torsional, axial-torsional) for the analysis of the geometric stiffness of beam elements.

8-2-3 Plane Stress Element

In the geometric stiffness calculation of a plane stress element, all the translational displacements in the x, y and z directions are considered in the element coordinate system.

$$\mathbf{u}_i = \{u_i \quad v_i \quad w_i\}^T \quad (8.18)$$

$$u = \sum_{i=1}^n N_i u_i, \quad v = \sum_{i=1}^n N_i v_i, \quad w = \sum_{i=1}^n N_i w_i \quad (8.19)$$

where,

n : Number of nodes

N_i : Shape functions based on the number of nodes

In-plane stresses are considered in the composition of \mathbf{S} .

$$\mathbf{S} = \begin{bmatrix} \bar{\mathbf{S}} & \mathbf{0} & \mathbf{0} \\ \mathbf{0} & \bar{\mathbf{S}} & \mathbf{0} \\ \mathbf{0} & \mathbf{0} & \bar{\mathbf{S}} \end{bmatrix}, \quad \bar{\mathbf{S}} = \begin{bmatrix} \sigma_{xx} & \tau_{xy} \\ \tau_{xy} & \sigma_{yy} \end{bmatrix} \quad (8.20)$$

The relationship of nodal displacement and displacement derivative function, \mathbf{G}_i , is noted as Eq. (8.21),

$$\mathbf{G}_i = \begin{bmatrix} \frac{\partial N_i}{\partial x} & \frac{\partial N_i}{\partial y} & 0 & 0 & 0 & 0 \\ 0 & 0 & \frac{\partial N_i}{\partial x} & \frac{\partial N_i}{\partial y} & 0 & 0 \\ 0 & 0 & 0 & 0 & \frac{\partial N_i}{\partial x} & \frac{\partial N_i}{\partial y} \end{bmatrix}^T \quad (8.21)$$

Using the matrix, \mathbf{G}_i , the geometric stiffness of a plane stress element can be expressed as,

$$\mathbf{K}_{Gij} = t \int_{A_e} \mathbf{G}_i^T \mathbf{S} \mathbf{G}_j dA \quad (8.22)$$

where,

t : Thickness

A_e : Element area

8-2-4 Plate Element

In the geometric stiffness calculation of a plate element, all the translational displacements in the x, y and z directions in the element coordinate system are expressed in nodal d.o.f, which reflect rotations.

$$\mathbf{u}_i = \{u_i \quad v_i \quad w_i \quad \theta_{xi} \quad \theta_{yi}\}^T \quad (8.23)$$

$$u = \sum_{i=1}^n (N_i u_i + z N_i \theta_{yi}), \quad v = \sum_{i=1}^n (N_i v_i - z N_i \theta_{xi}), \quad w = \sum_{i=1}^n N_i w_i \quad (8.24)$$

where,

n : Number of nodes

N_i : Shape functions based on the number of nodes

Since Eq. (8.24) does not consider curvature of an element, it can only be applied to a linear plate element. In the formation of \mathbf{S} , all the stress components except for σ_{zz} are considered.

$$\mathbf{S} = \begin{bmatrix} \bar{\mathbf{S}} & \mathbf{0} & \mathbf{0} \\ \mathbf{0} & \bar{\mathbf{S}} & \mathbf{0} \\ \mathbf{0} & \mathbf{0} & \bar{\mathbf{S}} \end{bmatrix}, \quad \bar{\mathbf{S}} = \begin{bmatrix} \sigma_{xx} & \tau_{xy} & \tau_{zx} \\ \tau_{xy} & \sigma_{yy} & \tau_{yz} \\ \tau_{zx} & \tau_{yz} & 0 \end{bmatrix} \quad (8.25)$$

The relationship of nodal displacement and displacement derivative function, \mathbf{G}_i , is noted as Eq. (8.26),

$$\mathbf{G}_i = \begin{bmatrix} \frac{\partial N_i}{\partial x} & \frac{\partial N_i}{\partial y} & 0 & 0 & 0 & 0 & 0 & 0 & 0 \\ 0 & 0 & 0 & \frac{\partial N_i}{\partial x} & \frac{\partial N_i}{\partial y} & 0 & 0 & 0 & 0 \\ 0 & 0 & 0 & 0 & 0 & 0 & \frac{\partial N_i}{\partial x} & \frac{\partial N_i}{\partial y} & 0 \\ 0 & 0 & 0 & -z \frac{\partial N_i}{\partial x} & -z \frac{\partial N_i}{\partial y} & -N_i & 0 & 0 & 0 \\ z \frac{\partial N_i}{\partial x} & z \frac{\partial N_i}{\partial y} & N_i & 0 & 0 & 0 & 0 & 0 & 0 \end{bmatrix}^T \quad (8.26)$$

Using the matrix, \mathbf{G}_i , the geometric stiffness of a plate element can be expressed as,

$$\mathbf{K}_{Gij} = \int_{V_e} \mathbf{G}_i^T \mathbf{S} \mathbf{G}_j dV \quad (8.27)$$

where,

V_e : Element volume

In case of a higher order plate element, the curvature of the element is considered, and a coordinate system is defined for rotational d.o.f. at each node. Other than these, the geometric stiffness can be calculated in a similar process.

8-2-5 Solid Element

In the geometric stiffness calculation of a solid element, all the translational displacements in the x, y and z directions in the element coordinate system are considered.

$$\mathbf{u}_i = \{u_i \quad v_i \quad w_i\}^T \quad (8.28)$$

$$u = \sum_{i=1}^n N_i u_i, \quad v = \sum_{i=1}^n N_i v_i, \quad w = \sum_{i=1}^n N_i w_i \quad (8.29)$$

where,

n : Number of nodes

N_i : Shape functions based on the number of nodes

In the formation of \mathbf{S} , all the stress components are considered.

$$\mathbf{S} = \begin{bmatrix} \bar{\mathbf{S}} & \mathbf{0} & \mathbf{0} \\ \mathbf{0} & \bar{\mathbf{S}} & \mathbf{0} \\ \mathbf{0} & \mathbf{0} & \bar{\mathbf{S}} \end{bmatrix}, \quad \bar{\mathbf{S}} = \begin{bmatrix} \sigma_{xx} & \tau_{xy} & \tau_{zx} \\ \tau_{xy} & \sigma_{yy} & \tau_{yz} \\ \tau_{zx} & \tau_{yz} & \sigma_{zz} \end{bmatrix} \quad (8.30)$$

The relationship of nodal displacement and displacement derivative function, \mathbf{G}_i , is noted as Eq. (8.31),

$$\mathbf{G}_i = \begin{bmatrix} \frac{\partial N_i}{\partial x} & \frac{\partial N_i}{\partial y} & \frac{\partial N_i}{\partial z} & 0 & 0 & 0 & 0 & 0 & 0 \\ 0 & 0 & 0 & \frac{\partial N_i}{\partial x} & \frac{\partial N_i}{\partial y} & \frac{\partial N_i}{\partial z} & 0 & 0 & 0 \\ 0 & 0 & 0 & 0 & 0 & 0 & \frac{\partial N_i}{\partial x} & \frac{\partial N_i}{\partial y} & \frac{\partial N_i}{\partial z} \end{bmatrix}^T \quad (8.31)$$

Using the matrix, \mathbf{G}_i , the geometric stiffness of a solid element can be expressed as,

$$\mathbf{K}_{Gij} = \int_{V_e} \mathbf{G}_i^T \mathbf{S} \mathbf{G}_j dV \quad (8.32)$$

where,

V : Element volume

8-3 Critical Load Factor Calculation

The eigenvalue problem of equation (8.6) in linear buckling analysis can be simply expressed as.

$$(\mathbf{K} + \lambda_m \mathbf{K}_G) = \mathbf{0} \quad (8.33)$$

where,

λ_m : Critical load factor

ϕ_m : Buckling mode shape

MIDAS uses the Lanczos iteration method for solving an eigenvalue problem such as equation (8.33). The Lanczos iteration method is explained in the Chapter Modal Analysis. Equation (8.33) is similar to an eigenvalue problem of free vibration analysis, but the geometric stiffness, \mathbf{K}_G is not positive definite unlike the mass matrix. Consequently, a shift invert technique must be applied in linear buckling analysis by substituting $\lambda_m = \sigma \theta_m / (1 - \theta_m)$. The calculated critical load factors are output in the order from the smallest absolute value upward.

8-4 Optional Parameters

In linear buckling analysis the critical load factor α may have either a positive or a negative sign depending on the direction of the reference load \mathbf{p} . In case of a complex finite element model with complex loads, the sign of the critical load factor can change depending on the buckling mode. Therefore, MIDAS provides a function, which can calculate only the critical loads with a positive sign if necessary.

Although specific loads such as self weight generally remain constant unlike the reference load, \mathbf{p} , MIDAS provides a function that allows selection of load types so that they can be used as either a reference load or a constant load. The load, which has been selected as a constant load will remain constant irrespective of the load factor, α , but generates only the geometric stiffness. The linear buckling analysis, which includes constant loads, becomes an eigenvalue problem in the following form:

$$(\mathbf{K} + \mathbf{K}_G^* + \lambda_m \mathbf{K}_G) = 0 \quad (8.34)$$

where,

\mathbf{K}_G^* : Geometric stiffness for stresses induced by constant loads

In a linear buckling analysis the Lanczos iterative process expects for plate elements that the drilling d.o.f. is activated. When this is not the case MIDAS will restrain the rotations in the local Z-direction.

Chapter 9. Load and Boundary

9-1 Constraint Conditions

In MIDAS, 3 translational degrees of freedom and 3 rotational degrees of freedom may be assigned to a single node, depending on the type of elements that are connected to the node. Constraint conditions are defined to a node when not all 6 degrees of freedom are addressed by the elements connected to the nodes, or when the user wants to define special constraints to restrain a node from any directional movements in the Global Coordinate System (GCS).

Different element types activate the following nodal degrees of freedom:

- Truss-element: Only 2D or 3D translations
- Beam-elements: 2D or 3D translations and rotations
- Plane stress, plane strain and axisymmetric: Only 2D displacements.
- Plate elements: 3D translations and only out of plane rotations
- Plate elements with drilling dof's: 3D translations and rotations
- Solids: Only 3D translations

Degrees of freedom in a node that are not activated by elements connected to that node are automatically constrained, unless the Automatic Constraint option has been switched off in the Control Analysis dialogue. When a 2D Analysis or an axisymmetric model has been chosen in this dialogue box automatically the out-of-plane degrees of freedom will be constrained. When nodal constraints are assigned to a node, the corresponding reactions are produced at the node.

The nodal reactions are produced in the GCS.

User defined constraints can be defined with respect to the Global Coordinate System (GCS) or to the Nodal Local Coordinate System (NCS).

Fig. 9-(1) illustrates a method of specifying constraints on the degrees of freedom of a plane frame model. Since this is a two dimensional beam-element model defined in the GCS X-Z plane, the displacement d.o.f. in the GCS Y-direction and the rotational d.o.f. about the GCS X and Z

axes need to be restrained in all the nodes.

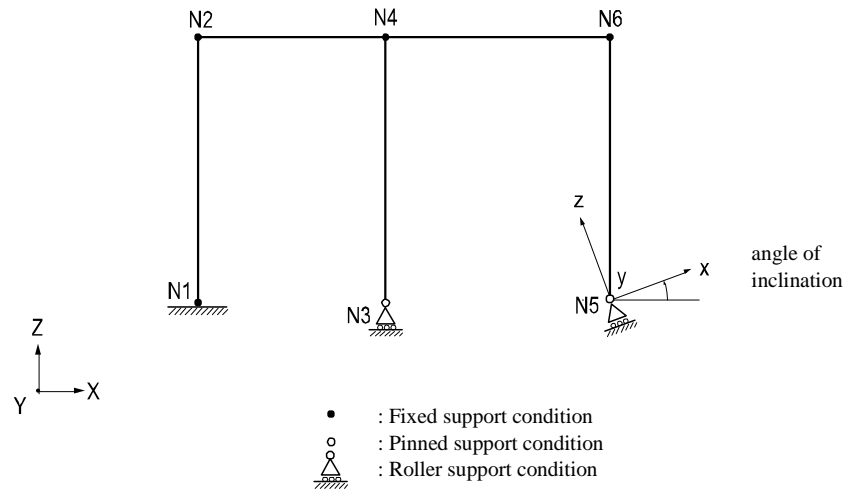
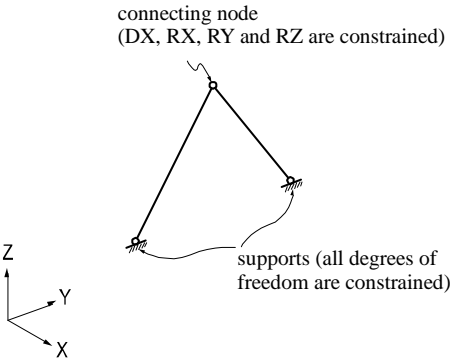


Figure 9-(1) Plane frame model with constraints on d.o.f.

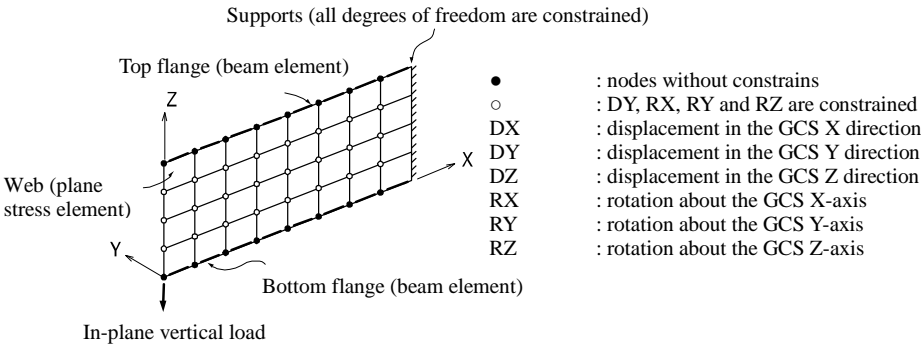
For node **N1**, which is a fixed support, the Constraints dialogue is used to additionally restrain the translations in the GCS X and Z-directions and the rotations about the GCS Y-axis. For node **N3**, which is a roller support, the translation in the GCS Z direction is restrained. For node **N5**, which is a roller support in an NCS, the NCS is defined first at an angle to the GCS X-axis. Then the corresponding translation is restrained in the NCS.

Fig. 9-(2) shows examples of constraining the not-connected degrees of freedom in nodes. In Fig. 9-(2) (a), the translation in the direction of the X-axis and all rotations in the connecting node are constrained because of truss elements have only axial translational degrees of freedom. Fig. 9-(2) (b) represents an I-beam where the top and bottom flanges are modeled as beam elements and the web is modeled with plane stress elements with drilling degrees of freedom. 3D beam elements have 6 d.o.f.'s at each node, and therefore, in those nodes where the plane stress elements are connected to the beam elements, no additional

nodal constraints are required. At the same time the out-of-plane translation in the Y direction and all the rotational degrees of freedom are constrained in the nodes of the plane stress elements that are not connected to the beams. Plane stress elements with drilling degrees of freedom have only in-plane translational and out-of plane rotational degrees of freedom. If the structure does not have enough stiffness, users can assign small stiffness, which does not affect the whole structural analysis, to prevent instability in analysis.



(a) Connection of truss elements



(b) Modeling of an I-shaped cantilever beam, top/bottom flanges modeled as beam elements, and web modeled as plane stress elements

Figure 9-(2) Examples of constraints on degrees of freedom

9-2 Skewed (Inclined) Support Condition

Skewed support conditions are modeled using constraint conditions in the NCS (nodal coordinate system). When a NCS is defined in a node, the support conditions are interpreted with reference to the NCS, whereas the nodal reactions on the skewed supports are produced in the GCS (global coordinate system).

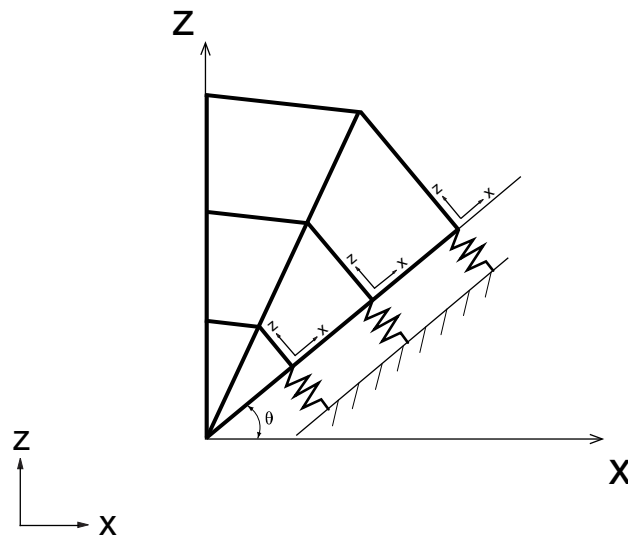


Figure 9-(3) Example of skewed support condition

9-3 Constraint Equation

A constraint equation can be defined to subordinate the movement of a specific node to the movement of other nodes. In that case the specific subordinated node is called the constraint node, and the nodes that define the movement of the subordinated nodes are called independent nodes. The linear relationship between the constraint node and the independent nodes is defined as.

$$U_{M,m} = a_1 U_{I,i} + a_2 U_{J,j} + \dots + b_1 R_{I,i} + b_2 R_{J,j} + \dots \quad \text{- Translational Constraint} \quad (9.1)$$

$$R_{M,m} = c_1 U_{I,i} + c_2 U_{J,j} + \dots + d_1 R_{I,i} + d_2 R_{J,j} + \dots \quad \text{- Rotational Constraint} \quad (9.2)$$

where,

$U_{M,m}$: Linear displacement of constraint node, m in M-direction

$U_{I,i}$: Linear displacement of independent node, i in I-direction

$R_{M,m}$: Rotational displacement of constraint node, m about M-direction

$R_{I,i}$: Rotational displacement of independent node, i about I-direction

a_i, b_i, c_i, d_i : Coefficients defining correlation among degrees of freedom

The constraint equations (9.1) and (9.2) allow to constrain any node and any degree of freedom. The constrain equations are defined to the degrees of freedom in GCS.

Fig. 9-(4) shows an application example in which a connection is made between a 3-D structure consisting of solid elements and a thin plate consisting of plate elements. Since solid elements do not have any rotational degrees of freedom, they cannot restrain the rotational behavior of the connected plate. When the rotations of the plate elements are restrained such as defined by equation (9.3), the plate elements will be connected perpendicularly to the solid elements and bending of the plate will be transferred into bending of the solid elements.

$$R_{y,3} = \frac{1}{h} U_{x,1} - \frac{1}{h} U_{x,2} \quad (9.3)$$

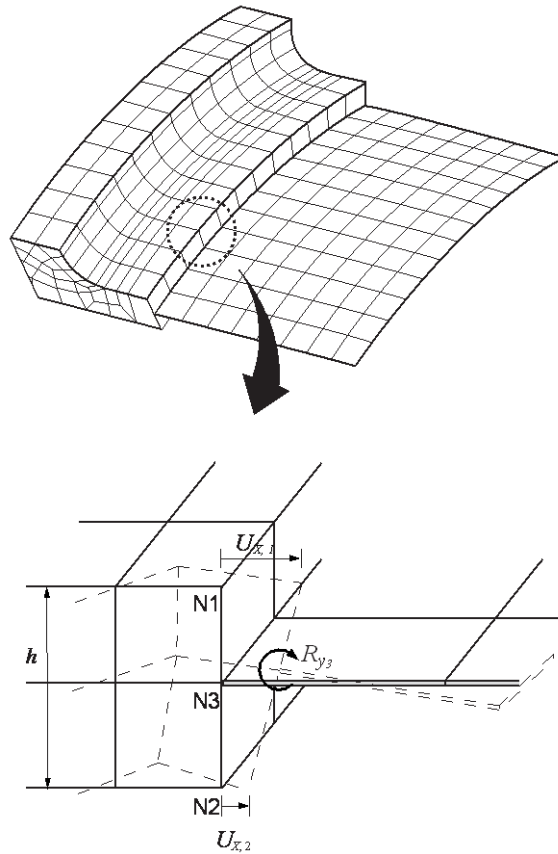


Figure 9-(4) Example of constraint equation application

It must be emphasized that the constraint equation which is explained in above is not a rigid link. A rigid link is a set of constraint relations that each equals the movement of one node to the movement of a single node. While in constraint equations the movement of a single node is

subordinated to the movements of a number of independent nodes.

There are two methods for assigning constraint equations. By using the explicit method constraint equations are defined by directly entering all the degrees of freedom and coefficients of equations (9.1) or (9.2). Alternatively the weighted displacement method can be used, in which the movement of the constraint node is prescribed to be equal to the average displacement of independent nodes. Both of which are outlined below.

Explicit

- Select a constraint node and a degree of freedom (multi-selection is not allowed).
- Select independent nodes and a degree of freedom (multi-selection is not allowed), and input coefficients (a_i, b_i or c_i, d_i).

Information for independent nodes can be input more than once, and the equations (9.1) or (9.2) are defined based on this information.

Weighted displacement

- Select a constraint node.
- Select degrees of freedom (multi-selection is allowed) to be equal to the constraint node and independent nodes.
- Define for each independent node a weight factor, w_i .

Information on independent nodes can be input more than once, and the following constraint equations are defined by this information:

$$U_{I,m} = \sum_i \frac{w_i}{S} U_{I,i} \quad \text{or} \quad R_{I,m} = \sum_i \frac{w_i}{S} R_{I,i}$$

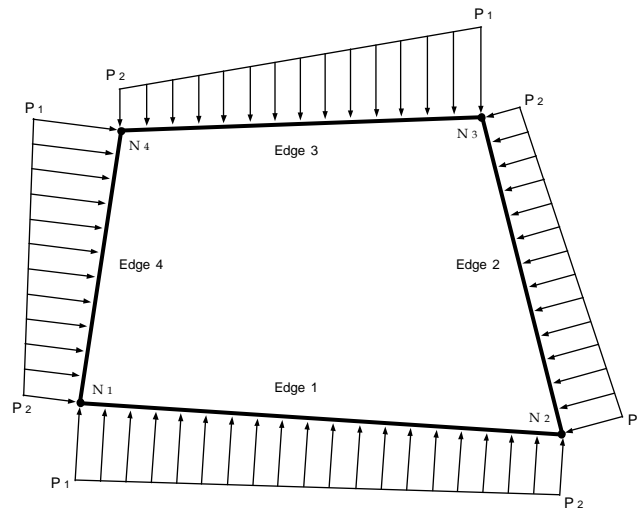
where, S is the sum of the weight factors ($\sum_i w_i$). MIDAS does not allow to couple translational and rotational displacements.

9-4 Nodal Load

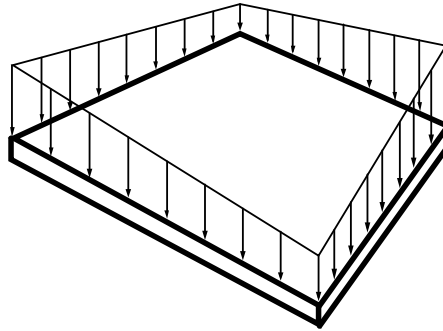
The nodal load is the most basic load, which enables us to define 6 directional load values for each node. The direction of a nodal load can be defined in any particular coordinate system.

9-5 Element Pressure Load

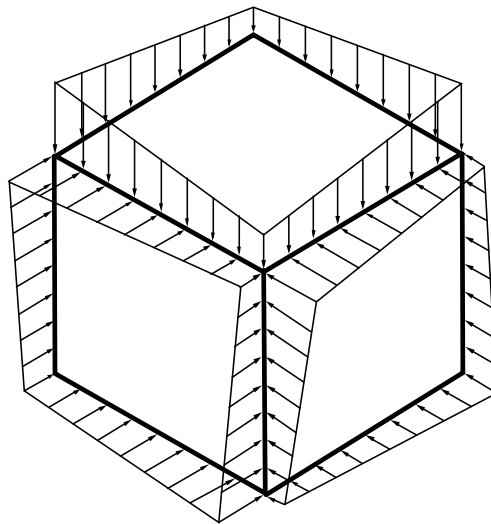
Element pressure load is input in a form of uniformly distributed loads on surfaces or edges. Element pressure loads can be applied to 2-D elements (plate, plane stress, plane strain and axisymmetric) and 3-D elements (solid). Internally MIDAS converts element pressure loads into equivalent nodal loads. The load directions can be defined in either ECS or GCS. Fig. 9-(5) shows examples of element pressure loads.



(a) Pressure load applied to a plate element, plane stress element, plane strain element or axisymmetric element in normal direction to edges



(b) Pressure load acting on the surface of a plate element or plane stress element



(c) Pressure load acting on surfaces of a 3D element in the normal direction

Figure 9-(5) Pressure loads acting on elements

9-6 Body Force

In general the body force is used to define the self-weight or inertia force of a structure. This load is applied to all the elements and is defined in GCS X, Y and Z-directions. The basic definition of the body force is given in equation (9.4), and the magnitudes of ω_x , ω_y , ω_z are calculated as the product of the density and the gravitational acceleration in each direction. The shape function is identical to that used in the element stiffness calculation.

$$\mathbf{F}_i = \int_{V_e} N_i \begin{Bmatrix} \omega_x \\ \omega_y \\ \omega_z \end{Bmatrix} dV \quad (9.4)$$

Where,

- \mathbf{F}_i : Body Force
- ω_x : Unit Weight in the X-direction
- ω_y : Unit Weight in the Y-direction
- ω_z : Unit Weight in the Z-direction
- N_i : *Shape Function*

9-7 Prescribed Displacement

Prescribed displacement is used when the location of a particular node after deformation is known. Prescribed displacement is basically defined in the Global Coordinate System, but can be defined together with Nodal Coordinate System to express displacements in any directions. Prescribed displacement is classified as loading because it generates structural deformation, but is similar to a boundary condition as it generates reactions.

Especially, a node with a specified displacement results in adaptations in the stiffness of the corresponding elements. Therefore, one should be careful when the structure is analyzed for a number of load cases in the same analysis-run. For example, a prescribed displacement in a node will remain in place for all the load cases which are applied to the structure when boundary conditions are not changed accordingly.

Chapter 10. Construction Stage Analysis

10-1 Introduction

A structure is completed in a number of construction stages. The configurations of the structure, loadings, boundary conditions and even the physical properties of structural members change during the construction stages. Such changes in the structural system are induced from the installation and removal of temporary structural members required in the process of construction and staged erection of permanent structural members. In the case of concrete, the material properties change with time. If the structural system continues to change as the construction progresses, the true behavior of the finally erected structure may be different from that of the structure analyzed without reflecting the construction stages. Also the maximum member forces may take place during the construction rather than at the completion of the construction or at the service stage.

If a structure undergoes various construction stages until its completion, the structure needs to be analyzed for time dependent effects. This is intended to include member forces induced from the process of construction in design in addition to the member forces resulting from the loads conventionally accounted for. The time dependent properties of concrete include creep, shrinkage, change in compressive strength, etc. The time effects should be taken into account for the construction of new structures as well as existing structures under retrofit and reinforcement.

MIDAS considers the following changes in structural systems in construction stage analysis:

Creation and removal of structural members

Loading and unloading

Change in boundary conditions

MIDAS considers the following time-dependent properties of concrete for construction stage analysis:

Compressive strength gain with time in concrete members

Creep deformation in concrete members

Shrinkage deformation in concrete members

The following steps outline the procedure used in MIDAS for carrying out time dependent analysis reflecting construction stages:

1. Create a structural model. Assign elements, loads and boundary conditions to groups of the 3 categories, which will be activated or deactivated at each construction stage.
2. Define time dependent material properties such as creep and shrinkage. The time dependent material properties can be defined using the standards such as ACI or CEB-FIP. The user may also define them directly.
3. Compose construction stages based on the true sequence of construction.
Define construction stages using the previously defined element groups, boundary condition groups and loading groups.
4. Carry out a structural analysis after specifying the desired analysis conditions.

10-2 Composition of Construction Stages

In order to compose a construction stage model, a base model needs to be created first followed by assigning construction stages to the corresponding structural members associated with loads and boundary conditions.

10-2-1 Generation of a base model

In order to activate (create) and deactivate (delete) structural members according to construction stages, the total structure needs to be classified into element groups, boundary condition groups and load groups separately.

10-2-2 Composition of construction stages

The user composes construction stages by activating and/or deactivating element groups, boundary condition groups and load groups for each stage. Sub-time steps can be added to each construction stage, and load groups can be added or deleted at each time step. Activation and deactivation of element groups and boundary condition groups causing changes in the structural system can take place only at the first step of a construction stage. If the structure is insensitive to time dependent properties, times need not be input for construction stages. However, if a number of load groups are sequentially applied in a construction stage, the corresponding time intervals need to be defined.

Each construction stage is composed by defining activation and deactivation of element groups, boundary condition groups and load groups. The structure at a particular construction stage is composed of added and deleted element, boundary condition and load groups accumulated on the structure at the previous construction stage.

The following are the contents, which can be included in each construction stage:

Activation (creation) and deactivation (deletion) of elements with certain ages (maturities)

Activation and deactivation of loadings applied at specific times

Changes in boundary conditions

The concept of construction stages used in MIDAS is illustrated in Figure 10-(1). Construction stages can be readily defined by duration for each stage. A construction stage with '0' duration is possible, and the first and last steps are basically created once a construction stage is defined. Activation and deactivation of elements, boundary conditions and loadings are accomplished within the time duration of each stage.

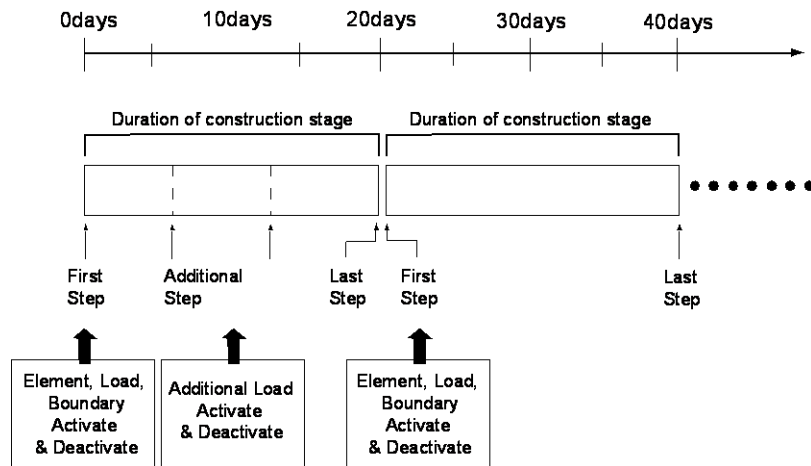


Figure 10-(1) Concept of composing construction stages

Changing conditions such as new and deleted elements, change in boundary conditions and addition and removal of loadings basically take place at the first step of each construction stage. Accordingly, each construction stage is created to reflect specific changes in the structural system associated with specific timing in the construction schedule. That is, the number of construction stages increases with the increase in the number of interim structural conditions until its

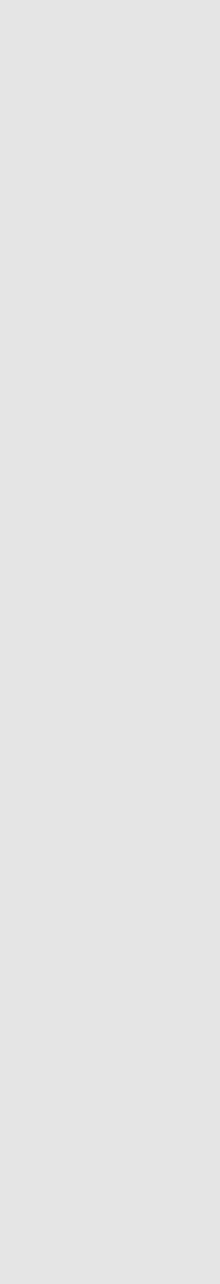
completion.

Structural system changes in elements and boundary conditions can be defined only at the first step of each construction stage. However, additional steps can be defined within a given construction stage for ease of analysis to reflect addition and removal of loadings. This allows us to specify delayed loadings representing, for instance, temporary construction loads while maintaining the same structural system without creating additional construction stages.

If many additional steps are defined in a construction stage, the accuracy in analysis results will improve since the time dependent analysis closely reflects creep, shrinkage and compressive strengths. However, if too many steps are defined, the analysis time may be excessive, thereby compromising efficiency. On the contrary, if time dependent properties are not selected and the analysis is subsequently carried out, the analysis results do not change irrespective of the number of steps defined.

Subsequent to activating certain elements with specific ages (maturities) in a construction stage, the ages continue to increase with the passage of subsequent construction stages. MIDAS automatically calculates the properties of concrete elements using the elements' ages accumulated over the duration of the previous construction stages.

When specific elements are activated in a construction stage, the corresponding ages must be assigned to the elements. Creating elements with '0' age represents the instant when the fresh concrete is cast. However, a structural analysis model does not typically include temporary structures such as formwork/falsework, and as such unexpected analysis results may be produced if the analysis model includes immature concrete elements. Especially, if elements of '0' age are activated, and an analysis is carried out reflecting the time dependent compressive strength gains, meaningless large displacements may result due to the fact that no concrete strength can be expected in the first 24 hours of casting. A correct method of modeling a structure in a construction stage will be that the wet concrete with the formwork is considered as loading, and that the activation of the concrete elements are assumed after a period of time upon removal of the



formwork/falsework.

If new elements are activated in a particular construction stage, the total displacements or stresses accumulated up to the immediately preceding construction stage do not affect the new elements. That is, new elements are activated with '0' internal stresses regardless of the loadings applied to the structure previously.

If a loading is applied in a construction stage, the loading remains in effect in all the subsequent construction stages unless it is deliberately removed. Elements are similarly activated for a given construction stage. Only the elements pertaining to the relevant construction stage are activated as opposed to activating all the necessary elements for the stage. Once-activated elements cannot be activated again, and only those elements can be deactivated.

10-3 Time Dependent Material Properties

MIDAS can reflect time dependent concrete properties such as creep, shrinkage and compressive strength gains.

10-3-1 Creep

Creep and shrinkage simultaneously occur in real structures as presented in Figure 10-(2). Accordingly, elastic shortening, creep and shrinkage can not be physically separated. However, for the purpose of practical analysis and design, they are separately considered.

The true elastic strain in the figure 10-(1) represents the reduction in elastic strain as a result of concrete strength gains (increase in modulus of elasticity) relative to time. In general cases, the apparent elastic strain is considered as elastic strain. MIDAS, however, reflects the true elastic strain in analysis since it can consider the time-variant concrete strength gains.

Creep strain in a member is proportional to elastic strain at the time of loading. And high strength concrete yields less creep strain relative to lower strength concrete under the same stress. The magnitude of creep strain can be 1.5~3.0 times that of elastic strain. About 50% of the total creep strain takes place within the first few months followed by a slower development of creep strain for some time, and the majority of creep strain will have occurred in about 5 years.

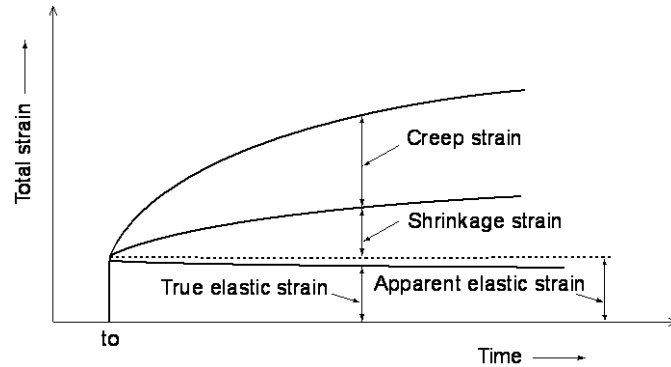


Figure 10-(2) Concrete strain over the passage of time

Most materials retain the property of creep. However, it is more pronounced in the concrete materials, and it contributes to the increase in deformation relative to time, which can not be ignored in design. In normal concrete structures, sustained dead loads and external forces cause creep. Additional creep occurs in pre-stressed/post-tensioned concrete structures due to the pre-stress effects.

The sum of elastic strain and creep strain in concrete under the state of uni-axial stress can be expressed as,

$$\varepsilon(t) = \varepsilon_i(\tau) + \varepsilon_c(t, \tau) = \sigma \cdot J(t, \tau) \quad (10.1)$$

where,

$J(t, \tau)$: Total strain under the unit stress, defined as creep function
τ	: Time at which the specified stress starts acting, loading time
t	: Time at which the resulting strain is calculated

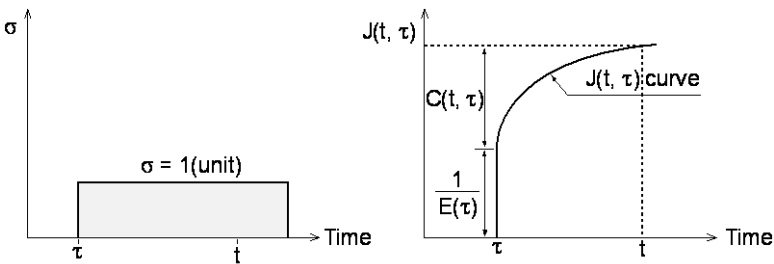


Figure 10-(3) Definition of creep function and specific creep

As shown in Figure 10-(3), the creep function $J(t, \tau)$ can be presented by the sum of the initial elastic strain and creep strain as follows:

$$J(t, \tau) = \frac{1}{E(\tau)} + C(t, \tau) \tag{10.2}$$

where,

$E(\tau)$: Modulus of elasticity at the time of loading
$C(t, \tau)$: Resulting creep deformation at the age t, which is referred to as specific creep

The creep function $J(t, \tau)$ can be also expressed in terms of a ratio relative to the elastic deformation.

$$J(t, \tau) = \frac{1 + \phi(t, \tau)}{E(\tau)} \tag{10.3}$$

where,

$\phi(t, \tau)$: Creep coefficient, which represents the ratio of the creep to the elastic deformation
-----------------	---

From the above two equations, the relationship between the specific creep and the creep coefficient can be also expressed as follows:

$$\phi(t, \tau) = E(\tau) \cdot C(t, \tau) \quad (10.4)$$

$$C(t, \tau) = \frac{\phi(t, \tau)}{E(\tau)} \quad (10.5)$$

MIDAS allows us to specify creep coefficients or shrinkage strains calculated by the equations presented in CEB-FIP, ACI, etc., or we may also directly specify the values obtained from experiments.

The user-defined property data can be entered in the form of creep coefficient, creep function or specific creep (see Figure 10-(4)).

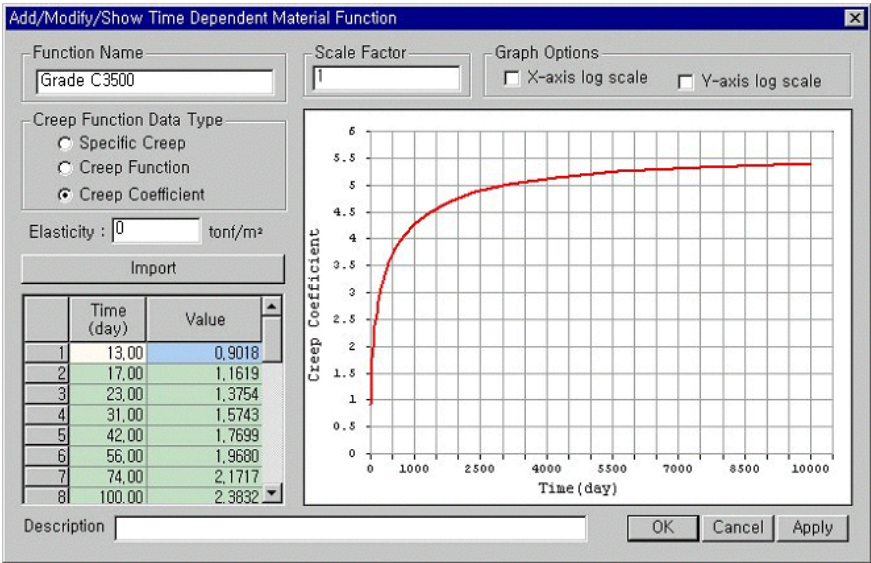


Figure 10-(4) Dialog box for specifying user-defined creep coefficients

The concrete creep function varies with the time of loading as shown in Fig. 10-(5). The later the load application time, the smaller is the immediate elastic strain due to the concrete strength gain with time. As for the deformation at a time after the time of loading, it will become smaller if the

loading time is later.

The reasons why the elastic and creep strains decrease as the loading time is delayed are the development of compressive strength and the hydration of concrete. When the user defines the creep functions, the property of concrete strength gain must be well reflected. The range of the loading times for creep functions must include the element ages (loading times), which exist in a time dependent analysis. The accuracy of analysis results improves with an increase in the number of creep functions for different loading times.

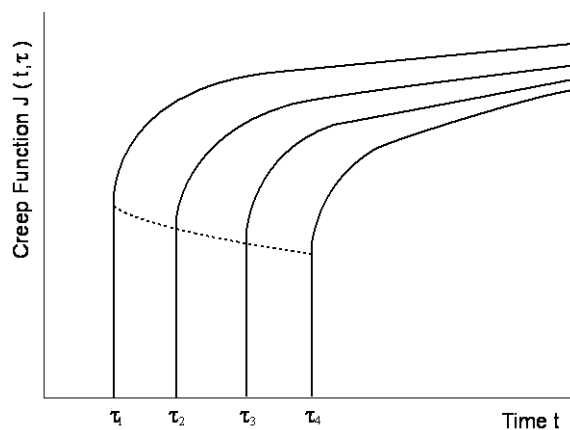


Figure 10-(5) Creep functions varying with different loading times

10-3-2 Methods of calculating creep

The creep function, which is used to calculate creep is a function of the time of a specific stress applied (τ) and the current time (t). That is, various creep functions as shown in Fig. 10-(5) can be used depending on the time of the specific stress applied. If the stress changes with time, the increased/decreased stress at each time requires an independent creep function. Creep strain at a particular time is calculated through superposition of individually calculated strains due to the stresses increased/decreased from the time that stress starts changing. In order to use the superposition method, the histories of all the element stresses are saved, and the creep strains are calculated from the initial steps to the present for all the stresses at every step. Extensive data storage and calculations are thus required to use the superposition method. However, MIDAS does not save the entire histories of stresses, rather MIDAS uses the following integration method to increase the calculation efficiency.

The following outlines the method of calculating creep strain at the time t due to the stresses at the time τ_j using creep coefficients:

$$\varepsilon_c(t, \tau_j) = \phi(t, \tau_j) \varepsilon(\tau_j) : \text{Creep strain} \quad (10.6)$$

$$P_{cr} = \int_A E(t) \varepsilon_c(t, \tau_j) dA : \text{Loading due to creep strain} \quad (10.7)$$

where,

$\varepsilon(\tau_j)$: Strain due to stress at time τ_j
$\phi(t, \tau_j)$: Creep coefficient for the time from τ_j to t
$\varepsilon_c(t, \tau_j)$: Creep strain at time t due to elastic strain at time τ_j

The following outlines the method in which specific functions of creep are numerically expressed, and stresses are integrated over time. The total creep from a particular time τ to a final time t can be expressed as an (superposition) integration of creeps due to the stresses resulting from each stage.

$$\varepsilon_c(t) = \int_0^t C(t, \tau) \frac{\partial \sigma(\tau)}{\partial \tau} d\tau \quad (10.8)$$

where,

$\varepsilon_c(t)$: Creep strain at time t
$C(t, \tau)$: Specific creep
τ	: Time at which the load is applied

If we assume from the above expression that the stress at each stage is constant, the total creep strain can be expressed as a sum of the strains at each stage.

$$\varepsilon_{c,n} = \sum_{j=1}^{n-1} \Delta \sigma_j C(t_n, \tau_j) \quad (10.9)$$

Using the above expression, the incremental creep strain $\Delta \varepsilon_{c,n}$ between the times t_n and t_{n-1} can be expressed as follows:

$$\Delta \varepsilon_{c,n} = \varepsilon_{c,n} - \varepsilon_{c,n-1} = \sum_{j=1}^{n-1} \Delta \sigma_j C(t_n, \tau_j) - \sum_{j=1}^{n-2} \Delta \sigma_j C(t_{n-1}, \tau_j) \quad (10.10)$$

If the specific creep is expressed by the degenerate kernel (Dirichlet functional summation), the incremental creep strain can be calculated without having to save the entire stress history.

$$C(t, \tau) = \sum_{i=1}^m a_i(\tau) \left[1 - e^{-(t-\tau)/\Gamma_i} \right] \quad (10.11)$$

where,

$a_i(\tau)$: Coefficients related to the initial shapes of specific creep curves at the time τ of loading
Γ_i	: Values related to the shapes of specific creep curves over a period of time

The coefficients $a_i(\tau)$ related to the initial shapes of the specific creep curves are expressed as follows:

1. Define m , and Γ_i which will be used for calculation. Define the time of loading τ_j . The time of loading needs to be distributed evenly over the total time for analysis.
2. Select the time t_i at which creep strain needs to be calculated. Because the creep strain calculation is based on the time of loading, the time at which creep needs to be calculated t_i must be always greater than the loading time τ_j .
3. Calculate the creep compliance values, $C(t_i, \tau_j)$. The user may use the creep compliance values, which may have been measured or calculated using national standards. The number of the creep compliance values should be evenly distributed over the total analysis time, and sufficient data needs to be secured.
4. By using the values obtained from the above steps, the following expression can be constructed:

$$\begin{bmatrix} 1 - e^{-(t_1 - \tau_j)/\Gamma_1} & 1 - e^{-(t_1 - \tau_j)/\Gamma_2} & \dots & 1 - e^{-(t_1 - \tau_j)/\Gamma_m} \\ 1 - e^{-(t_2 - \tau_j)/\Gamma_1} & 1 - e^{-(t_2 - \tau_j)/\Gamma_2} & \dots & 1 - e^{-(t_2 - \tau_j)/\Gamma_m} \\ \vdots & \vdots & \ddots & \vdots \\ 1 - e^{-(t_n - \tau_j)/\Gamma_1} & 1 - e^{-(t_n - \tau_j)/\Gamma_2} & \dots & 1 - e^{-(t_n - \tau_j)/\Gamma_m} \end{bmatrix} \begin{Bmatrix} a_1(\tau_j) \\ a_2(\tau_j) \\ \vdots \\ a_m(\tau_j) \end{Bmatrix} = \begin{Bmatrix} C(t_1, \tau_j) \\ C(t_2, \tau_j) \\ \vdots \\ C(t_n, \tau_j) \end{Bmatrix}$$

$$\begin{aligned} A_{i,1} &= \Delta\sigma_0 a_i(\tau_j) \\ \mathbf{A}_{n \times m} \mathbf{a}_{m \times 1} &= \mathbf{C}_{n \times 1} \quad (n > m) \end{aligned} \quad (10.12)$$

5. The Least Square Method is used to obtain the solution to Eq. 10.12.

$$\mathbf{A}^T \mathbf{A} \mathbf{a} = \mathbf{A}^T \mathbf{C}$$

$$\mathbf{a} = (\mathbf{A}^T \mathbf{A})^{-1} (\mathbf{A}^T \mathbf{C})$$

In order to optimize the values of m and Γ_i , the following conditions need to be satisfied.

- Minimize errors in the Least Square Method.
- The ultimate creep strain calculated using $\sum a_i(\tau_j)$ need to be very close to the predicted.
- Participation from each value of $a_i(\tau_j) \left[1 - e^{-(t-\tau_j)/\Gamma_i} \right]$ needs to be close to one another.

Having gone through the steps 3~5 using different loading times τ_j , the corresponding values of $a_i(\tau_j)$ are obtained and subsequently saved. If a specified loading time does not coincide with any of the specific creep curves, the loading times τ_j and the corresponding $a_i(\tau_j)$ are interpolated.

Using the above specific creep equation, the incremental strain can be rearranged as follows:

$$\Delta \varepsilon_{c,n} = \sum_{i=1}^m \left[\sum_{j=1}^{n-2} \Delta \sigma_j a_i(\tau_j) e^{-(t-\tau_j)/\Gamma_i} + \Delta \sigma_{n-1} a_i(\tau_{n-1}) \right] \left[1 - e^{-(t-\tau_j)/\Gamma_i} \right] \quad (10.13)$$

$$\Delta \varepsilon_{c,n} = \sum_{i=1}^m A_{i,n} \left[1 - e^{-(t-\tau_j)/\Gamma_i} \right]$$

$$A_{i,n} = \sum_{j=1}^{n-2} \Delta \sigma_j a_i(\tau_j) e^{-(t-\tau_j)/\Gamma_i} + \Delta \sigma_{n-1} a_i(\tau_{n-1})$$

From the equation for $A_{i,n}$, $A_{i,n-1}$ can be expressed as,

$$A_{i,n-1} = \sum_{j=1}^{n-3} \Delta \sigma_j a_i(\tau_j) e^{-(t-\tau_j)/\Gamma_i} + \Delta \sigma_{n-2} a_i(\tau_{n-2}).$$

Therefore, the relationship between $A_{i,n}$ and $A_{i,n-1}$ is given by,

$$A_{i,n} = A_{i,n-1} e^{-(t-\tau_{n-1})/\Gamma_i} + \Delta\sigma_{n-1} a_i(\tau_{n-1})$$

$$A_{i,1} = \Delta\sigma_0 a_i(\tau_0)$$

Using the above method, the incremental strain for each element at each stage can be obtained from the stress resulted from the immediately preceding stage and the modified stress $\Delta\sigma_{n-1}$ accumulated up to the immediately preceding stage. This method thus eliminates the need for saving the stress histories of the members and calculating the strains from the initial stage at every stage. This method provides rather accurate analysis reflecting change in stresses. Once the user enters the required material properties, the user need not separately calculate the creep coefficients since the program automatically calculates them. The fact that the equations from the standard specifications are used, this method retains some drawbacks. The user can not directly enter own values based on experience, and the user can not assign specific creep values to specific elements. This method is greatly affected by the time interval of analysis. The time intervals for construction stages in general cases are relatively short and hence do not present problems. However, if a long time interval is specified for a stage, it is necessary to divide the interval into sub-time intervals to closely reflect the creep effects.

Time intervals based on the characteristics of creep should be divided into a log scale. Once the user specifies the number of intervals, MIDAS automatically divides the time intervals into a log scale. There is no fast rule for an appropriate number of time intervals. But more divisions result in approaching the exact solution. In case of a long construction stage interval, it may be necessary to divide the stage into a number of time steps.

10-3-3 Shrinkage

Shrinkage is a phenomenon in which the volume of concrete contracts over time. MIDAS reflects shrinkage property curves presented in various standards and specifications in analysis.

Shrinkage is a function of time, which is independent from stresses in concrete members. Shrinkage strain from a time t_0 to a time t can be expressed as,

$$\varepsilon_s(t, t_0) = \varepsilon_\infty \cdot f(t, t_0) \quad (10.14)$$

where,

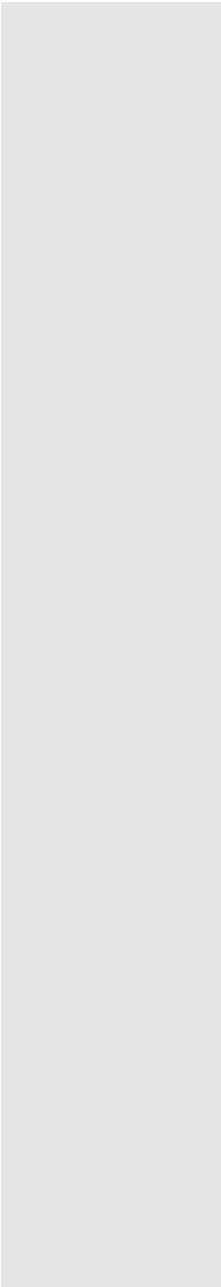
ε_∞	: Shrinkage coefficient at the final time
$f(t, t_0)$: A function of time
t	: Time of observation
t_0	: Initial time of shrinkage

MIDAS allows us to use the characteristic curves of shrinkage presented in various Standards such as CEB-FIP Model Code and ACI 209 and user defined curves based on experimental data.

Shrinkage strain at a corresponding construction stage is calculated using the characteristic curves of shrinkage.

$$\varepsilon_{sh}(t_2, t_1) = \varepsilon_{sh}(t_2, t_0) - \varepsilon_{sh}(t_1, t_0)$$

$\varepsilon_{sh}(t_2, t_1)$: Shrinkage strain from the construction stage t_1 to t_2
$\varepsilon_{sh}(t_1, t_0)$: Shrinkage strain from the initial time of shrinkage t_0 to t_1
$\varepsilon_{sh}(t_2, t_0)$: Shrinkage strain from the initial time of shrinkage t_0 to t_2



Shrinkage strains are non-mechanical strains such as thermal strains and creep strains. So the strains associated with calculation of concrete member forces are obtained by subtracting the shrinkage strains from the strains due to displacement.

$$F = EA(\varepsilon - \varepsilon_{sh})$$

If a structural member is not constrained in the axial direction, the effect of shrinkage on the member causes only displacement without generating member forces. Also, member forces caused by shrinkage may induce creep strains without the presence of external loadings. Shrinkage strains are thus affected by boundary conditions and time.

10-3-4 Change in modulus of elasticity with time

Concrete compressive strength and the modulus of elasticity change with time. In practice, considering the aging effects (maturity) is essential to ensure that the intended structure attains the planned geometry and strength.

MIDAS reflects the changes in concrete compressive strength gain relative to the ages of concrete members in analysis. The compressive strength gain functions can be defined from the standard specifications such as ACI 209 and CEB-FIP as shown in Figure 10-(6), or it could be a user-defined function. MIDAS thus refers to the concrete compressive strength gain curves, and it automatically calculates the strengths corresponding to the times defined in the construction stages, which are used in analysis.

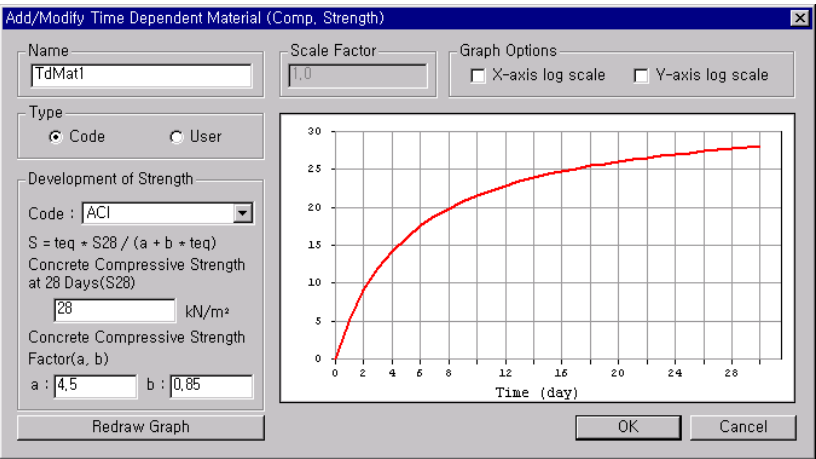


Figure 10-6 Definition of concrete compressive strength gain curve based on Standards

MIDAS uses the following standards:

1. Korean Bridge Standards (2005)

Equations for creep calculation

$$\varepsilon_{c\sigma} = f_c(t') / E_{ci} \cdot \phi(t, t')$$

$$\varepsilon_{c\sigma}(t, t') = f_c(t') \left[\frac{1}{E_{ci}(t')} + \frac{\phi(t, t')}{E_{ci}} \right]$$

$$\phi(t, t') = \phi_0 \beta_c(t - t')$$

$$\phi_0 = \phi_{RH} \beta(f_{cu}) \beta(t')$$

$$\phi_{RH} = 1 + \frac{1 - 0.01RH}{0.10 \sqrt[3]{h}}$$

$$\beta(f_{cu}) = \frac{16.8}{\sqrt{f_{cu}}}$$

$$\beta(t') = \frac{1}{0.1 + (t')^{0.2}}$$

$$\beta_c(t - t') = \left[\frac{(t - t')}{\beta_H + (t - t')} \right]^{0.3}$$

$$\beta_H = 1.5 \left\{ 1 + (0.012RH)^{18} \right\} h + 250 \leq 1500$$

$$h = \frac{2A_c}{u}$$

ε_{cc}	: Creep strain in concrete
$\sigma_c(t')$: Sustained stress at loading time (t')
E_{ci}	: Initial tangential modulus of elasticity of concrete at 28-days
$\phi(t, t')$: Creep coefficient of concrete
ϕ_o	: Notional creep coefficient
f_{cu}	: Mean 28-day compressive strength (MPa)
RH	: Relative humidity (%)
h	: Notional size of a member (mm)
A_c	: Cross sectional area of a member (mm^2)
u	: Perimeter of cross section exposed to atmosphere (mm)
t'	: Age at the time of loading sustained load (day)
t	: Time of measurement (day)

Equations for shrinkage calculation

$$\varepsilon_{sh}(t, t_s) = \varepsilon_{sho} \cdot \beta_s(t - t_s)$$

$$\varepsilon_{sho} = \varepsilon_s(f_{cu}) \beta_{RH}$$

$$\varepsilon_s(f_{cu}) = \left[160 + 10 \beta_{sc} \left(9 - \frac{f_{cu}}{10} \right) \right] \times 10^{-6}$$

$$\beta_{RH} = \begin{cases} -1.55 \left[1 - \left(\frac{RH}{100} \right)^3 \right] & (40\% \leq RH \leq 99\%) \\ 0.25 & (RH \geq 99\%) \end{cases}$$

$$\beta_s(t - t_s) = \sqrt{\frac{(t - t_s)}{0.035h^2 + (t - t_s)}}$$

$\varepsilon_{cs}(t, t_s)$: Creep strain from the time of initial creep (t_s) to a particular time (t)
ε_{cso}	: Notional creep strain
$\beta_s(t - t_s)$: Function for manifestation of shrinkage
β_{sc}	: Coefficient for cement type
	$\beta_{sc} = 4$ for a Type II cement
	$\beta_{sc} = 5$ for a Type I & V cement
	$\beta_{sc} = 6$ for a Type III cement

2. ACI209

Equations for creep calculation

$$\varepsilon_c(t, t') = \sigma_c(t')$$

$$J(t, t') = \frac{I}{E_{ci}(t')} [1 + \phi(t, t')]$$

$$\phi(t, t') = \frac{(t - t')^{0.6}}{10 + (t - t')^{0.6}} \phi_u$$

$$\phi_u = 2.35 C_{cu} C_h C_i C_s C_f C_a$$

1) Curing conditions (C_{cu})

$$C_{cu} = \begin{cases} 1.25(t')^{-0.118} & (\text{moist cured}) \\ 1.13(t')^{-0.094} & (\text{steam cured}) \end{cases}$$

2) Relative humidity (C_h)

$$C_h = \begin{cases} 1.27 - 0.0067H & (H > 40) \\ 1.0 & (H \leq 40) \end{cases}$$

3) Volume-surface ratio (C_i)

$$C_i = \frac{2}{3} \left[1 + 1.13e^{-0.0213 \text{ v/s}} \right] \quad (mm)$$

4) Slump (C_s)

$$C_s = 0.82 + 0.00264 S \quad (mm)$$

5) Fine aggregate percentage (C_f)

$$C_f = 0.88 + 0.0024 \psi$$

6) Air content (C_a)

$$C_a = 0.46 + 0.09A \geq 1.0$$

t'	: Concrete age at the time of loading
H	: Relative humidity (%)
v / s	: Volume-surface ratio
S	: Slump value
ψ	: Ratio of fine aggregate to the total aggregate by weight (%)
A	: Air content (%)

Equations for shrinkage calculation

$$\varepsilon_{sh}(t, t_0) = \begin{cases} \frac{(t - t_0)}{35 + (t - t_0)} \varepsilon_{sh,u} & (\text{moist cured}) \\ \frac{(t - t_0)}{55 + (t - t_0)} \varepsilon_{sh,u} & (\text{steam cured}) \end{cases}$$

$$\varepsilon_{sh,u} = -780 \times 10^{-6} C_{sh}$$

$$C_{sh} = C_{cp} C_h C_t C_s C_f C_a C_c$$

1) Correction factors for the age of curing (C_{cp})

Age of moist curing (day)	1	3	7	14	28	90
Correction factor (C_{cp})	1.2	1.1	1.0	0.93	0.86	0.75

2) Relative humidity (C_h)

$$C_h = \begin{cases} 1.40 - 0.010H & (40 \leq H \leq 80) \\ 3.00 - 0.030H & (80 \leq H \leq 100) \end{cases}$$

3) Volume-surface ratio (C_t)

$$C_t = 1.2e^{-0.00472 v/s} \quad (mm)$$

4) Slump (C_s)

$$C_s = 0.89 + 0.00161S \quad (mm)$$

- 5) Fine aggregate percentage (C_f)

$$C_f = \begin{cases} 0.30 + 0.014\psi & (\psi \leq 50) \\ 0.90 + 0.002\psi & (\psi \geq 50) \end{cases}$$

- 6) Air content (C_a)

$$C_a = 0.95 + 0.008A$$

- 7) Cement content of concrete (C_c)

$$C_c = 0.75 + 0.00061C \quad (kg/m^3)$$

$\epsilon_{sh}(t, t_0)$: Shrinkage strain from the time of initial shrinkage (t_0) to a particular time (t)
$\epsilon_{sh,u}$: Final shrinkage strain
t_0	: Initial time at which shrinkage starts (<i>day</i>)
H	: Relative humidity (%)
v / s	: Volume-surface ratio
S	: Slump value
ψ	: Ratio of fine aggregate to the total aggregate by weight (%)
A	: Air content (%)
C	: Cement content of concrete (kg/m^3)

3. CEB-FIP Model Code 90

Equations for creep calculation

$$\varepsilon_{cc}(t, t_0) = \sigma_c(t_0) / E_{ci} \cdot \phi(t, t_0)$$

$$\phi(t, t_0) = \phi_0 \beta_c(t - t_0)$$

$$\phi_0 = \phi_{RH} \beta(f_{cm}) \beta(t_0)$$

$$\phi_0 = \phi_{RH} \beta(f_{cm}) \beta(t_0)$$

$$\phi_{RH} = 1 + \frac{1 - RH / RH_o}{0.46(h / h_0)^{1/3}}$$

$$\beta(f_{cm}) = \frac{5.3}{(f_{cm} / f_{cmo})^{0.5}}$$

$$\beta(t_0) = \frac{1}{0.1 + (t_o / t_l)^{0.2}}$$

$$h = \frac{2A_c}{u}$$

$$\beta_c(t - t_0) = \left[\frac{(t - t_o) / t_l}{\beta_H + (t - t_o) / t_l} \right]^{0.3}$$

$$\beta_H = 150 \left\{ 1 + \left(1.2 \frac{RH}{RH_o} \right)^{18} \right\} \frac{h}{h_o} + 250 \leq 1500$$

ε_{cc}	: Creep strain in concrete
$\sigma_c(t_o)$: Sustained stress at loading time (t_o)
E_{ci}	: Modulus of elasticity of concrete at 28-days
$\phi(t, t_o)$: Creep coefficient for concrete
ϕ_o	: Notional creep coefficient
f_{cm}	: Mean 28-day compressive strength (<i>MPa</i>) $f_{cmo} = 10 \text{ MPa}$
RH	: Relative humidity $RH_o = 100\%$
h	: Notional size of a member $h_o = 100 \text{ mm}$
A_c	: Cross sectional area of a member (<i>mm</i> ²)
u	: Perimeter length exposed to atmosphere (<i>mm</i>)
t_o	: Effective age at the time of loading (day)
t	: Time of measurement (day) $t_1 = 1 \text{ day}$

Equations for shrinkage calculation

$$\varepsilon_{cs}(t, t_s) = \varepsilon_{cso} \cdot \beta_s(t - t_s)$$

$$\varepsilon_{cso} = \varepsilon_s(f_{cm}) \beta_{RH}$$

$$\varepsilon_s(f_{cm}) = [160 + 10\beta_{sc}(9 - f_{cm}/f_{cmo})] \times 10^{-6}$$

$$\beta_{RH} = -1.55\beta_{sRH} \quad (40\% \leq RH \leq 99\%)$$

$$\beta_{RH} = +0.25 \quad (RH \geq 99\%)$$

$$\beta_{sRH} = 1 - \left(\frac{RH}{RH_o} \right)^3$$

$$\beta_s(t - t_s) = \left[\frac{(t - t_s)/t_1}{350(h/h_o)^2 + (t - t_s)/t_1} \right]^{0.5}$$

$\varepsilon_{cs}(t, t_s)$: Shrinkage strain from the time of initial shrinkage (t_s) to a particular time (t)
ε_{cso}	: Notional shrinkage strain
$\beta_s(t - t_s)$: Function for manifestation of shrinkage
β_{sc}	: Coefficient for cement type
	$\beta_{sc} = 4$ Slowly hardening cements
	$\beta_{sc} = 5$ Normal or Rapid hardening cements
	$\beta_{sc} = 8$ Rapid hardening high strength cements

4. JSCE (Japanese concrete standard specifications - 2002)

Equations for creep calculation

$$\varepsilon'_{cc} = \phi \sigma'_{cp} / E_{ct}$$

$$\varepsilon'_{cc}(t, t', t_0) = \left[1 - e^{-0.09(t-t')^{0.6}} \right] \cdot \varepsilon'_{cr}$$

$$\varepsilon'_{cr} = \varepsilon'_{bc} + \varepsilon'_{dc}$$

$$\varepsilon'_{bc} = 15(C + W)^{2.0} (W / C)^{2.4} (\log_e t')^{-0.67}$$

$$\varepsilon'_{dc} = 4500(C + W)^{1.4} (W / C)^{4.2} [\log_e (V / S / 10)]^{-2.2} (1 - RH / 100)^{0.36} t_0^{-0.30}$$

ε'_{cc}	: Compressive creep strain of concrete
ϕ	: Creep coefficient
σ'_{cp}	: Compressive strength
E_{ct}	: Modulus of elasticity at the time of loading
ε'_{cr}	: Final value of creep strain under a unit stress ($\times 10^{-10} / (N / mm^2)$)
ε'_{bc}	: Final value of basic creep strain under a unit stress ($\times 10^{-10} / (N / mm^2)$)
ε'_{dc}	: The final value of drying creep strain under a unit stress ($\times 10^{-10} / (N / mm^2)$)
C	: Cement content of concrete (kg/m^3) ($260 \text{ kg} / m^3 \leq C \leq 500 \text{ kg} / m^3$)
W	: Unit weight (kg / m^3) ($130 \text{ kg} / m^3 \leq C \leq 230 \text{ kg} / m^3$)
W / C	: Water-cement ratio ($40\% \leq C \leq 65\%$)
RH	: Relative humidity ($45\% \leq C \leq 80\%$)
V	: Volume (mm^3)
S	: Area exposed to atmosphere (mm^2)
V / S	: Volume-surface ratio (mm) ($100 \text{ mm} \leq V / S \leq 300 \text{ mm}$)
t_0	: Time at which shrinkage starts (day)
t'	: Effective age at loading (day)
t	: Time of measurement (day)

Equations for shrinkage calculation

$$\varepsilon_{cs}'(t, t_0) = \left[1 - e^{-0.108(t-t_0)^{0.56}} \right] \cdot \varepsilon_{sh}'$$
$$\varepsilon_{sh}' = -50 + 78 \left[1 - e^{(RH/100)} \right] + 38 \log_e W - 5 \left[\log_e (V/S/10) \right]^2$$

$\varepsilon_{sh}'(t, t_0)$: Shrinkage strain from concrete age t_0 to t ($\times 10^{-5}$)
ε_{sh}'	: Final shrinkage strain ($\times 10^{-5}$)

5. Japan bridge specification (Hisei Year 14)

Equations for creep calculation

$$\varepsilon_{cc} = \phi \sigma_c / E_{ct}$$

$$\phi(t, t_0) = \phi_{d0} \cdot \beta_d(t - t_0) + \phi_{f0} [\beta_f(t) - \beta_f(t_0)]$$

$$h_{th} = \lambda \cdot \frac{A_c}{u}$$

ε_{cc}	: Creep strain in concrete
σ_c	: Stress due to sustained load (N / mm^2)
E_c	: Modulus of elasticity of concrete (N / mm^2)
ϕ	: Creep coefficient for concrete
ϕ_{d0}	: Creep coefficient for delayed elastic strain due to sustained load
$\beta_d(t - t_0)$: Function for manifestation of ϕ_{d0} with time (see Figure 10-(7))
ϕ_{f0}	: Creep coefficient for permanent creep strain
$\beta_f(t)$: Function for manifestation of ϕ_{f0} with time (see Figure 10-(8))
RH	: Relative humidity ($45\% \leq C \leq 80\%$)
λ	: Environmental coefficient corresponding to relative humidity (see Table 10.1)
A_c	: Surface area of a member (mm^2)
u	: Perimeter length exposed to atmosphere (mm)
h_{th}	: Fictitious member thickness (mm)
t_0	: Effective age at loading (day)
t	: Time of measurement (day)

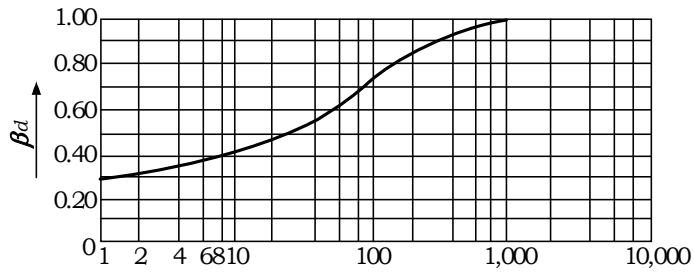


Figure 10-(7) Function for manifestation of ϕ_{d0} of concrete with time ($\beta_d(t-t_0)$)

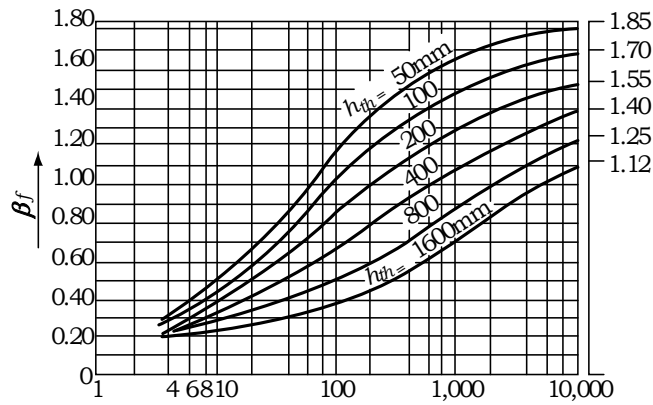


Figure 10-(8) Function for manifestation of ϕ_{f0} of concrete with time ($\beta_f(t)$)

Environment condition	ϕ_{f0}	λ
Submerged	0.8	60
Relative humidity 90%	1.3	10
Relative humidity 70%	2.0	3
Relative humidity 40%	3.0	2

Table 10.1 ϕ_{f0} and λ corresponding to environmental conditions

Equations for shrinkage calculation

$\epsilon_{cs}(t,t_0) = \epsilon_{so} \cdot \beta_s(t-t_0)$

$\epsilon_{cs}(t,t_0)$: Shrinkage strain from concrete age t_0 to t
ϵ_{so}	: Final strain of basic shrinkage in concrete
$\beta_s(t)$: Function for manifestation of shrinkage

:

Environmental condition	ϵ_{so}
Submerged	-10×10^{-5}
Relative humidity 90%	$+10 \times 10^{-5}$
Relative humidity 70%	$+25 \times 10^{-5}$
Relative humidity 40%	$+50 \times 10^{-5}$

Table 10.2 ϵ_{so} values corresponding to environmental conditions

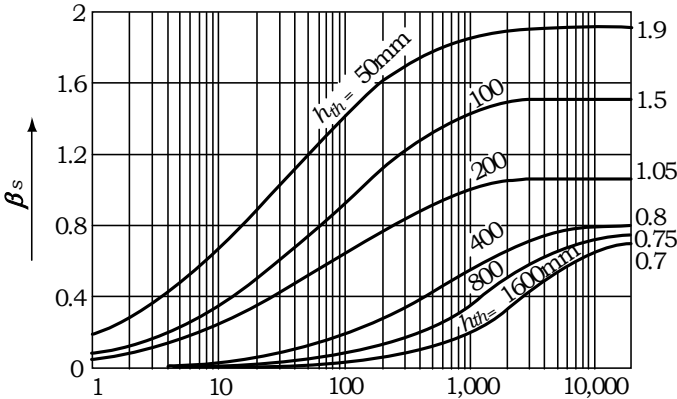


Figure 10-(9) Function for manifestation of concrete shrinkage (β_s)

Chapter 11. Thermal Analysis

11-1 Introduction

Thermal stresses due to heat of hydration in a mass concrete structure may cause detrimental cracking, thereby reducing its durability as well as impeding structural safety. In order to avoid such problems in casting mass concrete, heat of hydration is analyzed to control cracking through calculation of temperature and stress distribution. Mass concrete structures requiring heat of hydration analysis depend on their dimensions, structural types, cement types and construction conditions. In practice, heat of hydration analyses are normally carried out for slabs or mats in excess of 800~1000 mm in thickness and walls confined at bottom in excess of about 500 mm in thickness.

Surface cracking may develop initially due to the temperature difference between the surface and the center. Through-cracks can also develop as a result of contraction restrained by external boundary conditions in the cooling process of high heat of hydration. Heat of hydration analysis is largely classified into thermal transfer and thermal stress analyses. Thermal transfer analysis entails conduction, convection, heat source, etc., and thermal stress analysis entails changes in the modulus of elasticity, creep and shrinkage, which are influenced by temperature, curing conditions, maturities, etc.

11-2 Heat Transfer Analysis

MIDAS calculates changes in nodal temperatures with time due to conduction, convection and heat source in the process of cement hydration. The following outlines the pertinent items considered in MIDAS and some of the main concepts in heat transfer analysis.

Conduction

In the case of fluids, molecular movements or direct collisions; and in the case of solids, movements of electrons cause the heat transfer through energy exchange from a high temperature zone to a low temperature zone. The rate of heat transfer through conduction is proportional to the area perpendicular to heat flux multiplied by the temperature gradient in that direction (Fourier's law).

$$Q_x = q_x A = -kA \frac{\partial T}{\partial x} \quad (11.1)$$

where,

Q_x	: Rate of heat transfer in X-direction
q_x	: Heat flux
A	: Area
k	: Thermal conductivity
$\frac{\partial T}{\partial x}$: Temperature gradient

In general, the thermal conductivity of saturated concrete ranges between 1.21~3.11, and its unit is $kcal/(m^2 \cdot h \cdot ^\circ C)$. The thermal conductivity of concrete tends to decrease with increases in temperature, but the effect is rather insignificant in the ambient temperature range.

Convection

When a fluid flows on a solid or in a pipe with different temperatures between the solid and the fluid, heat is transmitted between the fluid and the surface of the solid through the fluid's relative molecular motion. This heat transfer is called convection.

Heat transfer by forced convection occurs if a fluid is forced to flow on a surface such that an artificial fluid flow is formed. If the fluid flow is naturally created by a buoyancy effect due to a difference in density resulting from a difference in temperature within the fluid, such heat transfer is referred to as a free convection. Since the fluid flow affects the temperature field in this type of heat transfer, it is not a simple task to determine the temperature distribution and convection heat transfer in practice.

The convection coefficient h_c is defined to simply calculate the heat transfer between a solid and a fluid. T and T_∞ represent the surface temperature of the solid and the average temperature of the fluid flowing on the solid surface respectively.

$$q = h_c(T - T_\infty) \quad : \text{Heat flux on a solid} \quad (11.2)$$

The convection coefficient (h_c) widely varies with many factors such as flow type, the geometric configuration of the object, the area in contact with the flow, physical properties of the fluid, average temperature on the surface subjected to convection, location, etc. Therefore, it is very difficult to formulate the coefficient. In general, convection problems associated with temperature analyses of mass concrete structures relate to the type of heat transfer taking place between the concrete surface and the atmosphere. Accordingly, the following empirical formula is often used, which is a function of the atmospheric wind speed.

$$h_c = h_n + h_f = 5.2(kcal/(m^2 \cdot h \cdot ^\circ C)) + 3.2V \text{ (m/sec)} \quad (11.3)$$

The unit for convection coefficient is $kcal/(m^2 \cdot h \cdot ^\circ C)$.

Heat Source

Heat source is intended to model the amount of heat generated by the hydration process in mass concrete. The internal heat generation from the hydration heat source for a unit time and a unit volume is obtained by differentiating the equation for adiabatic temperature rise and multiplying the specific heat and the density of concrete. Adiabatic conditions are said to occur without loss or gain of heat or change in entropy; i.e., as isothermal.

Internal heat generation per unit time and volume ($kcal/(m^3 \cdot h)$) is expressed by,

$$g = \frac{1}{24} \rho c K \alpha e^{-\alpha t / 24}, \quad (11.4)$$

while the adiabatic temperature rise ($^{\circ}C$) is given by,

$$T = K(1 - e^{-\alpha t}) \quad (11.5)$$

where,

T	: Adiabatic temperature ($^{\circ}C$)
K	: Maximum adiabatic temperature rise ($^{\circ}C$)
α	: Response speed
t	: Time (days)

Pipe cooling

Pipe cooling is accomplished by embedding pipes into a concrete structure. These pipes are used to reduce the temperature rise from heat of hydration by passing a lower temperature fluid through the pipes. The heat transfer process takes place between the fluid and the pipe surfaces, and the temperature of the fluid increases as it passes through the pipes. The heat transfer by convection between the fluid and pipe surfaces is expressed as follows:

$$q_{conv} = h_p A_s (T_s - T_m) = h_p A_s \left(\frac{T_{s,i} + T_{s,o}}{2} - \frac{T_{m,i} + T_{m,o}}{2} \right) \quad (11.6)$$

where,

h_p	: Convection coefficient of fluid in pipes ($kcal / m^2 \cdot h \cdot ^\circ C$)
A_s	: Surface area of a pipe (m^2)
T_s, T_m	: Pipe surface and coolant temperatures ($^\circ C$)
$T_{s,i}, T_{s,o}$: Pipe inlet and outlet temperatures ($^\circ C$)
$T_{m,i}, T_{m,o}$: Coolant temperatures at pipe inlet and outlet ($^\circ C$)

Initial temperature

Initial temperature is an average temperature of water, cement and aggregates at the time of concrete casting, which becomes the initial condition for analysis. MIDAS allows the user to define different initial temperatures for different construction stages.

Ambient temperature

Ambient temperature represents the curing temperature, which may be defined as a constant value, *sine* function or time-dependent function.

Prescribed temperature

A prescribed temperature represents a boundary condition for a heat transfer analysis and always remains a constant temperature. The nodes that are not specified with the convection conditions or constant temperatures are analyzed under the adiabatic condition without any heat transfer. In a symmetrical model, the plane of symmetry is considered an adiabatic boundary condition.

Solution to heat equilibrium equations

The basic equilibrium equation expressed in Eq. 11.7 is used to analyze heat transfer. Analysis results are expressed in terms of nodal temperatures varying with time.

$$CT + (K + H)T = F_Q + F_h + F_q = R \quad (11.7)$$

$C = \left[\int_V \rho c N_i N_j dx dy dz \right]$: Capacitance (mass)
$K = \left[\int_V \left(k_{xx} \frac{\partial N_i}{\partial x} \frac{\partial N_j}{\partial x} + k_{yy} \frac{\partial N_i}{\partial y} \frac{\partial N_j}{\partial y} + k_{zz} \frac{\partial N_i}{\partial z} \frac{\partial N_j}{\partial z} \right) dx dy dz \right]$: Conduction
$H = \left[\int_S h_c N_i N_j dS_h \right]$: Convection
$F_Q = \int_V N_i Q dx dy dz$: Heat load due to heat source/sink
$F_h = \int_S h_c T_e N_i dS_h$: Heat load due to convection
$F_q = - \int_S q N_i dS_q$: Heat load due to heat flux

Table 11.1 Basic equilibrium equations used for heat transfer analysis

where,

ρ	: Density
c	: Specific heat
$k_{xx} \ k_{yy} \ k_{zz}$: Heat conductivity
h_c	: Convection coefficient
Q	: Rate of heat flow
T_e	: Ambient temperature
q	: Heat flux
T	: Nodal temperature
\dot{T}	: Differential of nodal temperature with respect to time
R	: Thermal loads

If the temperature T_i at the time t_i and the temperature T_{i+1} at the time t_{i+1} are assumed to have the relationship given by Eq. (11.8),

$$\alpha \dot{T}_{i+1} + (1-\alpha) \dot{T}_i = \frac{T_{i+1} - T_i}{\Delta t_{i+1}}, \quad (11.8)$$

and we rearrange the equilibrium equation; we then obtain Eq. (11.9), Eq. (11.10) and Eq. (11.11).

$$C \dot{T}_i + (K + H) T_i = R_i \quad (11.9)$$

$$C \dot{T}_{i+1} + (K + H) T_{i+1} = R_{i+1}$$

Taking the weighted average of the equilibrium Eq. (11.9) at the times t_i and t_{i+1} , Eq. (11.10) is obtained.

$$C \left(\alpha \dot{T}_{i+1} + (1-\alpha) \dot{T}_i \right) + (K + H) \left(\alpha T_{i+1} + (1-\alpha) T_i \right) = \alpha R_{i+1} + (1-\alpha) R_i. \quad (11.10)$$

By introducing Eq. (11.8) into Eq. (11.10), the equilibrium equation Eq. (11.11) can be expressed

as a function of temperature. Nodal temperatures are calculated by using equivalent heat-resistance and thermal loads.

$$\begin{aligned}
 [C + \alpha \Delta t_{i+1} (K + H)] T_{i+1} &= \\
 [C - (1 - \alpha) \Delta t_{i+1} (K + H)] T_i + \Delta t_{i+1} [\alpha R_{i+1} + (1 - \alpha) R_i] & \quad (11.11) \\
 \bar{K} T_{i+1} &= \bar{R} \\
 \bar{K} &= [C + \alpha \Delta t_{i+1} (K + H)] T_{i+1} \\
 \bar{R} &= [C - (1 - \alpha) \Delta t_{i+1} (K + H)] T_i + \Delta t_{i+1} [\alpha R_{i+1} + (1 - \alpha) R_i]
 \end{aligned}$$

The integral variable α used in Eq. (11.8) is classified below, which will affect the convergence condition.

$\alpha = 0.0$: Euler-Forward differentiation method (Conditional convergence depending on the magnitude of Δt)

$\alpha = 0.5$: Crank-Nicolson (Central differential) method (Unconditional convergence)

$\alpha = 2/3$: Galerkin method (Unconditional convergence)

$\alpha = 1.0$: Backward method (Unconditional convergence)

11-3 Thermal Stress Analysis

Stresses in mass concrete at each stage of construction are obtained by considering the results of heat transfer analysis such as nodal temperature distribution, changes in material properties due to changes in time and temperature, time-dependent shrinkage, time and stress-dependent creep, etc. The following outlines some important concepts associated with thermal stress analysis and pertinent items considered in MIDAS.

Equivalent concrete age based on temperature and time

Changes in material properties resulting from the process of maturing concrete can be expressed in terms of temperature and time. Even a group of nodes have been cast at the same time, the strength gains can be different if the temperature distribution is uneven. In order to reflect such phenomenon, an equivalent concrete age is created on the basis of time and temperature. The equivalent concrete age is used to calculate the concrete strength gain and is calculated using CEB-FIP MODEL CODE 90.

Equivalent concrete age based on CEB-FIP MODEL CODE 90 is given by,

$$t_{eq} = \sum_{i=1}^n \Delta t_i \exp \left[13.65 - \frac{4000}{273 + T(\Delta t_i) / T_0} \right]$$

where,

t_{eq}	: Equivalent concrete age (days)
Δt_i	: Time interval at each analysis stage (days)
$T(\Delta t_i)$: Temperature during each analysis stage (° C)
T_0	: 1 ° C

Calculation of compressive strength of concrete using equivalent concrete age

Various national standards are used to calculate compressive strength of concrete, which is then used to calculate the modulus of elasticity, tensile strength, etc.

ACI 209

$$\sigma_c(t) = \frac{t}{a + bt_{eq}} \sigma_{c(28)}$$

where,

a, b	: Coefficients based on the cement classification
$\sigma_{c(28)}$: Concrete compressive strength at 28 days

CEB-FIP MODEL CODE 90

$$\sigma_c(t) = \exp \left\{ s \left[1 - \left(\frac{28}{t_{eq}/t_1} \right)^{1/2} \right] \right\} \sigma_{c(28)}$$

where,

s	: Coefficients based on cement classification
$\sigma_{c(28)}$: Concrete compressive strength at 28 days
t_1	: 1 day

Japanese Concrete Standard Specifications 2002

$$\sigma_c(t) = \frac{dt}{a + bt_{eq}} \sigma_{c(28)}$$

$$\sigma_{tensile}(t) = c \sqrt{\sigma_c(t)}$$

where,

$\sigma_{c(28)}$: Concrete compressive strength at 28 days
a, b, d	: Coefficients based on cement classification $a = 4.5, b = 0.95, d = 1.11$ (Normal Portland cement) $a = 6.2, b = 0.93, d = 1.15$ (Moderate Portland cement) $a = 2.9, b = 0.97, d = 1.07$ (High-early-strength cement)
c	: Tensile strength development coefficient (0.44)

KS concrete code (1996)

$$\sigma_c(t) = \frac{t}{a + bt_{eq}} \sigma_{c(91)}$$

where,

a, b	: Coefficients based on cement classification
$\sigma_{c(91)}$: Concrete compressive strength at 91 days

Deformations resulting from temperature changes

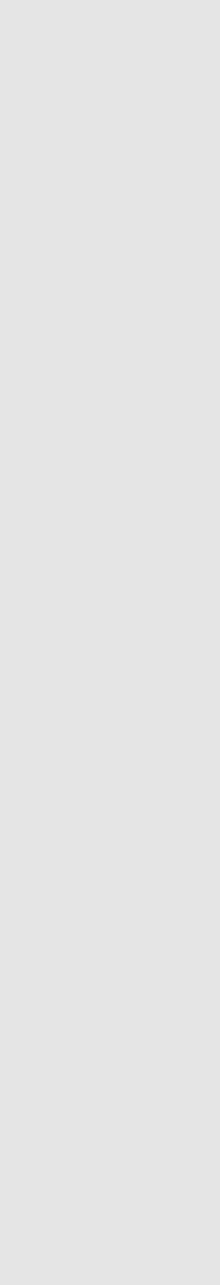
By using the changes in nodal temperatures at each stage obtained from heat transfer analysis, thermal strains are calculated followed by calculating equivalent loads based on the stiffness.

Deformations due to Shrinkage

Additional deformations and stresses develop due to shrinkage after initial curing of concrete in formwork supported on falsework. MIDAS adopts ACI 209 and CEB-FIP MODEL CODE, etc. to include the shrinkage effects in thermal stress analyses, which reflect the cement type, structural configuration and time.

Deformations due to Creep

Additional deformations and stresses develop as a result of sustained stresses in concrete

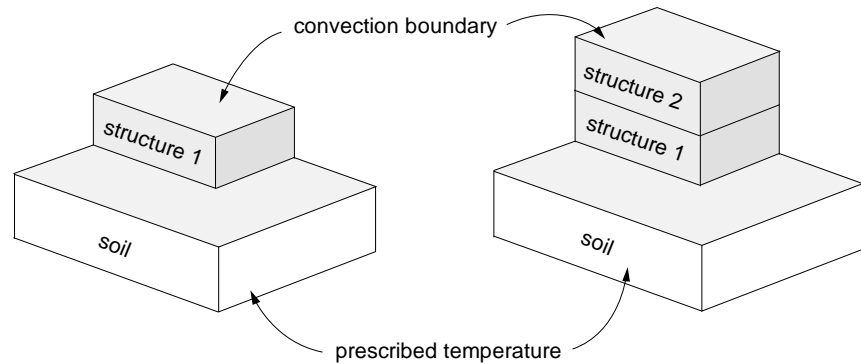


structures. MIDAS adopts ACI 209, CEB-FIP MODEL CODE 90, Japanese Code, etc. to consider the effects of creep.

11-4 Heat of Hydration Analysis Considering Construction Stages

Heat of hydration analysis is a time-dependent analysis, and as such construction stages need to be reflected in the analysis. During the construction stages, changes in geometric configurations and boundary conditions of structures take place, and prestress and additional loads may be introduced. Fig. 11-(1) shows a change in a structural model based on construction stages. Structures are added and thermal boundary conditions are changed at different construction stages. However, the analysis model and the structural boundary conditions must remain unchanged at a given construction stage. Each construction stage consists of a number of time steps, and loads may be added or removed at each time step. The self weight of a new structural model becomes reflected only once at the first time step of each construction stage.

Input data at each construction stage are structural models, structural and heat boundary conditions and loads at different time steps. Note that the user can only add the structural models and structural boundary conditions at each construction stage. However, the user is allowed to add or remove heat boundary conditions. In addition, it is possible to add or remove the loads at any time step of a construction stage.



(a) First construction stage model (b) Second construction stage model

Figure 11-(1) Construction stage models for heat of hydration analysis

11-5 Results of heat of hydration analysis

Heat of hydration analysis retains the results of heat transfer analysis and thermal stress analysis. The results of heat transfer analysis include nodal temperatures and nodal compressive and nodal tensile strengths based on the equivalent concrete age. The results of thermal stress analysis include nodal displacements, element stresses and crack ratio in which a ratio of the element stress to the tensile stress is expressed. The user can check all the results at each time step of any construction stage.

Results of heat transfer analysis

- a. Nodal temperatures
- b. Compressive and tensile strengths at nodes based on the equivalent concrete age

Results of thermal stress analysis

- a. Nodal displacements.
- b. Stresses in elements
- c. Crack ratio

Chapter 12. Material Models

12-1 Introduction

12-1-1 Overview

Unlike elastic material behaviors, plastic material behaviors exhibit permanent or irreversible deformations even after unloading applied loads in a structure. In order to reflect such properties, deformations are formulated by assuming separation of elastic and plastic components of the total deformations.

$$\boldsymbol{\varepsilon} = \boldsymbol{\varepsilon}_e + \boldsymbol{\varepsilon}_p \quad (12.1)$$

Hook's law defines the stress and strain relationship in the elastic range. Applying Eq. (12.1), can we then define the stress as follows:

$$\boldsymbol{\sigma} = \mathbf{E}\boldsymbol{\varepsilon}_e = \mathbf{E}(\boldsymbol{\varepsilon} - \boldsymbol{\varepsilon}_p) \quad (12.2)$$

where, \mathbf{E} represents Young's Modulus.

The stress at a point in a structure subjected to loading is a measure of defining the elastic-plastic state of the point. Such basis varies from materials to materials of specific material properties such as steel, concrete, etc., which is referred to as yield criterion. The yield criterion of a material is defined through experiments on various stress states. The stresses at the point of instigating plastic flow can be expressed by a function in the space of stresses.

$$f(\boldsymbol{\sigma}, \kappa) = 0 \quad (12.3)$$

where, f is the yield function, and κ is the hardening parameter. If the yield function, f is less than zero, plastic flow does not occur, and if it is greater than zero, plastic flow takes place.

12-1-2 Flow rule

Plastic strain is expressed by separating the scalar and vector components according to the Koiter's rule.

$$\dot{\boldsymbol{\epsilon}}_p = \sum_{i=1}^n \dot{\lambda}_i \frac{\partial g_i}{\partial \boldsymbol{\sigma}} = \sum_{i=1}^n \dot{\lambda}_i \mathbf{m}_i \quad (12.4)$$

where, g_i is the plastic potential function, which is a function, $g_i(\boldsymbol{\sigma}, \kappa)$, of the stress and hardening parameter, κ . $\dot{\lambda}_i$ is a plastic multiplier, which must satisfy the Kuhn-Tucker conditions.

$$f \leq 0; \quad \dot{\lambda}_i \geq 0; \quad \dot{\lambda}_i f = 0 \quad (12.5)$$

From the above conditions, we note that if the yield function, f is less than zero, $\dot{\lambda}_i$ always becomes zero and plastic flow does not occur. \mathbf{m} in Eq. (12.4) represents the vector defining the direction of plastic strain. If at this point we define the direction of plastic strain as $\partial f / \partial \boldsymbol{\sigma}$ using the yield function, f , rather than using the plastic potential function, g , then this is referred to as the associated flow rule. Conversely, the non-associated flow rule refers to the method by which the direction of plastic strain is defined as $\partial g / \partial \boldsymbol{\sigma}$ using the plastic potential function. Generally for those material models such as von Mises and Tresca, which show constant deviatoric stresses along the hydrostatic pressure in the space of stresses, the use of the associated flow rule is common. However, for such materials as Mohr-Coulomb and Drucker-Prager, which show deviatoric stresses varying with the hydrostatic pressure in the space of stresses, the non-associated flow rule is used. Applying the non-associated flow rule for a material model in which deviatoric stresses vary with the hydrostatic pressure, has the effect of constraining the phenomenon of excessive volumetric expansion due to non-coincident directions of stresses and strains. However, this results in a non-symmetric stiffness matrix, which requires a non-symmetric solver and has the drawback of slow convergence.

In case of concrete structures where concrete is generally confined by ties or hollow steel sections, plastic analysis can be quite sensitive to the effect of such confinement. The non-associated flow

rule is recommended for such a case.

12-1-3 Hardening behavior

Hardening behavior in an elasto-plastic model can be divided into strain hardening and plastic work hardening. The strain hardening can be defined by using the normalized equivalent plastic strain.

$$\dot{\kappa} = \sqrt{\frac{2}{3} (\dot{\epsilon}^p)^T \mathbf{Q} \dot{\epsilon}^p} \quad (12.6)$$

where, $\mathbf{Q} = \text{diag}[1, 1, 1, 1/2, 1/2, 1/2]$ represents a diagonal matrix. Plastic work hardening defines its behavior using the plastic work done by a unit stress.

$$\dot{\kappa} = \boldsymbol{\sigma}^T \dot{\epsilon}^p \quad (12.7)$$

All the above two types of hardening are integrated over time, t , to calculate the hardening parameter up to the present load step.

$$\kappa = \int \dot{\kappa} dt \quad (12.8)$$

MIDAS currently supports strain hardening only. Depending on the properties of hardening behavior expressed by the hardening parameter, κ , the hardening rule is classified into ‘isotropic hardening’, ‘kinematic hardening’ and ‘mixed hardening’ of the two types. Isotropic hardening exhibits the behavior of isotropic expansion or contraction of the yield surface depending on the hardening parameter as shown in Fig. 12-(1a). Kinematic hardening on the other hand exhibits the behavior of translation of the origin of the yield surface without any expansion or contraction of the yield surface as shown in Fig. 12-(1b). Mixed hardening exhibits the combined behavior of the two behaviors above as shown in Fig. 12-(1c). MIDAS currently supports isotropic hardening only.

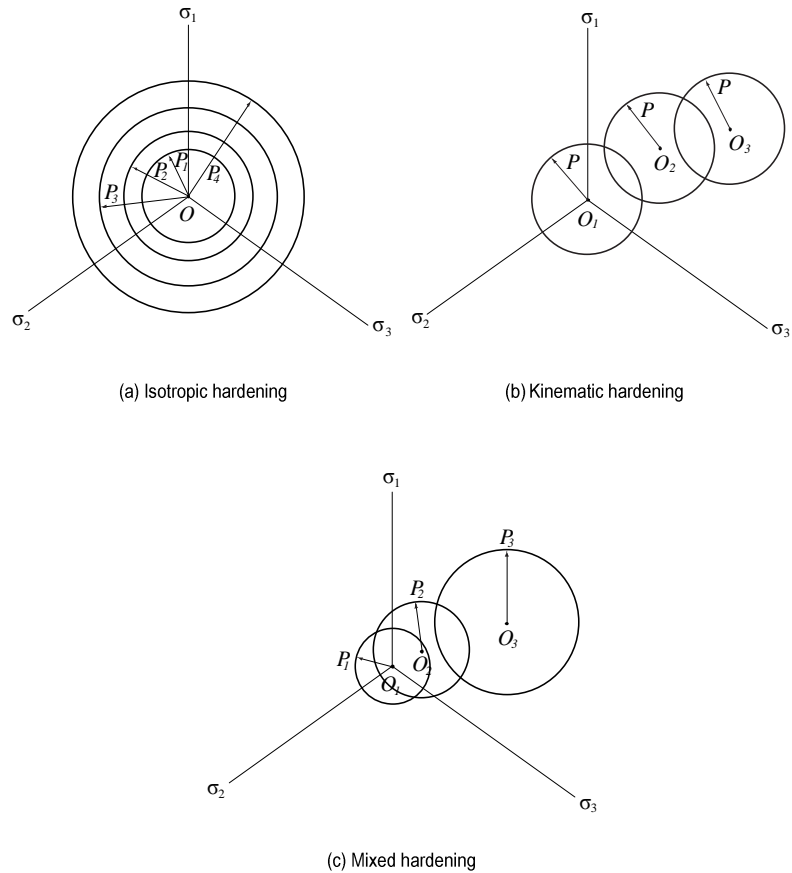


Figure 12-1) Hardening behavior of yield functions

12-1-4 Linearized consistency condition

The state of internal change of an elasto-plastic material is defined by the incremental constitutive relationship, which is expressed by the type of finite increases. Plastic flow begins upon reaching the yield condition and is controlled by plastic state parameters like κ . The constitutive equation for the state of finite strain in non-associated flow can be based on Eq. (12.2), which is written as,

$$\dot{\boldsymbol{\sigma}} = \mathbf{E}(\dot{\boldsymbol{\varepsilon}} - \dot{\boldsymbol{\varepsilon}}_p) = \mathbf{E}(\dot{\boldsymbol{\varepsilon}} - \dot{\lambda} \mathbf{m}) \quad (12.9)$$

When the state of stress lies on the yield surface, the linearized consistency condition is defined by expanding the first order of the Taylor function as below.

$$\dot{f}(\boldsymbol{\sigma}, \kappa) = \left(\frac{\partial f}{\partial \boldsymbol{\sigma}} \right)^T \dot{\boldsymbol{\sigma}} + \frac{\partial f}{\partial \kappa} \frac{\partial \kappa}{\partial \lambda} \dot{\lambda} = \mathbf{n}^T \dot{\boldsymbol{\sigma}} - h \dot{\lambda} = 0 \quad (12.10)$$

where, $\mathbf{n} = \frac{\partial f}{\partial \boldsymbol{\sigma}}$, h is hardening modulus, and $h = -\frac{\partial f}{\partial \kappa} \frac{\partial \kappa}{\partial \lambda} \dot{\lambda}$

By substituting Eq. (12.9) into Eq. (12.10), we can arrange the plastic multiplier, $\dot{\lambda}$ as,

$$\dot{\lambda} = \frac{\mathbf{n}^T \mathbf{E}}{h + \mathbf{n}^T \mathbf{E} \mathbf{m}} \dot{\boldsymbol{\varepsilon}} \quad (12.11)$$

Substituting Eq. (12.11) into Eq. (12.9), the constitutive equation is expressed in the form of an incremental relationship of stress and strain as,

$$\dot{\boldsymbol{\sigma}} = \left(\mathbf{E} - \frac{\mathbf{E} \mathbf{m} \mathbf{n}^T \mathbf{E}}{h + \mathbf{n}^T \mathbf{E} \mathbf{m}} \right) \dot{\boldsymbol{\varepsilon}} = \mathbf{E}_{ep} \dot{\boldsymbol{\varepsilon}} \quad (12.12)$$

where, \mathbf{E}_{ep} is the elasto-plastic tangent operator, which is the tangent stiffness matrix of the material. By introducing the non-associated flow rule at this point, \mathbf{E}_{ep} becomes non-symmetrical due to $\mathbf{m} \neq \mathbf{n}$.

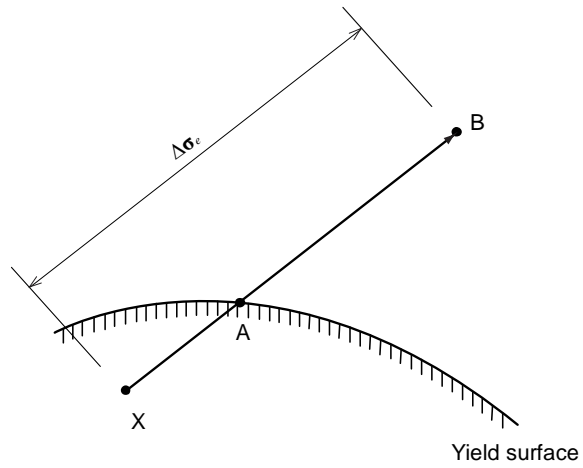
12-1-5 Integration of rate form

Integration methods for an incremental type of equations can be largely classified into an explicit forward Euler algorithm with sub-incrementation and an implicit backward Euler algorithm. In the explicit forward Euler algorithm, the direction of plastic flow is calculated at the point A (Fig. 12-(2) and 12-(3)) where an incremental stress and the yield surface meet. Whereas in the implicit backward Euler algorithm, it is calculated at the final stress point B (Fig. 12-(4)).

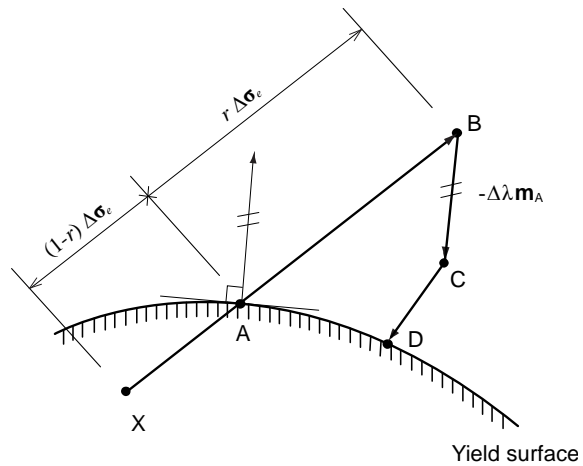
The explicit forward Euler algorithm is relatively simple and does not require the process of iterative calculations at the integration points, but has the following drawbacks:

- It is stable only in certain conditions.
- Sub-increments are required to attain permissible accuracy. (Fig. 12-(3)).
- Additional corrective measures are required to return to the yield surface. (Fig. 12-(3)).

Also, the explicit forward Euler algorithm can not constitute a consistent tangent stiffness matrix. On the contrary, the implicit backward Euler algorithm can sufficiently obtain accurate results without sub-incrementation and artificial return and is stable unconditionally, but requires the process of iterative calculations at the integration points. However, this algorithm is more efficient than the explicit forward Euler algorithm in that it allows us to formulate a consistent tangent stiffness matrix.



(a) Location of intersection point A



(b) Corrected to point D after moving from point A to point C in the tangential direction

Figure 12-(2) Explicit forward Euler algorithm

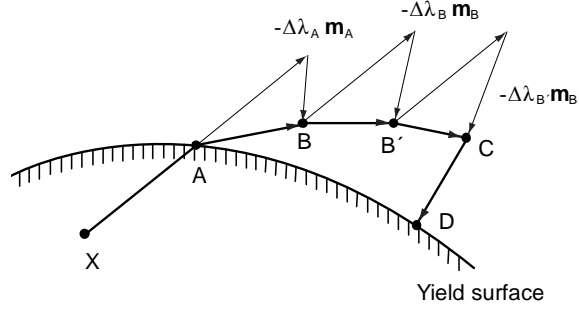


Figure 12-(3) Sub-incrementation in explicit forward Euler algorithm

12-1-6 Forward Euler method

In the explicit forward Euler method, elastic strain is first assumed, and then elastic incremental stress is calculated. (point B in Fig. 12-(2a)).

$$\begin{aligned}\Delta\sigma_e &= \mathbf{E}\Delta\epsilon \\ \sigma_B &= \sigma_X + \Delta\sigma_e\end{aligned}\quad (12.13)$$

The next step is to calculate the magnitude of incremental stress defining the elastic limit. The initial elastic incremental stress is divided into the admissible stress increment, $(1-r)\Delta\sigma_e$ within the elastic limit and the inadmissible stress increment, $r\Delta\sigma_e$ beyond the yield function. The incremental stress defining the elastic limit is calculated using the equation below. (point A in Fig. 12-(2a)).

$$\begin{aligned}f(\sigma_X + (1-r)\Delta\sigma_e, \kappa) &= 0 \\ r &= \frac{f_B}{f_B - f_X}\end{aligned}\quad (12.14)$$

The subscripts in Eq. (12.14) and Eq. (12.15) are referred to in Fig. 12-(2).

In order to use the sub-incrementation method, the incremental stress, $r\Delta\sigma_e$, which has deviated from the yield surface, is divided into k small sub-incremental stresses for convergence. (Fig. 12-(3)). The number of sub-increments is directly related to the margin of error, which is calculated

as Eq. (12.15).

$$k = \text{INT} \left[8(\sigma_{\text{effB}} - \sigma_{\text{effA}}) / \sigma_{\text{effA}} \right] + 1 \quad (12.15)$$

σ_{effA} and σ_{effB} represent the effective stresses at the points A and B in Fig. 12-(2a) respectively. If the state of the final stress does not lie on the yield surface, the stress state is moved to the yield surface by the following artificial return method (point D in Fig. 12-(3)):

$$\begin{aligned} \Delta\lambda_c &= \frac{f_c}{h + \mathbf{n}_c^T \mathbf{E} \mathbf{m}_c} \\ \boldsymbol{\sigma}_D &= \boldsymbol{\sigma}_c - \Delta\lambda_c \mathbf{E} \mathbf{m}_c \end{aligned} \quad (12.16)$$

12-1-7 Backward Euler method

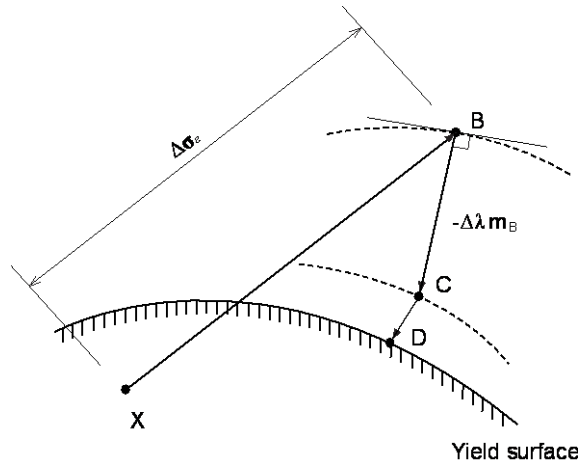


Figure 12-(4) Implicit backward Euler method

The fact that the explicit forward Euler method predicts the next stress value using the component in the direction perpendicular to the yield surface at the point A, the stress at the intersection must be calculated. If the component in the direction perpendicular to the yield surface is predicted at

the point B in Fig. 12-(4), the stress calculation at the intersection becomes unnecessary.

$$\boldsymbol{\sigma}_C = \boldsymbol{\sigma}_X + \Delta\boldsymbol{\sigma}_e - \Delta\lambda\mathbf{E}\mathbf{m}_B = \boldsymbol{\sigma}_B - \Delta\lambda\mathbf{E}\mathbf{m}_B \quad (12.17)$$

If the yield function, f is thus first-order expanded about the point B using a Taylor series, we obtain,

$$f = f_B + \left(\frac{\partial f}{\partial \boldsymbol{\sigma}} \right)^T \Delta\boldsymbol{\sigma} + \frac{\partial f}{\partial \kappa} \Delta\kappa = f_B - \Delta\lambda \mathbf{n}_B^T \mathbf{E} \mathbf{m}_B - h_B \Delta\lambda \quad (12.18)$$

The failure function at the newly calculated point becomes zero. The above equation is then rearranged for $\Delta\lambda$ as,

$$\Delta\lambda = \frac{f_B}{h_B + \mathbf{n}_B^T \mathbf{E} \mathbf{m}_B} \quad (12.19)$$

Using this, $\boldsymbol{\sigma}_C$ is calculated by the implicit backward Euler method as follows:

$$\boldsymbol{\sigma}_C = \boldsymbol{\sigma}_B - \Delta\lambda \mathbf{E} \mathbf{m}_B \quad (12.20)$$

At this point, $\boldsymbol{\sigma}_C$ at the point C always does not lie on the yield surface. In order to treat this, the point C now becomes a reference point to predict a new stress value, and the above calculations are iteratively performed until the stress value falls on the yield surface.

12-1-8 Constitutive matrix

The plastic constitutive equation is formulated as below. The finite incremental stress is determined by the elastic part of the finite incremental strain vector as,

$$\dot{\boldsymbol{\sigma}} = \mathbf{E}(\dot{\boldsymbol{\varepsilon}} - \dot{\boldsymbol{\varepsilon}}_p) = \mathbf{E}\dot{\boldsymbol{\varepsilon}} - \dot{\lambda}\mathbf{E}\mathbf{m} \quad (12.21)$$

Since the present stress must be always located on the yield surface, Eq. (12.21) must satisfy the consistency condition. After substituting Eq. (12.11) into Eq. (12.21) and rearranging it for finite incremental strain, the finite incremental stress can be calculated as Eq. (12.22).

$$\dot{\boldsymbol{\sigma}} = \left(\mathbf{E} - \frac{\mathbf{E} \mathbf{m} \mathbf{n}^T \mathbf{E}}{h + \mathbf{n}^T \mathbf{E} \mathbf{m}} \right) \dot{\boldsymbol{\varepsilon}} = \mathbf{E}_{ep} \dot{\boldsymbol{\varepsilon}} \quad (12.22)$$

If a consistent tangent stiffness matrix is used in conjunction with the Newton-Raphson iterative process in the explicit forward Euler method, much faster convergence is achieved due to the characteristic of the 2nd order convergence in the Newton-Raphson iterative process. In order to reflect the 2nd order characteristic, Eq. (12.18) is differentiated, which then becomes,

$$\dot{\boldsymbol{\sigma}} = \mathbf{E} \dot{\boldsymbol{\varepsilon}} - \dot{\lambda} \mathbf{E} \mathbf{m} - \Delta \lambda \mathbf{E} \frac{\partial \mathbf{m}}{\partial \boldsymbol{\sigma}} \dot{\boldsymbol{\sigma}} - \Delta \lambda \mathbf{E} \frac{\partial \mathbf{m}}{\partial \kappa} \frac{\partial \kappa}{\partial \lambda} \dot{\lambda} \quad (12.23)$$

where, $\dot{\lambda}$ represents the magnitude of the change in $\Delta \lambda$. Eq. (12.23) is rearranged as,

$$\mathbf{A} \dot{\boldsymbol{\sigma}} = \mathbf{E} \dot{\boldsymbol{\varepsilon}} - \dot{\lambda} \mathbf{E} \bar{\mathbf{m}} \quad (12.24)$$

$$\text{where, } \mathbf{A} = \mathbf{I} + \Delta \lambda \mathbf{E} \frac{\partial \mathbf{m}}{\partial \boldsymbol{\sigma}}, \quad \bar{\mathbf{m}} = \mathbf{m} + \Delta \lambda \frac{\partial \mathbf{m}}{\partial \kappa} \frac{\partial \kappa}{\partial \lambda}$$

If we now define $\mathbf{H} = \mathbf{A}^{-1} \mathbf{E}$, Eq. (12.24) is rearranged as,

$$\dot{\boldsymbol{\sigma}} = \mathbf{H} (\dot{\boldsymbol{\varepsilon}} - \dot{\lambda} \bar{\mathbf{m}}) \quad (12.25)$$

If we rearrange Eq. (12.25) in the total strain term using the linearized consistency condition, the next equation is obtained.

$$\dot{\boldsymbol{\sigma}} = \left(\mathbf{H} - \frac{\mathbf{H} \bar{\mathbf{m}} \mathbf{n}^T \mathbf{H}}{h + \mathbf{n}^T \mathbf{H} \bar{\mathbf{m}}} \right) \dot{\boldsymbol{\varepsilon}} = \mathbf{C}_{ep} \dot{\boldsymbol{\varepsilon}} \quad (12.26)$$

\mathbf{E}_{ep} in Eq. (12.22) is referred to as a tangent stiffness matrix, and \mathbf{C}_{ep} in Eq. (12.26) is referred to as a consistent tangent stiffness matrix.

MIDAS limitations

Isotropic Plasticity Only

Isotropic Hardening Only

Strain Hardening Only

12-2 Yield Criteria

Presenting an yield function in terms of stress components in the generally used state of multi-axes accompanies many difficulties geometrically and physically. Therefore, an yield function is typically presented using independent components on stress coordinate axes. The yield condition is defined using the following principal stresses.

$$f(\sigma_1, \sigma_2, \sigma_3) = 0 \quad (12.27)$$

One of the convenient methods for presenting an yield function is to use stress invariants.

12-2-1 Stress invariants

(1) Stress invariants

Stress occurring at any point in a material is presented using the stress tensor, σ_{ij} . And using the directional vector, n_j defining the direction of the principal stress, the following equation is established.

$$(\sigma_{ij} - \sigma \delta_{ij}) n_j = 0 \quad (12.28)$$

where, δ_{ij} is Kronecker delta.

In the above Eq. (12.28), $n_j \neq 0$, and the necessary condition to satisfy Eq. (12.28) is noted as,

$$|\sigma_{ij} - \sigma \delta_{ij}| = 0 \quad (12.29)$$

The matrix Eq. (12.29) can be presented in a cubic equation for principal stress as follows:

$$\sigma^3 - I_1 \sigma^2 + I_2 \sigma - I_3 = 0 \quad (12.30)$$

where,

$$\begin{aligned}
 I_1 &= \sigma_x + \sigma_y + \sigma_z = \sigma_{ii} \\
 I_2 &= (\sigma_x \sigma_y + \sigma_y \sigma_z + \sigma_z \sigma_x) - (\tau_{xy}^2 + \tau_{yz}^2 + \tau_{zx}^2) = \frac{1}{2} (I_1^2 - \sigma_{ij} \sigma_{ji}) \\
 I_3 &= \begin{vmatrix} \sigma_x & \tau_{xy} & \tau_{xz} \\ \tau_{yx} & \sigma_y & \tau_{yz} \\ \tau_{zx} & \tau_{zy} & \sigma_z \end{vmatrix} = \frac{1}{3} \sigma_{ij} \sigma_{jk} \sigma_{ki} - \frac{1}{2} I_1 \sigma_{ij} \sigma_{ji} + \frac{1}{6} I_1^3
 \end{aligned} \tag{12.31}$$

I_1 , I_2 and I_3 can be represented using the principal stresses, σ_1 , σ_2 and σ_3 .

$$\begin{aligned}
 I_1 &= \sigma_1 + \sigma_2 + \sigma_3 \\
 I_2 &= \sigma_1 \sigma_2 + \sigma_2 \sigma_3 + \sigma_3 \sigma_1 \\
 I_3 &= \sigma_1 \sigma_2 \sigma_3
 \end{aligned} \tag{12.32}$$

(2) Deviatoric stress invariants

The stress tensor, σ_{ij} is divided into hydrostatic pressure and deviatoric stress components, which can be expressed as,

$$\sigma_{ij} = s_{ij} + \sigma_m \delta_{ij} \tag{12.33}$$

where, $\sigma_m = (\sigma_x + \sigma_y + \sigma_z)/3 = I_1/3$, which is referred to as mean stress. And $s_{ij} = \sigma_{ij} - \sigma_m \delta_{ij}$ is referred to as deviatoric stress, which exhibits the state of pure shear. In order to calculate the invariants for deviatoric stress, it is transformed into the type of calculating invariants of the stress tensor, σ_{ij} .

$$|s_{ij} - s \delta_{ij}| = 0 \tag{12.34}$$

Eq. (12.34) is expressed in an equation form as,

$$s^3 - J_1 s^2 + J_2 s - J_3 = 0 \tag{12.35}$$

where,

$$\begin{aligned}
 J_1 &= s_{ii} = s_x + s_y + s_z = 0 \\
 J_2 &= \frac{1}{2} s_{ij} s_{ji} \\
 &= \frac{1}{6} \left[(\sigma_x - \sigma_y)^2 + (\sigma_y - \sigma_z)^2 + (\sigma_z - \sigma_x)^2 \right] + \tau_{xy}^2 + \tau_{yz}^2 + \tau_{zx}^2 \quad (12.36) \\
 J_3 &= \frac{1}{3} s_{ij} s_{jk} s_{ki} = \begin{vmatrix} s_x & \tau_{xy} & \tau_{xz} \\ \tau_{yx} & s_y & \tau_{yz} \\ \tau_{zx} & \tau_{zy} & s_z \end{vmatrix}
 \end{aligned}$$

J_1 , J_2 and J_3 are expressed in terms of deviatoric principal stresses, s_1 , s_2 and s_3 .

$$\begin{aligned}
 J_1 &= s_1 + s_2 + s_3 = 0 \\
 J_2 &= \frac{1}{2} (s_1^2 + s_2^2 + s_3^2) = \frac{1}{6} \left[(\sigma_1 - \sigma_2)^2 + (\sigma_2 - \sigma_3)^2 + (\sigma_3 - \sigma_1)^2 \right] \quad (12.37) \\
 J_3 &= \frac{1}{3} (s_1^3 + s_2^3 + s_3^3) = s_1 s_2 s_3
 \end{aligned}$$

I_1 , I_2 , I_3 , J_1 , J_2 and J_3 are all invariants expressed in scalar retaining independent characteristics on coordinate axes. In order to present the yield function in a geometrically convenient way, three invariants, I_1 , J_2 and J_3 among these are mainly used. I_1 , J_2 and J_3 are referred to as 1st, 2nd and 3rd invariant respectively.

(3) Geometric meaning of three stress invariants

Yielding in most material models is mainly predominated by the deviatoric stresses. Accordingly, the representation of an yield function by hydrostatic and deviatoric stress components is very conveniently used to define the geometric shape of the yield function. Next we will review the method of representing the stress state of a point $\mathbf{P}(\sigma_1, \sigma_2, \sigma_3)$ in terms of hydrostatic axis and deviatoric axis components.

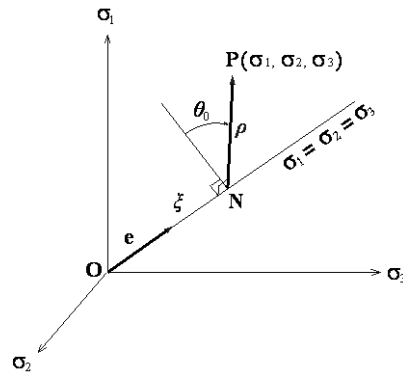


Figure 12-(5) Definition of stress state in the space of principal stresses

In case a point $P(\sigma_1, \sigma_2, \sigma_3)$ is defined, which is expressed in a stress state in the space of principal stresses, as in Fig. 12-(5), a vector \mathbf{OP} can be defined. The vector \mathbf{OP} can be divided into the vector \mathbf{ON} , which follows the hydrostatic axis, and the vector \mathbf{NP} , which exists on the deviatoric plane perpendicular to the hydrostatic axis. Their scalars are as follows:

$$\begin{aligned} |\mathbf{ON}| &= \xi = \frac{1}{\sqrt{3}} I_1 \\ |\mathbf{NP}| &= \rho = \sqrt{2J_2} \end{aligned} \quad (12.38)$$

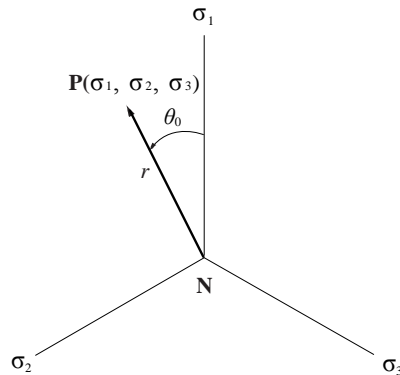


Figure 12-(6) Definition of stress state on the deviatoric plane

Fig. 12-(6) shows the deviatoric plane, which is perpendicular to the hydrostatic axis. The previously defined vector **NP** needs to be rotated by θ_0 from the σ_1 axis in order to define the point P on the deviatoric plane. This θ_0 is referred to as similarity angle, which is written as,

$$\theta_0 = \frac{1}{3} \cos^{-1} \left(\frac{3\sqrt{3}}{2} \frac{J_3}{J_2^{3/2}} \right) \quad (12.39)$$

θ_0 retains the following range:

$$0 \leq \theta_0 \leq \frac{\pi}{3} \quad (12.40)$$

For numerical analysis, the use of Lode Angle θ is more convenient than using θ_0 , which is defined as.

$$\theta = \frac{1}{3} \sin^{-1} \left(-\frac{3\sqrt{3}}{2} \frac{J_3}{J_2^{3/2}} \right) \quad (12.41)$$

Here, $\theta = \theta_0 - \frac{\pi}{6}$ whose range is as follows:

$$-\frac{\pi}{6} \leq \theta \leq \frac{\pi}{6} \quad (12.42)$$

12-2-2 Rankine Model (*In a later version*)

The Rankine model defines the yielding of a material using the maximum principal stress, σ_1 , which is expressed as,

$$f(\boldsymbol{\sigma}, \kappa) = \sigma_1 - \sigma_t(\kappa) = 0 \quad (12.43)$$

Expressing Eq. (12.43) using the invariants, I_1 , J_2 and θ , we obtain,

$$f(I_1, J_2, \theta, \kappa) = \frac{2}{\sqrt{3}} \sqrt{J_2} \left(\sin \left(\theta + \frac{2}{3} \pi \right) \right) + \frac{I_1}{3} - \sigma_t(\kappa) = 0 \quad (12.44)$$

Also expressing Eq. (12.43) in terms of ξ , ρ and θ , we find,

$$f(\xi, \rho, \theta, \kappa) = \frac{2}{\sqrt{6}} \rho \left(\sin \left(\theta + \frac{2}{3} \pi \right) \right) + \frac{\xi}{\sqrt{3}} - \sigma_t(\kappa) = 0 \quad (12.45)$$

The Rankine model is mainly defined with tension cutoff behavior. Together with the Mohr-Coulomb or Drucker-Prager model, it is used to define tension behaviors of soils, concrete, etc.

Fig. 12-(7) shows the 3-dimensional shape of the Rankine model in the space of stresses. As in Fig. 12-(8), the shape on the π plane is a triangle, and it can be defined in a linear function for hydrostatic axis on the meridian plane.

Hardening

The hardening behavior model follows the strain hardening hypothesis, which assumes that hardening progresses with increase in plastic deformation. The relationship between the plastic strain, $\boldsymbol{\varepsilon}_p$ and the hardening parameter, κ is thus defined as,

$$\dot{\kappa} = \sqrt{\frac{2}{3} (\boldsymbol{\varepsilon}_{p1} \boldsymbol{\varepsilon}_{p1} + \boldsymbol{\varepsilon}_{p2} \boldsymbol{\varepsilon}_{p2} + \boldsymbol{\varepsilon}_{p3} \boldsymbol{\varepsilon}_{p3})} \quad (12.46)$$

Rearranging the above,

$$\dot{\kappa} = \dot{\lambda} \quad (12.47)$$

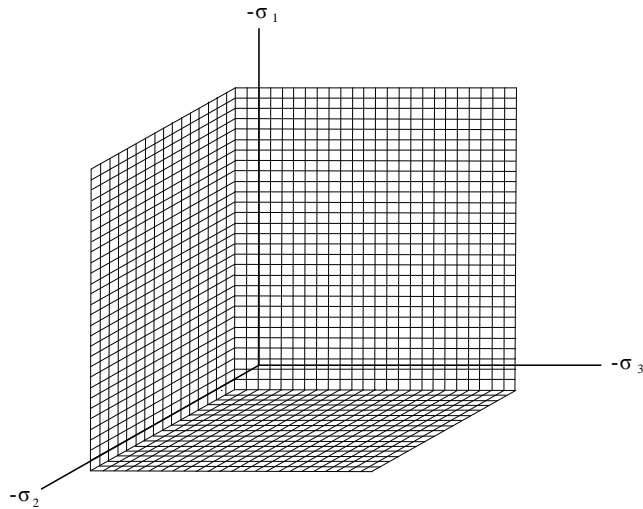
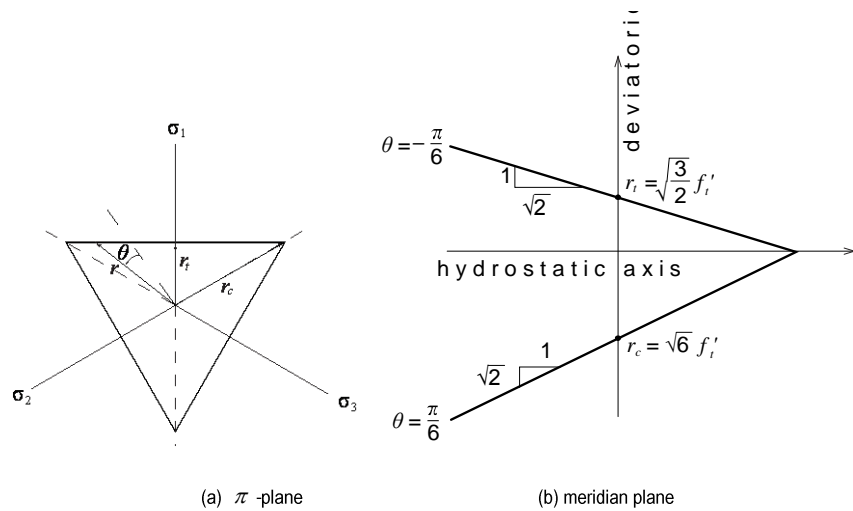


Figure 12-7) Rankine yield function

Figure 12-8) Rankine yield surface in π -plane & meridian plane

12-2-3 Tresca Model

The Tresca model has been developed for an yield criterion of metallic materials. When the maximum shear stress at a point in a material reaches the limiting value, k , the material is assumed to yield as follows:

$$f(\sigma, k) = \frac{1}{2} |\sigma_1 - \sigma_3| - k = 0 \quad (12.48)$$

where, $\sigma_1 \geq \sigma_2 \geq \sigma_3$

If Eq. (12.48) is expressed in terms of stress invariants, J_2 and θ ,

$$\begin{aligned} f(J_2, \theta) &= \frac{2}{\sqrt{3}} \sqrt{J_2} \left[\sin\left(\theta + \frac{2}{3}\pi\right) - \sin\left(\theta + \frac{4}{3}\pi\right) \right] - 2k \\ &= 2\sqrt{J_2} \cos\theta - Y(\kappa) = 0 \end{aligned} \quad (12.49)$$

where, $Y(\kappa) = 2k$, which represents the yield stress.

If Eq. (12.48) is expressed in terms of invariants, ρ and θ ,

$$f(\rho, \theta) = \sqrt{2}\rho \cos\theta - Y(\kappa) = 0 \quad (12.50)$$

Since this criterion does not consider the effect of hydrostatic pressure acting on the yield surface, it is unrelated to the stress I_1 on the hydrostatic pressure surface, and deviatoric stress varies with Lode angle on the deviatoric surface. As such, the Tresca yield criterion becomes a regular hexagonal column parallel with the hydrostatic axis in the space of principal stresses as shown in Fig. 12-(9), and it is depicted as a regular hexagon on the deviatoric plane. Fig 12-(10) shows the yield surface on the π -plane and the meridian plane.

Hardening

The hardening behavior model follows the strain hardening hypothesis, which assumes that hardening progresses with increase in plastic deformation. The relationship between the plastic strain, ϵ_p and the hardening parameter, κ is thus defined as,

$$\dot{\kappa} = \sqrt{\frac{2}{3} (\epsilon_{p1}\epsilon_{p1} + \epsilon_{p2}\epsilon_{p2} + \epsilon_{p3}\epsilon_{p3})} \quad (12.51)$$

From Eq. (12.51), principal plastic strains are appropriately calculated and rearranged to give the relationship between the hardening parameter and the plastic multiplier as,

$$\dot{\kappa} = \frac{2}{\sqrt{3}} \dot{\lambda} \quad (12.52)$$

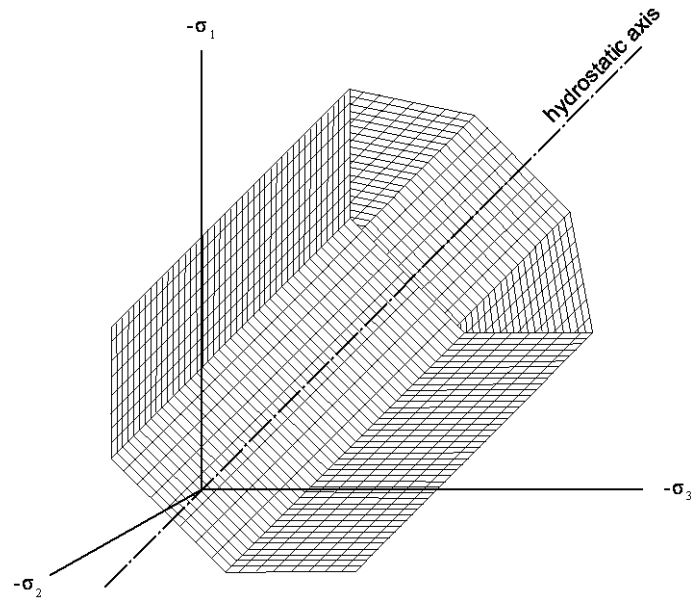


Figure 12-(9) Tresca yield surface

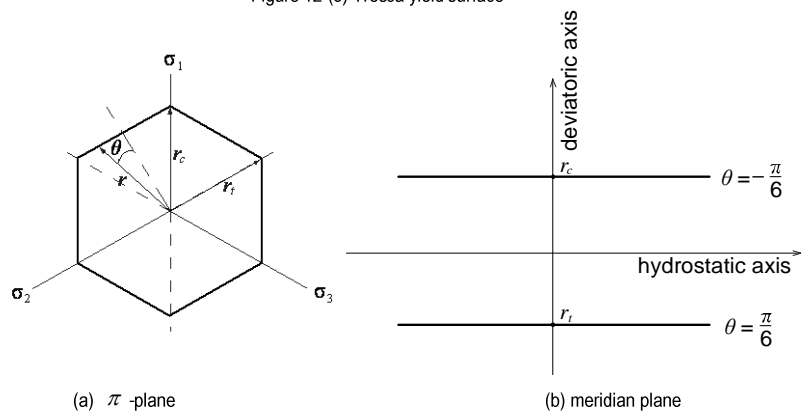


Figure 12-(10) Tresca yield surface in π -plane & meridian plane

12-2-4 Von Mises Model

The Von Mises model is one that is mostly used for analysis of metallic materials. It assumes that yielding occurs when a regular octahedral shear stress, τ_{oct} reaches the limit, which is formulated as,

$$f(\tau_{oct}) = \tau_{oct} - \sqrt{\frac{2}{3}}k = 0 \quad (12.53)$$

or,

$$f(J_2) = J_2 - k^2 = 0 \quad (12.54)$$

Expressing in terms of the principal stresses, σ_1 , σ_2 and σ_3 ,

$$(\sigma_1 - \sigma_2)^2 + (\sigma_2 - \sigma_3)^2 + (\sigma_3 - \sigma_1)^2 = 6k^2 \quad (12.55)$$

Here, k = yield stress under pure shear

If we consider the uni-axial case,

$$f(\sqrt{J_2}) = \sqrt{3}\sqrt{J_2} - Y(\kappa) = 0 \quad (12.56)$$

Here, $Y(\kappa) = k$, which represents the yield stress. Eq. (12.56) is the most widely used form, which is only dependent on the stress invariant, J_2 and is also referred to as the J_2 theory. The Von Mises yield surface retains a circular shape, which is parallel with the hydrostatic axis in the space of principal stresses as shown in Fig. 12-(11). If the von Mises and Tresca criteria are coincided at the compressive meridian and the tensile meridian, i.e., $r_c(\theta = -\pi/6)$ and $r_t(\theta = \pi/6)$, the von Mises' surface becomes a circle circumscribing the Tresca's hexahedral surface (Fig. 12-(12a)). In this case, the maximum difference in expected yield stress occurs along the shear meridian ($\theta = 0$), and the ratio of the yield shear stresses of the von Mises and Tresca criteria is $2/\sqrt{3} = 1.15$. On the other hand, if the two criteria are coincided at the shear meridian (identical k value), the von Mises' circle is inscribed by the Tresca's hexahedron. The maximum expected difference between the two criteria occurs along the compressive meridian ($\theta = -\pi/6$) and the tensile meridian ($\theta = \pi/6$) (Fig. 12-(12b)).

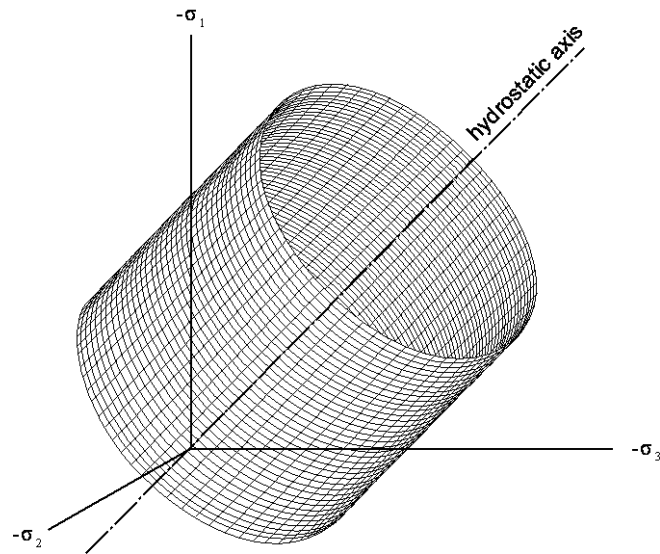
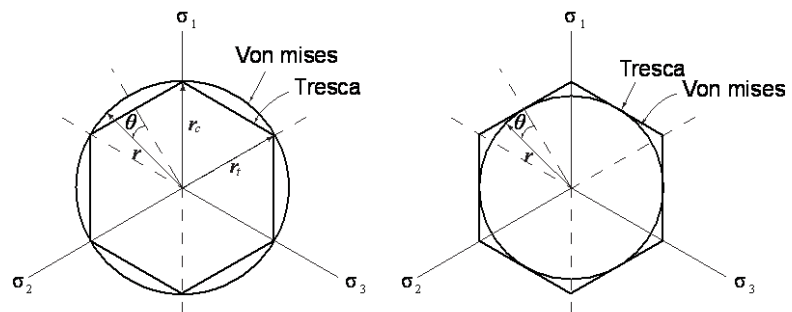
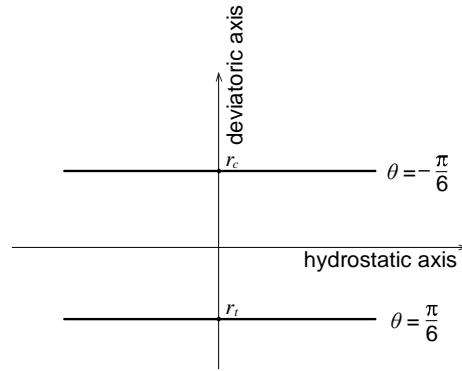


Figure 12-(11) Von Mises yield surface

(a) circumscribed circle in π -plane(b) inscribed circle in π -plane



(c) meridian plane

Figure 12-(12) Von Mises yield surface in π -plane & meridian plane

Hardening

Like the Tresca model, the Von Mises hardening behavior model follows the strain hardening hypothesis, which assumes that hardening progresses with increase in plastic deformation. The relationship between the plastic strain, ϵ_p , and the hardening parameter, κ is thus defined as,

$$\dot{\kappa} = \sqrt{\frac{2}{3}(\epsilon_{p1}\epsilon_{p1} + \epsilon_{p2}\epsilon_{p2} + \epsilon_{p3}\epsilon_{p3})} \quad (12.57)$$

Rearranging Eq. (12.57), we obtain,

$$\dot{\kappa} = \dot{\lambda} \quad (12.58)$$

12-2-5 Mohr-Coulomb Model

The material yield criterion of the Mohr (1900) model is defined as,

$$|\tau| = F(\sigma) \quad (12.59)$$

The peak shear strength, τ on a plane is assumed to be only related to the normal stress on the same plane. Eq. (12.59) describes the yield surface of a Mohr circle, and the yield function, $F(\sigma)$ is determined by experiments. The Mohr criterion assumes that a material yields at the instant when the largest Mohr circle becomes in contact with the Coulomb yield surface. This means that the middle principal stress σ_2 ($\sigma_1 \geq \sigma_2 \geq \sigma_3$) does not influence the yield criterion. The simplest form of the Coulomb yield surface is a straight line whose equation for the envelope of this line is written as,

$$|\tau| = c + \sigma \tan \phi \quad (12.60)$$

where, c, ϕ = shear strength parameters of materials
 c = cohesion
 ϕ = internal friction angle

The yield criterion of Eq. (12.60) is said to be the Mohr-Coulomb criterion. The fact that the criterion is simple and very accurate, it is widely used for materials, which exhibit the property of changing shear strengths with change in compressive stresses.

Expressing the Mohr-Coulomb equation in terms of principal stresses, we obtain,

$$\sigma_1 \frac{(1 - \sin \phi)}{2c \cos \phi} - \sigma_3 \frac{(1 + \sin \phi)}{2c \cos \phi} = 1 \quad (12.61)$$

Eq. (12.61) can be written in terms of I_1, J_2 and θ as,

$$f(I_1, J_2, \theta) = -\frac{1}{3}I_1 \sin \phi + \sqrt{J_2} \left(\cos \theta + \frac{1}{\sqrt{3}} \sin \theta \sin \phi \right) - c \cos \phi = 0 \quad (12.62)$$

The Mohr-Coulomb criterion retains the shape of an irregular hexagonal pyramid in the space of

principal stresses, and the meridian is a straight line as shown in Fig. 12-(13). And the deviatoric shape on the π -plane ($\sigma_1 + \sigma_2 + \sigma_3 = 0$) becomes an irregular hexagon as shown in Fig. 12-(14a). In order to draw the irregular hexagon, the lengths of r_{t0} and r_{c0} are required on the meridian plane at $\theta = -\pi/6$ as shown in Fig. 12-(14b), which are defined as,

$$r_{t0} = \frac{2\sqrt{6}c \cos \phi}{3 + \sin \phi} \quad (12.63)$$

$$r_{c0} = \frac{2\sqrt{6}c \cos \phi}{3 - \sin \phi} \quad (12.64)$$

From Eq. (12.63) and Eq. (12.64), r_{t0} / r_{c0} is found.

$$\frac{r_{t0}}{r_{c0}} = \frac{3 - \sin \phi}{3 + \sin \phi} \quad (12.65)$$

The fact that all deviatoric sections of the Mohr-Coulomb yield surface geometrically resemble one another, the ratio, r_t / r_c of any deviatoric plane (i.e., for different values of I_1 or ξ) remains constant.

$$\frac{r_t}{r_c} = \frac{r_{t0}}{r_{c0}} = \frac{3 - \sin \phi}{3 + \sin \phi} \quad (12.66)$$

For the purpose of controlling the phenomenon of excessive volumetric expansion, the non-associated flow rule can be applied here. For this, the plastic potential function can be defined using the expansion angle, ψ instead of using the internal friction angle, ϕ as follows:

$$g(I_1, J_2, \theta) = -\frac{1}{3}I_1 \sin \psi + \sqrt{J_2} \left(\cos \theta + \frac{1}{\sqrt{3}} \sin \theta \sin \psi \right) \quad (12.67)$$

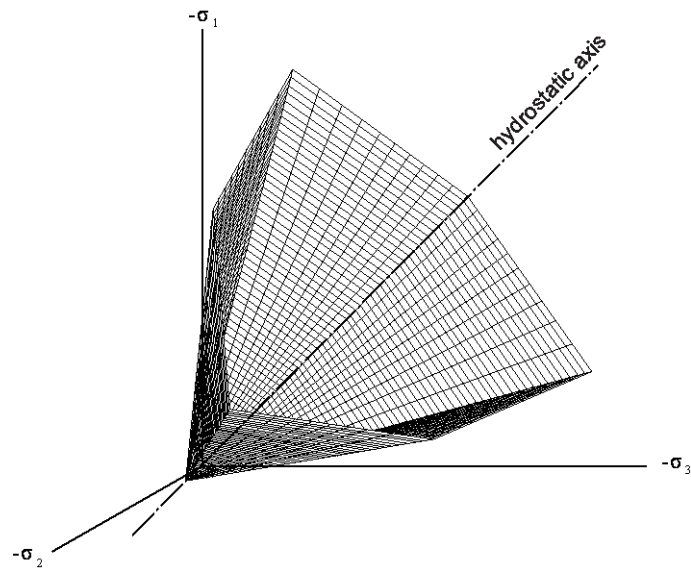
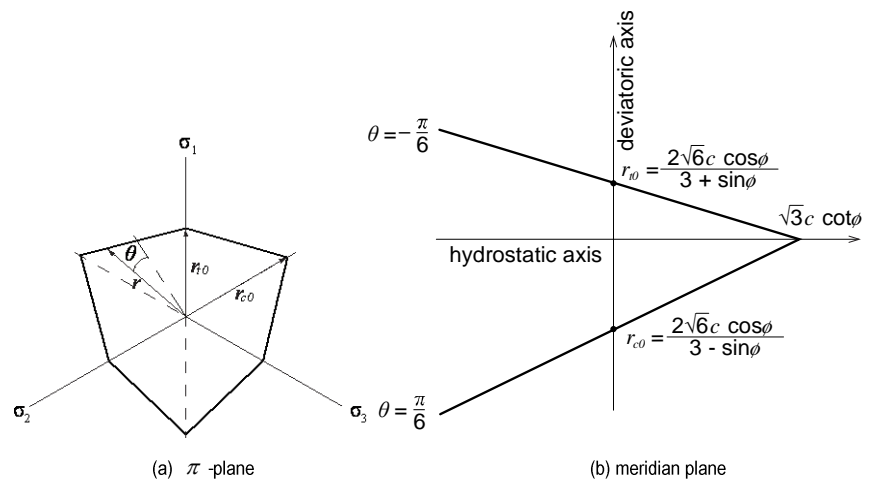


Figure 12-(13) Mohr-Coulomb yield surface

Figure 12-(14) Mohr-Coulomb yield surface in π -plane & meridian plane

Hardening

The hardening behavior model follows the strain hardening hypothesis, which assumes that hardening progresses with increase in plastic deformation. The relationship between the plastic strain, ϵ_p and the hardening parameter, κ is thus defined as,

$$\dot{\kappa} = \sqrt{\frac{2}{3}(\epsilon_{p1}\epsilon_{p1} + \epsilon_{p2}\epsilon_{p2} + \epsilon_{p3}\epsilon_{p3})} \quad (12.68)$$

Rearranging Eq. (12.68), we obtain,

$$\dot{\kappa} = \dot{\lambda} \sqrt{\frac{1}{3}(1 + \sin^2 \psi)} \quad (12.69)$$

12-2-6 Drucker-Prager Model

The Drucker-Prager model has originated from the von Mises model, which has been modified and extended by Drucker and Prager (1952) and widely used for practical problems. It is also referred to as an extended von Mises criterion. Expressing the yield function and plastic potential function of the Drucker-Prager model in terms of stress invariants, I_1 and J_2 , we obtain,

$$\begin{aligned} f(I_1, J_2) &= \sqrt{J_2} - \alpha I_1 - k = 0 \\ g(I_1, J_2) &= \sqrt{J_2} - \gamma I_1 \end{aligned} \quad (12.70)$$

$$\text{where, } \alpha = \frac{2\sin\phi}{\sqrt{3}(3-\sin\phi)}, \quad k = \beta c, \quad \beta = \frac{6\cos\phi}{\sqrt{3}(3-\sin\phi)}, \quad \gamma = \frac{2\sin\psi}{\sqrt{3}(3-\sin\psi)}$$

If α is zero, Eq. (12.70) reverts to the von Mises yield criterion. In order to define the value γ of the plastic potential function, g , the value of the angle of expansion, ψ is additionally required. Fig. 12-(15) shows the Drucker-Prager yield surface in the space of principal stresses. The yield surface retains the shape of a cone with the axis of a spatial diagonal line (stress axis of hydrostatic plane, $\sigma_1 = \sigma_2 = \sigma_3$).

The Drucker-Prager yield surface can be considered to have been tailored to the behaviors of concrete and foundation materials in that the von Mises yield surface has been extended to vary along the hydrostatic pressure.

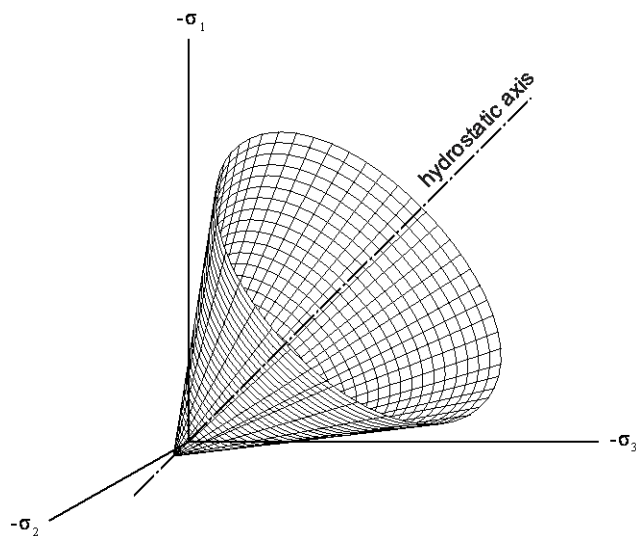
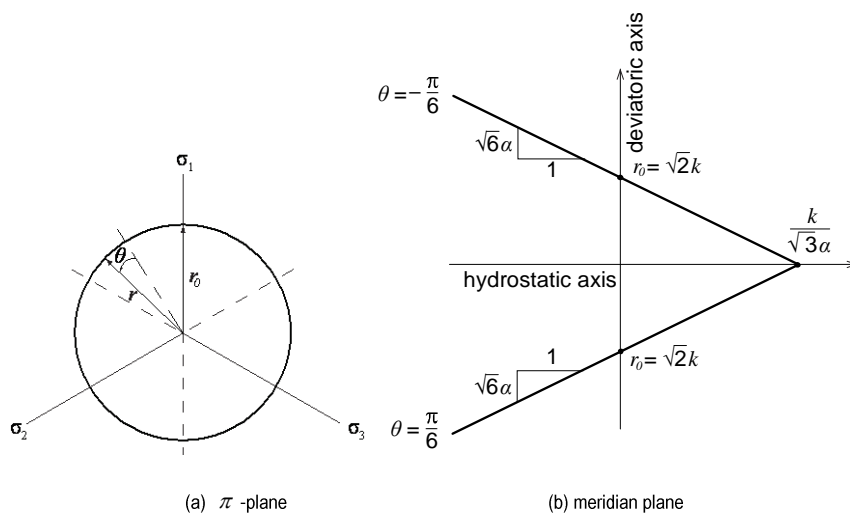


Figure 12-(15) Drucker-Prager yield surface

Figure 12-(16) Drucker-Prager yield surface in π -plane & meridian plane

Hardening

The hardening behavior model follows the strain hardening hypothesis, which assumes that hardening progresses with increase in plastic deformation. The relationship between the plastic strain, ϵ_p and the hardening parameter, κ is thus defined as,

$$\dot{\kappa} = \sqrt{\frac{2}{3}(\epsilon_{p1}\epsilon_{p1} + \epsilon_{p2}\epsilon_{p2} + \epsilon_{p3}\epsilon_{p3})} \quad (12.71)$$

Rearranging Eq. (12.57), we obtain,

$$\dot{\kappa} = \dot{\lambda}\sqrt{1 + 2\gamma^2} \quad (12.72)$$

Chapter 13. Total Strain Crack

13-1 Introduction

13-1-1 Concrete Crack Models

Analysis models for concrete cracking can be classified into a discrete crack model [discontinuum model] and a smeared crack model [continuum model] (see Fig. 13-(1)). The discrete crack model uses finite elements at which concrete cracks are separately represented as boundaries. In the smeared crack model, concrete cracks are assumed to be scattered and distributed, such that discrete elements are not used at the crack locations.

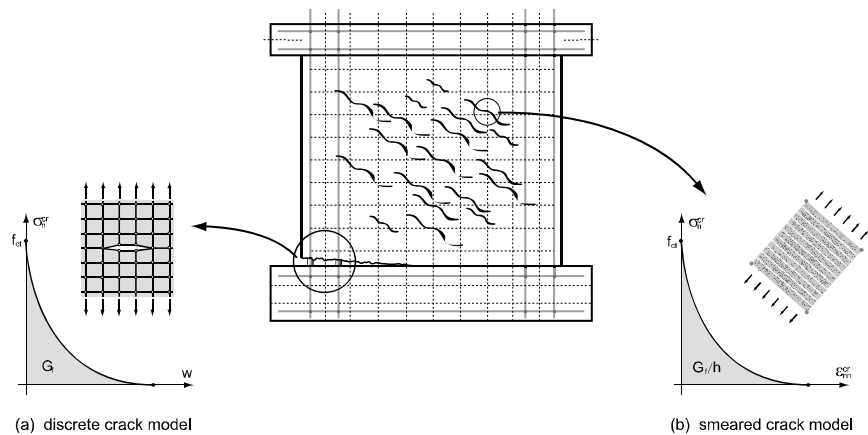


Figure 13-(1) Concrete crack models

The discrete crack model has the advantage of being able to specifically represent such behaviors as physical discontinuity due to concrete cracking and failure and bond slips of reinforcing bars. However, it has some disadvantages in that the accuracy of analysis significantly depends on the material properties required, and that finite element modeling can be quite complex. Cracks can be modeled by automatically dividing elements at the crack locations and adding interface elements in advance at the locations where cracks are expected. Interface non-linearity in Chapter 14 explains the use of interface elements in a discrete crack model.

The smeared crack model assumes that locally generated cracks are evenly scattered over a wide surface. This model is known to be suitable for reinforced concrete structures with reasonable amount of reinforcement, and its finite element modeling is relatively simple. The smeared crack model can be classified into orthogonal and non-orthogonal crack models depending on the assumption of angles of crack development. The orthogonal crack model assumes orthogonal crack directions, whereas the non-orthogonal crack model assumes non-orthogonal directions of cracks. Also, depending on the numerical analysis methods for cracks, the smeared crack model is further classified into various models such as a decomposed-strain model and a total strain model.

The decomposed-strain model in the smeared crack model calculates the total strain in terms of material strain and crack strain. The material strain is quite versatile in its expandability since it can include elastic strain, plastic strain, creep strain, thermal strain, etc. The crack strain also can be expanded into a non-orthogonal multi-directional crack model as it can include a number of crack strains at different angles. However, its disadvantages exist in that the algorithm is complex; selection of material properties is difficult; and convergence may become an issue.

The total strain model in the smeared crack model can be rather simply formulated using total strain without having to decompose it into the strain components. In addition, its algorithm is easy to understand because the total strain model uses only one stress-strain relationship for tensile behavior including cracks and one for compressive behavior. It is also more practical since the input for material properties for defining nonlinear behaviors is relatively simple enough.

13-1-2 Total Strain Crack Model

MIDAS uses the total strain crack model classified under the smeared crack model. As shown in Fig. 13-(2), it provides two methods, which are separated into the fixed crack model and the rotating crack model depending on the reference crack axes. The former assumes that the axes of cracks remain unchanged once the crack axes are defined. On the contrary, the latter is a method in which the directions of the cracks are assumed to continuously rotate depending on the changes in the axes of principle strains.

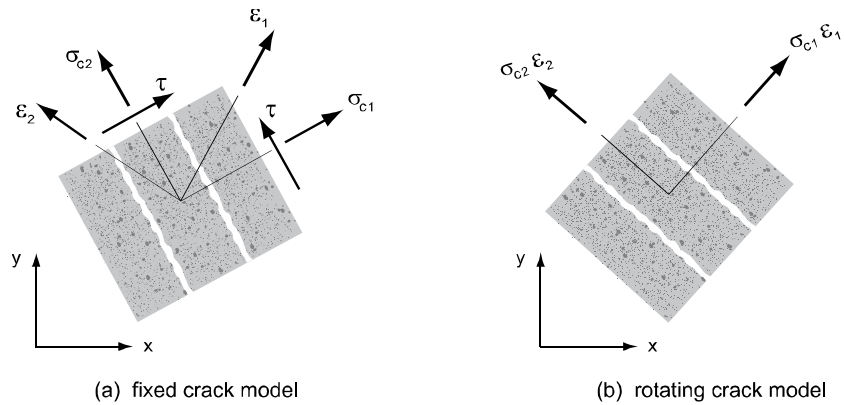


Figure 13-2) Orthogonal crack models

In both cases of the fixed and rotating models, the first crack at the integral points always initiates in the directions of the principle strains. Concrete materials exhibit isotropic properties prior to cracking and anisotropic properties after cracking. MIDAS treats the properties of concrete as orthotropic materials after cracking. As such, the normal stresses and shear stresses are calculated on the crack surfaces. Since we assume that the directions of the incipient cracks remain unchanged in the fixed crack model, the normal stresses and shear stresses exist on the crack surfaces as shown in Fig. 13-(2a). However, new cracks are assumed to develop in the directions of the current principle strains in the rotating crack model, while ignoring the cracks developed at the previous stage. Thus, only the normal stresses are present on the crack surfaces as shown in Fig. 13-(2b). As a result, the fixed crack model and the rotating crack model can be said to use the concepts of fixed stress-strain and coaxial stress-strain respectively. Since MIDAS considers only the cases of perpendicular crack angles, the fixed crack model and the rotating crack model in MIDAS can be classified into an orthogonal crack model.

Although the fixed crack model can realistically reflect the physical characteristics of the crack phenomena, the orthogonal crack model tends to somewhat overestimate the stiffness and strength

of materials in comparison with a non-orthogonal crack model. On the contrary, the algorithm for the rotating crack model is relatively simple, and its convergence is superior due to the fact that this model is unrelated to the previous cracking conditions. Because of such merits, the rotating crack model has been used for nonlinear analyses of reinforced concrete structures over the years.

The constitutive model on the basis of total strain is founded on the Modified Compression Field Theory proposed by Vecchio and Collins¹. This theory was formulated on the basis of two-dimensional models. MIDAS has been implemented with an extension into 3-dimensional models based on the theory proposed by Selby and Vecchio².

1 Vecchio, F. J., and Collins, M. P. *The modified compression field theory for reinforced concrete elements subjected to shear*. ACI Journal 83, 22 (1986), 219–231.

2 Selby, R. G., and Vecchio, F. J., *Three-dimensional Constitutive Relations for Reinforced Concrete*. Tech. Rep. 93-02, Univ. Toronto, dept. Civil Eng., Toronto, Canada, 1993.

13-2 Basic Properties

The following parameters need to be defined in order to analyze the Total Strain Crack Model.

- Crack Model Type
- General Concrete Properties
- Tensile Behavior
- Compressive Behavior
- Shear Behavior
- Lateral Influences

13-2-1 Crack Model Type

The total strain crack model implemented in MIDAS contains the smeared fixed crack model (SFCM) and smeared rotating crack model (SRCM). The rotating crack model and the fixed crack model are known to well represent the cracking behaviors of general reinforced concrete structures. Especially the fixed crack model has been recognized to accurately simulate the physical behaviors of concrete cracks. The difference between the two models exists in the process of determining the crack directions, which is explained in the Transformation of Crack Direction section in detail.

13-2-2 General Concrete Properties

The required material properties to analyze crack models can be defined either by the user or automatically by the program using pertinent codes (MIDAS currently uses CEB-FIP 1990).

(1) Direct User Input

The user-defined material properties are as follows:

- 1) Young's Modulus
- 2) Poisson's Ratio *[default = 0.0]*
- 3) Tensile Strength
- 4) Compressive Strength
- 5) Fracture Energy *[if necessary]*

(2) Code Based Input

This is used when the user wishes to define the values presented in codes. Material properties are now calculated by CEB-FIP 1990 and applied to analysis. By entering the following two values, material properties are obtained through the equation of the relationship between compressive strength and tensile strength as well as the equation of the relationship between compression strength and fracture energy, as presented in CEB-FIP 1990.

- (1) Grade: Characteristic compressive strength $[N/mm^2]$
- (2) D_{max} : Maximum aggregate size $[mm]$

In order to properly define the necessary material properties in the total strain crack model, the user needs to input the concrete grade and the maximum aggregate size (D_{max}). The concrete grade represents f_{ck} (characteristic compressive strength), which is classified below.

Concrete classes: C12, C20, C30, C40, C50, C60, C70 and C80

C60 here means $f_{ck}=60 [N/mm^2]$.

CEB-FIP 1990 uses Grade and D_{max} to calculate the Young's modulus, mean compressive strength, mean tensile strength and fracture energy.

The mean compressive strength is expressed by,

$$f_{cm} = f_{ck} + \Delta f \quad (13.1)$$

where, $\Delta f = 8 \text{ [MPa]}$.

The Young's modulus is expressed in terms of the mean compressive strength (f_{cm}),

$$E_c = E_{c0} \left(\frac{f_{cm}}{f_{cm0}} \right)^{\frac{1}{3}} \quad (13.2)$$

where, $E_{c0} = 2.15 \times 10^4 \text{ [N/mm}^2\text{]}$, and the reference mean compressive strength, f_{cm0} is 10 $\text{[N/mm}^2\text{]}$.

The mean tensile strength is calculated as,

$$f_{ct,m} = f_{ctk0,m} \left(\frac{f_{ck}}{f_{ck0}} \right)^{\frac{2}{3}} \quad (13.3)$$

where, f_{ctk0} is 1.40 $\text{[N/mm}^2\text{]}$, and f_{ck0} is 10 $\text{[N/mm}^2\text{]}$.

The fracture energy is related to the compressive strength and the maximum aggregate size, D_{\max} , which uses the following equation:

$$G_f = G_{f0} \left(\frac{f_{cm}}{f_{cm0}} \right)^{0.7} \quad (13.4)$$

f_{cm0} is 10 $\text{[N/mm}^2\text{]}$. Table 13.1 shows the values of G_{f0} corresponding to the maximum size of aggregates.

$D_{\max} \text{ (mm)}$	$G_{f0} \text{ (J/m}^2\text{)}$
8	25
16	30
32	58

Table 13.1 G_{f0} corresponding to D_{\max}

13-3 Loading and Unloading

The total strain crack model implemented in MIDAS depicts all the ultimate states of materials such as cracking and crushing, and especially shear behavior can be clearly defined through the relationship between shear stress and shear strain. In case of unloading, the total strain crack model is intended to point towards the origin point in the stress-strain curve. The detailed analytical process is outlined below.

Concrete subjected to loadings resists tensile or compressive forces, and it can reach the ultimate states of materials such as cracking and crushing. In case the fixed crack model is used, the shear behavior can be explicitly presented. The material deterioration by cracking and crushing of concrete can be assessed by means of a vector field α , which comprises six internal damage variables, α_k ($k = 1, \dots, 2 \times nstr$). $nstr$ represents the number of the principal stresses. The variables ($k = 1, \dots, nstr$) related to the maximum tensile strain will be greater than or equal to zero. And the variables ($k = 1 + nstr, \dots, 2 \times nstr$) identifying the minimum compressive strain will be less than zero. The fact that no damage recovery is assumed to take place, the absolute values of the internal damage variables can only increase.

The loading-unloading-reloading conditions can be understood by additional unloading constraints (variables r_k). The unloading constraint variables are determined for both tension and compression zones individually, which are used to represent stiffness degradation in each zone separately.

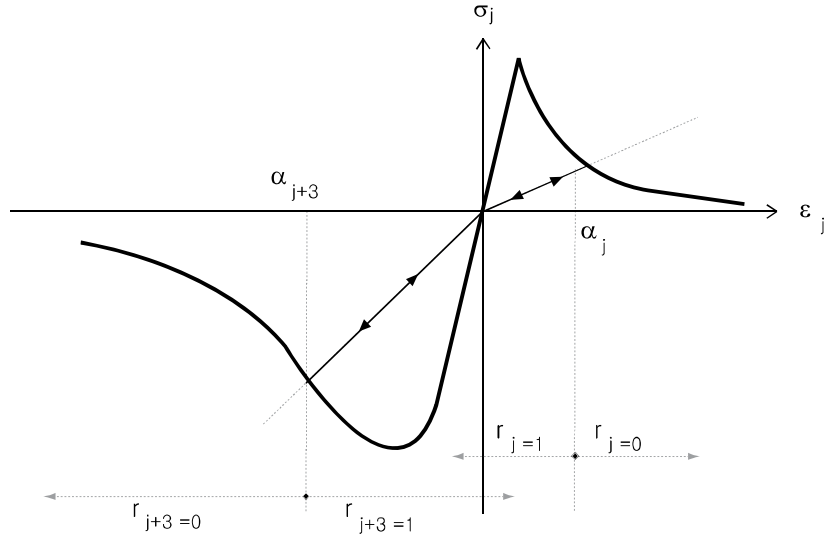


Figure 13-(3) Loading-Unloading

The unloading constraint variable in the tensile zone is expressed by,

$$r_k = \begin{cases} 0 & \text{if } {}^{t+\Delta t}_{i+1}\epsilon_k > \alpha_k \\ 1 & \text{if } {}^{t+\Delta t}_{i+1}\epsilon_k \leq \alpha_k \end{cases} \quad (k = 1, \dots, nstr) \quad (13.5)$$

The unloading constraint variable in the compression zone is expressed by,

$$r_k = \begin{cases} 0 & \text{if } {}^{t+\Delta t}_{i+1}\epsilon_{k-3} < \alpha_k \\ 1 & \text{if } {}^{t+\Delta t}_{i+1}\epsilon_{k-3} \geq \alpha_k \end{cases} \quad (k = 1 + nstr, \dots, 2 \times nstr) \quad (13.6)$$

The internal variables are updated as follows:

$${}^{t+\Delta t}_{i+1}\mathbf{a} = {}^t\mathbf{a} + \mathbf{W}\Delta\epsilon \quad (13.7)$$

where,

$$\mathbf{W} = \begin{cases} W_{k,k} = 1 - r_k & k = 1, \dots, nstr \\ W_{k+nstr,k} = 1 - r_k & k = 1 + nstr, \dots, 2 \times nstr \end{cases} \quad (13.8)$$

Assuming that damage recovery does not occur, the stress in the j direction can be expressed as,

$$\sigma_j = f_j(\mathbf{\alpha}, \boldsymbol{\varepsilon}_{nst}) \cdot g_j(\mathbf{\alpha}, \boldsymbol{\varepsilon}_{nst}) \quad (13.9)$$

In addition to the internal variable α_j in the j direction representing the uniaxial stress and strain relationship, the internal variables and strains in the remaining directions influence the stress, which is the reason for expressing it as a function of variable $\mathbf{\alpha}$ and the principal strain tensor $\boldsymbol{\varepsilon}_{nst}$. If unloading and reloading are defined by the secant method considering the maximum and minimum strains in each crack direction, the loading-unloading function denoted by g_j can be expressed by,

$$g_j = \begin{cases} 1 - \frac{\alpha_j - \varepsilon_j}{\alpha_j} = \frac{\varepsilon_j}{\alpha_j} & \text{if } \varepsilon_j > 0 \\ 1 - \frac{\alpha_{j+nstr} - \varepsilon_j}{\alpha_{j+nstr}} = \frac{\varepsilon_j}{\alpha_{j+nstr}} & \text{if } \varepsilon_j < 0 \end{cases} \quad [0 \leq g \leq 1] \quad (13.10)$$

The uniaxial stress–strain relationship (13.9) is based on the basic strength in the crack directions f , multiplied by the loading–unloading function g . The material model implemented in MIDAS takes into account the effect of confinement and the effect of lateral cracking on the basic strength. These factors need to be properly considered because they influence not only the maximum strength, but generally the shape of the stress–strain curve.

13-4 Crack Strain Transformation

The constitutive model of the total strain crack model is defined as stress as a function of the total strain. This concept is also known as hypo-elasticity if loading and unloading follow the same stress-strain path. In MIDAS, loading and unloading take place on separate stress-strain paths. Especially unloading takes place with a secant slope. For the stress-strain relationship of the total strain crack model, it is possible to use a number of approaches applying user-defined models in addition to the hysteretic curves provided by MIDAS.

The concept of orthogonal crack models, which will be explained in this section, is a representative method widely used for crack analysis. It defines the stress-strain relationship depending on the principal directions of strain vectors.

The rotating crack model is also known as a coaxial stress-strain method. This model has been recognized to predict the behaviors of reinforced concrete structures very well. On the other hand, the fixed crack model is known as a fixed stress-strain method. This model defines the stress-strain relationships of all subsequent cracks based on the fixed coordinate axes of the incipient crack direction. The above two concepts can be easily explained in a similar framework even if they differ in crack directions (nst) being fixed or rotated.

The basic concept of the total strain crack model is that stresses are calculated considering the crack directions. The strains in the element coordinate system are renewed by considering the incremental strain $\Delta\epsilon_{xyz}$.

$${}^{t+\Delta t}_{i+1}\epsilon_{xyz} = {}^t\epsilon_{xyz} + {}^{t+\Delta t}_{i+1}\Delta\epsilon_{xyz} \quad (13.11)$$

The strains in the crack directions are calculated by multiplying the strains in the element coordinate system by the transformation matrix.

$${}^{t+\Delta t}_{i+1}\boldsymbol{\varepsilon}_{nst} = \mathbf{T}{}^{t+\Delta t}_{i+1}\boldsymbol{\varepsilon}_{xyz} \quad (13.12)$$

The transformation matrix \mathbf{T} in the rotating crack model is determined by the current strain expressed by,

$$\mathbf{T} = \mathbf{T}({}^{t+\Delta t}_{i+1}\boldsymbol{\varepsilon}_{xyz}). \quad (13.13)$$

On the other hand, the transformation matrix in the fixed crack model is fixed by the incipient crack direction.

The strain transformation matrix is obtained by the Jacobi method. If the strain tensor is expressed in its general form by,

$$\mathbf{E} = \begin{bmatrix} \varepsilon_{xx} & \varepsilon_{xy} & \varepsilon_{xz} \\ \varepsilon_{yx} & \varepsilon_{yy} & \varepsilon_{yz} \\ \varepsilon_{zx} & \varepsilon_{zy} & \varepsilon_{zz} \end{bmatrix} \quad (13.14)$$

the eigenvectors are saved in the rotation matrix \mathbf{R} below.

$$\mathbf{R} = [\mathbf{n} \quad \mathbf{s} \quad \mathbf{t}] = \begin{bmatrix} c_{xn} & c_{xs} & c_{xt} \\ c_{yn} & c_{ys} & c_{yt} \\ c_{zn} & c_{zs} & c_{zt} \end{bmatrix} \quad (13.15)$$

$c_{xn} = \cos \phi_{ij}$ is the cosine between the i axis and the j axis. The strain transformation matrix \mathbf{T} is then calculated by substituting the appropriate values,

$$\mathbf{T} = \begin{bmatrix} c_{xn}^2 & c_{yn}^2 & c_{zn}^2 & c_{xn}c_{yn} & c_{yn}c_{zn} & c_{zn}c_{xn} \\ c_{xs}^2 & c_{ys}^2 & c_{zs}^2 & c_{xs}c_{ys} & c_{ys}c_{zs} & c_{zs}c_{xs} \\ c_{xt}^2 & c_{yt}^2 & c_{zt}^2 & c_{xt}c_{yt} & c_{yt}c_{zt} & c_{zt}c_{xt} \\ 2c_{xn}c_{xs} & 2c_{yn}c_{ys} & 2c_{zn}c_{zs} & c_{xn}c_{ys} + c_{yn}c_{xs} & c_{yn}c_{zs} + c_{zn}c_{ys} & c_{zn}c_{xs} + c_{xn}c_{zs} \\ 2c_{xs}c_{xt} & 2c_{ys}c_{yt} & 2c_{zs}c_{zt} & c_{xs}c_{yt} + c_{ys}c_{xt} & c_{ys}c_{zt} + c_{zs}c_{yt} & c_{zs}c_{xt} + c_{xs}c_{zt} \\ 2c_{xt}c_{xn} & 2c_{yt}c_{yn} & 2c_{zt}c_{zn} & c_{xt}c_{yn} + c_{yt}c_{xn} & c_{yt}c_{zn} + c_{zn}c_{yn} & c_{zt}c_{xn} + c_{xt}c_{zn} \end{bmatrix} \quad (13.16)$$

in a general three-dimensional stress situation. For the other stress situations the appropriate sub-matrix should be taken. The constitutive model is then formulated in the crack coordinate system, which is generally given by,

$${}^{t+\Delta t}_{i+1}\sigma_{nst} = \sigma({}^{t+\Delta t}_{i+1}\epsilon_{nst}) \quad (13.17)$$

Finally the stress vectors in the crack coordinate systems are transformed into the element coordinate systems and renewed.

$${}^{t+\Delta t}_{i+1}\sigma_{xyz} = \mathbf{T}^T {}^{t+\Delta t}_{i+1}\sigma_{nst} \quad (13.18)$$

In the rotating crack model, the transformation matrix \mathbf{T} is determined like $\mathbf{T}^T({}^{t+\Delta t}_{i+1}\epsilon_{xyz})$ by the current strain. In the fixed crack model, the transformation matrix defined by the incipient crack is used.

13-5 Stiffness Matrix

An iterative scheme is used for concrete crack analysis because of its nonlinearity. In order to satisfy the equilibrium between external and internal force vectors, one of the incremental iterative procedures such as the Newton-Raphson method is used. To this end, the constitutive model needs to be defined by a proper stiffness matrix. MIDAS uses the secant stiffness and tangent stiffness approaches to determine the stiffness matrix. The secant stiffness approach is especially suitable for finding excellent and stable solutions to analyses of reinforced concrete structures, which widely develop cracks. On the contrary, the tangent stiffness approach is known to be very appropriate for analyses of local cracking or crack propagation.

13-5-1 Tangent Stiffness Matrix

The tangent stiffness matrix in the element coordinate system is given by,

$$\mathbf{D} = \mathbf{T}^T \mathbf{D}_{\text{tangent}} \mathbf{T} \quad (13.19)$$

where, \mathbf{T} represents the strain transformation matrix, and $\mathbf{D}_{\text{tangent}}$ represents the tangent stiffness matrix in the crack coordinate systems.

The tangent stiffness matrix can be decomposed into four sub-matrices as follows:

$$\mathbf{D}_{\text{tangent}} = \begin{bmatrix} \mathbf{D}_{nn} & \mathbf{D}_{n\theta} \\ \mathbf{D}_{\theta n} & \mathbf{D}_{\theta\theta} \end{bmatrix} \quad (13.20)$$

\mathbf{D}_{nn} is the tangent stiffness sub-matrix of the normal components of the local (crack) strain; $\mathbf{D}_{\theta\theta}$ represents the tangent stiffness sub-matrix of the shear components of the local strain; and $\mathbf{D}_{n\theta}$ and $\mathbf{D}_{\theta n}$ are the tangent stiffness sub-matrices representing the coupling terms between the normal and the shear strain.

In a co-rotational concept, the coupling sub-matrices are equal to zero and the sub-matrix $\mathbf{D}_{\square\square}$ is dependent on the principal stress components as has been derived by several authors³. The sub-matrix then becomes,

$$\mathbf{D}_{\theta\theta} = \begin{bmatrix} \frac{\sigma_1 - \sigma_2}{2(\varepsilon_1 - \varepsilon_2)} & 0 & 0 \\ 0 & \frac{\sigma_2 - \sigma_3}{2(\varepsilon_2 - \varepsilon_3)} & 0 \\ 0 & 0 & \frac{\sigma_3 - \sigma_1}{2(\varepsilon_3 - \varepsilon_1)} \end{bmatrix} \quad (13.21)$$

It is clear that the shear stiffness terms are not independent on the stresses in the principal directions. This is a direct result of the spin of the principal coordinate system. In a fixed concept the coupling sub-matrices are not necessarily zero but depend on the specific relationship between the shear-retention and the normal strain components. In general, the sub-matrix $\mathbf{D}_{n\square}$ is equal to zero because the normal stress components are not dependent on the shear components of the strain vector. On the other hand, the sub-matrix $\mathbf{D}_{\square n}$ is given by,

3 Crisfield, M. A., and Wills, J., *Analysis of R/C panels using different concrete models*, J. Eng. Mech. Div., ASCE 115, 3 (1989),

578–597.

Feenstra, P. H., *Computational Aspects of Biaxial Stress in Plain and Reinforced Concrete*, PhD thesis, Delft University of Technology, 1993.

Rots, J. G., *Computational Modeling of Concrete Fracture*, PhD thesis, Delft University of Technology, 1988.

Willam, K. J., Pramono, E., and Sture, S., *Fundamental issues of smeared crack models*, In Proc. SEM/RILEM Int. Conf. on Fracture of Concrete and Rock, Houston 1987 (New York, 1989), S. P. Shah and S. E. Schwartz, Eds., Springer-Verlag, pp. 142–157.

$$\mathbf{D}_{\theta n} = \begin{bmatrix} \frac{\partial \sigma_{ns}}{\partial \varepsilon_{nn}} & \frac{\partial \sigma_{ns}}{\partial \varepsilon_{ss}} & \frac{\partial \sigma_{ns}}{\partial \varepsilon_{tt}} \\ \frac{\partial \sigma_{st}}{\partial \varepsilon_{nn}} & \frac{\partial \sigma_{st}}{\partial \varepsilon_{ss}} & \frac{\partial \sigma_{st}}{\partial \varepsilon_{tt}} \\ \frac{\partial \sigma_m}{\partial \varepsilon_{nn}} & \frac{\partial \sigma_m}{\partial \varepsilon_{ss}} & \frac{\partial \sigma_m}{\partial \varepsilon_{tt}} \end{bmatrix} \quad (13.22)$$

This matrix becomes zero when the shear retention is independent from the normal (crack) strain. The shear terms of the tangent stiffness matrix is usually given by,

$$\mathbf{D}_{\theta\theta} = \begin{bmatrix} \frac{\partial \sigma_{ns}}{\partial \gamma_{ns}} & 0 & 0 \\ 0 & \frac{\partial \sigma_{st}}{\partial \gamma_{st}} & 0 \\ 0 & 0 & \frac{\partial \sigma_m}{\partial \gamma_m} \end{bmatrix} \quad (13.23)$$

The normal stiffness terms, \mathbf{D}_{nn} , are partial derivatives as can be expected. Because coupling due to lateral strain effects is included in the calculation of the principal stresses, the off-diagonal terms are not equal to zero, and the resulting matrix is non-symmetric.

$$\mathbf{D}_{nn} = \begin{bmatrix} \frac{\partial \sigma_{nn}}{\partial \varepsilon_{nn}} & \frac{\partial \sigma_{nn}}{\partial \varepsilon_{ss}} & \frac{\partial \sigma_{nn}}{\partial \varepsilon_{tt}} \\ \frac{\partial \sigma_{ss}}{\partial \varepsilon_{nn}} & \frac{\partial \sigma_{ss}}{\partial \varepsilon_{ss}} & \frac{\partial \sigma_{ss}}{\partial \varepsilon_{tt}} \\ \frac{\partial \sigma_{tt}}{\partial \varepsilon_{nn}} & \frac{\partial \sigma_{tt}}{\partial \varepsilon_{ss}} & \frac{\partial \sigma_{tt}}{\partial \varepsilon_{tt}} \end{bmatrix} \quad (13.24)$$

The starting point for the derivation of the stiffness terms \mathbf{D}_{nst} is the stress-strain relation given in (13.9). The derivative with respect to the principal strain vector, ε_{nst} , becomes,

$$\frac{\partial \sigma_i}{\partial \boldsymbol{\varepsilon}_{nst}} = g_i(\boldsymbol{\alpha}, \boldsymbol{\varepsilon}_{nst}) \left\{ \frac{\partial \boldsymbol{\alpha}^T}{\partial \boldsymbol{\varepsilon}_{nst}} \frac{\partial f_i}{\partial \boldsymbol{\alpha}} + \frac{\partial f_i}{\partial \boldsymbol{\varepsilon}_{nst}} \right\} + f_i(\boldsymbol{\alpha}, \boldsymbol{\varepsilon}_{nst}) \left\{ \frac{\partial \boldsymbol{\alpha}^T}{\partial \boldsymbol{\varepsilon}_{nst}} \frac{\partial g_i}{\partial \boldsymbol{\alpha}} + \frac{\partial g_i}{\partial \boldsymbol{\varepsilon}_{nst}} \right\} \quad (13.25)$$

The derivative of the internal variables with respect to the strain vector $\partial \boldsymbol{\alpha} / \partial \boldsymbol{\varepsilon}_{nst}$, given by the matrix \mathbf{W} in (13.8), results in,

$$\frac{\partial \sigma_i}{\partial \boldsymbol{\varepsilon}_{nst}} = g_i(\boldsymbol{\alpha}, \boldsymbol{\varepsilon}_{nst}) \left\{ \mathbf{W}^T \frac{\partial f_i}{\partial \boldsymbol{\alpha}} + \frac{\partial f_i}{\partial \boldsymbol{\varepsilon}_{nst}} \right\} + f_i(\boldsymbol{\alpha}, \boldsymbol{\varepsilon}_{nst}) \left\{ \mathbf{W}^T \frac{\partial g_i}{\partial \boldsymbol{\alpha}} + \frac{\partial g_i}{\partial \boldsymbol{\varepsilon}_{nst}} \right\} \quad (13.26)$$

This is elaborated as,

$$\begin{aligned} \mathbf{D}_{nst} = & \begin{bmatrix} \{m_1 r_1 + (1 - m_1) r_4\} \overline{E_1} & 0 & 0 \\ 0 & \{m_2 r_2 + (1 - m_2) r_5\} \overline{E_2} & 0 \\ 0 & 0 & \{m_3 r_3 + (1 - m_3) r_6\} \overline{E_3} \end{bmatrix} \\ & + \begin{bmatrix} g_1 & 0 & 0 \\ 0 & g_2 & 0 \\ 0 & 0 & g_3 \end{bmatrix} \begin{bmatrix} \frac{\partial f_1}{\partial \varepsilon_1} & \frac{\partial f_1}{\partial \varepsilon_2} & \frac{\partial f_1}{\partial \varepsilon_3} \\ \frac{\partial f_2}{\partial \varepsilon_1} & \frac{\partial f_2}{\partial \varepsilon_2} & \frac{\partial f_2}{\partial \varepsilon_3} \\ \frac{\partial f_3}{\partial \varepsilon_1} & \frac{\partial f_3}{\partial \varepsilon_2} & \frac{\partial f_3}{\partial \varepsilon_3} \end{bmatrix} \\ & + \begin{bmatrix} g_1 & 0 & 0 \\ 0 & g_2 & 0 \\ 0 & 0 & g_3 \end{bmatrix} \begin{bmatrix} \frac{\partial f_1}{\partial \alpha_1} & \frac{\partial f_1}{\partial \alpha_2} & \dots & \frac{\partial f_1}{\partial \alpha_6} \\ \frac{\partial f_2}{\partial \alpha_1} & \frac{\partial f_2}{\partial \alpha_2} & \dots & \frac{\partial f_2}{\partial \alpha_6} \\ \frac{\partial f_3}{\partial \alpha_1} & \frac{\partial f_3}{\partial \alpha_2} & \dots & \frac{\partial f_3}{\partial \alpha_6} \end{bmatrix} \begin{bmatrix} 1 - r_1 & 0 & 0 \\ 0 & 1 - r_2 & 0 \\ 0 & 0 & 1 - r_3 \\ 1 - r_4 & 0 & 0 \\ 0 & 1 - r_5 & 0 \\ 0 & 0 & 1 - r_6 \end{bmatrix} \end{aligned} \quad (13.27)$$

where, m_i is introduced for the state of strain,

$$m_i = \begin{cases} 1 & \text{if } \varepsilon_i > 0 \\ 0 & \text{if } \varepsilon_i \leq 0 \end{cases} \quad (13.28)$$

The secant stiffness terms in the tensile and compressive regimes respectively are given by,

$$\overline{E}_j = \frac{f_j(\mathbf{a}, \boldsymbol{\varepsilon}_{nst})}{\alpha_j} \quad , \quad \overline{E}_j = \frac{f_j(\mathbf{a}, \boldsymbol{\varepsilon}_{nst})}{\alpha_{j+nstr}} \quad (13.29)$$

The tangent stiffness terms are calculated with a forward-difference approach in which the j -th component is disturbed with a small magnitude h according to,

$$\begin{aligned} \frac{\partial f_i}{\partial \varepsilon_j} &= \frac{f_i(\mathbf{a}, \boldsymbol{\varepsilon}_{nst} + h\mathbf{e}_j) - f_i(\mathbf{a}, \boldsymbol{\varepsilon}_{nst})}{h} \\ \frac{\partial f_i}{\partial \alpha_j} &= \frac{f_i(\mathbf{a} + h\mathbf{a}_j, \boldsymbol{\varepsilon}_{nst}) - f_i(\mathbf{a}, \boldsymbol{\varepsilon}_{nst})}{h} \end{aligned} \quad (13.30)$$

The components of the vector \mathbf{e}_j are equal to zero except for the j -th component. This holds true also for the vector \mathbf{a}_j . The step length h for the forward difference approximation is taken equal to $\text{tol} \cdot \varepsilon_j$, respectively $\text{tol} \cdot \alpha_j$. tol is the square-root of the machine precision, which is assumed equal to 1×10^{-16} .

The diagonal stiffness terms of the stiffness matrix \mathbf{D}_{nst} given in (13.27) are elucidated by writing the stiffness terms as,

$$\begin{aligned} \frac{\partial \sigma_i}{\partial \varepsilon_i} &= \\ &= \{m_i r_i + (1 - m_i) r_{i+nstr}\} \overline{E}_i + g_i \left\{ (1 - r_i) \frac{\partial f_i}{\partial \alpha_i} + (1 - r_{i+nstr}) \frac{\partial f_i}{\partial \alpha_{i+nstr}} \right\} \end{aligned} \quad (13.31)$$

If a tensile strain state is active, i.e., $m_i = 1$ and $r_{i+nstr} = 1$, the stiffness term further reduces to,

$$\frac{\partial \sigma_i}{\partial \varepsilon_i} = r_i \overline{E}_i + g_i (1 - r_i) \frac{\partial f_i}{\partial \alpha_i} \quad (13.32)$$

In a more convenient format, we obtain,

$$\frac{\partial \sigma_i}{\partial \varepsilon_i} = \begin{cases} \overline{E}_i & \text{if unloading, } (r_i = 1, g_i \leq 1) \\ \frac{\partial f_i}{\partial \alpha_i} & \text{if loading, } (r_i = 0, g_i = 1) \end{cases} \quad (13.33)$$

In a compressive strain state, i.e., $m_i = 0$ and $r_i = 1$, the stiffness term reduces to,

$$\frac{\partial \sigma_i}{\partial \varepsilon_i} = r_{i+nstr} \overline{E}_i + g_i (1 - r_{i+nstr}) \frac{\partial f_i}{\partial \alpha_{i+nstr}} \quad (13.34)$$

This results in,

$$\frac{\partial \sigma_i}{\partial \varepsilon_i} = \begin{cases} \overline{E}_i & \text{if unloading, } (r_{i+nstr} = 1, g_i \leq 1) \\ \frac{\partial f_i}{\partial \alpha_{i+nstr}} & \text{if loading, } (r_{i+nstr} = 0, g_i = 1) \end{cases} \quad (13.35)$$

13-5-2 Secant Stiffness Matrix

The secant approach is used according to the stiffness of an orthotropic material with zero Poisson's ratio in all directions. This results in the secant stiffness matrix in the principal coordinate system.

$$\mathbf{D}_{\text{secant}} = \begin{bmatrix} \overline{E}_1 & 0 & 0 & 0 & 0 & 0 \\ & \overline{E}_2 & 0 & 0 & 0 & 0 \\ & & \overline{E}_3 & 0 & 0 & 0 \\ & & & \overline{G}_{12} & 0 & 0 \\ \text{sym.} & & & & \overline{G}_{23} & 0 \\ & & & & & \overline{G}_{31} \end{bmatrix} \quad (13.36)$$

13-6 Compression Models

Concrete subjected to compressive stresses shows a pressure-dependent behavior, i.e., the strength and ductility increase with increasing isotropic stress. Due to the lateral confinement, the compressive stress–strain relationship is modified to incorporate the effects of the increased isotropic stress. Furthermore, it is assumed that the compressive behavior is influenced by lateral cracking. To model the lateral confinement effect, the parameters of the compressive stress–strain function, f_{cf} and $\epsilon_{p,cr}$, are determined with a failure function. The failure function gives the compressive stress, which causes failure as a function of the confining stresses in the lateral directions.

If the material is cracked in the lateral direction, the parameters are reduced with the factor $\beta_{\epsilon_{cr}}$ for the peak strain, and with the factor $\beta_{\sigma_{cr}}$ for the peak stress. A possible relationship is given in section 13.9.3. It is tacitly assumed that the base curve in compression is determined by the peak stress value $f_p = \beta_{\sigma_{cr}} \cdot f_{cf}$ and the corresponding peak strain value $\alpha_p = \beta_{\epsilon_{cr}} \cdot \epsilon_p$. The effect of these coefficients will be explained in detail in section 13.9. In summary,

$$f_p = \beta_{\sigma_{cr}} \cdot f_{cf} \qquad \alpha_p = \beta_{\epsilon_{cr}} \cdot \epsilon_p \qquad (13.37)$$

The base function in compression, with the parameters f_p and α_p , is modeled with a number of different predefined and user-defined curves. The predefined curves are the constant curve and the brittle curve, and the linear and exponential softening curves based on the compressive fracture energy, G_c . The linear hardening and the saturation hardening curves are available. Figure 13.4 shows the available hardening-softening curves in compression. Hardening-softening lines, which are available to express compression, are divided into the parabolic, parabolic exponential and hardening curve suggested by Thorenfeldt et. al.⁴.

⁴ Thorenfeldt, E., Tomaszewicz, A., and Jensen, J. J., *Mechanical properties of high-strength concrete and applications in design*, In Proc. Symp. Utilization of High-Strength Concrete (Stavanger, Norway) (Trondheim, 1987), Tapir.

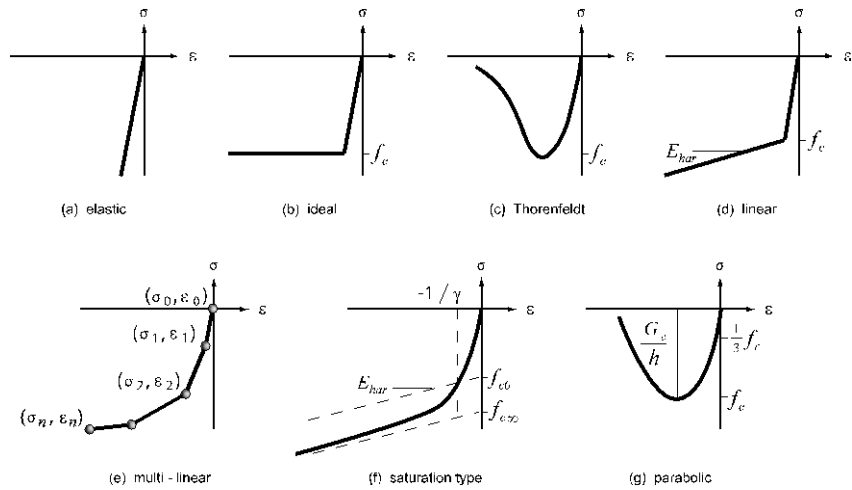


Figure 13-(4) Compression Models

13-6-1 Elastic Model

Young's modulus is used for a general elastic model. There is no additional input (see Fig. 13-4a).

13-6-2 Ideal Model

The ideal model is that when a tensile stress exceeds the tensile strength, the stress does not increase any more (See 13-(4b)).

The compressive strength is defined as, $f_c > 0.0$

13-6-3 Thorenfeldt Model

The Thorenfeldt model uses the value of compressive strength as, $f_c > 0.0$ (see Fig. 13-(4c)).

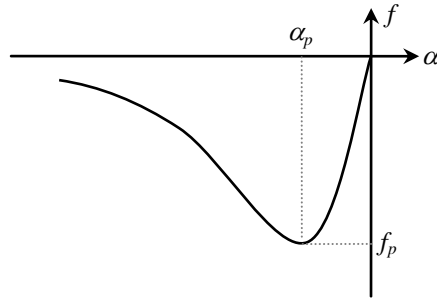


Figure 13-(5) Thorenfeldt compression curve

The equation of the Thorenfeldt curved line is expressed by,

$$f = -f_p \frac{\alpha_i}{\alpha_p} \left(\frac{n}{n-1 + \left(\frac{\alpha_i}{\alpha_p} \right)^{nk}} \right) \quad (13.38)$$

$$\text{where, } n = 0.80 + \frac{f_{cc}}{17}, \quad k = \begin{cases} 1 & \text{if } 0 > \alpha > \alpha_p \\ 0.67 + \frac{f_{cc}}{62} & \text{if } \alpha \leq \alpha_p \end{cases}$$

13-6-4 Linear Hardening Model

The linear hardening model is that after yielding at the compressive yielding point f_c , the compressive behavior depends on the reduced stiffness E_{har} , which changes linearly (See Fig. 13-4d).

Use $f_c > 0.0$, $E_{har} > 0.0$ for input

13-6-5 Multi-Linear Hardening Model

The user can define a stress curve by assigning a certain stress-strain function. The user can input 30 points maximum; the first point should be 0.d0 (see Fig. 13-4e).

[for the condition $< 0.d0$, strain will be monotonically increased.]

13-6-6 Saturation Model

The Saturation Model uses the following material properties as a set of input variables (see Fig. 13-4f).

Initial compressive strength: $f_{co} > 0.0$

Ultimate compressive strength: $f_{c\infty} > 0.0$

Constant hardening modulus: $E_{har} > 0.0$

Decaying factor: $\gamma > 0.0$

13-6-7 Parabolic Model

The Parabolic Model suggested by Feenstra⁵ is derived on the basis of the fracture energy. This curved line is presented by the following three characteristic variables (see Fig. 13-4g).

Compressive strength: $f_c > 0.0$

Compressive fracture energy: $G_c > 0.0$

Characteristic element length: $h > 0.0$

5 FEENSTRA, P. H., *Computational Aspects of Biaxial Stress in Plain and Reinforced Concrete*, PhD thesis, Delft University of Technology, 1993.

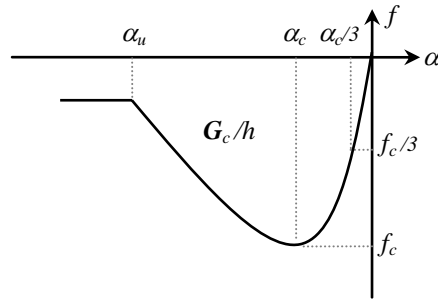


Figure 13-(6) Parabolic compression curve

The strain $\alpha_{c/3}$, at which one-third of the maximum compressive strength f_c is reached, is

$$\alpha_{c/3} = \frac{1}{3} \frac{f_c}{E} \quad (13.39)$$

The strain α_c , at which the maximum compressive strength is reached, is

$$\alpha_c = -\frac{4}{3} \frac{f_c}{E} = 4\alpha_{c/3} \quad (13.40)$$

Note that $\alpha_{c/3}$ and α_c are determined irrespective of the element size or compressive fracture energy. Finally, the ultimate strain α_u , at which the material is completely softened in compression, is

$$\alpha_u = \alpha_c - \frac{3}{2} \frac{G_c}{h f_c} \quad (13.41)$$

Based on the above variables, the following curved line is defined:

$$f = \begin{cases} -f_c \frac{1}{3} \frac{\alpha_j}{\alpha_{c/3}} & \text{if } 0 \leq \alpha_j < \alpha_{c/3} \\ -f_c \frac{1}{3} \left(1 + 4 \left(\frac{\alpha_j - \alpha_{c/3}}{\alpha_c - \alpha_{c/3}} \right) - 2 \left(\frac{\alpha_j - \alpha_{c/3}}{\alpha_c - \alpha_{c/3}} \right)^2 \right) & \text{if } \alpha_{c/3} \leq \alpha_j < \alpha_c \\ -f_c \left(1 - \left(\frac{\alpha_j - \alpha_c}{\alpha_u - \alpha_c} \right)^2 \right) & \text{if } \alpha_c \leq \alpha_j < \alpha_u \\ 0 & \text{if } \alpha_u \leq \alpha_j \end{cases} \quad (13.42)$$

It could now easily be verified that the fracture energy G_c and the characteristic element length h govern the softening part of the curve only:

$$\int_{\alpha_c}^{\alpha_u} f \, d\alpha_j = f_c \left(\alpha_j - \frac{1}{3} \left(\frac{\alpha_j - \alpha_c}{\alpha_u - \alpha_c} \right)^3 \right) \bigg|_{\alpha_c}^{\alpha_u} = \frac{G_c}{h} \quad (13.43)$$

13-7 Tension Models

13-7-1 Background Theory about Tension Softening Relations

The relationship between the crack stress σ_{nn}^{cr} and the crack strain ε_{nn}^{cr} in the normal direction can be written as a multiplicative relation.

$$\sigma_{nn}^{cr}(\varepsilon_{nn}^{cr}) = f_t \cdot y\left(\frac{\varepsilon_{nn}^{cr}}{\varepsilon_{nn,ult}^{cr}}\right) \quad (13.44)$$

f_t is the tensile strength, and $\varepsilon_{nn,ult}^{cr}$ is the ultimate crack strain. The general function $y(\cdot)$ represents the actual softening diagram.

If the softening behavior on the constitutive level is related to the Mode-I fracture energy G_f^I through an equivalent length or crack bandwidth denoted as h , the following relation can be derived:

$$G_f^I = h \int_{\varepsilon_{nn}^{cr}=0}^{\varepsilon_{nn}^{cr}=\infty} \sigma_{nn}^{cr}(\varepsilon_{nn}^{cr}) d\varepsilon_{nn}^{cr} \quad (13.45)$$

Substituting Eq. (13.44) into Eq. (13.45) results in,

$$G_f^I = h f_t \int_{\varepsilon_{nn}^{cr}=0}^{\varepsilon_{nn}^{cr}=\infty} y\left(\frac{\varepsilon_{nn}^{cr}}{\varepsilon_{nn,ult}^{cr}}\right) d\varepsilon_{nn}^{cr} \quad (13.46)$$

with the assumption that f_t is a constant. Changing from the variable ε_{nn}^{cr} to

$$x = \frac{\varepsilon_{nn}^{cr}}{\varepsilon_{nn,ult}^{cr}} \quad (13.47)$$

and consequently $\varepsilon_{nn}^{cr} = \varepsilon_{nn,ult}^{cr} dx$ results in the relation,

$$G_f^I = h f_t \left(\int_{x=0}^{x=\infty} y(x) dx \right) \varepsilon_{nn,ult}^{cr} \quad (13.48)$$

It is tacitly assumed that the ultimate crack strain $\varepsilon_{m,ult}^{cr}$ is finite. The final expression for the ultimate crack strain is now given by,

$$\varepsilon_{m,ult}^{cr} = \frac{1}{\alpha} \cdot \frac{G_f^I}{h f_t} \quad (13.49)$$

The factor α is determined by the integral,

$$\alpha = \int_{x=0}^{x=\infty} y(x) dx \quad (13.50)$$

The factor $\varepsilon_{m,ult}^{cr}$ is assumed to be constant during the analysis and is considered to be an element-related material property, which can be calculated from the material properties, the tensile strength f_t , the fracture energy G_f^I and the element area represented by the equivalent length h .

A snap-back in the constitutive model is possible if the absolute value of the initial slope of the softening diagram is greater than the Young's modulus of the material, and if it is assumed that the initial tangent of the tension softening diagram results in the greatest value of the tangent stiffness. The condition, which has to be fulfilled then is noted as,

$$\left. \frac{d\sigma_m^{cr}}{d\varepsilon_m^{cr}} \right|_{\varepsilon_m^{cr}=0} \geq -E \quad (13.51)$$

This can be expressed as,

$$\left. \frac{f_t}{\varepsilon_{m,ult}^{cr}} \frac{dy}{dx} \right|_{x=0} \geq -E \quad (13.52)$$

This results in an expression for the ultimate crack strain, which is noted as,

$$\varepsilon_{m,ult}^{cr} \geq -\frac{f_t}{E} \frac{dy}{dx} \bigg|_{x=0} = \varepsilon_{m,ult}^{cr, \min} \quad (13.53)$$

with $\varepsilon_{m,ult}^{cr}$ determined by Eq. (13.49). If the condition given in (13.53) is violated, there are

various possibilities to solve this problem. Firstly, it is possible to decrease the equivalent length h , but this property is an element property and consequently a fixed value. Secondly, it is possible to increase the fracture energy G_f^I since this will result in an increase in the ductility of the material. The final possibility is to decrease the tensile strength f_t , which implicitly results in an increase in the ductility since the fracture energy remains constant in this case.

The most obvious choice is to reduce the tensile strength because this has some physical meaning. The probability of reduced strength is higher if the sampling area is larger. This implies that the tensile strength should be reduced in larger elements since stress concentrations are not captured with these elements. So, if the condition of (13.53) is violated, the tensile strength should be reduced to,

$$f_{t,red}^2 = - \frac{G_f^I E}{\alpha h \frac{dy}{dx} \Big|_{x=0}} \quad (13.54)$$

Alternatively, the element size could be reduced such that the crack bandwidth h , is equal to a maximum of

$$h_{max} = - \frac{G_f^I E}{\alpha f_t^2 \frac{dy}{dx} \Big|_{x=0}} \quad (13.55)$$

13-7-2 Tension Models in Total Strain Crack Model

The tensile behavior model defined by the total strain crack model has elastic, ideal, brittle, linear, exponential, hordijk, multi-linear and user-defined behaviors. These models can be divided on the basis of the different theories as follows:

The total strain crack model materializes the softening function based on the fracture energy. The models based on the softening function are: linear softening curve, exponential softening curve, and nonlinear softening curve suggested by Hordijk⁶. In case of a smeared crack model, these models have a relation with crack bandwidth. Next, there is a tensile behavior, which has no direct effect on the fracture energy. This behavior can be depicted in the concept of total strain. The models belonging to this group are defined as, the ideal (Constant tensile), multi-linear and brittle behaviors. Finally, MIDAS allows the user to use the user-defined subroutine, USRCRV, to assign a tensile behavior.

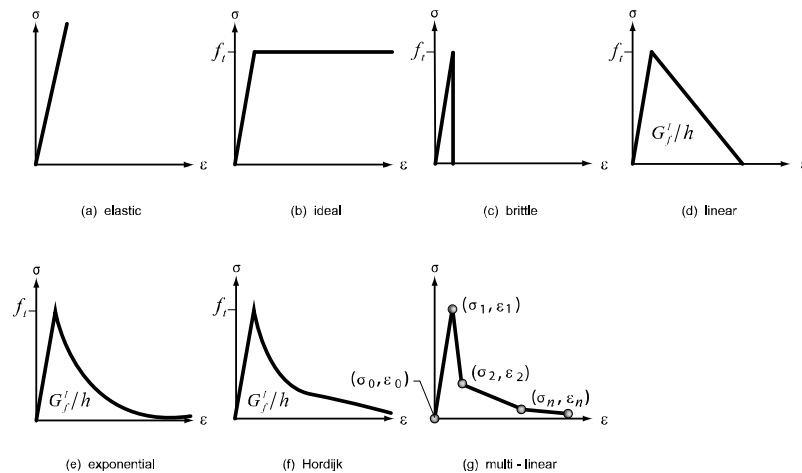


Figure 13-7) Tension Models

⁶ Hordijk, D. A., *Local approach to fatigue of concrete*, PhD thesis, Delft University of Technology, 1991.

(1) Elastic Model

The elastic model generally uses Young's modulus. There is no additional input (see Fig. 13-7a).

(2) Ideal Model

The ideal model is that when tensile stress exceeds the tensile strength, the stress remains unchanged (See 13-(7b)). In this case, the tensile strength is assigned by $f_t > 0.0$.

(3) Brittle Model

Brittle behavior is characterized by the full reduction of the strength after the strength criterion has been violated (Fig. 13-8). This model involves a discontinuity. Before the peak, there is only elastic strain. Beyond the peak, the stress drops to zero immediately; the elastic strain vanishes; and, we have only crack strain. The sudden stress drop, indicated by the dashed line in Fig. 13-8, in fact involves energy dissipation, which is related to the peak strain ε_{nn}^{peak} and the crack band width. In this case, the tensile strength is assigned by $f_t > 0.0$.

$$G_f = \frac{1}{2} f_t \varepsilon_{nn}^{peak} h \quad (13.56)$$

where, ε_{nn}^{peak} is a fixed value equal to f_t/E .

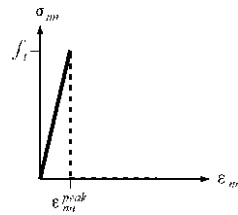


Figure 13-8) Brittle cracking behavior

(4) Linear Softening Model

The linear softening model is observed when tensile stress exceeds tensile strength (See Fig. 13-9).

Tensile fracture energy: $G_f^I > 0.0$

Crack band width: $h > 0.0$

Use the following values as input

Tensile strength: $f_t > 0.0$

Tensile fracture energy: $G_f^I > 0.0$

Crack band width: $h > 0.0$

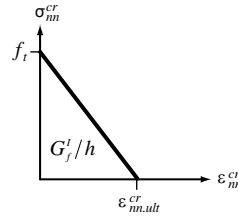


Figure 13-9) Linear tension softening

The relation of the crack stress is given by,

$$\frac{\sigma_{nn}^{cr}(\epsilon_{nn}^{cr})}{f_t} = \begin{cases} 1 - \frac{\epsilon_{nn}^{cr}}{\epsilon_{nn,ult}^{cr}} & \left(\text{if } 0 < \epsilon_{nn}^{cr} < \epsilon_{nn,ult}^{cr} \right) \\ 0 & \left(\text{if } \epsilon_{nn,ult}^{cr} < \epsilon_{nn}^{cr} < \infty \right) \end{cases} \quad (13.57)$$

The factor α for the ultimate crack strain is given by,

$$\alpha = \int_0^\infty y(x)dx = \int_0^1 y(x)dx + \int_0^\infty 0dx = \int_0^1 (1-x)dx = \frac{1}{2} \quad (13.58)$$

This results in an ultimate crack strain.

$$\varepsilon_{nn,ult}^{cr} = 2 \frac{G_f^I}{h f_t} \quad (13.59)$$

It is easily verified that

$$\left. \frac{dy}{dx} \right|_{x=0} = -1 \quad (13.60)$$

The minimum value of the ultimate crack strain becomes,

$$\varepsilon_{nn,ult,min}^{cr} = \frac{f_t}{E} \quad (13.61)$$

The reduced tensile strength is written as,

$$f_t = \sqrt{2 \frac{G_f^I E}{h}} \quad (13.62)$$

(5) Exponential Softening Model

The exponential softening model is that exponential softening occurs when tensile stress exceeds the tensile strength (See Fig. 13-7e). The slope of softening is determined on the basis of the fracture energy, G_f^I and crack band width, h .

Use the following values as input:

Tensile strength: $f_t > 0.0$

Tensile fracture energy: $G_f^I > 0.0$

Crack band width: $h > 0.0$

(6) Hordijk Model

Hordijk⁷, Cornelissen & Reinhardt⁸ proposed an expression for the softening behavior of concrete, which also results in a crack stress equal to zero at a crack strain $\varepsilon_{m,ult}^{cr}$ (Fig. 13-10).

Use the following values as input:

Tensile strength: $f_t > 0.0$

Tensile fracture energy: $G_f' > 0.0$

Crack band width: $h > 0.0$

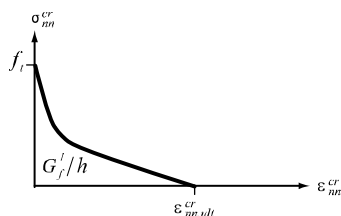


Figure 13-10) Non-linear tension softening (Hordijk et al.)

The function is defined by,

7 HORDIJK, D. A. Local Approach to Fatigue of Concrete. PhD thesis, Delft University of Technology, 1991.

8 CORNELISSEN, H. A. W., HORDIJK, D. A., AND REINHARDT, H. W.

Experimental determination of crack softening characteristics of normal weight and lightweight concrete.

Heron 31, 2 (1986).

$$\frac{\sigma_{nn}^{cr}(\varepsilon_{nn}^{cr})}{f_t} = \left\{ \begin{array}{ll} \left(1 + \left(c_1 \frac{\varepsilon_{nn}^{cr}}{\varepsilon_{nn,ult}^{cr}} \right)^3 \right) \exp \left(-c_2 \frac{\varepsilon_{nn}^{cr}}{\varepsilon_{nn,ult}^{cr}} \right) \dots & \\ - \frac{\varepsilon_{nn}^{cr}}{\varepsilon_{nn,ult}^{cr}} (1 + c_1^3) \exp(-c_2) & \left(\text{if } 0 < \varepsilon_{nn}^{cr} < \varepsilon_{nn,ult}^{cr} \right) \\ 0 & \left(\text{if } \varepsilon_{nn,ult}^{cr} < \varepsilon_{nn}^{cr} < 0 \right) \end{array} \right\} \quad (13.63)$$

The parameters are $c_1 = 3$ and $c_2 = 6.93$. The parameter α for the ultimate crack strain is given by,

$$\begin{aligned} \alpha &= \int_0^\infty y(x) dx = \int_0^1 y(x) dx + \int_1^\infty 0 dx \\ &= \int_0^1 (1 + (c_1 x)^3) \exp(-c_2 x) - x(1 + c_1^3) \exp(-c_2) dx \\ &= \frac{-12c_1^3 - 12c_1^3 c_2 - 6c_1^3 c_2^2 - 2c_2^3 - 2c_1^3 c_2^3}{\dots} \dots \dots \quad (13.64) \\ &\dots \frac{-c_2^4 - c_1^3 c_2^4 + 12c_1^3 \exp(c_2) + 2c_2^3 \exp(c_2)}{\dots 2c_2^4 \exp(c_2)} \end{aligned}$$

This results in $\alpha = 0.195$ for the parameters $c_1 = 3$, and $c_2 = 6.93$. The ultimate crack strain then is written as,

$$\varepsilon_{nn,ult}^{cr} = 5.136 \frac{G_f^I}{h f_t} \quad (13.65)$$

For the softening diagram of Hordijk et al., the following relation can be derived:

$$\begin{aligned} \left. \frac{dy}{dx} \right|_{x=0} &= \left(3c_1(c_1 x)^2 - c_2(1 + (c_1 x)^3) \right) \exp(-c_2 x) - (1 + c_1^3) \exp(-c_2) \Big|_{x=0} \quad (13.66) \\ &= -c_2 - (1 + c_1^3) \exp(-c_2) \end{aligned}$$

The minimum value of the ultimate crack strain is then given by,

$$\varepsilon_{nn,ult,min}^{cr} = 6.957 \frac{f_t}{E} \quad (13.67)$$

and the reduced tensile strength is written as,

$$f_t = \left(0.739 \frac{G_f' E}{h} \right)^{\frac{1}{2}} \quad (13.68)$$

(7) Multi-linear Model

The multi-linear model is that softening occurs when tensile stress exceeds the tensile strength (See Fig. 13-7g). At most 30 nodes can be defined as input, and the first node should be $0.d0$.

[for the condition $> 0.d0$, strain will be monotonically increased.]

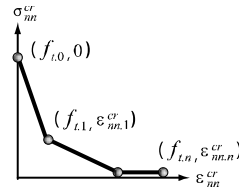


Figure 13-11) Multilinear tension softening

The following condition should be satisfied for the initial tangential slope:

$$\frac{f_{t,1} - f_{t,0}}{\varepsilon_{nn,1}^{cr}} \geq -E \quad (13.69)$$

13-8 Shear Models

The modeling of the shear behavior is only necessary in the fixed crack concept where the shear stiffness is usually reduced after cracking. For the current implementation in MIDAS, only a constant shear stiffness reduction is modeled, i.e.,

$$G^{cr} = \beta G \quad (13.70)$$

where, β the shear retention factor, $0 \leq \beta \leq 1$. For the rotating crack concept, the shear retention factor can be assumed equal to one.

13-9 Lateral Influence

13-9-1 Lateral Expansion effects due to Poisson's Ratio

The Poisson effect on a material determines the lateral displacement of a specimen subjected to a uniaxial tensile or compressive loading. If these displacements are constrained, a passive lateral confinement will act on the specimen. This effect is considered important in a three-dimensional modeling of reinforced concrete structures. In the work of Selby & Vecchio⁹ this effect is modeled through a pre-strain concept in which the lateral expansion effects are accounted for with an additional external loading on the structure. This implies that the computational flow of the finite element engine is adapted to this method. The Poisson effect is taken into account via the equivalent uniaxial strain concept. In case of linear-elastic behavior, the constitutive relationship in a three-dimensional stress-strain situation is given by,

$$\boldsymbol{\sigma}_{nst} = \frac{E}{(1+\nu)(1-2\nu)} \begin{bmatrix} 1-\nu & \nu & \nu \\ \nu & 1-\nu & \nu \\ \nu & \nu & 1-\nu \end{bmatrix} \boldsymbol{\epsilon}_{nst} \quad (13.71)$$

which can be expressed as,

$$\boldsymbol{\sigma}_{nst} = \begin{bmatrix} E & 0 & 0 \\ 0 & E & 0 \\ 0 & 0 & E \end{bmatrix} \cdot \begin{bmatrix} \frac{1-\nu}{(1+\nu)(1-2\nu)} & \frac{\nu}{(1+\nu)(1-2\nu)} & \frac{\nu}{(1+\nu)(1-2\nu)} \\ \frac{\nu}{(1+\nu)(1-2\nu)} & \frac{1-\nu}{(1+\nu)(1-2\nu)} & \frac{\nu}{(1+\nu)(1-2\nu)} \\ \frac{\nu}{(1+\nu)(1-2\nu)} & \frac{\nu}{(1+\nu)(1-2\nu)} & \frac{1-\nu}{(1+\nu)(1-2\nu)} \end{bmatrix} \boldsymbol{\epsilon}_{nst} \quad (13.72)$$

⁹ Selby, R. G., and Vecchio, F. J., *Three-dimensional Constitutive Relations for Reinforced Concrete*, Tech. Rep. 93-02, Univ. Toronto, dept.Civil Eng., Toronto, Canada, 1993.

This relationship is now expressed in terms of equivalent uniaxial strains as,

$$\boldsymbol{\sigma}_{nst} = \begin{bmatrix} E & 0 & 0 \\ 0 & E & 0 \\ 0 & 0 & E \end{bmatrix} \tilde{\boldsymbol{\epsilon}}_{nst} \quad (13.73)$$

The equivalent uniaxial strain vector $\tilde{\boldsymbol{\epsilon}}_{nst}$ is defined by

$$\tilde{\boldsymbol{\epsilon}}_{nst} = \begin{Bmatrix} \tilde{\epsilon}_1 \\ \tilde{\epsilon}_2 \\ \tilde{\epsilon}_3 \end{Bmatrix} = \begin{bmatrix} \frac{1-\nu}{(1+\nu)(1-2\nu)} & \frac{\nu}{(1+\nu)(1-2\nu)} & \frac{\nu}{(1+\nu)(1-2\nu)} \\ \frac{\nu}{(1+\nu)(1-2\nu)} & \frac{1-\nu}{(1+\nu)(1-2\nu)} & \frac{\nu}{(1+\nu)(1-2\nu)} \\ \frac{\nu}{(1+\nu)(1-2\nu)} & \frac{\nu}{(1+\nu)(1-2\nu)} & \frac{1-\nu}{(1+\nu)(1-2\nu)} \end{bmatrix} \begin{Bmatrix} \epsilon_1 \\ \epsilon_2 \\ \epsilon_3 \end{Bmatrix} \quad (13.74)$$

$$\tilde{\boldsymbol{\epsilon}}_{nst} = \mathbf{P} \boldsymbol{\epsilon}_{nst} \quad (13.75)$$

This concept can be performed for a nonlinear material model. The stress vector in the principal coordinate system, (13.17), is evaluated in terms of the equivalent uniaxial strain vector, $\tilde{\boldsymbol{\epsilon}}_{123}$, and not in terms of the principal strain vector, $\boldsymbol{\epsilon}_{nst}$. The equivalent uniaxial strain vector is simply determined when the principal strain vector and the (constant) Poisson's ratio are known. The tangent stiffness sub-matrix \mathbf{D}_{nst} is slightly modified due to the equivalent uniaxial strain concept. The matrix is given by,

$$\mathbf{D}_{nst} = \frac{\partial \boldsymbol{\sigma}_{nst}}{\partial \boldsymbol{\epsilon}_{nst}} = \frac{\partial \boldsymbol{\sigma}_{nst}}{\partial \tilde{\boldsymbol{\epsilon}}_{nst}} \mathbf{P} \quad (13.76)$$

where, the matrix $\partial \boldsymbol{\sigma}_{nst} / \partial \tilde{\boldsymbol{\epsilon}}_{nst}$ is given by (13.26) with $\tilde{\boldsymbol{\epsilon}}_{nst}$ substituted for $\boldsymbol{\epsilon}_{nst}$.

13-9-2 Compressive Behavior with Lateral Confinement

The increase in the strength with increasing isotropic stress is modeled with the four-parameter Hsieh-Ting-Chen failure surface, which is defined as,

$$f = 2.0108 \frac{J_2}{f_{cc}^2} + 0.9714 \frac{\sqrt{J_2}}{f_{cc}} + 9.1412 \frac{f_{c1}}{f_{cc}} + 0.2312 \frac{I_1}{f_{cc}} - 1 = 0 \quad (13.77)$$

with the invariants I_1 and J_2 and defined in terms of the stress in the concrete σ_{ci} according to

$$I_1 = \sigma_{c1} + \sigma_{c2} + \sigma_{c3} \quad (13.78)$$

$$J_2 = \frac{1}{6} \left\{ (\sigma_{c1} - \sigma_{c2})^2 + (\sigma_{c2} - \sigma_{c3})^2 + (\sigma_{c3} - \sigma_{c1})^2 \right\} \quad (13.79)$$

and the maximum principle stress¹⁰ f_{c1} .

$$f_{c1} = \max(\sigma_{c1}, \sigma_{c2}, \sigma_{c3}) \quad (13.80)$$

This is not the maximum *tensile stress* but the maximum *principal stress*. The parameters in Eq. (13.77) are determined by fitting of the uniaxial tensile and compressive strength, the biaxial compressive strength and experimental data of triaxial tests on concrete specimen. The stress f_{c3} is assumed to result in failure and is determined by scaling the linear elastic stress vector $\sigma_c = s \cdot E \cdot \epsilon_{nst}$ such that Eq. (13.77) holds true. The compressive failure stress in multi-axial stress situation is then given by,

$$f_{c3} = s \cdot \min(\sigma_{c1}, \sigma_{c2}, \sigma_{c3}) \quad (13.81)$$

If the scaling factor s is negative, thus resulting in a positive failure stress f_{c3} , the stress vector is

¹⁰ Braa, H. Private communication, 1997.

scaled to the tensile side of the failure surface, and the failure strength is set equal to a large negative value ($-30f_{cc}$). The failure strength f_{cf} is given by,

$$f_{cf} = -f_{c3} \quad (13.82)$$

The peak stress factor K_σ is given by Selby¹¹,

$$K_\sigma = \frac{f_{cf}}{f_{cc}} \geq 1 \quad (13.83)$$

and the peak strain factor is assumed to be given by,

$$K_\epsilon = K_\sigma \quad (13.84)$$

In unconfined compression, the values at the peak are given by the values of uniaxial compressive strength, and the peak stress factor is equal to one. The parameters of the compressive stress-strain function now become,

$$f_{cf} = K_\sigma f_{cc}, \quad \epsilon_p = K_\sigma \epsilon_0 \quad (13.85)$$

The value of the initial strain ϵ_0 is given by the relationship,

$$\epsilon_0 = -\frac{n}{n-1} \cdot \frac{f_{cc}}{E_c} \quad (13.86)$$

The equations given above result in a gradual increase in the maximum strength in confined compression, with an initial slope of the stress-strain diagram given by the Young's modulus. In a full triaxial stress situation, the failure surface cannot be reached and a linear stress-strain relation is obtained (see Fig. 13-12).

11 Selby, R. G., and Vecchio, F. J., *Three-dimensional Constitutive Relations for Reinforced Concrete*, Tech. Rep. 93-02, Univ. Toronto, dept. Civil Eng., Toronto, Canada, 1993.

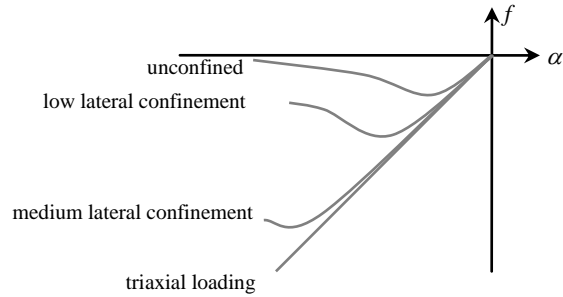


Figure 13-(12) Influence of lateral confinement on compressive stress-strain curve

The increased ductility of confined concrete is modeled by a linear adoption of the descending branch of the Thorenfeldt curve according to,

$$f_j = -f_p \left(1 - (1-r) \frac{\alpha_j - \alpha_p}{\alpha_u - \alpha_p} \right) \leq -r f_p \quad (13.87)$$

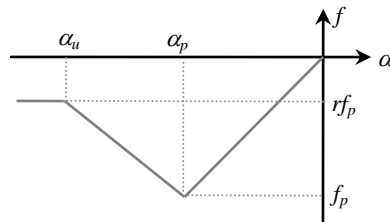


Figure 13-(13) Compressive behavior under lateral confinement

r is the factor, which models the residual strength of the material (see Fig. 13.13). The ultimate strain in compression is assumed to be determined by the ratio between the peak strength and the compression strength and the strain at the peak according to,

$$\alpha_u = \left(\frac{f_p}{f_{cc}} \right)^\gamma \alpha_p \quad (13.88)$$

The scalar \square needs to be determined; currently $\square = 3$ is assumed. The residual strength $r f_p$ also depends on the ratio between the peak strength and the compressive strength according to,

$$r = \left(\frac{f_p}{f_{cc}} \right)^\gamma r_0 \quad (13.89)$$

r_0 is an initial value. Assume $r_0 = 0.1$.

The linear compression–softening relationship is only applied to the Thorenfeldt curve if the peak value f_p is considerably larger than the compressive strength f_{cc} . Assume $f_p / f_{cc} > 1.05$. In case lateral compression and lateral cracking result in $f_p / f_{cc} < 1.05$, the ductility of the material will not increase.

13-9-3 Compressive Behavior with Lateral Cracking

In cracked concrete, large tensile strains perpendicular to the principal compressive direction reduce the concrete compressive strength. The compressive strength f_p is consequently not only a function of the internal variable \square_p , but is also a function of the internal variables governing the tensile damage in the lateral directions, $\square_{l,1}$ and $\square_{l,2}$. The reduction factors due to lateral cracking are denoted as $\beta_{ccr} = \beta_{ccr}(\alpha_{lat})$ and $\beta_{\sigma cr} = \beta_{\sigma cr}(\alpha_{lat})$, which are functions of the average lateral damage variable given by $\alpha_{lat} = \sqrt{\alpha_{l,1}^2 + \alpha_{l,2}^2}$.

The relationship for reduction due to lateral cracking is the model according to Vecchio and Collins¹² (see Fig. 13.14).

$$\beta_{\sigma_{cr}} = \frac{1}{1 + K_c} \leq 1 \quad (13.90)$$

$$\text{where, } K_c = 0.27 \left(-\frac{\alpha_{lat}}{\varepsilon_0} - 0.37 \right) \quad \text{and} \quad \beta_{\varepsilon_{cr}} = 1 .$$

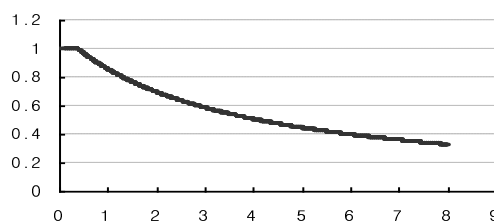


Figure 13-(14) Reduction factor due to lateral cracking

12 Vecchio, F. J., and Collins, M. P., *Compression response of cracked reinforced concrete*, J. Str. Eng., ASCE 119, 12 (1993), 3590–3610.

Chapter 14. Interface Nonlinearity

14-1 Introduction

The modeling of geometric discontinuities such as discrete cracks in concrete, joints in rock and masonry, and bond-slip layers in reinforced concrete is most conveniently done using the multipurpose structural interface elements implemented in MIDAS. These elements relate the forces acting on the interface to the relative displacement of the two sides of the interface as shown in Figure (14-1) for the two-dimensional configuration.

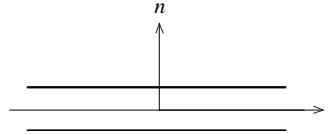


Figure 14-(1) Two-dimensional interface element

Interface elements are dealt with in Chapter 4, and this Chapter covers the nonlinear behaviors of interface elements. In this section, we describe the relations for the two-dimensional configuration, i.e., the line interface elements. In general, the relations are also valid for three-dimensional cases. The traction vector \mathbf{t} is defined for the two-dimensional case as,

$$\mathbf{t} = \begin{Bmatrix} t_n \\ t_t \end{Bmatrix} \quad (14.1)$$

And the vector, which collects the relative displacements, is expressed as,

$$\Delta \mathbf{u} = \begin{Bmatrix} \Delta u_n \\ dt \end{Bmatrix} \quad (14.2)$$

The linear constitutive relation between the traction vector and the relative displacement vector is given by,

$$\begin{Bmatrix} t_n \\ t_t \end{Bmatrix} = \begin{bmatrix} k_n & 0 \\ 0 & k_t \end{bmatrix} \begin{Bmatrix} \Delta u_n \\ dt \end{Bmatrix} \quad (14.3)$$

k_n and k_t are usually assigned large penalty values to model the initial continuous geometry. Application of a Gaussian integration scheme to interface elements can lead to spurious kinematic element performance under certain conditions. See for instance Gens et al.¹, Rots², Hohberg³ and Schellekens⁴. It is therefore recommended to use a lumped integration scheme for interface elements with large dummy stiffnesses. The Newton-Cote scheme has been adopted in MIDAS to overcome to the above problem.

The general constitutive relation is assumed to be incrementally linear.

$$\dot{t} = D \Delta \dot{u} \quad (14.4)$$

t is the traction vector; Δu is the vector with the relative displacements; and D is the tangential stiffness matrix defined as,

$$D = \begin{bmatrix} D_{11} & D_{12} \\ D_{21} & D_{22} \end{bmatrix} \quad (14.5)$$

The stiffness coefficients generally depend on Δu_n , dt , t_n , t_t and possibly on other state parameters. The constitutive relations are discussed in the following sections.

1 Gens, A., Carol, I., and Alonso, E. E. *An interface element formulation for the analysis of soil– reinforcement interaction*. Comp. Geotechnics 7 (1988), 133–151.

2 Rots, J. G. *Computational Modeling of Concrete Fracture*. PhD thesis, Delft University of Technology, 1988.

3 Hohberg, J. M. *A note on the spurious kinematic oscillations in FEM joint elements*. Earthq. Engrg. Struct. Dynamics 19 (1990), 773–779.

4 Schellekens, J. C. J. *Computational Strategies for Composite Structures*. PhD thesis, Delft University of Technology, 1992.

14-2 Discrete cracking

The constitutive law for discrete cracking in MIDAS is based on a total deformation theory, which expresses the tractions as a function of the total relative displacements, the crack width Δu_n and the crack slip dt (Fig. 14-2).

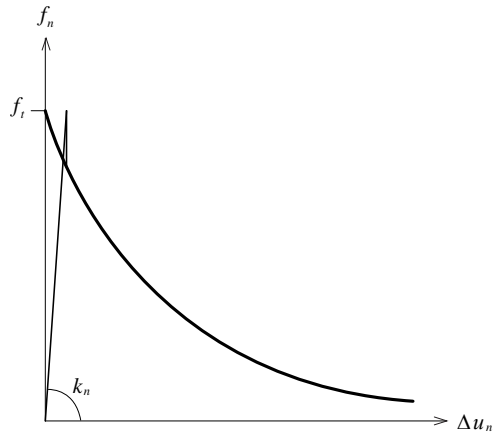


Figure 14-2) Discrete cracking

The relationship between normal traction and crack width and the relationship between shear traction and slip are assumed as nonlinear functions.

$$\begin{cases} t_n = f_n(\Delta u_n) \\ t_r = f_r(dt) \end{cases} \quad (14.6)$$

Differentiating Eq. (14.6) results in expressions for the tangential stiffness coefficients,

$$\begin{cases} D_{11} = \frac{\partial f_n}{\partial \Delta u_n} \\ D_{12} = 0 \\ D_{21} = 0 \\ D_{22} = \frac{\partial f_t}{\partial dt} \end{cases} \quad (14.7)$$

In general, the normal traction t_n is governed by a tension softening relation. For structural interface elements, MIDAS supports the following relations:

- Brittle cracking model
- Linear tension softening model
- Nonlinear tension softening model (Hordijk et al.)

14-2-1 Brittle cracking model

Brittle behavior is characterized by the full reduction of the strength after the strength criterion has been violated (Fig. 14-3).

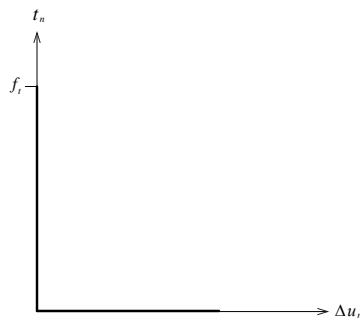


Figure 14-(3) Brittle cracking behavior

This behavior can be written as

$$\frac{f_n(\Delta u_n)}{f_t} = \begin{cases} 1 & \text{if } \Delta u_n \leq 0 \\ 0 & \text{if } 0 < \Delta u_n < \infty \end{cases} \quad (14.8)$$

14-2-1 Linear Tension softening

In case of linear tension softening (Fig. 14-4), the relation of the crack stress is given by,

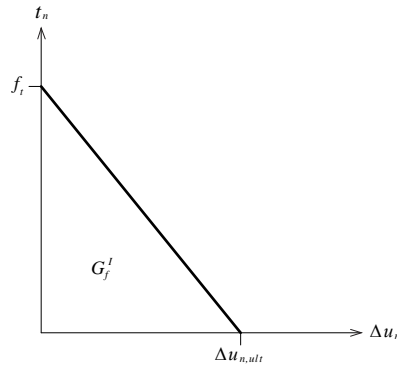


Figure 14-4) Linear tension softening

$$\frac{f_n(\Delta u_n)}{f_t} = \begin{cases} 1 - \frac{\Delta u_n}{\Delta u_{n,ult}} & \text{if } 0 < \Delta u_n < \Delta u_{n,ult} \\ 0 & \text{if } \Delta u_{n,ult} < \Delta u_n < \infty \end{cases} \quad (14.9)$$

with the ultimate crack strain

$$\Delta u_{n,ult} = 2 \frac{G_f'}{f_t} \quad (14.10)$$

Unloading and reloading can be modeled according to a secant approach or an elastic approach.

In the secant approach, the relation between the traction and the relative normal displacement is linear up to the origin, after which the initial stiffness is recovered. In the elastic approach, the initial stiffness is recovered immediately after the relative normal displacement has become less than the current maximum relative normal displacement (Fig. 14-4).

14-2-2 Nonlinear tension softening model (Hordijk et al.)

Hordijk⁵, Cornelissen & Reinhardt⁶ proposed an expression for the softening behavior of concrete, which also results in a crack stress equal to zero at a crack width $\Delta u_{n,ult}$ (Fig. 14-5).

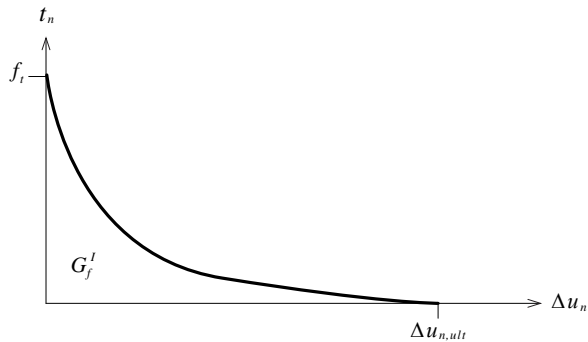


Figure 14-5) Nonlinear tension softening (Hordijk et al.)

The function is defined by,

⁵ Hordijk, D. A. *Local Approach to Fatigue of Concrete*. PhD thesis, Delft University of Technology, 1991.

⁶ Cornelissen, H. A. W., Hordijk, D. A., and Reinhardt, H. W. *Experimental determination of crack softening characteristics of normalweight and lightweight concrete*. Heron 31, 2 (1986).

$$\frac{f_n(\Delta u_n)}{f_t} = \begin{cases} \left(1 + \left(c_1 \frac{\Delta u_n}{\Delta u_{n,ult}}\right)^3\right) \exp\left(-c_2 \frac{\Delta u_n}{\Delta u_{n,ult}}\right) \\ - \frac{\Delta u_n}{\Delta u_{n,ult}} (1 + c_1^3) \exp(-c_2) & \text{if } 0 < \Delta u_n < \Delta u_{n,ult} \\ 0 & \text{if } \Delta u_{n,ult} < \Delta u_n < \infty \end{cases} \quad (14.11)$$

where, the parameters $c_1 = 3$ and $c_2 = 6.93$ with the ultimate crack strain defined by,

$$\Delta u_{n,ult} = 5.136 \frac{G_f^I}{f_t} \quad (14.12)$$

Unloading and reloading can be modeled according to a secant approach, an elastic approach or by application of hysteresis. In the secant approach, the relation between the traction and the relative normal displacement is linear up to the origin, after which the initial stiffness is recovered. In the elastic approach, the initial stiffness is recovered immediately after the relative normal displacement has become less than the current maximum relative normal displacement (Fig. 14-5). The third possibility is to apply the hysteresis model of Hordijk^{5,7} in which unloading and reloading follow different paths (Fig. 14-6).

7 Janssen, J. G. *Mode-I Fracture of Plain Concrete Under Monotonic and Cyclic Loading*. Tech. Rep. BI-90-110, TNO Building and Construction Research, Rijswijk, The Netherlands, 1990.

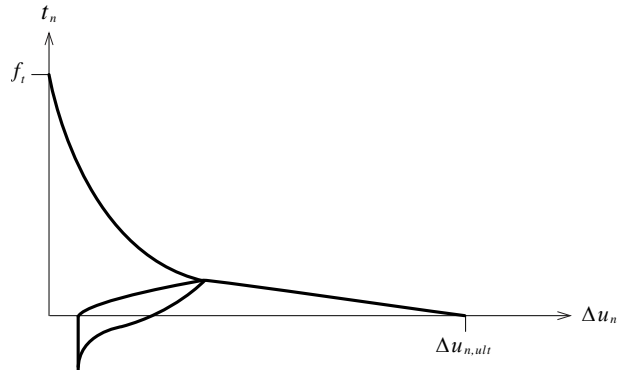


Figure 14-(6) Hysteresis model (Hordijk)

14-2-3 Shear Retention

In general, the shear traction t_i is reduced after cracking according to

$$f_t = \begin{cases} k_i dt & \text{if } \Delta u_n < \frac{f_t}{k_n} \\ \beta k_i dt & \text{if } \Delta u_n \geq \frac{f_t}{k_n} \end{cases} \quad (14.13)$$

where, βk_i is the reduced shear stiffness while $0 \leq \beta \leq 1$.

In general, β may vary between 0.1 to 0.3. If the crack surface is assumed to be smooth, i.e. crack Mode-I, β is defined as zero. But generally, it is assumed that the crack surface is not smooth and hence $0 < \beta \leq 1$.

14-3 Crack Dilatancy

A crack can be considered open when its normal relative displacement Δu_n has become greater than the ultimate magnitude of the normal relative displacement $\Delta u_{n,ult}$ of a softening model. For such an open crack, the constitutive model of a rough crack can be utilized. The constitutive relation of the rough, open crack is mobilized when the displacement tangential to the crack faces has become greater than zero, in the absolute sense. Consider an open crack, which is planar but microscopically rough (Fig. 14-7).

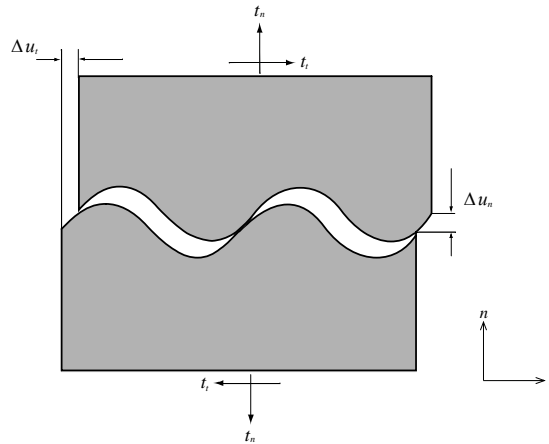


Figure 14-(7) Rough crack (Saw teeth effect)

The global crack displacements Δu_n and Δu_t are the relative displacements of the two parts of the structure, separated by the crack. With this definition, the global crack width is independent of the global crack sliding, but the local sliding and width will vary along the crack, depending on the crack geometry.

Due to the complexity of the problem, the constitutive laws for crack dilatancy, which have been

proposed by various authors, are mostly based on a total deformation theory. This theory expresses the tractions as a function of the total relative displacements. See for instance Bažant & Gambarova⁸,

$$\begin{cases} t_n = f_n(\Delta u_n, dt) \\ t_t = f_t(\Delta u_n, dt) \end{cases} \quad (14.14)$$

Differentiating (14.14) results in expressions for the crack stiffness coefficients:

$$\begin{cases} D_{11} = \frac{\partial f_n}{\partial \Delta u_n} \\ D_{12} = \frac{\partial f_n}{\partial dt} \\ D_{21} = \frac{\partial f_t}{\partial \Delta u_n} \\ D_{22} = \frac{\partial f_t}{\partial dt} \end{cases} \quad (14.15)$$

The mathematical models for crack dilatancy can be classified into two categories. The first category is based on experimental results and has an empirical formulation, which we will denote it as empirical crack models. The second category is based on an assumption of the shape of the crack surface and has a rational formulation, which we will denote this category as physical crack models. Although there are many models which give good results, the ones supported by MIDAS have been restricted to a few models that are characteristic of their class.

Empirical crack models

- Rough crack model (Bazant & Gambarova)

⁸ Bažant, Z. P., and Gambarova, P. G. *Rough crack models in reinforced concrete*. J. Struct. Eng., ASCE 106, 4 (1980), 819–842.

- Rough crack model (Gambarova & Karakoc)
- Aggregate interlock model (Walraven & Reinhardt)

Physical crack model

- Two-phase model (Walraven)
- Contact density model (Li et al.)

14-3-1 Rough Crack Model (Bažant and Gambarova)

Bažant & Gambarova⁸ introduced a rough crack model by considering the crack surface as a regular array of trapezoidal asperities. Fig. 14-8 shows the response diagram of this model, which has been used merely in qualitative sense, i.e., to introduce the general properties to be expected.

- The wedging effects of the interface asperities make the shear stress primarily dependent on the displacement ratio $r = dt / \Delta u_n$.
- For large values of the displacement ratio r , the shear stress must exhibit an asymptote because of micro-cracking and crushing in the mortar close to the aggregate particles.
- For large values of the normal crack displacement, the contact at the interface is lost, $\Delta u_n > 0.5D_{\max}$, where D_{\max} is the maximum aggregate size.

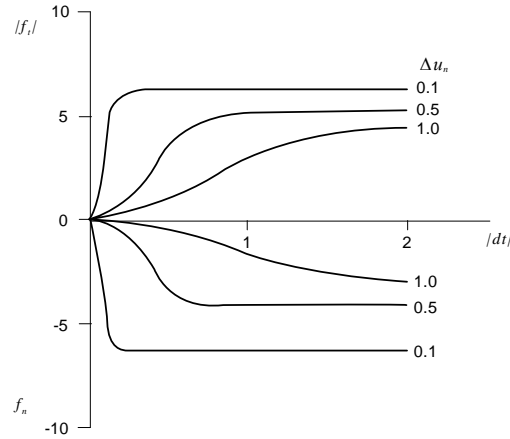


Figure 14-(8) Rough crack model (Bazant and Gambarova)

The constitutive model is determined by optimizing the fits of Paulay & Loeber's⁹ test results at constant crack width. The relations are,

$$f_t = \tau_u r \frac{a_3 + a_4 |r|^3}{1 + a_4 r^4} \quad (14.16)$$

$$f_n = -\frac{a_1}{\Delta u_n} (a_2 |f_t|)^p$$

where,

$$p = 1.30 \times \left(1 - \frac{0.231}{1 + 0.185 \Delta u_n + 5.63 (\Delta u_n)^2} \right), \quad r = \frac{dt}{\Delta u_n}, \quad \tau_u = \frac{\tau_0 a_0}{a_0 + (\Delta u_n)^2},$$

$$a_0 = 0.01 D_{\max}^2, \quad a_1 = 0.000534, \quad a_2 = 145.0, \quad a_3 = \frac{2.45}{\tau_0}, \quad a_4 = 2.44 \times \left(1 - \frac{4}{\tau_0} \right),$$

$$\tau_0 = 0.245 f_c = 0.195 f_{cc}$$

⁹ Paulay, T., and Loeber, P. J. *Shear transfer by aggregate interlock*. ACI-Special Publication SP, 42 (1974), 1-15.

The notation f_c is used for the compressive cylindrical strength of the concrete, and the more frequently used compressive cube strength is denoted by f_{cc} .

14-3-2 Rough Crack Model (Gambarova and Karakoc)

An improvement to the rough crack model of Bažant & Gambarova has been proposed by Gambarova & Karakoç¹⁰. Fig. 14-9 shows the response diagram for this model. The authors claim that their model gives a better formulation for the relation between the normal traction and the crack displacements, because this relation is based on tests with a constant confinement stress by Daschner & Kupfer¹¹. Further, this formulation takes the effect of aggregate size into account.

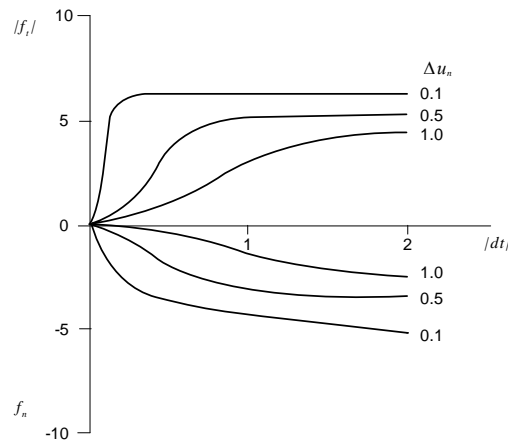


Figure 14-9) Rough crack model (Gambarova and Karakoc)

10 Gambarova, P. G., and Karakoç. *A new approach to the analysis of the confinement role in regularly cracking concrete elements*. In Trans. 7th Struct. Mech. in Reactor Tech. (1983), vol. H, pp. 251–261.

11 Daschner, F., and Kupfer, H. *Versuche zur Schubkraftübertragung in Risse von Normal- und Leichtbeton*. Bauingenieur 57 (1982), 57–60.

The relations are,

$$\begin{aligned} f_t &= \tau_0 \left(1 - \sqrt{\frac{2\Delta u_n}{D_{\max}}} \right) r \frac{a_3 + a_4 |r|^3}{1 + a_4 r^4} \\ f_n &= -a_1 a_2 \sqrt{\Delta u_n} \frac{r}{(1 + r^2)^{0.25}} f_t \end{aligned} \quad (14.17)$$

where,

$$a_1 a_2 = 0.62, \quad a_3 = \frac{2.45}{\tau_0}, \quad a_4 = 2.44 \times \left(1 - \frac{4}{\tau_0} \right), \quad \tau_0 = 0.25 f_c = 0.2 f_{cc}$$

14-3-3 Aggregate Interlock Relation (Walraven and Reinhardt)

Walraven & Reinhardt¹² have deduced linear relations, which fit their experiments¹³ on lightweight and gravel concrete. We only consider the relations restricted to gravel concrete because the main subject of this section is the analysis of crack dilatancy models for gravel concrete. Fig. 14.10 shows the response diagram for this model.

¹² Walraven, J. C., and Reinhardt, H. W. *Theory and experiments on the mechanical behavior of cracks in plain and reinforced concrete subjected to shear loading*. Heron 26, 1(a) (1981), 5–68.

¹³ Walraven, J. C., Vos, E., and Reinhardt, H. W. *Experiments on Shear Transfer in Cracks in Concrete. Part I: Description of Results*. Tech. Rep. 5-79-3, Stevin Laboratory, Delft University of Technology, Delft, 1979.

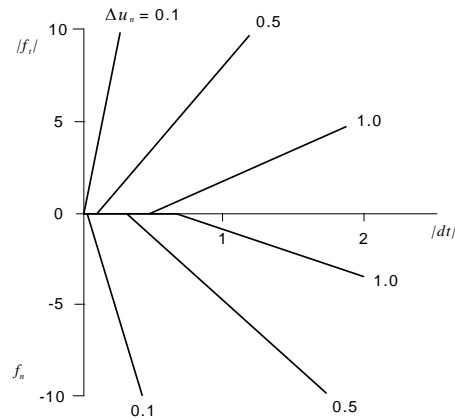


Figure 14-(10) Aggregate interlock relation (Walraven and Reinhardt)

The relations which fit the results with the greatest accuracy are,

$$\begin{aligned} f_t &= -\frac{f_{cc}}{30} + \left(1.8\Delta u_n^{-0.80} + (0.234\Delta u_n^{-0.707} - 0.20) f_{cc} \right) dt \\ f_n &= \frac{f_{cc}}{20} - \left(1.35\Delta u_n^{-0.63} + (0.191\Delta u_n^{-0.552} - 0.15) f_{cc} \right) dt \end{aligned} \quad (14.18)$$

in which $dt \geq 0$, $f_t \geq 0$ and $f_n \leq 0$.

14-3-4 Two-phase Model (Walraven)

The two-phase model proposed by Walraven¹⁴ is based on the following assumptions:

- The concrete is regarded as a two-phase material, with perfectly stiff spherical

¹⁴ Walraven, J. C. *Aggregate Interlock: a Theoretical and Experimental Analysis*. PhD thesis, Delft University of Technology, 1980.

inclusions and a perfectly plastic matrix.

- The grading of the aggregate matches Fuller's curve.
- The active contact areas between the inclusions and the matrix are related to interface displacements via geometric relations and take into account the statistics of aggregate distribution.
- The compressive contact strength of the matrix is related to the concrete strength while the shear contact strength is related linearly to the compressive contact strength via a constant friction coefficient.

Walraven has developed this theoretical model for pure aggregate interlock, i.e., aggregate interlock in cracks, which are not intersected by reinforcing bars. Fig. 14-11 shows the response diagram for this model. Shear stress and normal stress are obtained from equilibrium when a given tangential and normal crack displacement occurs.

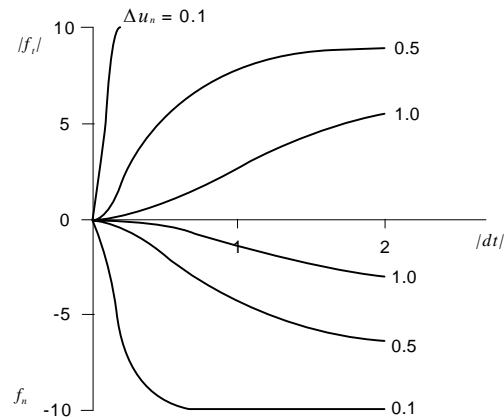


Figure 14-(11) Two-phase model (Walraven)

The formulation is given by,

$$\begin{aligned} f_t &= \sigma_{pu} (A_n + \mu A_t) \\ f_n &= -\sigma_{pu} (A_t - \mu A_n) \end{aligned} \quad (14.19)$$

A_n and A_t are the averaged contact areas in the directions n and t between the inclusions and the matrix. σ_{pu} is the matrix compressive strength. μ is the coefficient of friction between the inclusion and the matrix. The tangential stiffness terms are functions of the crack displacement dt , the normal crack displacement Δu_n and the distribution of the aggregate. See Feenstra¹⁵.

14-3-5 Contact Density Model (Li et al.)

The Contact Density model is based on two proposals and three assumptions by Li et al.¹⁶, which can be summarized as follows:

- A crack plane consists of a number of areas (contact units) with various inclinations. These inclinations θ from $-\pi/2$ to $\pi/2$ can be described by a contact density probability function $\Omega(\theta)$.
- The direction of each contact stress is proposed to be fixed and normal to the initial contact direction denoted as θ .
- The density function $\Omega(\theta)$ is assumed as a trigonometric function, which is independent of the size and the grading of the aggregate, and of the strength and kinds

¹⁵ Feenstra, P. H. *Numerical Simulation and Stability Analysis of Crack Dilatancy Models*. Tech. Rep. BI-89-191, TNO Building and Construction Research, Rijswijk, The Netherlands, 1989.

¹⁶ Li, N., Maekawa, L., and Okamura, H. *Contact density model for stress transfer across cracks in concrete*. J. of the Faculty of Engineering, University of Tokyo XL, 1 (1989), 9–52.

of coarse aggregates.

- The contact force is computed with a simple elastic perfectly plastic model for the contact stress prediction σ_{con} .
- The effective ratio of contact area $K(\Delta u_n)$ expresses the loss of contact when the normal crack displacement Δu_n is large enough compared with the roughness of the crack surface.

Fig. 14-12 shows the response diagram for this model.

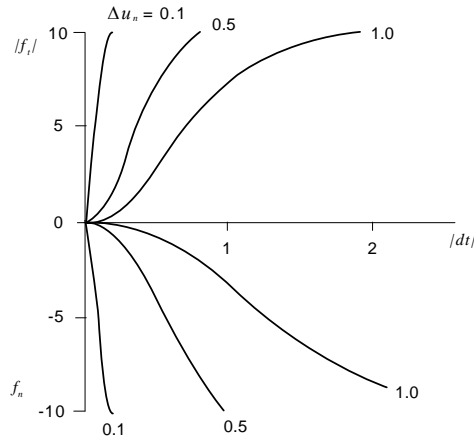


Figure 14-(12) Contact density model (Li et al.)

The mathematical formulation is given by

$$f_t = \int_{-\frac{1}{2}\pi}^{\frac{1}{2}\pi} \sigma_{con} K(\Delta u_n) A_i \Omega(\theta) \sin \theta d\theta$$

$$f_n = \int_{-\frac{1}{2}\pi}^{\frac{1}{2}\pi} \sigma_{con} K(\Delta u_n) A_i \Omega(\theta) \cos \theta d\theta$$
(14.20)

in which the surface area of the crack A_i is 1.27 multiplied by the sectional area of the crack plane.

14-4 Bond Slip

In reinforced concrete, the interaction between the reinforcement and the concrete is highly complex. The interaction is governed by secondary transverse and longitudinal cracks in the vicinity of the reinforcement. This behavior can be modeled with a bond-slip mechanism where the relative slip of the reinforcement and the concrete is described in a phenomenological sense. The mechanical behavior of the slip zone is then described by the interface element with a zero thickness.

The constitutive laws for bond-slip, which have been proposed, are mostly based on a total deformation theory, which expresses the tractions as a function of the total relative displacements. In MIDAS, the relationship between the normal traction and the normal relative displacement is assumed to be linear elastic, whereas the relationship between the shear traction and the slip is assumed as a nonlinear function.

$$\begin{aligned} t_n &= k_n \Delta u_n \\ t_i &= f_i(dt) \end{aligned} \quad (14.21)$$

Differentiating (14.21) results in expressions for the tangential stiffness coefficients.

$$\begin{cases} D_{11} = k_n \\ D_{12} = 0 \\ D_{21} = 0 \\ D_{22} = \frac{\partial f_i}{\partial dt} \end{cases} \quad (14.22)$$

MIDAS offers two predefined curves for the relationships between shear traction and slip, a

Cubic function according to Dörr¹⁷, and a Power Law relation proposed by Noakowski¹⁸. Moreover, a user-defined multi-linear diagram is available.

14-4-1 Cubic Function (Dörr)

Dörr¹⁷ proposed a polynomial relation between shear traction and slip, which shows a limit if the slip is larger than a certain value dt^0 (Fig. 14-13).

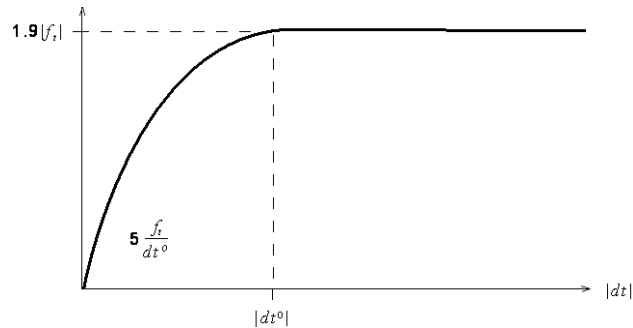


Figure 14-(13) Cubic function for bond-slip (Dörr)

The formulation of this relationship is given by a cubic function.

$$f_t = \begin{cases} f_t \left(5 \left(\frac{dt}{dt^0} \right) - 4.5 \left(\frac{dt}{dt^0} \right)^2 + 1.4 \left(\frac{dt}{dt^0} \right)^3 \right) & \text{if } 0 \leq dt \leq dt^0 \\ 1.9 f_t & \text{if } dt \geq dt^0 \end{cases} \quad (14.23)$$

Unloading and reloading of the interface shear behavior is modeled using a secant approach.

17 Dörr, K. *Ein Beitrag zur Berechnung von Stahlbetonscheiben unter besonderer Berücksichtigung des Verbundverhaltens*. PhD thesis, University of Darmstadt, 1980.

18 Noakowski, P. *Die Berechnung von Stahlbetonscheiben bei Zwangsbeanspruchung infolge Temperatur*. Deutscher Ausschuß für Stahlbeton 296 (1978).

14-4-2 Power Law (Noakowski)

The relationship between shear traction and slip proposed by Noakowski¹⁸ depicts a kind of stick-slip behavior (Fig. 14-14). The initial shear stiffness is kept linear to avoid unrealistically high stiffness when the slip is smaller than an initial value Δu_t^0 .

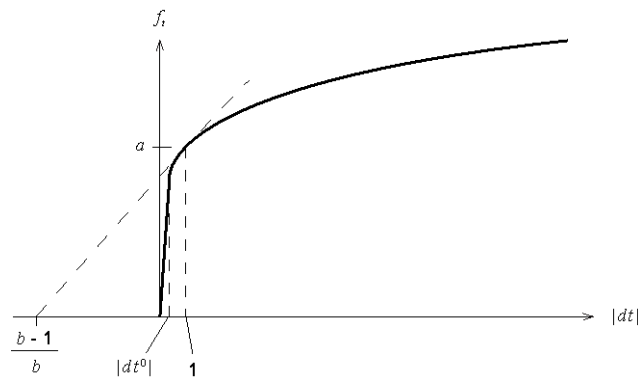


Figure 14-14) Power Law for bond-slip (Noakowski)

This relation is formulated with a Power Law.

$$f_t = \begin{cases} a(dt)^b & \text{if } dt \geq dt^0 \\ a(dt)^{b-1} dt & \text{if } 0 \leq dt \leq dt^0 \end{cases} \quad (14.24)$$

where, $b < 1$. Unloading and reloading is modeled with a secant approach.

14-5 Coulomb friction

In general, the interface between two parts of a structure is governed by a frictional behavior. This behavior can be modeled with the Coulomb friction model, which has close resemblance with the Mohr–Coulomb plasticity model for continuum elements. The assumption of the decomposition of the total relative displacement rate $\Delta \dot{\mathbf{u}}$, into a reversible part $\Delta \dot{\mathbf{u}}^e$, and an irreversible part $\Delta \dot{\mathbf{u}}^p$ is,

$$\Delta \dot{\mathbf{u}} = \Delta \dot{\mathbf{u}}^e + \Delta \dot{\mathbf{u}}^p \quad (14.25)$$

This results in the traction rate vector.

$$\dot{\mathbf{t}} = \mathbf{D}^e \Delta \dot{\mathbf{u}}^e = \mathbf{D}^e (\Delta \dot{\mathbf{u}} - \Delta \dot{\mathbf{u}}^p) \quad (14.26)$$

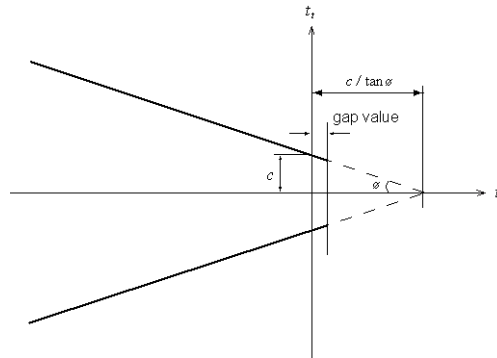


Figure 14-(15) Coulomb friction criterion

The basic unknown is the irreversible relative displacement rate $\Delta \dot{\mathbf{u}}^p$, which is determined following the flow theory of plasticity. The Coulomb friction model is basically given by the yield

surface and the plastic potential surface:

$$\begin{cases} f = \sqrt{t_i^2} + t_n \tan \phi(\kappa) - \bar{c}(\kappa) = 0 \\ g = \sqrt{t_i^2} + t_n \tan \psi \end{cases} \quad (14.27)$$

$\tan \phi(\kappa)$ is the friction coefficient as a function of the internal parameter κ , and $\bar{c}(\kappa)$ is the cohesion as a function of the internal parameter κ . The direction of the irreversible displacements is given by the plastic potential function g where the “uplift” is determined by the dilatancy angle ψ , where

$$\Delta \dot{\mathbf{u}}^p = \dot{\lambda} \frac{\partial g}{\partial \mathbf{t}} \quad (14.28)$$

MIDAS assumes this angle to be constant. During the process of irreversible relative displacements, the consistency condition $\dot{f} = 0$ has to be fulfilled, which can be elaborated as,

$$\dot{f} = \frac{\partial f^T}{\partial \mathbf{t}} \dot{\mathbf{t}} + \frac{\partial f}{\partial \kappa} \dot{\kappa} = 0 \quad (14.29)$$

which yields the expression of the multiplier $\dot{\lambda}$.

$$\dot{\lambda} = \frac{1}{-\frac{\partial f}{\partial \kappa}} \frac{\partial f^T}{\partial \mathbf{t}} \dot{\mathbf{t}} = -\frac{1}{h} \frac{\partial f^T}{\partial \mathbf{t}} \dot{\mathbf{t}} \quad (14.30)$$

Finally, the evolution of the internal parameter κ is assumed to be given by the irreversible relative displacement component in the t direction.

$$\dot{\kappa} = \left| \Delta \dot{\mathbf{u}}_t^p \right| \quad (14.31)$$

The derivation of the tangent stiffness matrix now becomes straightforward.

$$\begin{aligned}
 \dot{\mathbf{t}} &= \mathbf{D}^e \left\{ \Delta \dot{\mathbf{u}} - \Delta \dot{\mathbf{u}}^p \right\} = \mathbf{D}^e \left\{ \Delta \dot{\mathbf{u}} - \lambda \frac{\partial \mathbf{g}}{\partial \mathbf{t}} \right\} \\
 &= \mathbf{D}^e \left\{ \Delta \dot{\mathbf{u}} - \frac{1}{h} \frac{\partial \mathbf{g}}{\partial \mathbf{t}} \frac{\partial \mathbf{f}^T}{\partial \mathbf{t}} \dot{\mathbf{t}} \right\} = \left\{ \mathbf{D}^e - \frac{\mathbf{D}^e \frac{\partial \mathbf{g}}{\partial \mathbf{t}} \frac{\partial \mathbf{f}^T}{\partial \mathbf{t}} \mathbf{D}^e}{h + \frac{\partial \mathbf{f}^T}{\partial \mathbf{t}} \mathbf{D}^e \frac{\partial \mathbf{g}}{\partial \mathbf{t}}} \right\} \Delta \dot{\mathbf{u}}
 \end{aligned} \quad (14.32)$$

which is written in components,

$$\dot{\mathbf{t}} = \frac{1}{h + k_n \tan \phi \tan \psi + k_t} \begin{bmatrix} k_n(h + k_t) & -k_n k_t \tan \psi \frac{t_t}{|t_t|} \\ -k_n k_t \tan \phi(k) \frac{t_t}{|t_t|} & k_t(h + k_n \tan \phi \tan \psi) \end{bmatrix} \Delta \dot{\mathbf{u}} \quad (14.33)$$

It is obvious that the tangent stiffness matrix becomes nonsymmetrical if the friction angle is not equal to the dilatancy angle, i.e. $\phi \neq \psi$. A non-associated flow rule models may cause a significant increase in the size of allocated memory and analysis time. MIDAS recommends the user to define a value in the range of $\phi - \psi \leq 20^\circ$. The analysis may fail to converge due to a significant difference between ϕ and ψ .

14-6 Combined Cracking-Shearing-Crushing

This interface material model, also known as the ‘Composite Interface model’, is appropriate to simulate fracture, frictional slip as well as crushing along material interfaces, for instance at joints in masonry. Usually the brick units are modeled as linear elastic, or viscoelastic continua, while the mortar joints are modeled with interface elements, which obey the nonlinear behavior described by this combined cracking–shearing–crushing model (Fig. 14-16b) (see Lourenço & Rots¹⁹, and Van Zijl²⁰). In some cases, it is justified to model also the mortar with continuum elements, and the interface elements and material behavior are employed to capture the physical interface between bricks and mortar (Fig. 14-16a).

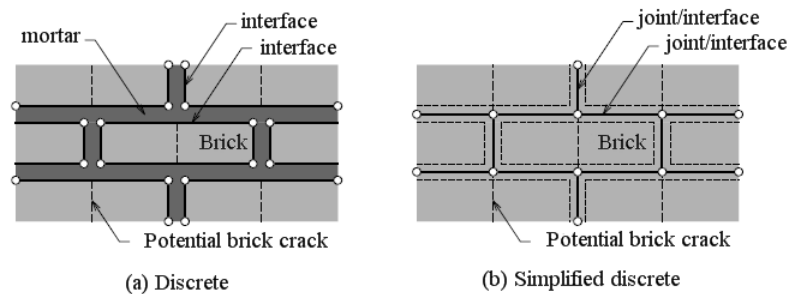


Figure 14-(16) Modeling strategies for masonry

¹⁹ Lourenço, P. B., and Rots, J. G. A multi-surface interface model for the analysis of masonry structures. *J. Struct. Eng.*, ASCE 123, 7 (1997), 660–668.

²⁰ van Zijl, G. P. A. G. *Computational Modelling of Masonry Creep and Shrinkage*. PhD thesis, Delft University of Technology, 2000.

14-6-1 Two-dimensional Interface Model

Two-dimensional interface model in MIDAS is based on the presented formula by Lourenço & Rots¹⁹ and enhanced by Van Zijl²⁰. It is based on multi-surface plasticity, comprising a Coulomb friction model combined with a tension cut-off and an elliptical compression cap (Fig. 14-16). Softening acts in all three modes and is preceded by hardening in the case of the cap mode. The interface model is derived in terms of the generalized stress and strain vectors.

$$\boldsymbol{\sigma} = \begin{pmatrix} \sigma \\ \tau \end{pmatrix}, \quad \boldsymbol{\varepsilon} = \begin{pmatrix} u \\ v \end{pmatrix} \quad (14.34)$$

where, σ and u are the stress and relative displacement respectively in the normal direction of the interface, and τ and v are the shear stress and relative displacement respectively.

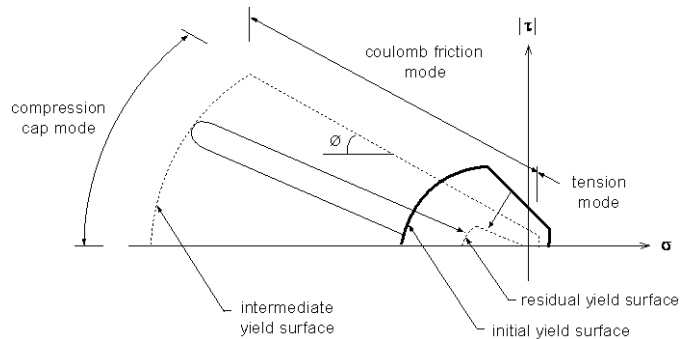


Figure 14-17) Two-dimensional interface model

In the elastic regime, the constitutive behavior is described by,

$$\boldsymbol{\sigma} = \mathbf{D}\boldsymbol{\varepsilon} \quad (14.35)$$

with the stiffness matrix

$$\mathbf{D} = \text{diag} [k_n \quad k_s] \quad (14.36)$$

Shear slipping

A Coulomb friction yield/crack initiation criterion

$$f = |\tau| + \sigma\Phi - c \quad (14.37)$$

describes the shear-slipping, with the friction coefficient Φ equal to the friction angle $\tan \phi$, and c is the adhesion. Both adhesion softening and friction softening are captured. The adhesion softening is described by,

$$c(\sigma, \kappa) = c_0 e^{-\frac{c_0}{G_f^H} \kappa} \quad (14.38)$$

where, c_0 is the initial adhesion of the brick-mortar interface and G_f^H is the shear slip fracture energy. The friction softening is coupled to the adhesion softening via,

$$\Phi(\sigma, \kappa) = \Phi_0 + (\Phi_r - \Phi_0) \frac{c_0 - c}{c_0} \quad (14.39)$$

where, Φ_0 and Φ_r are the initial and the residual friction coefficients respectively. The adhesion and friction parameters are found by linear regression of the micro-shear experimental data, while the fracture energy is determined by the appropriate integration of the stress-crack width response.

The experimentally observed linear relation between the fracture energy and the normal confining stress is captured by letting,

$$G_f'' = \begin{cases} a\sigma + b & \text{if } \sigma < 0 \\ b & \text{if } \sigma \geq 0 \end{cases} \quad (14.40)$$

where, a and b are constants to be determined by linear regression of the experimental data.

Dilatancy

The flow rule is expressed as,

$$\dot{\mathbf{\epsilon}}_p = \begin{Bmatrix} \dot{u}_p \\ \dot{v}_p \end{Bmatrix} = \dot{\lambda} \frac{\partial g}{\partial \boldsymbol{\sigma}} \quad (14.41)$$

which provides a way of describing the dilatancy, by choice of a suitable potential function

$$\frac{\partial g}{\partial \boldsymbol{\sigma}} = \begin{Bmatrix} \Psi \\ \text{sign}(\tau) \end{Bmatrix} \quad (4.42)$$

$\Psi = \tan \psi$ is the mobilized dilatancy coefficient. Following directly from the flow rule, Eq. (14.43) is derived.

$$\psi = \frac{\dot{u}_p}{\dot{v}_p} \text{sign}(\tau) \quad (14.43)$$

By integration, the shear-slip induced normal uplift is found to be,

$$u_p = \int \Psi d|\Delta v_p| \quad (14.44)$$

There is experimental evidence that dilatancy depends on the confining stress and the shear-slip. A dilatancy formulation of separate variables, i.e.,

$$\Psi = \Psi_1(\sigma) \Psi_2(v_p) \quad (14.45)$$

simplifies curve fitting and ensures convexity of the potential function g .

$$g = \int \left(\frac{\partial g}{\partial \sigma} \right)^T d\sigma = |\tau| + \Psi_2(v_p) \int \Psi_1(\sigma) d\sigma \quad (14.46)$$

Therefore, a description of the normal uplift upon shear-slipping is chosen as,

$$u_p = \begin{cases} 0 & \text{if } \sigma < \sigma_u \\ \frac{\Psi_0}{\delta} \left(1 - \frac{\sigma}{\sigma_u} \right) (1 - e^{-\delta v_p}) & \text{if } \sigma_u \leq \sigma < 0 \\ \frac{\Psi_0}{\delta} (1 - e^{-\delta v_p}) & \text{if } \sigma \geq 0 \end{cases} \quad (14.47)$$

which yields after differentiation.

$$\Psi = \begin{cases} 0 & \text{if } \sigma < \sigma_u \\ \Psi_0 \left(1 - \frac{\sigma}{\sigma_u} \right) e^{-\delta v_p} & \text{if } \sigma_u \leq \sigma < 0 \\ \Psi_0 e^{-\delta v_p} & \text{if } \sigma \geq 0 \end{cases} \quad (14.48)$$

Ψ_0 is the dilatancy at zero normal confining stress and shear slip. σ_u is the confining (compressive) stress at which the dilatancy becomes zero. The dilatancy shear slip degradation coefficients δ are material parameters to be obtained by, for instance, a least squares fit of (14.47) to experimental test data. Note that for tensile stress, a stress-independent dilatancy coefficient is assumed.

Softening

A strain softening hypothesis is employed, where the softening is governed by shear-slipping, yielding upon substitution of (14.41) and (14.42).

$$\Delta \kappa = |v_p| = \Delta \lambda \quad (14.49)$$

The stress-update can be cast in the standard plasticity predictor–corrector fashion and the corrected stresses, together with the plastic strain increment $\Delta \kappa$, or $\Delta \lambda$, can be solved by a Newton–Raphson iterative scheme. A consistent tangent modulus is employed for the global convergence iterations, which ensures quadratic convergence (see Van Zijl²⁰).

Tension cut-off

The yield function for the tension cut-off (criterion number 2 of the interface model) is,

$$f_2 = \sigma - \sigma_t \quad (14.50)$$

where, σ_t is the tensile or brick-mortar bond strength. The strength is assumed to soften exponentially.

$$\sigma_t = f_t e^{-\frac{f_t}{G_f^I} \kappa_2} \quad (14.51)$$

f_t is the bond strength, and G_f^I is the Mode-I fracture energy. The softening is governed by a strain softening hypothesis.

$$\Delta \kappa_2 = |\Delta u_p| \quad (14.52)$$

Upon consideration of an associated flow rule,

$$\Delta \varepsilon_p = \Delta \lambda_2 \frac{\partial f_2}{\partial \sigma} \quad (14.53)$$

reduces to

$$\Delta \kappa_2 = \Delta \lambda_2 \quad (14.54)$$

Compression cap

The yield function for the compression cap, here referred to as criterion number 3 (with 1 being the shear mode), is

$$f_3 = \sigma^2 + C_s \tau^2 - \sigma_c^2 \quad (14.55)$$

C_s is a parameter controlling the shear stress contribution to failure, and σ_c is the compressive strength. The latter is assumed to evolve according to the strain hardening hypothesis.

$$\Delta \kappa_3 = \sqrt{\Delta \boldsymbol{\varepsilon}_p^T \Delta \boldsymbol{\varepsilon}_p} \quad (14.56)$$

Upon consideration of an associated flow rule,

$$\Delta \boldsymbol{\varepsilon}_p = \Delta \lambda_3 \frac{\partial f_3}{\partial \boldsymbol{\sigma}} \quad (14.57)$$

becomes

$$\Delta \kappa_3 = 2 \Delta \lambda_3 \sqrt{\sigma^2 + (C_s \tau)^2} \quad (14.58)$$

The yield surface hardens, as described by a parabolic hardening rule, followed by parabolic/exponential softening (Fig. 14-18). The peak strength $f_{c,x}$ is reached at the plastic strain κ_p . Subsequently, the softening branch is entered, governed by the fracture energy G_{fc} .

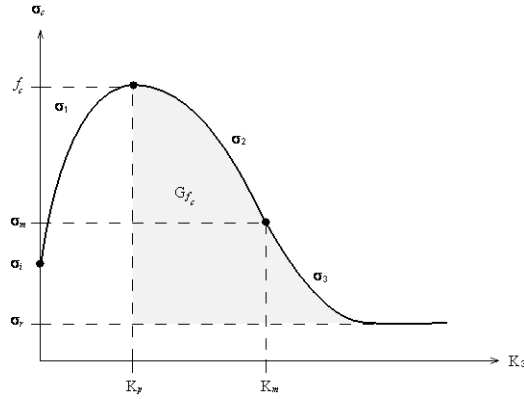


Figure 14-18) Hardening-softening law for interface compression cap

For practical reasons, all stress values in Fig. 14.18 are related to the peak strengths f_c as follows: $\bar{\sigma}_i = \frac{1}{3} f_c$, $\bar{\sigma}_m = \frac{1}{2} f_c$ and $\bar{\sigma}_r = \frac{1}{7} f_c$. The three regions of this hardening-softening rule are given by,

$$\begin{aligned}
 \bar{\sigma}_1(\kappa_3) &= \bar{\sigma}_i + (f_c - \bar{\sigma}_i) \sqrt{\frac{2\kappa_3 - \kappa_3^2}{\kappa_p^2 - \kappa_p^2}} \\
 \bar{\sigma}_2(\kappa_3) &= f_c + (\bar{\sigma}_m - f_c) \left(\frac{\kappa_3 - \kappa_p}{\kappa_m - \kappa_p} \right)^2 \\
 \bar{\sigma}_3(\kappa_3) &= \bar{\sigma}_r + (\bar{\sigma}_m - \bar{\sigma}_r) \exp \left(2 \left(\frac{\bar{\sigma}_m - f_c}{\kappa_m - \kappa_p} \right) \left(\frac{\kappa_3 - \kappa_m}{\bar{\sigma}_m - \bar{\sigma}_r} \right) \right)
 \end{aligned} \tag{14.59}$$

Corners

At each of the intersections of the Coulomb friction criterion with the tension cut-off and the compression cap, the plastic strain increment is given by,

$$\Delta \varepsilon_p = \Delta \lambda_1 \frac{\partial g_1}{\partial \sigma} + \Delta \lambda_i \frac{\partial g_i}{\partial \sigma} \quad (14.60)$$

The subscript 1 refers to the shear criterion, and i refers to tension cut-off ($i = 2$) and to the compression cap ($i = 3$). Lourenço²¹ describes this procedure in detail. The corners are treated consistently. In both the shear/tension corner and the shear/compression corner, the stress corrections can be written in a standard predictor–corrector fashion and solved for, together with the two plastic strain increments $\Delta \lambda_1$ or $\Delta \lambda_i$, by a Newton–Raphson iterative scheme. Also consistent tangent moduli here are employed for the global convergence iterations to ensure quadratic convergence.

14-6-2 Three-dimensional Interface Model

The two-dimensional interface model is extended to a three-dimension (see Van Zijl²⁰), which enables the description of delamination (tension cut-off) and relative shear-slipping of two planes (Coulomb friction). No three-dimensional compression cap is implemented in MIDAS. Now the generalized stress and strain vectors are,

$$\boldsymbol{\sigma} = \begin{Bmatrix} \sigma \\ \tau_s \\ \tau_t \end{Bmatrix} ; \quad \boldsymbol{\varepsilon} = \begin{Bmatrix} u \\ v \\ w \end{Bmatrix} \quad (14.61)$$

Here, the shear stresses τ_s and τ_t act in the local plane of the interface; v and w are the relative shearing displacements in the interface plane; and σ and u are the stress and relative displacement respectively normal to the plane. The stiffness matrix is defined as,

21 Lourenço, P. B. *Computational Strategies for Masonry Structures*. PhD thesis, Delft University of Technology, 1996.

$$\mathbf{D} = \text{diag}[k_n \quad k_s \quad k_t] \quad (14.62)$$

Fig. 14-19 shows the three-dimensional interface material law.

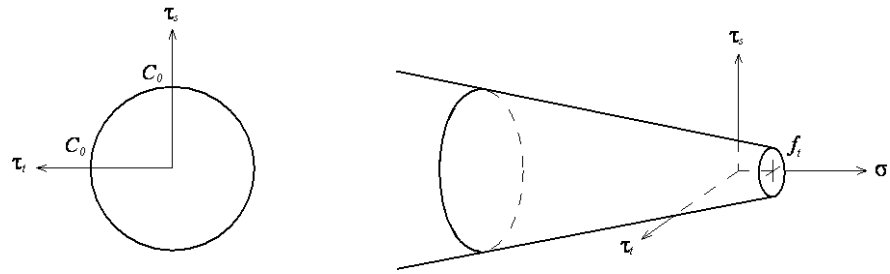


Figure 14-19) Three-dimensional interface yield function

Apart from the added stress and strain components, the two-dimensional tension criterion f_2 of (14.50) remains unchanged. For the Coulomb friction part, the yield function becomes,

$$f = \sqrt{\tau_s^2 + \tau_t^2} + \sigma \Phi - c \quad (14.63)$$

As for the two-dimensional case, adhesion softening and friction softening are modeled as described by (14-38) and (14-39). A non-associated plastic potential is chosen, giving the flow rule.

$$\Delta \epsilon_p = \Delta \lambda \frac{\partial g}{\partial \sigma} = \Delta \lambda \begin{bmatrix} \psi \\ \frac{\tau_s}{\sqrt{\tau_s^2 + \tau_t^2}} \\ \frac{\tau_t}{\sqrt{\tau_s^2 + \tau_t^2}} \end{bmatrix} \quad (14.63)$$

The mobilized dilatancy Ψ is defined as before by (14.48). However, now the strain softening is governed by the equivalent shear displacement.

$$\Delta \kappa = \sqrt{(\Delta v_p)^2 + (\Delta w_p)^2} = \Delta \lambda \quad (14.64)$$

Chapter 15. Geometric Nonlinearity

15-1 Introduction

If a structure undergoes large deformation, the geometrical shape of the structure will change. As a result, the relationship between strain and displacement may no longer remain linear. Fig. 15-(1)-A shows a structure in its equilibrium position. This structure is deformed by a load [a plumb bob] (Fig.15-(1)-B). At this point, the load and deflection interaction becomes nonlinear.

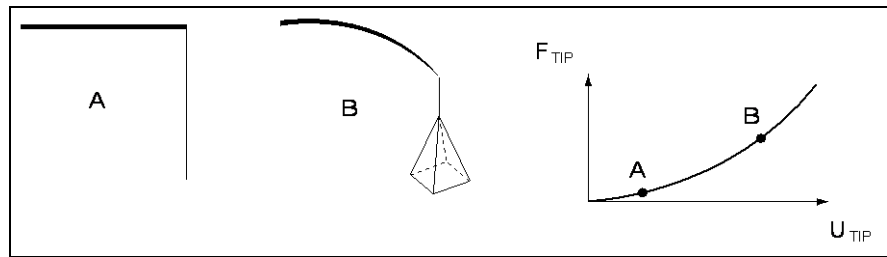


Figure 15-(1) Schematic representation of a large deformation

Since the geometric shape of the structure changes while being in the process of deformation, geometric nonlinear analysis assumes that the shape of the structure before deformation (initial configuration) differs from that after deformation. Also assumed here is that strains and rotations are not small. Accordingly, the stiffness matrix (\mathbf{K}) becomes a function of displacements (\mathbf{u}) in geometric nonlinear analysis.

Generally, the formulations used in geometric nonlinear analysis include the Total Lagrangian formulation (TL) and the Updated Lagrangian formulation (UL). The formulations for both types are essentially the same, except that they have different ways to express the strains and stresses. The stresses and strains used in TL are the second Piola-Kirchhoff stress and the Green-Lagrangian strain respectively. The stresses and strains used in UL are the Cauchy stress and the incremental linear Eulerian strain. The stresses and strains in TL and UL represent the shapes prior to deformation and after deformation respectively. In case of one dimensional analysis for

example, the second Piola-Kirchhoff stress represents the relationship of force and area before deformation (F / A_0), whereas the Cauchy stress represents the relationship of force and area after deformation (F / A).

Fig. 15-(2) shows the state of a body being deformed from its initial state (prior to deformation) at time= 0 to its current state (after deformation) at time= t . Ω_0 and Ω represent the initial state and the current state respectively. $\bar{\mathbf{X}}$ represents the spatial coordinate at the initial state, and \mathbf{x} represents the spatial coordinate after the passage of time, t .

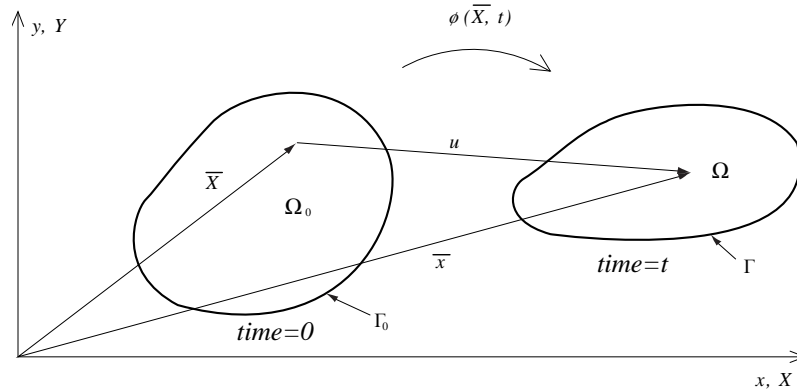


Figure 15-(2) Schematic representation of a deformed body

The Green-Lagrangian strain is defined using the coordinates of undeformed configuration, which is given by,

$$\mathbf{E} = \frac{1}{2} (\mathbf{F}^T \mathbf{F} - \mathbf{I}) \text{ or } E_{ij} = \frac{1}{2} (u_{i,j} + u_{j,i} + u_{k,i} u_{k,j}) \quad (15.1)$$

$$\mathbf{F} = \frac{\partial \mathbf{x}}{\partial \bar{\mathbf{X}}} = \frac{\partial (\bar{\mathbf{X}} + \mathbf{u})}{\partial \bar{\mathbf{X}}} = \mathbf{I} + \frac{\partial \mathbf{u}}{\partial \bar{\mathbf{X}}}$$

where,

\mathbf{E} or E_{ij} : Green-Lagrangian strain

\mathbf{F} : Deformation gradient

\mathbf{F} links the undeformed shape of the body to the deformed shape.

In case of a one dimensional structure, Eq.(15.1) can be written as,

$$E_{11} = \frac{1}{2} \frac{L^2 - \bar{L}^2}{\bar{L}^2} \quad (15.2)$$

In Eq. (15.2), \bar{L} represents the element length prior to deformation, and L represents the element length after deformation. If the deformation in Eq.(15.2) is extremely small, the Green-Lagrangian strain can be expressed in the context of small (linear) strain as,

$$\begin{aligned} E_{11} &= \frac{1}{2} \frac{(L - \bar{L})(L + \bar{L})}{\bar{L}^2} = \frac{1}{2} \frac{L - \bar{L}}{\bar{L}} \left(\frac{L - \bar{L}}{\bar{L}} + \frac{2\bar{L}}{\bar{L}} \right) = \frac{1}{2} \left(\frac{L - \bar{L}}{\bar{L}} \right)^2 + \frac{L - \bar{L}}{\bar{L}} \\ &\cong \frac{L - \bar{L}}{\bar{L}} \end{aligned} \quad (15.3)$$

In order to examine the meaning of the second Piola-Kirchhoff stress in a general three dimensional continuum, we will induce the relationship with the Cauchy stress. The fundamental laws of thermodynamics state that the amount of energy produced by the Cauchy stress or the second Piola-Kirchhoff stress, whichever is used, is the same. Therefore, the virtual work can be written as,

$$r = \int \mathbf{S} : \delta \mathbf{E} dV_0 = \int \boldsymbol{\sigma} : \delta \boldsymbol{\varepsilon} dV = \int J \boldsymbol{\sigma} : \delta \boldsymbol{\varepsilon} dV_0, \quad J = \det(\mathbf{F}) \quad (15.4)$$

where,

\mathbf{S} : Second Piola-Kirchhoff stress

$\boldsymbol{\sigma}$: Cauchy stress

$\delta \boldsymbol{\varepsilon}$: Incremental linear Eulerian strain, $\boldsymbol{\varepsilon} = \frac{1}{2} (u_{i,j} + u_{j,i})$

J : The *Jacobian* determinant

First, if the Green-Lagrangian strain and the deformation gradient are differentiated, each of them

is expressed as,

$$\delta \mathbf{E} = \frac{1}{2} (\delta \mathbf{F}^T \mathbf{F} + \mathbf{F}^T \delta \mathbf{F}) \quad (15.5)$$

$$\delta \mathbf{F} = \frac{\partial \delta \mathbf{u}}{\partial \bar{\mathbf{X}}} = \frac{\partial \delta \mathbf{u}}{\partial \mathbf{x}} \frac{\partial \mathbf{x}}{\partial \bar{\mathbf{X}}} = \frac{\partial \delta \mathbf{u}}{\partial \mathbf{x}} \mathbf{F} \quad (15.6)$$

Substituting Eq. (15.6) into Eq.(15.5) results in Eq. (15.7).

$$\delta \mathbf{E} = \frac{1}{2} \left(\left(\frac{\partial \delta \mathbf{u}}{\partial \mathbf{x}} \mathbf{F} \right)^T \mathbf{F} + \mathbf{F}^T \left(\frac{\partial \delta \mathbf{u}}{\partial \mathbf{x}} \mathbf{F} \right) \right) = \mathbf{F}^T \left(\frac{1}{2} \left(\frac{\partial \delta \mathbf{u}^T}{\partial \mathbf{x}} + \frac{\partial \delta \mathbf{u}}{\partial \mathbf{x}} \right) \right) \mathbf{F} = \mathbf{F}^T \delta \mathbf{e} \mathbf{F} \quad (15.7)$$

Substituting Eq.(15.7) into Eq.(15.4), the virtual work can be rewritten as,

$$r = \int \mathbf{S} : \delta \mathbf{E} dV_0 = \int \mathbf{S} : (\mathbf{F}^T \delta \mathbf{e} \mathbf{F}) dV_0 = \int \mathbf{F} \mathbf{S} \mathbf{F}^T : \delta \mathbf{e} dV_0 = \int J \boldsymbol{\sigma} : \delta \mathbf{e} dV_0 \quad (15.8)$$

Now, the relationship between the Cauchy stress and the second Piola-Kirchhoff stress can be expressed as,

$$\boldsymbol{\sigma} = \frac{1}{J} \mathbf{F} \mathbf{S} \mathbf{F}^T, \quad \mathbf{S} = J \mathbf{F}^{-1} \boldsymbol{\sigma} \mathbf{F}^{-T} \quad (15.9)$$

At time $t + \Delta t$, the virtual work theorem can be expressed in terms of the second Piola-Kirchhoff stress and the Green-Lagrange strain as Eq. (15.10).

$${}^{t+\Delta t} r = \int {}^{t+\Delta t} S_{ij} \delta {}^{t+\Delta t} E_{ij} dV_0 \quad (15.10)$$

$$\begin{aligned} {}^{t+\Delta t} S_{ij} &= {}^t S_{ij} + \Delta S_{ij} \\ {}^{t+\Delta t} E_{ij} &= {}^t E_{ij} + \Delta E_{ij} \end{aligned} \quad (15.11)$$

$$\delta {}^{t+\Delta t} E_{ij} = \frac{1}{2} \left(\delta u_{i,j} + \delta u_{j,i} + {}^t u_{k,i} \delta u_{k,j} + \delta u_{k,i} {}^t u_{k,j} + \delta u_{k,i} \Delta u_{k,j} + \delta u_{k,j} \Delta u_{k,i} \right)$$

where, r is virtual work caused by external forces.

Substituting Eq.(15.11) into Eq.(15.10), we obtain,

$$\int \Delta S_{ij} \delta e_{ij} dV_0 + \int {}^t S_{ij} \delta \eta_{ij} dV_0 = {}^{t+\Delta t} r - \int {}^t S_{ij} \delta e_{ij} dV_0 \quad (15.12)$$

where,

$$\delta e_{ij} = \frac{1}{2}(\delta u_{k,j} + \delta u_{j,i} + {}^t u_{k,i} \delta u_{k,j} + \delta u_{k,i} {}^t u_{k,j}) \quad : \text{Linear term}$$

$$\delta \eta_{ij} = \frac{1}{2}(\delta u_{k,i} \Delta u_{k,j} + \delta u_{k,j} \Delta u_{k,i}) \quad : \text{Nonlinear term}$$

ΔS_{ij} is expanded by using the Taylor series as follows:

$$\Delta S_{ij} = {}^{t+\Delta t} S_{ij} - {}^t S_{ij} = \left({}^t S_{ij} + \frac{\partial {}^t S_{ij}}{\partial {}^t E_{kl}} \Delta E_{kl} + \text{high order} \right) - {}^t S_{ij} \quad (15.13)$$

Substituting Eq. (15.13) into the first term of Eq. (15.12) and ignoring the second order and the higher order terms of ΔE_{kl} , the first term becomes a linearized equation as Eq. (15.14).

$$\begin{aligned} \int \Delta S_{ij} \delta e_{ij} dV_0 &= \int \left(\frac{\partial {}^t S_{ij}}{\partial {}^t E_{kl}} \Delta E_{kl} \right) \delta e_{ij} dV_0 = \int D_{ijkl} \Delta E_{kl} \delta e_{ij} dV_0 \\ \Delta E_{ij} &= \Delta e_{ij} = \frac{1}{2}(\Delta u_{i,j} + \Delta u_{j,i} + {}^t u_{k,i} \Delta u_{k,j} + \Delta u_{k,i} {}^t u_{k,j}) \end{aligned} \quad (15.14)$$

Also, using the property of ${}^t S_{ij} = {}^t S_{ji}$, the second term of Eq. (15.12) can be arranged as,

$$\int {}^t S_{ij} \delta \eta_{ij} dV_0 = \int {}^t \mathbf{S} : (\delta \mathbf{L}^T \Delta \mathbf{L}) dV_0, \quad L_{ij} = \frac{\partial u_i}{\partial X_j} \quad (15.15)$$

From the right side of Eq. (15.12), each term can be expressed as Eq. (15.16).

$$\begin{aligned} {}^{t+\Delta t} \mathbf{r} &= \delta \mathbf{u}^T {}^{t+\Delta t} \mathbf{f}_{ext} \\ \int {}^t S_{ij} \delta e_{ij} dV_0 &= \int {}^t \mathbf{S} : \delta \mathbf{e} dV_0 = \delta \mathbf{u}^T {}^t \mathbf{f}_{int} \end{aligned} \quad (15.16)$$

where,

$$\delta \mathbf{u} = [\delta u_1 \quad \delta v_1 \quad \delta w_1 \quad \delta u_2 \quad \delta v_2 \quad \delta w_2 \quad \cdots \quad \delta u_N \quad \delta v_N \quad \delta w_N]^T$$

Accordingly, the right side of Eq. (15.12) is arranged using Eq. (15.16) to Eq. (15.17).

$${}^{t+\Delta t} \mathbf{r} - \int {}^t \mathbf{S} : \delta \mathbf{e} dV_0 = \delta \mathbf{u}^T ({}^{t+\Delta t} \mathbf{f}_{ext} - {}^t \mathbf{f}_{int}) \quad (15.17)$$

Substituting Eq.(15.14-15, 17) into Eq.(15.12) results in Eq. (15.18). The first term of the left side in Eq. (15.18) represents the virtual work done by linear strains, and the second term represents the virtual work done by nonlinear strains.

$$\int \delta \mathbf{e}^T \mathbf{D} \Delta \mathbf{e} dV_0 + \int {}^t \mathbf{S} : \delta \mathbf{L}^T \Delta \mathbf{L} dV_0 = \delta \mathbf{u}^T ({}^{t+\Delta t} \mathbf{f}_{ext} - {}^t \mathbf{f}_{int}) \quad (15.18)$$

Eq. (15.18) is expressed as Eq. (15.19). The stiffness matrices, \mathbf{K}_L^e and \mathbf{K}_{NL}^e are determined by the element shape functions, which are detailed in the subsequent sections.

$$({}^t \mathbf{K}_L^e + {}^t \mathbf{K}_{NL}^e) \Delta \mathbf{u} = {}^{t+\Delta t} \mathbf{f}_{ext} - {}^t \mathbf{f}_{int} \quad (15.19)$$

15-2 Truss Element

A truss element has translational displacements, u , v and w in the Element Coordinate System, which are expressed using the shape function, N_i , as follows:

$$u = \sum_{i=1}^N N_i u_i, \quad v = \sum_{i=1}^N N_i v_i, \quad w = \sum_{i=1}^N N_i w_i \quad (15.20)$$

The stress and strain used for truss elements can be expressed as,

$$\mathbf{S} = \{S_{xx}\}, \quad \mathbf{E} = \{E_{xx}\} \quad (15.21)$$

where, x : Element Coordinate System

The linear term, $\delta \mathbf{e}$ of virtual strains in Eq. (15.19) can be written as,

$$\delta \mathbf{e} = \{\delta u_{,x}\} + \{\delta u_{,x} {}'u_{,x} + \delta v_{,x} {}'v_{,x} + \delta w_{,x} {}'w_{,x}\} \quad (15.22)$$

Eq. (15.22) is expressed in terms of the product of the virtual displacement term, $\delta \mathbf{u}$ and the matrix, \mathbf{B}_L .

$$\delta \mathbf{e} = \mathbf{B}_{L0} \delta \mathbf{u} + \mathbf{B}_{L1} \delta \mathbf{u} = \mathbf{B}_L \delta \mathbf{u} \quad (15.23)$$

The linear term of incremental strains can also be expressed in a similar way.

$$\Delta \mathbf{e} = \mathbf{B}_{L0} \Delta \mathbf{u} + \mathbf{B}_{L1} \Delta \mathbf{u} = \mathbf{B}_L \Delta \mathbf{u} \quad (15.24)$$

From Eq. (15.23) and Eq. (15.24), the displacement-strain relationship matrix is written as,

$$\mathbf{B}_{L0} = \{N_{1,x} \quad 0 \quad 0 \quad N_{2,x} \quad 0 \quad 0\} \quad (15.25)$$

$$\mathbf{B}_{L1} = \{ {}'u_{,x} N_{1,x} \quad {}'v_{,x} N_{1,x} \quad {}'w_{,x} N_{1,x} \quad {}'u_{,x} N_{2,x} \quad {}'v_{,x} N_{2,x} \quad {}'w_{,x} N_{2,x} \} \quad (15.26)$$

$\delta \mathbf{L}$, which composes the nonlinear term of the virtual strain in Eq. (15.19), is written as,

$$\delta \mathbf{L} = \{\delta u_{,x} \quad \delta v_{,x} \quad \delta w_{,x}\}^T \quad (15.27)$$

Eq. (15.27) is expressed by the product of the virtual displacement term, $\delta \mathbf{u}$ and the matrix, \mathbf{B}_{NL} .

$$\delta \mathbf{L} = \mathbf{B}_{NL} \delta \mathbf{u} \quad (15.28)$$

$\Delta \mathbf{L}$ also can be expressed in a similar way.

$$\Delta \mathbf{L} = \mathbf{B}_{NL} \Delta \mathbf{u} \quad (15.29)$$

where,

$$\mathbf{B}_{NL} = \begin{bmatrix} N_{1,x} & 0 & 0 & N_{2,x} & 0 & 0 \\ 0 & N_{1,x} & 0 & 0 & N_{2,x} & 0 \\ 0 & 0 & N_{1,x} & 0 & 0 & N_{2,x} \end{bmatrix} \quad (15.30)$$

Substituting Eq. (15.23-24) and Eq. (15.28-29) into Eq. (15.19), we can obtain a linearized equilibrium equation.

$$\delta \mathbf{u}^T (\mathbf{K}_L^e + \mathbf{K}_{NL}^e) \Delta \mathbf{u} = \delta \mathbf{u}^T ({}^{t+\Delta t} \mathbf{f}_{ext}^e - {}^t \mathbf{f}_{int}^e) \quad (15.31)$$

Each term of Eq. (15.31) is as follows:

$$\begin{aligned} {}^t \mathbf{K}_L^e &= \int_{L_e} A \mathbf{B}_L^T \mathbf{D} \mathbf{B}_L dL \\ {}^t \mathbf{K}_{NL}^e &= \int_{L_e} A {}^t \mathbf{B}_{NL}^T {}^t \hat{\mathbf{S}} {}^t \mathbf{B}_{NL} dL \\ {}^t \mathbf{f}_{int}^e &= \int_{L_e} A {}^t \mathbf{B}_L^T {}^t \mathbf{S} dL \end{aligned} \quad (15.32)$$

where,

A : section area

The matrix, ${}^t \hat{\mathbf{S}}$ composed of stress components is as follows:

$${}^t \hat{\mathbf{S}} = \begin{bmatrix} {}^t \mathbf{S} & \mathbf{0} & \mathbf{0} \\ \mathbf{0} & {}^t \mathbf{S} & \mathbf{0} \\ \mathbf{0} & \mathbf{0} & {}^t \mathbf{S} \end{bmatrix} \quad {}^t \mathbf{S} = [{}^t S_{xx}] \quad (15.33)$$

As a result of the truss element analysis, nodal stresses and element forces exist similarly to linear analysis. In addition to the nodal results, stresses at the integral points can be tabulated.

15-3 Plane Stress Element

Plane stress elements, which consider geometric nonlinearity, consist of isoparametric elements of 3, 4, 6 and 8 nodes. Each element uses a shape function identical to that of the linear element, and incompatible modes are not used. A plane stress element has translational displacements, u and v in the Element Coordinate System, which are expressed using the shape function, N_i , as follows:

$$u = \sum_{i=1}^N N_i u_i, \quad v = \sum_{i=1}^N N_i v_i \quad (15.34)$$

The stresses and strains used in plane stress elements can be expressed as,

$$\mathbf{S} = \begin{Bmatrix} S_{xx} & S_{yy} & S_{xy} \end{Bmatrix}^T, \quad \mathbf{E} = \begin{Bmatrix} E_{xx} & E_{yy} & E_{xy} \end{Bmatrix}^T \quad (15.35)$$

The linear term, $\delta \mathbf{e}$ of virtual strains in Eq. (15.19) can be written as,

$$\delta \mathbf{e} = \begin{Bmatrix} \delta u_{,x} \\ \delta v_{,y} \\ \delta u_{,y} + \delta v_{,x} \end{Bmatrix} + \begin{Bmatrix} \delta u_{,x} {}^t u_{,x} + \delta v_{,x} {}^t v_{,x} \\ \delta u_{,y} {}^t u_{,y} + \delta v_{,y} {}^t v_{,y} \\ \delta u_{,x} {}^t u_{,y} + \delta v_{,x} {}^t v_{,y} + \delta u_{,y} {}^t u_{,x} + \delta v_{,y} {}^t v_{,x} \end{Bmatrix} \quad (15.36)$$

Eq. (15.36) is expressed in terms of the product of the virtual displacement term, $\delta \mathbf{u}$ and the matrix, \mathbf{B}_L .

$$\delta \mathbf{e} = \mathbf{B}_{L0} \delta \mathbf{u} + \mathbf{B}_{L1} \delta \mathbf{u} = \mathbf{B}_L \delta \mathbf{u} \quad (15.37)$$

The linear term of incremental strains can also be expressed in a similar way.

$$\Delta \mathbf{e} = \mathbf{B}_{L0} \Delta \mathbf{u} + \mathbf{B}_{L1} \Delta \mathbf{u} = \mathbf{B}_L \Delta \mathbf{u} \quad (15.38)$$

From Eq. (15.37) and Eq. (15.38), the displacement-strain relationship matrix is written as,

$$\mathbf{B}_{L0} = \begin{bmatrix} N_{1,x} & 0 & \cdots & N_{N,x} & 0 \\ 0 & N_{1,y} & \cdots & 0 & N_{N,y} \\ N_{1,y} & N_{1,x} & \cdots & N_{N,y} & N_{N,x} \end{bmatrix} \quad (15.39)$$

$$\mathbf{B}_{L1} = \begin{bmatrix} {}^t u_{,x} N_{1,x} & {}^t v_{,x} N_{1,x} & \cdots \\ {}^t u_{,y} N_{1,y} & {}^t v_{,y} N_{1,y} & \cdots \\ ({}^t u_{,x} N_{1,y} + {}^t u_{,y} N_{1,x}) & ({}^t v_{,x} N_{1,y} + {}^t v_{,y} N_{1,x}) & \cdots \\ {}^t u_{,x} N_{n,x} & {}^t v_{,x} N_{n,x} & \\ {}^t u_{,y} N_{n,y} & {}^t v_{,y} N_{n,y} & \\ ({}^t u_{,x} N_{n,y} + {}^t u_{,y} N_{n,x}) & ({}^t v_{,x} N_{n,y} + {}^t v_{,y} N_{n,x}) & \end{bmatrix} \quad (15.40)$$

$\delta \mathbf{L}$, which composes the nonlinear term of the virtual strain in Eq. (15.19), is written as,

$$\delta \mathbf{L} = \left\{ \delta u_{,x} \quad \delta u_{,y} \quad \delta v_{,x} \quad \delta v_{,y} \right\}^T \quad (15.41)$$

Eq. (15.41) is expressed by the product of the virtual displacement term, $\delta \mathbf{u}$ and the matrix, \mathbf{B}_{NL} .

$$\delta \mathbf{L} = \mathbf{B}_{NL} \delta \mathbf{u} \quad (15.42)$$

$\Delta \mathbf{L}$ also can be expressed in a similar way.

$$\Delta \mathbf{L} = \mathbf{B}_{NL} \Delta \mathbf{u} \quad (15.43)$$

where,

$$\mathbf{B}_{NL} = \begin{bmatrix} N_{1,x} & 0 & \cdots & N_{N,x} & 0 \\ N_{1,y} & 0 & \cdots & N_{N,y} & 0 \\ 0 & N_{1,x} & \cdots & 0 & N_{N,x} \\ 0 & N_{1,y} & \cdots & 0 & N_{N,y} \end{bmatrix} \quad (15.44)$$

Substituting Eq. (15.37-38) and Eq. (15.42-43) into Eq. (15.19), we can obtain a linearized equilibrium equation.

$$\delta \mathbf{u}^T ({}^t \mathbf{K}_L + {}^t \mathbf{K}_{NL}) \Delta \mathbf{u} = \delta \mathbf{u}^T ({}^{t+\Delta t} \mathbf{f}_{ext}^e - {}^t \mathbf{f}_{int}^e) \quad (15.45)$$

Each term of Eq. (15.45) is as follows:

$$\begin{aligned}
{}^t\mathbf{K}_L^e &= \int_{A_e} {}^t\mathbf{B}_L^T \mathbf{D} \mathbf{B}_L dA \\
{}^t\mathbf{K}_{NL}^e &= \int_{A_e} {}^t {}^t\mathbf{B}_{NL}^T {}^t\hat{\mathbf{S}} {}^t\mathbf{B}_{NL} dA \\
{}^t\mathbf{f}_{\text{int}}^e &= \int_{A_e} {}^t {}^t\mathbf{B}_L^T {}^t\mathbf{S} dA
\end{aligned} \tag{15.46}$$

where,

t : thickness

The matrix, ${}^t\hat{\mathbf{S}}$ composed of stress components is as follows:

$${}^t\hat{\mathbf{S}} = \begin{bmatrix} {}^t\mathbf{S} & \mathbf{0} \\ \mathbf{0} & {}^t\mathbf{S} \end{bmatrix} \quad {}^t\mathbf{S} = \begin{bmatrix} {}^tS_{xx} & {}^tS_{xy} \\ {}^tS_{xy} & {}^tS_{yy} \end{bmatrix} \tag{15.47}$$

As a result of the plane stress element analysis, nodal stresses and strains exist similarly to linear analysis. In addition to the nodal results, stresses and strains at the integral points can be tabulated.

The order of integration is as follows:

- 3-node triangle : 1 point Gauss integration
- 4-node quadrilateral: 4 point Gauss integration
- 6-node triangle : 3 point Gauss integration
- 8-node quadrilateral: 9 point Gauss integration

15-4 Plate Element

Plate elements, which consider geometric nonlinearity, use a “degenerated plate approach”. Plate elements can consider in-plane deformation of the plane stress state and out-of-plane deformation consisting of flexure and shear. Plate elements reflecting geometric nonlinearity do not consider the drilling degree of freedom. They consider the shear deformation based on the Mindlin plate theory. Similar to the linear elements, the element types include 3, 4, 6 and 8 node elements.

Although tensile stresses in the thickness direction are generally ignored in plate elements, all the stress and strain components are considered in the process of formulation.

$$\mathbf{S} = \{S_{xx} \quad S_{yy} \quad S_{zz} \quad S_{xy} \quad S_{yz} \quad S_{zx}\}^T, \quad \mathbf{E} = \{E_{xx} \quad E_{yy} \quad E_{zz} \quad E_{xy} \quad E_{yz} \quad E_{zx}\}^T \quad (15.48)$$

The translation displacement at a position in an element can be separately expressed in terms of the translational displacement and rotation of the neutral plane.

$$\mathbf{U} = \mathbf{u}_0 + \mathbf{t} \quad (15.49)$$

where, the vector, \mathbf{t} represents the effect of rotation.

$$\mathbf{t} = \frac{t}{2} \zeta (\mathbf{T} - \bar{\mathbf{T}}) \quad (15.50)$$

Here,

\mathbf{T} : deformed unit shell normal vector

$\bar{\mathbf{T}}$: undeformed unit shell normal vector

The linear term, $\delta \mathbf{e}$ of virtual stains in Eq. (15.19) can be written as,

$$\begin{aligned}
\delta \mathbf{e} = & \left\{ \begin{array}{c} \delta(u_{0,x} + t_{x,x}) \\ \delta(v_{0,y} + t_{y,y}) \\ \delta(w_{0,z} + t_{z,z}) \\ \delta(u_{0,y} + t_{x,y}) + \delta(v_{0,x} + t_{y,x}) \\ \delta(v_{0,z} + t_{y,z}) + \delta(w_{0,y} + t_{z,y}) \\ \delta(w_{0,x} + t_{z,x}) + \delta(u_{0,z} + t_{x,z}) \end{array} \right\} \\
& + \left\{ \begin{array}{c} \delta(\mathbf{u}_{0,x} + \mathbf{t}_{,x})^T (\mathbf{t}_{0,x} + \mathbf{t}_{,x}) \\ \delta(\mathbf{u}_{0,y} + \mathbf{t}_{,y})^T (\mathbf{t}_{0,y} + \mathbf{t}_{,y}) \\ \delta(\mathbf{u}_{0,z} + \mathbf{t}_{,z})^T (\mathbf{t}_{0,z} + \mathbf{t}_{,z}) \\ \delta(\mathbf{u}_{0,x} + \mathbf{t}_{,x})^T (\mathbf{t}_{0,y} + \mathbf{t}_{,y}) + \delta(\mathbf{u}_{0,y} + \mathbf{t}_{,y})^T (\mathbf{t}_{0,x} + \mathbf{t}_{,x}) \\ \delta(\mathbf{u}_{0,y} + \mathbf{t}_{,y})^T (\mathbf{t}_{0,z} + \mathbf{t}_{,z}) + \delta(\mathbf{u}_{0,z} + \mathbf{t}_{,z})^T (\mathbf{t}_{0,y} + \mathbf{t}_{,y}) \\ \delta(\mathbf{u}_{0,z} + \mathbf{t}_{,z})^T (\mathbf{t}_{0,x} + \mathbf{t}_{,x}) + \delta(\mathbf{u}_{0,x} + \mathbf{t}_{,x})^T (\mathbf{t}_{0,z} + \mathbf{t}_{,z}) \end{array} \right\} \quad (15.51)
\end{aligned}$$

$\delta \mathbf{L}$, which composes the nonlinear term of the virtual strain in Eq. (15.19), is written as,

$$\delta \mathbf{L} = \left\{ \begin{array}{c} \delta(u_{0,x} + t_{x,x}) \\ \delta(u_{0,y} + t_{x,y}) \\ \delta(u_{0,z} + t_{x,z}) \\ \delta(v_{0,x} + t_{y,x}) \\ \delta(v_{0,y} + t_{y,y}) \\ \delta(v_{0,z} + t_{y,z}) \\ \delta(w_{0,x} + t_{z,x}) \\ \delta(w_{0,y} + t_{z,y}) \\ \delta(w_{0,z} + t_{z,z}) \end{array} \right\} \quad (15.52)$$

The matrices \mathbf{B}_L and \mathbf{B}_{NL} , which are required for real calculation, are not explained in this section. For the calculation of the element stiffness or forces, the stresses and strains in Eq. (15.48) are transformed into the coordinate system in contact with the element's neutral plane. The method of presenting the rotational displacement and the characteristics of the elements of different numbers of nodes are explained below.

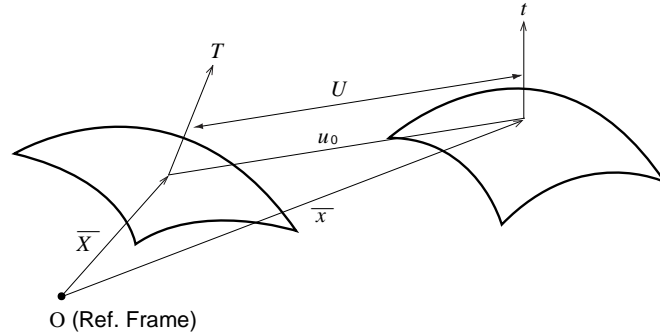


Figure 15-(3) Initial and current configurations of a plate

All the 3 translational displacements and 3 rotational displacements are considered in the global coordinate system for a flat plate having 3 nodes or 4 nodes. However, the components perpendicular to the vector in the thickness direction in incremental rotation displacements are excluded through the process of orthogonalization.

$$\mathbf{u}_i = \{u_i \quad v_i \quad w_i \quad \theta_{xi} \quad \theta_{yi} \quad \theta_{zi}\}^T \quad (15.53)$$

The 4-node plate element uses the Lagrangian shape function. The vector in the thickness direction deformed by finite rotation is calculated by accumulating the rotational matrix such as $\mathbf{T} = \delta\mathbf{R}\mathbf{R}^T$. The increment of rotational stiffness, $\delta\mathbf{R}$ is written as,

$$\delta\mathbf{R} = \mathbf{I} + \frac{\sin \delta\theta}{\delta\theta} \mathbf{S}(\delta\theta) + \frac{1 - \cos \delta\theta}{\delta\theta^2} \mathbf{S}(\delta\theta) \mathbf{S}(\delta\theta) \quad (15.54)$$

where,

$\mathbf{S}(\delta\theta)$: skew symmetric matrix

Shear strains are calculated from the ANS (assumed natural strain) at the 4 sides as in Fig. 15-(4), and the locking phenomenon is prevented.

$$\gamma_{\xi\xi} = \frac{1}{2}(1-\eta)\gamma_{\xi\xi}(0,-1) + \frac{1}{2}(1+\eta)\gamma_{\xi\xi}(0,1) \quad (15.55)$$

$$\gamma_{\xi\eta} = \frac{1}{2}(1-x)\gamma_{\xi\eta}(-1,0) + \frac{1}{2}(1+x)\gamma_{\xi\eta}(1,0) \quad (15.56)$$

$$\begin{Bmatrix} \gamma_{z\alpha} \\ \gamma_{z\beta} \end{Bmatrix} = \mathbf{P} \begin{Bmatrix} \gamma_{\xi\xi} \\ \gamma_{\xi\eta} \end{Bmatrix} \quad (15.57)$$

where,

\mathbf{P} : coordinate transform matrix

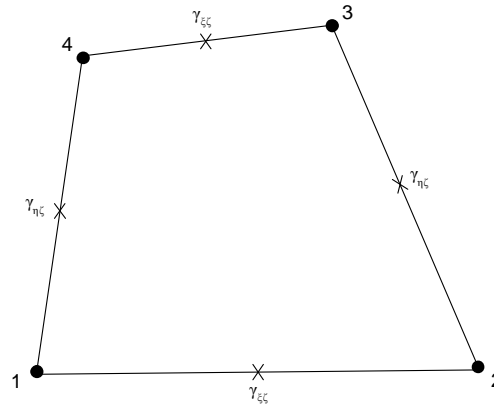


Figure 15(4) Tying point for interpolation of assumed shear strain

The calculation of the 3-node element uses the degenerated method, which makes the 4th node of the 4-node element to have the same coordinates as the 3rd node.

Curved plate elements consisted of 6 nodes or 8 nodes have 3 translational displacements and the rotations about the two in-plane directions, \mathbf{V}_{1i} and \mathbf{V}_{2i} defined at a node in the global coordinate system. \mathbf{V}_{1i} and \mathbf{V}_{2i} are defined in the formulation of linear elements.

$$\mathbf{u}_i = \{u_i \quad v_i \quad w_i \quad \theta_{1i} \quad \theta_{2i}\}^T \quad (15.58)$$

A curved plate uses the Lagrangian shape function. The vector in the thickness direction deformed by finite rotation is calculated by accumulating the rotational matrix in the same way as for a flat plate element. Considering only the components in the \mathbf{V}_{1i} and \mathbf{V}_{2i} directions among the incremental rotation displacements, the effect of orthogonalization is implicitly obtained.

The analysis output of geometric nonlinear plate elements includes nodal stresses/strains and element internal forces as for the linear analysis. In addition, stresses and strains at Gauss points can be also tabulated. Stresses and strains are calculated at two points across the thickness in the z axis direction. The basic locations are at the top ($z = t/2$) and the bottom ($z = -t/2$) on the basis of the thickness associated with in-plane behavior. The plate elements, which consider geometric nonlinearity, carry out three point Simpson integration in the thickness direction, and the order of integration for the area is as follows:

- 3-node triangle : 1 point Gauss integration
- 4-node quadrilateral: 4 point Gauss integration
- 6-node triangle : 3 point Gauss integration
- 8-node quadrilateral : 4 point Gauss integration

15-5 Plane Strain Element

Plane strain elements, which consider geometric nonlinearity, consist of isoparametric elements of 3, 4, 6 and 8 nodes. Each element uses a shape function identical to that of the linear element, and incompatible modes are not used. A plane strain element has translational displacements, u and v in the Element Coordinate System. The process of developing formulation is identical to that for plane stress elements. The finally linearized equilibrium equation for plain stress elements is derived as,

$$\delta \mathbf{u}^T ({}^t \mathbf{K}_L + {}^t \mathbf{K}_{NL}) \Delta \mathbf{u} = \delta \mathbf{u}^T ({}^{t+\Delta t} \mathbf{f}_{ext}^e - {}^t \mathbf{f}_{int}^e) \quad (15.59)$$

Except for the matrix, \mathbf{D} , which defines the relationship of stress and strain, each term of Eq. (15.59) is identical to that of plane stress elements. The analysis output of geometric nonlinear plane strain elements includes nodal stresses and strains as for the linear analysis. In addition, stresses and strains at Gauss points can be also tabulated. The order of integration is as follows:

- 3-node triangle: 1 point Gauss integration
- 4-node quadrilateral: 4 point Gauss integration
- 6-node triangle: 3 point Gauss integration
- 8-node quadrilateral: 9 point Gauss integration

15-6 Axisymmetric Element

Axisymmetric elements, which consider geometric nonlinearity, consist of isoparametric elements of 3, 4, 6 and 8 nodes. Each element uses a shape function identical to that of the linear element. An axisymmetric element has translational displacements, u and v in the Element Coordinate System, which are expressed using the shape function, N_i , as follows:

$$u = \sum_{i=1}^N N_i u_i, \quad v = \sum_{i=1}^N N_i v_i \quad (15.60)$$

The stresses and strains used in axisymmetric elements can be expressed as,

$$\mathbf{S} = \{S_{xx} \quad S_{yy} \quad S_{xy} \quad S_{zz}\}^T, \quad \mathbf{E} = \{E_{xx} \quad E_{yy} \quad E_{xy} \quad E_{zz}\}^T \quad (15.61)$$

The linear term, $\delta \mathbf{e}$ of virtual strains in Eq. (15.19) can be written as,

$$\delta \mathbf{e} = \begin{Bmatrix} \delta u_{,x} \\ \delta v_{,y} \\ \delta u_{,y} + \delta v_{,x} \\ \frac{\delta u}{r} \end{Bmatrix} + \begin{Bmatrix} \delta u_{,x} {}^t u_{,x} + \delta v_{,x} {}^t v_{,x} \\ \delta u_{,y} {}^t u_{,y} + \delta v_{,y} {}^t v_{,y} \\ \delta u_{,x} {}^t u_{,y} + \delta v_{,x} {}^t v_{,y} + \delta u_{,y} {}^t u_{,x} + \delta v_{,y} {}^t v_{,x} \\ \frac{\delta u {}^t u}{r^2} \end{Bmatrix} \quad (15.62)$$

Eq. (15.62) is expressed in terms of the product of the virtual displacement term, $\delta \mathbf{u}$ and the matrix, \mathbf{B}_L .

$$\delta \mathbf{e} = \mathbf{B}_{L0} \delta \mathbf{u} + \mathbf{B}_{L1} \delta \mathbf{u} = \mathbf{B}_L \delta \mathbf{u} \quad (15.63)$$

The linear term of incremental strains can also be expressed in a similar way.

$$\Delta \mathbf{e} = \mathbf{B}_{L0} \Delta \mathbf{u} + \mathbf{B}_{L1} \Delta \mathbf{u} = \mathbf{B}_L \Delta \mathbf{u} \quad (15.64)$$

From Eq. (15.63) and Eq. (15.64), the displacement-strain relationship matrix is written as,

$$\mathbf{B}_{L0} = \begin{bmatrix} N_{1,x} & 0 & \cdots & N_{N,x} & 0 \\ 0 & N_{1,y} & \cdots & 0 & N_{N,y} \\ N_{1,y} & N_{1,x} & \cdots & N_{N,y} & N_{N,x} \\ \frac{N_1}{r} & 0 & \cdots & \frac{N_N}{r} & 0 \end{bmatrix} \quad (15.65)$$

$$\mathbf{B}_{L1} = \begin{bmatrix} {}^t u_{,x} N_{1,x} & {}^t v_{,x} N_{1,x} & \cdots \\ {}^t u_{,y} N_{1,y} & {}^t v_{,y} N_{1,y} & \cdots \\ ({}^t u_{,x} N_{1,y} + {}^t u_{,y} N_{1,x}) & ({}^t v_{,x} N_{1,y} + {}^t v_{,y} N_{1,x}) & \cdots \\ {}^t u \frac{N_1}{r^2} & 0 & \cdots \\ {}^t u_{,x} N_{N,x} & {}^t v_{,x} N_{N,x} & \cdots \\ {}^t u_{,y} N_{N,y} & {}^t v_{,y} N_{N,y} & \cdots \\ ({}^t u_{,x} N_{N,y} + {}^t u_{,y} N_{N,x}) & ({}^t v_{,x} N_{N,y} + {}^t v_{,y} N_{N,x}) & \cdots \\ {}^t u \frac{N_N}{r^2} & 0 & \cdots \end{bmatrix} \quad (15.66)$$

$\delta \mathbf{L}$, which composes the nonlinear term of the virtual strain in Eq. (15.19), is written as,

$$\delta \mathbf{L} = \left\{ \delta u_{,x} \quad \delta u_{,y} \quad \delta v_{,x} \quad \delta v_{,y} \quad \frac{\delta u}{r} \right\}^T \quad (15.67)$$

Eq. (15.67) is expressed by the product of the virtual displacement term, $\delta \mathbf{u}$ and the matrix,

\mathbf{B}_{NL} .

$$\delta \mathbf{L} = \mathbf{B}_{NL} \delta \mathbf{u} \quad (15.68)$$

$\Delta \mathbf{L}$ also can be expressed in a similar way.

$$\Delta \mathbf{L} = \mathbf{B}_{NL} \Delta \mathbf{u} \quad (15.69)$$

where,

$$\mathbf{B}_{NL} = \begin{bmatrix} N_{1,x} & 0 & \cdots & N_{N,x} & 0 \\ N_{1,y} & 0 & \cdots & N_{N,y} & 0 \\ 0 & N_{1,x} & \cdots & 0 & N_{N,x} \\ 0 & N_{1,y} & \cdots & 0 & N_{N,y} \\ \frac{N_1}{r} & 0 & \cdots & \frac{N_N}{r} & 0 \end{bmatrix} \quad (15.70)$$

Substituting Eq. (15.63-64) and Eq. (15.68-69) into Eq. (15.19), we can obtain a linearized equilibrium equation.

$$\delta \mathbf{u}^T ({}^t \mathbf{K}_L + {}^t \mathbf{K}_{NL}) \Delta \mathbf{u} = \delta \mathbf{u}^T ({}^{t+\Delta t} \mathbf{f}_{ext}^e - {}^t \mathbf{f}_{int}^e) \quad (15.71)$$

Each term of Eq. (15.71) is as follows:

$$\begin{aligned} {}^t \mathbf{K}_L &= \int_{A_e} r \mathbf{B}_L^T \mathbf{D} \mathbf{B}_L dA \\ {}^t \mathbf{K}_{NL} &= \int_{A_e} r {}^t \mathbf{B}_{NL}^T {}^t \hat{\mathbf{S}} {}^t \mathbf{B}_{NL} dA \\ {}^t \mathbf{f}_{int}^e &= \int_{A_e} r {}^t \mathbf{B}_L^T {}^t \mathbf{S} dA \end{aligned} \quad (15.72)$$

where,

$${}^t \hat{\mathbf{S}} = \begin{bmatrix} {}^t S_{xx} & {}^t S_{xy} & \mathbf{0} \\ {}^t S_{xy} & {}^t S_{yy} & \mathbf{0} \\ \mathbf{0} & \mathbf{0} & {}^t \mathbf{S} \end{bmatrix} \quad {}^t \mathbf{S} = \begin{bmatrix} {}^t S_{xx} & {}^t S_{xy} & 0 \\ {}^t S_{xy} & {}^t S_{yy} & 0 \\ 0 & 0 & {}^t S_{zz} \end{bmatrix} \quad (15.73)$$

As a result of the axisymmetric element analysis, nodal stresses and strains exist similarly to linear analysis. In addition to the nodal results, stresses and strains at the integral points can be tabulated.

The order of integration is as follows:

- 3-node triangle : 1 point Gauss integration
- 4-node quadrilateral: 4 point Gauss integration
- 6-node triangle : 3 point Gauss integration
- 8-node quadrilateral: 9 point Gauss integration

15-7 Solid Element

Solid elements, which consider geometric nonlinearity, consist of isoparametric elements of 4, 6, 8, 10, 15 and 20 nodes. Each element uses a shape function identical to that of the linear element, and incompatible modes are not used. A solid element has translational displacements, u , v and w in the Element Coordinate System, which are expressed using the shape function, N_i , as follows:

$$u = \sum_{i=1}^N N_i u_i, \quad v = \sum_{i=1}^N N_i v_i, \quad w = \sum_{i=1}^N N_i w_i \quad (15.74)$$

The stresses and strains used in solid elements can be expressed as,

$$\mathbf{S} = \begin{Bmatrix} S_{xx} & S_{yy} & S_{zz} & S_{xy} & S_{yz} & S_{zx} \end{Bmatrix}^T, \quad \mathbf{E} = \begin{Bmatrix} E_{xx} & E_{yy} & E_{zz} & E_{xy} & E_{yz} & E_{zx} \end{Bmatrix}^T \quad (15.75)$$

The linear term, $\delta \mathbf{e}$ of virtual strains in Eq. (15.19) can be written as,

$$\delta \mathbf{e} = \begin{Bmatrix} \delta u_{,x} \\ \delta v_{,y} \\ \delta w_{,z} \\ \delta u_{,y} + \delta v_{,x} \\ \delta v_{,z} + \delta w_{,y} \\ \delta w_{,z} + \delta u_{,x} \end{Bmatrix} + \begin{Bmatrix} \delta u_{,x} {}^t u_{,x} + \delta v_{,x} {}^t v_{,x} + \delta w_{,x} {}^t w_{,x} \\ \delta u_{,y} {}^t u_{,y} + \delta v_{,y} {}^t v_{,y} + \delta w_{,y} {}^t w_{,y} \\ \delta u_{,z} {}^t u_{,z} + \delta v_{,z} {}^t v_{,z} + \delta w_{,z} {}^t w_{,z} \\ \delta u_{,x} {}^t u_{,y} + \delta v_{,x} {}^t v_{,y} + \delta w_{,x} {}^t w_{,y} + \delta u_{,y} {}^t u_{,x} + \delta v_{,y} {}^t v_{,x} + \delta w_{,y} {}^t w_{,x} \\ \delta u_{,y} {}^t u_{,z} + \delta v_{,y} {}^t v_{,z} + \delta w_{,y} {}^t w_{,z} + \delta u_{,z} {}^t u_{,y} + \delta v_{,z} {}^t v_{,y} + \delta w_{,z} {}^t w_{,y} \\ \delta u_{,z} {}^t u_{,x} + \delta v_{,z} {}^t v_{,x} + \delta w_{,z} {}^t w_{,x} + \delta u_{,x} {}^t u_{,z} + \delta v_{,x} {}^t v_{,z} + \delta w_{,x} {}^t w_{,z} \end{Bmatrix} \quad (15.76)$$

Eq. (15.76) is expressed in terms of the product of the virtual displacement term, $\delta \mathbf{u}$ and the matrix, \mathbf{B}_L .

$$\delta \mathbf{e} = \mathbf{B}_{L0} \delta \mathbf{u} + \mathbf{B}_{L1} \delta \mathbf{u} = \mathbf{B}_L \delta \mathbf{u} \quad (15.77)$$

The linear term of incremental strains can also be expressed in a similar way.

$$\Delta \mathbf{e} = \mathbf{B}_{L0} \Delta \mathbf{u} + \mathbf{B}_{L1} \Delta \mathbf{u} = \mathbf{B}_L \Delta \mathbf{u} \quad (15.78)$$

From Eq. (15.77) and Eq. (15.78), the displacement-strain relationship matrix is written as,

$$\mathbf{B}_{L0} = \begin{bmatrix} N_{1,x} & 0 & 0 & N_{2,x} & \cdots & N_{N,x} & 0 & 0 \\ 0 & N_{1,y} & 0 & 0 & \cdots & 0 & N_{N,y} & 0 \\ 0 & 0 & N_{1,z} & 0 & \cdots & 0 & 0 & N_{N,z} \\ N_{1,y} & N_{1,x} & 0 & N_{2,y} & \cdots & N_{N,y} & N_{N,x} & 0 \\ 0 & N_{1,z} & N_{1,y} & 0 & \cdots & 0 & N_{N,z} & N_{N,y} \\ N_{1,z} & 0 & N_{1,x} & N_{2,z} & \cdots & N_{N,z} & 0 & N_{N,x} \end{bmatrix} \quad (15.79)$$

$$\mathbf{B}_{L1} = \begin{bmatrix} {}^t u_{,x} N_{1,x} & {}^t v_{,x} N_{1,x} & {}^t w_{,x} N_{1,x} & {}^t u_{,x} N_{2,x} & \cdots & {}^t u_{,x} N_{N,1} \\ {}^t u_{,y} N_{1,y} & {}^t v_{,y} N_{1,y} & {}^t w_{,y} N_{1,y} & {}^t u_{,y} N_{2,y} & \cdots & {}^t u_{,y} N_{N,2} \\ {}^t u_{,z} N_{1,z} & {}^t v_{,z} N_{1,z} & {}^t w_{,z} N_{1,z} & {}^t u_{,z} N_{2,z} & \cdots & {}^t u_{,z} N_{N,3} \\ {}^t u_{,x} N_{1,y} + {}^t u_{,y} N_{1,x} & {}^t v_{,x} N_{1,y} + {}^t v_{,y} N_{1,x} & {}^t w_{,x} N_{1,y} + {}^t w_{,y} N_{1,x} & {}^t u_{,x} N_{2,y} + {}^t u_{,y} N_{2,x} & \cdots & {}^t w_{,x} N_{N,y} + {}^t w_{,y} N_{N,x} \\ {}^t u_{,y} N_{1,z} + {}^t u_{,z} N_{1,y} & {}^t v_{,y} N_{1,z} + {}^t v_{,z} N_{1,y} & {}^t w_{,y} N_{1,z} + {}^t w_{,z} N_{1,y} & {}^t u_{,y} N_{2,z} + {}^t u_{,z} N_{2,y} & \cdots & {}^t w_{,y} N_{N,z} + {}^t w_{,z} N_{N,y} \\ {}^t u_{,x} N_{1,z} + {}^t u_{,z} N_{1,x} & {}^t v_{,x} N_{1,z} + {}^t v_{,z} N_{1,x} & {}^t w_{,x} N_{1,z} + {}^t w_{,z} N_{1,x} & {}^t u_{,x} N_{3,z} + {}^t u_{,z} N_{3,x} & \cdots & {}^t w_{,x} N_{N,z} + {}^t w_{,z} N_{N,x} \end{bmatrix} \quad (15.80)$$

$\delta \mathbf{L}$, which composes the nonlinear term of the virtual strain in Eq. (15.19), is written as,

$$\delta \mathbf{L} = \left\{ \delta u_{,x} \quad \delta u_{,y} \quad \delta u_{,z} \quad \delta v_{,x} \quad \delta v_{,y} \quad \delta v_{,z} \quad \delta w_{,x} \quad \delta w_{,y} \quad \delta w_{,z} \right\}^T \quad (15.81)$$

Eq. (15.81) is expressed by the product of the virtual displacement term, $\delta \mathbf{u}$ and the matrix, \mathbf{B}_{NL} .

$$\delta \mathbf{L} = \mathbf{B}_{NL} \delta \mathbf{u} \quad (15.82)$$

$\Delta \mathbf{L}$ also can be expressed in a similar way.

$$\Delta \mathbf{L} = \mathbf{B}_{NL} \Delta \mathbf{u} \quad (15.83)$$

where,

$$\mathbf{B}_{NL} = \begin{bmatrix} \tilde{\mathbf{B}}_1 & \mathbf{0} & \mathbf{0} & \tilde{\mathbf{B}}_2 & \cdots & \tilde{\mathbf{B}}_N & \mathbf{0} & \mathbf{0} \\ \mathbf{0} & \tilde{\mathbf{B}}_1 & \mathbf{0} & \mathbf{0} & \cdots & \mathbf{0} & \tilde{\mathbf{B}}_N & \mathbf{0} \\ \mathbf{0} & \mathbf{0} & \tilde{\mathbf{B}}_1 & \mathbf{0} & \cdots & \mathbf{0} & \mathbf{0} & \tilde{\mathbf{B}}_N \end{bmatrix} \quad (15.84)$$

$$\tilde{\mathbf{B}}_i = \{N_{i,x} \quad N_{i,y} \quad N_{i,z}\}^T$$

Substituting Eq. (15.77-78) and Eq. (15.82-83) into Eq. (15.19), we can obtain a linearized equilibrium equation.

$$\delta \mathbf{u}^T ({}^t \mathbf{K}_L^e + {}^t \mathbf{K}_{NL}^e) \Delta \mathbf{u} = \delta \mathbf{u}^T ({}^{t+\Delta t} \mathbf{f}_{ext}^e - {}^t \mathbf{f}_{int}^e) \quad (15.85)$$

Each term of Eq. (15.85) is as follows:

$$\begin{aligned} {}^t \mathbf{K}_L^e &= \int_{V_e} \mathbf{B}_L^T \mathbf{D} \mathbf{B}_L dV \\ {}^t \mathbf{K}_{NL}^e &= \int_{V_e} {}^t \mathbf{B}_{NL}^T {}^t \hat{\mathbf{S}} {}^t \mathbf{B}_{NL} dV \\ {}^t \mathbf{f}_{int}^e &= \int_{V_e} {}^t \mathbf{B}_L^T {}^t \mathbf{S} dV \end{aligned} \quad (15.86)$$

where,

$${}^t \hat{\mathbf{S}} = \begin{bmatrix} {}^t \mathbf{S} & \mathbf{0} & \mathbf{0} \\ \mathbf{0} & {}^t \mathbf{S} & \mathbf{0} \\ \mathbf{0} & \mathbf{0} & {}^t \mathbf{S} \end{bmatrix} \quad {}^t \mathbf{S} = \begin{bmatrix} {}^t S_{xx} & {}^t S_{xy} & {}^t S_{zx} \\ {}^t S_{xy} & {}^t S_{yy} & {}^t S_{yz} \\ {}^t S_{zx} & {}^t S_{yz} & {}^t S_{zz} \end{bmatrix} \quad (15.87)$$

As a result of the solid element analysis, nodal stresses and strains exist similarly to linear analysis. In addition to the nodal results, stresses and strains at the integral points can be tabulated.

The order of integration is as follows:

- 4-node tetrahedron: 1 point Gauss integration
- 6-node pentahedron: 6 point Gauss integration
- 8-node hexahedron: 8 point Gauss integration
- 10-node tetrahedron: 4 point Gauss integration
- 15-node pentahedron: 9 point Gauss integration
- 20-node hexahedron: 27 point gauss integration

Chapter 16. Iteration Methods

16-1 Introduction

In nonlinear finite element analysis, the relation between a force vector and displacement vector is no longer linear. For several reasons, for instance in case of material nonlinearity, the relation becomes nonlinear, and the displacements often depend on the displacements at earlier stages, e.g. in case of plastic material behavior. Just as with a linear analysis, we wish to calculate a displacement vector that equilibrates the internal and external forces. In the linear case, the solution vector can be calculated right away, but not in the nonlinear case. To determine the state of equilibrium, we not only make the problems discrete in space (with finite elements), but also in time (with increments). To achieve equilibrium at the end of each increment, we can use an iterative solution algorithm. The combination of both is called an incremental-iterative solution procedure.

In this chapter, we will consider a vector of displacement increments that must yield an equilibrium condition between internal and external forces, and a stiffness matrix relating internal forces to incremental displacements. In reality, the physical meaning of items in the ‘displacement’ vector can also be e.g. a velocity or a Lagrange multiplier. In this chapter, the physical meaning of what we refer to as the displacement and force vectors and the stiffness matrix is irrelevant. Most often, it represents a continuous system that is approximated using the Principle of Virtual Work, Galerkin discretization or another method. A good starting point is to strive for an equilibrium state in which the internal force vector equals the external force vector, satisfying boundary conditions.

$$\mathbf{f}_{\text{int}} = \mathbf{f}_{\text{ext}} \quad (16.1)$$

$$\mathbf{u}_i = \mathbf{u}_i^0 \quad (i \text{ Prescribed}) \quad (16.2)$$

In nonlinear analysis, the internal force vector usually depends nonlinearly on the displacements (e.g. nonlinear elasticity). It can also depend on the displacements in the history. This is e.g. the

case if the material is ‘path dependent’ such as in plasticity and if large displacements facilitate multiple equilibrium solutions. The external force vector can also be displacement dependent. This is the case in geometrical nonlinear analysis, if the magnitude or the direction of the loading depends on the displacements such as with pressure on a wall. We can now write,

$$\mathbf{f}_{int}(\mathbf{u}, history) = \mathbf{f}_{ext}(\mathbf{u}) \quad (16.2)$$

The system described above is already discretized in space. To enable a numerical solution, a time discretization is performed as well. Here ‘time’ can have a real physical meaning e.g. in a creep analysis or it can be a pseudo-time, only to describe a sequence of situations. Starting at time t with an approximated solution ${}^t\mathbf{u}$, a solution ${}^{t+\Delta t}\mathbf{u}$ is searched for which (16.2) holds. Within the time-increment, only the displacements at start and end are known. The internal force vector, which may be path dependent, is calculated from the situation at time t , the time increment Δt and the displacement increment $\Delta\mathbf{u}$. The external forces only depend on the current geometry. If we consider only one increment, the time increment and the situation at the start of the increment (history) are fixed. The equilibrium equation within the increment then only depends on $\Delta\mathbf{u}$. We can write the nonlinear problem as: find $\Delta\mathbf{u}$ such that

$${}^{t+\Delta t}\mathbf{u} = {}^t\mathbf{u} + \Delta\mathbf{u} \quad (16.3)$$

and, with \mathbf{g} as the out-of-balance force vector (the residual forces).

$$\mathbf{g}(\Delta\mathbf{u}) = \mathbf{f}_{ext}(\Delta\mathbf{u}) - \mathbf{f}_{int}(\Delta\mathbf{u}) = \mathbf{0} \quad (16.3)$$

16-1-1 Iterative Procedures

A purely incremental method usually leads to inaccurate solutions in nonlinear analysis, unless very small step sizes are used. In an iterative process, the errors that occur can be reduced successively. This in fact realizes an implicit procedure. The allowable step size is usually higher

than in case of a process without iterations (e.g. an explicit process). The general procedure is the same for all iteration processes (Fig. 16-1). In all procedures, the total displacement increment $\Delta \mathbf{u}$ is adapted iteratively by iterative increments $\delta \mathbf{u}$ until equilibrium is reached, up to a prescribed tolerance. Indicating the iteration number with a right subscript, the incremental displacements at iteration $i + 1$ are calculated from

$$\Delta \mathbf{u}_{i+1} = \Delta \mathbf{u}_i + \delta \mathbf{u}_{i+1} \quad (16.4)$$

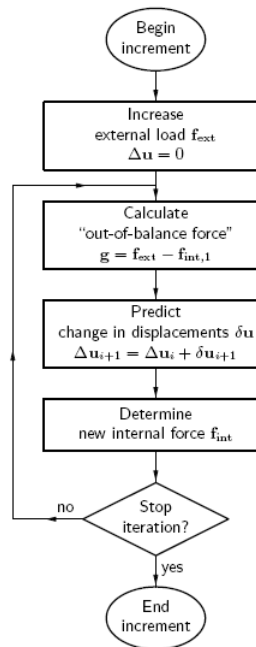


Figure 16-(1) Iteration process

The difference between several procedures is the way in which $\delta \mathbf{u}$ is determined. The iterative increments are calculated by use of a 'stiffness matrix' \mathbf{K} that represents some kind of linearized form of the relation between the force vector and the displacement vector. The stiffness matrix used can be changed at each iteration. The matrix that is used in iteration i is called \mathbf{K}_i . A direct

approach is to determine the iterative increments by,

$$\delta \mathbf{u}_i = \mathbf{K}_i^{-1} \mathbf{g}_i \quad (16.5)$$

where, \mathbf{g}_i is the out-of-balance force vector at the start of iteration i . In this case, a linear set of equations are solved at each iteration.

Next sections describe the methods that are available in MIDAS - the *Initial stiffness* method, the *Newton-Raphson* method, the *Modified Newton-Raphson* method, the *Arc-length* method and the *Displacement control*.

16-2 Initial Stiffness Method

The initial stiffness method uses the stiffness matrix, calculated at the beginning of the analysis stage. And regardless of the load level, the stiffness matrix remains unchanged during the entire process of analysis. This method is used for those analyses, which tend to exhibit instability. Stable solutions are generally found, but relatively small increments result in slow convergence.

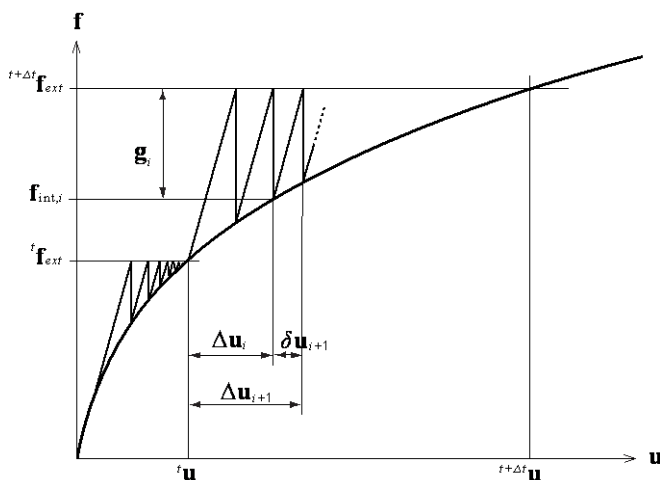


Figure 16-(2) Initial Stiffness iteration

16-3 Newton-Raphson Method

Within the class of Newton–Raphson methods, generally two subclasses are distinguished, the *Regular* and the *Modified* Newton–Raphson method. Both methods use Eq. (16.5) to determine the iterative increment of the displacement vector. In a Newton–Raphson method, the stiffness matrix \mathbf{K}_i represents the tangential stiffness of the structure.

$$\mathbf{K}_i = \frac{\partial \mathbf{g}}{\partial \Delta \mathbf{u}} \quad (16.6)$$

The difference between the Regular and the Modified Newton–Raphson method is the point at which the stiffness matrix is evaluated.

16-3-1 Regular Newton-Raphson

In the Regular Newton–Raphson iteration, the stiffness relation Eq. (16.6) is evaluated at each iteration (Fig. 16-3). This means that the prediction of Eq. (16.5) is based on the last known or predicted situation, even if this is not an equilibrium state. The Regular Newton–Raphson method yields a quadratic convergence characteristic, which means that the method converges to the final solution within only a few iterations. A disadvantage of the method is that the stiffness matrix has to be set up at each iteration and, if a direct solver is used to solve the linear set of equations, the time consuming decomposition of the matrix has to be performed every iteration as well. Moreover, the quadratic convergence is only guaranteed if a correct stiffness matrix is used and if the prediction is already in the neighborhood of the final solution. If the initial prediction is far from the final solution, the method easily fails to converge. In summary, the Regular Newton–Raphson method usually needs only a few iterations, but each iteration is relatively time consuming.

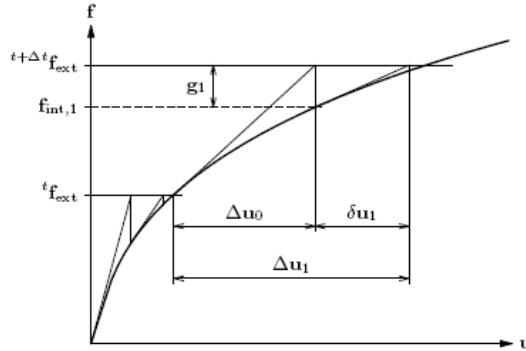


Figure 16-3) Regular Newton-Raphson iteration

16-3-2 Modified Newton-Raphson

The Modified Newton–Raphson method only evaluates the stiffness relation (16.6) at the start of the increment (Fig. 16-4). This means that the prediction is always based on a converged equilibrium state. Usually, Modified Newton–Raphson converges slower to equilibrium than Regular Newton–Raphson. However, for each iteration only the prediction of the iterative incremental displacements and the internal force vector has to be calculated. It is not necessary to set up a new stiffness matrix. If a direct solver for the linear set of equations is used, it is not necessary to perform the decomposition again; only the relatively fast substitution part will be needed. In summary, *the Modified Newton–Raphson method usually needs more iterations, but every iteration is faster than that in Regular Newton–Raphson.*

In situations where Regular Newton–Raphson no longer converges, the Modified Newton–Raphson process can sometimes still converge. Small variations of both processes are possible by

using the linear or previous stiffness for the first prediction and by setting up the current stiffness matrix after the first prediction. If unloading occurs, it can be advantageous to return to the linear stiffness, e.g. in a plasticity analysis.

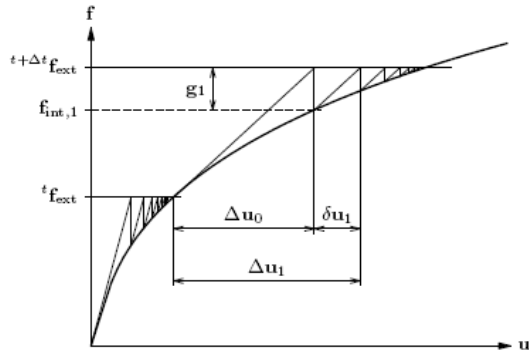


Figure 16-(4) Modified Newton-Raphson iteration

16-4 Arc-Length Method

In an ordinary iteration process, the predictions for the displacement increments can become very large. This is the case especially if the load–displacement curve is almost horizontal. If a fixed load increment is prescribed, this results in very large predictions for the displacements. The problem can be overcome with the use of an *Arc-length* method. Using the Arc-length method, the *snap through* behavior of Fig. (16-5a) can be analyzed, just as the displacement control could. However, it is possible to define a system of loads that could not be substituted by prescribed displacements. Moreover, the Arc-length method is also capable of passing snap-back behavior (Fig. 16-5b), where the displacement-control scheme fails.

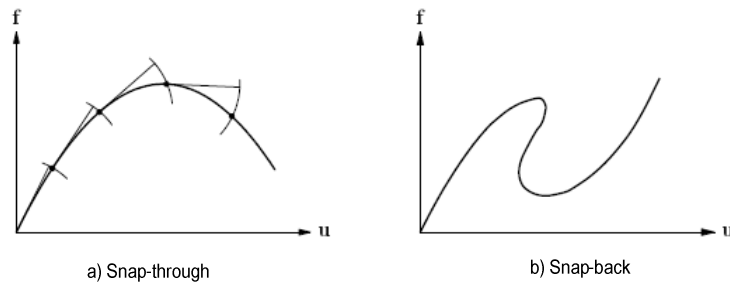


Figure 16-5) Arc-length control

The Arc-length method constrains the norm of the incremental displacements to a prescribed value. This is done by simultaneously adapting the size of the increment. Note that the size is adapted within the iteration process and is not fixed at the moment the increment starts. For this purpose, we define the external force vector at the start of the increment as \mathbf{f}_{ext} and the increment of the external force vector as $\Delta\lambda_i \hat{\mathbf{f}}$. The load factor $\Delta\lambda_i$ multiplies a unit load $\hat{\mathbf{f}}$ and can be changed at each iteration. Substitution in (16.5) results in,

$$\delta \mathbf{u}_i = \mathbf{K}_i^{-1} (\Delta \lambda_i \hat{\mathbf{f}} + {}^t \mathbf{f}_{int} - \mathbf{f}_{int,i}) \quad (16.7)$$

The solution $\delta \mathbf{u}_i$ is now split in two parts.

$$\delta \mathbf{u}_i^I = \mathbf{K}_i^{-1} ({}^t \mathbf{f}_{int} - \mathbf{f}_{int,i}) \quad \text{and} \quad \delta \mathbf{u}_i^{II} = \mathbf{K}_i^{-1} \hat{\mathbf{f}} \quad (16.8)$$

The total iterative increment is then derived from,

$$\delta \mathbf{u}_i = \delta \mathbf{u}_i^I + \Delta \lambda_i \delta \mathbf{u}_i^{II} \quad (16.9)$$

The load factor $\Delta \lambda_i$ is still undefined and can now be used to constrain the incremental displacement vector. MIDAS offers a quadratic and a linearized constraint, leading to the Spherical Path Arc-length method (Crisfield¹).

16-4-1 Spherical Path

In the spherical constraint, the constraint equation is,

$$\Delta \mathbf{u}_i^T \Delta \mathbf{u}_i = \Delta l^2 \quad (16.10)$$

where, Δl is the required arc length. Substitution of (16.4) and (16.9) into (16.10) gives the value for $\Delta \lambda$.

$$\Delta \lambda_i = \frac{-a_2 \pm \sqrt{a_2^2 - 4a_1a_3}}{2a_1} \quad (16.11)$$

with

¹ Crisfield, M. A. Non-linear Finite Element Analysis of Solids and Structures, vol. 1: Essentials. John Wiley & Sons, 1991.

$$\begin{aligned}
a_1 &= (\delta \mathbf{u}_i'')^T \delta \mathbf{u}_i'' \\
a_2 &= 2(\delta \mathbf{u}_i')^T \delta \mathbf{u}_i'' + 2(\Delta \mathbf{u})^T \delta \mathbf{u}_i'' \\
a_3 &= 2(\Delta \mathbf{u})^T \delta \mathbf{u}_i' + (\delta \mathbf{u}_i')^T \delta \mathbf{u}_i' + (\Delta \mathbf{u})^T \Delta \mathbf{u} - \Delta l^2
\end{aligned} \tag{16.12}$$

Normally, two solutions for $\Delta \lambda$ fulfill (16.10), but if the discriminant $a_2^2 - 4a_1a_3 < 0$, then MIDAS uses a linearized equivalent of the Spherical Path method as described by Forde and Stierner². To determine which of the two regular solutions should be used, the angle θ between the displacement increment vector of the previous iteration and the current iteration is calculated for both solutions.

$$\begin{aligned}
\cos(\theta) &= \frac{(\Delta \mathbf{u}_{i-1})^T \delta \mathbf{u}_i}{\|\Delta \mathbf{u}_{i-1}\| \|\delta \mathbf{u}_i\|} = \frac{\Delta \mathbf{u}_{i-1}^T (\Delta \mathbf{u}_{i-1} + \delta \mathbf{u}_i')}{\Delta l^2} + \delta \lambda_{i-1} \frac{\Delta \mathbf{u}_{i-1}^T \delta \mathbf{u}_i''}{\Delta l^2} \\
&= \frac{a_4 + a_5 \delta \lambda_i}{\Delta l^2}
\end{aligned} \tag{16.13}$$

where,

$$\begin{aligned}
a_4 &= \Delta \mathbf{u}_{i-1}^T (\Delta \mathbf{u}_{i-1} + \delta \mathbf{u}_i') \\
a_5 &= \Delta \mathbf{u}_{i-1}^T \delta \mathbf{u}_i''
\end{aligned} \tag{16.14}$$

If one of the solutions yields a negative cosine and the other yields a positive cosine, MIDAS chooses the solution with the positive cosine (acute angle). If both solutions yield acute angles, the solution closest to the linear solution $\Delta \lambda = -a_3/a_2$ is used.

From the results of the Eq. (16.11), $\delta \lambda_{i,1}$ and $\delta \lambda_{i,2}$, it may be written as,

$$\begin{aligned}
\Delta l^2 \cos \theta_1 &= a_4 + a_5 \delta \lambda_{i,1} \\
\Delta l^2 \cos \theta_2 &= a_4 + a_5 \delta \lambda_{i,2}
\end{aligned} \tag{16.15}$$

where,

² Forde, B. W. R., and Stierner, S. F. Improved Arc-length Orthogonality methods for nonlinear Finite Element Analysis. Computers & Structures 27, 5 (1987), 625–630.

$$\begin{cases} \delta\lambda_i = \delta\lambda_{i,1} & (\Delta l^2 \cos \theta_1 > \Delta l^2 \cos \theta_2) \\ \delta\lambda_i = \delta\lambda_{i,1} = \delta\lambda_{i,2} & (\Delta l^2 \cos \theta_1 = \Delta l^2 \cos \theta_2) \\ \delta\lambda_i = \delta\lambda_{i,2} & (\Delta l^2 \cos \theta_1 < \Delta l^2 \cos \theta_2) \end{cases} \quad (16.16)$$

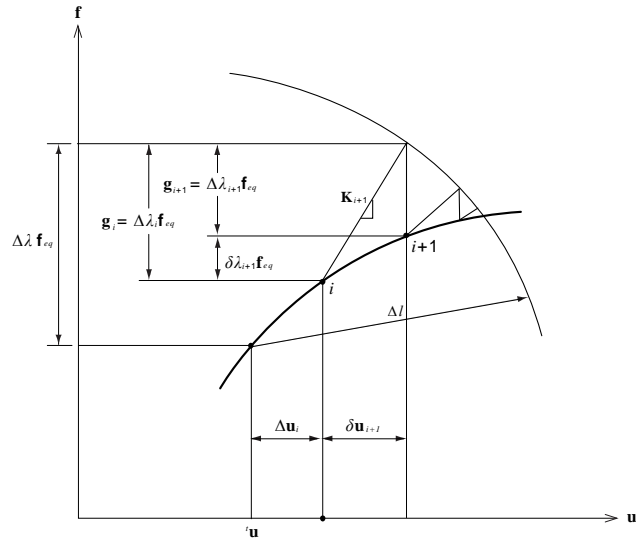


Figure 16-6) Spherical Arc-length method

16-5 Displacement Control

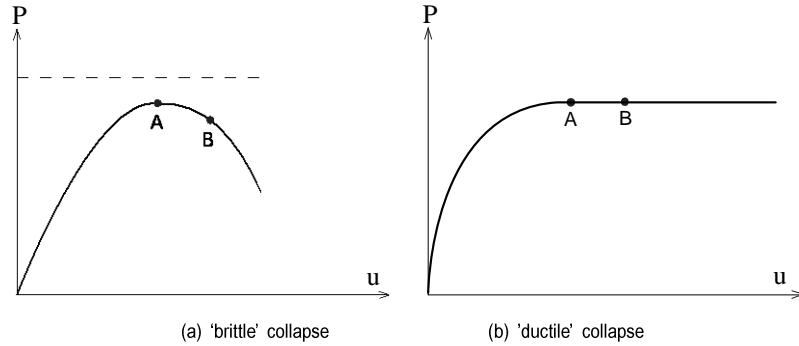


Figure 16-7) load deflection graphs

Fig. 16-7 shows two possible load-deflection curves involving limit load, snap-through and in some cases snap-back phenomena. Therefore, for each model, it is important to choose a stable scheme to obtain a correct equilibrium path. Among the different iterative methods, the displacement control method is considered in this section.

In the Displacement Control method, the target displacement defines the incremental load factor. Load increment factor is written as,

$$\delta u_i = \delta u_i^I + \Delta \lambda_i \delta u_i^{II} \quad (16.17)$$

The incremental load factor is defined through an iterative procedure at the initial load step. Initial incremental load factor coincide with the direction of displacement control at the controlled node. Because the initial incremental displacement and target displacement \hat{u} coincide, Eq. (16.17) is written as,

$$\delta u_1 = \delta u_1^I + \Delta \lambda_1 \delta u_1^{II} = \hat{u} \quad (16.18)$$

At the first iteration, the residual force is assumed to be zero. As a results, $\delta u_1^I = 0$, and the

initial load factor is expressed by,

$$\Delta\lambda_1 = \frac{\delta u_1 - \delta u_1^I}{\delta u_1^{II}} = \frac{\hat{u} - \delta u_1^I}{\delta u_1^{II}} = \frac{\hat{u}}{\delta u_1^{II}} \quad (i = 1) \quad (16.19)$$

\hat{u} has a constant value during the iteration and δu_i ($i > 1$) is zero.

From Eq. (16.17) and the above assumption, the incremental load factor $\Delta\lambda_i$ ($i > 1$) is obtained by,

$$\Delta\lambda_i = -\frac{\delta u_i^I}{\delta u_i^{II}} \quad (i > 1) \quad (16.20)$$

Finally, the updated total displacement is obtained from Eq. (16.20) and Eq. (16.17). Note that if the incremental load factor becomes zero, the iterative procedure will be terminated.

16-6 Convergence Criteria

The iteration process must be stopped if the results are satisfactory (Fig. 16-1). For this purpose, MIDAS offers several convergence norms. Besides stopping the iteration in case of convergence, the iteration process is also stopped if a specified maximum number of iterations has been reached, or if the iteration obviously leads to divergence. The detection of divergence is based on the same norms as the detection of convergence. Fig. 16-8 specifies the items used to set up the various norms.

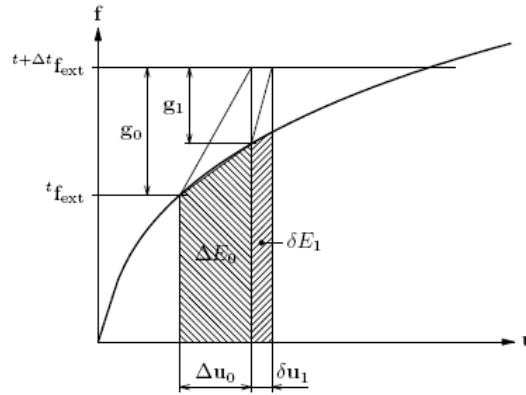


Figure 16-8) Norm items

16-6-1 Force Norm

The force norm is the Euclidian norm of the out-of-balance force vector \mathbf{g} . To check convergence, the force norm after the current iteration is checked against the norm of the initial unbalance \mathbf{g}_0 .

$$\text{Force norm ratio} = \frac{\sqrt{\mathbf{g}_i^T \mathbf{g}_i}}{\sqrt{\mathbf{g}_0^T \mathbf{g}_0}} \quad (16.21)$$

Because the reference force norm is known before the first prediction of displacements, the force norm ratio can be calculated directly after the first prediction, $i = 1$ in (16.21). This means that if the first prediction is correct (nearly linear behavior), the force norm can detect convergence right away and no unnecessary iterations have to be performed.

16-6-2 Displacement Norm

The displacement norm is the Euclidian norm of the iterative displacement increment. To check convergence, the displacement norm is checked against the norm of the displacement increments in the first prediction of the increment.

$$\text{Displacement norm ratio} = \frac{\sqrt{\delta \mathbf{u}_i^T \delta \mathbf{u}_i}}{\sqrt{\Delta \mathbf{u}_0^T \Delta \mathbf{u}_0}} \quad (16.22)$$

From Eq. (16.22), it is clear that the ratio of the displacement norm after the first prediction (iteration 0) equals 1 by definition. To check convergence, always one additional iteration is necessary.

16-6-3 Energy Norm

A third way to check convergence is the energy norm. This norm is composed of internal forces and relative displacements as indicated in Fig. 16-8 with $\Delta \mathbf{E}_0$ and $\delta \mathbf{E}_i$. To determine convergence, the energy ratio is calculated as,

$$\text{Energy norm ratio} = \left| \frac{\delta \mathbf{u}_i^T (\mathbf{f}_{int,i+1} + \mathbf{f}_{int,i})}{\Delta \mathbf{u}_0^T (\mathbf{f}_{int,1} + \mathbf{f}_{int,0})} \right| \quad (16.23)$$

Note that here the internal force is used and not the out-of-balance force. As with the displacement norm, the energy norm also requires an additional iteration to detect convergence.

16-7 Auto-Switching

MIDAS provides an option to automatically switch from load/displacement control to arc-length control. This feature is activated when the equilibrium path is reached to the limit point.

To measure the degree of nonlinearity, the current stiffness parameter k is introduced. This parameter measures the stiffness of the system with respect to the tangential predictor as follows:

$$k_i = \frac{\mathbf{g}_i^T \Delta \mathbf{u}_i}{\Delta \mathbf{u}_i^T \Delta \mathbf{u}_i} \quad (16.24)$$

The scaled current stiffness parameter is expressed by,

$$C_s = \frac{k}{k_1} \quad (16.25)$$

where, k is the current value of the stiffness parameter, and k_0 is the initial value of the stiffness parameter.

During an iterative procedure within a load step, the scaled stiffness parameter is defined by, ΔC_s . Accordingly, ΔC_{s1} and ΔC_{sd} are defined as the initial and the current scaled stiffness parameters respectively. The automatic-switching function will be activated when the equilibrium path is getting closer to the limit point, and as a result, the current scaled stiffness parameter is converged towards zero. Therefore, the updated automatic-switching control parameter $\Delta C_{sd} / \Delta C_{s1}$ will satisfy the user defined value for this ratio.

Chapter 17. Equation Solver

17-1 Introduction

Solving linear simultaneous equations in a matrix form can be expressed by,

$$\mathbf{K}\mathbf{u} = \mathbf{p}, \quad (17.1)$$

where \mathbf{K} represents a stiffness matrix, and \mathbf{p} represents external forces acting on the structure.

The solution to the above equation is to find the displacement vector field, \mathbf{u} .

The equation (17.1) is used to analyze almost all structural problems including the linear system of equations, eigenvalue/ buckling problems, dynamic models and nonlinear problems. The solution schemes are largely classified into direct and iterative methods. MIDAS provides the following methods and corresponding options;

Direct methods

- Skyline
- Multi-frontal (default)

Iterative methods

- CG (default): Pre-conditioner : ILUT (default), Jacobi
- GMRES : Pre-conditioner : ILUT (default), Jacobi

17-2 Direct Method

Two main steps are considered in the direct method. The first step is decomposition and the second step is Forward-Backward Substitution (FBS).

A symmetric stiffness matrix, **K** is decomposed into,

$$\mathbf{LL}^T \mathbf{u} = \mathbf{p} \quad \text{or} \quad \mathbf{LDL}^T \mathbf{u} = \mathbf{p}. \quad (17.2)$$

Here, **L** is a lower-triangular matrix, and **D** is a diagonal matrix. In general, the decomposition method, which includes **D**, is required for a matrix, which is not positive definite. The decomposed matrix, **K** ($= \mathbf{LL}^T$ or $= \mathbf{LDL}^T$) is used to find solutions through the process of Forward-Backward Substitution. Substituting it into $\mathbf{v} = \mathbf{L}^T \mathbf{u}$ or $\mathbf{v} = \mathbf{DL}^T \mathbf{u}$, can we then express it as,

$$\mathbf{Lv} = \mathbf{p}, \quad (17.3)$$

And the solutions to $\mathbf{Lv} = \mathbf{p}$, that is **v**, can be obtained by the characteristics of the lower-triangular matrix. Once **v** is obtained, **u** can be calculated using $\mathbf{v} = \mathbf{L}^T \mathbf{u}$ or $\mathbf{v} = \mathbf{DL}^T \mathbf{u}$. An important point for applying the direct method is to appropriately use the sparsity of the matrix. Typically, in the context of finite element analysis, the matrix **K** is a sparse matrix. Depending on how the sparsity is handled, the required memory allocation and analysis time can significantly vary.

MIDAS provides a skyline solver, which uses a front matrix and a multi-frontal solver, which uses multi-front matrices.

17-2-1 Skyline Solver

The Skyline solver performs matrix decomposition using a single front matrix and uses the skyline type for saving the matrix.

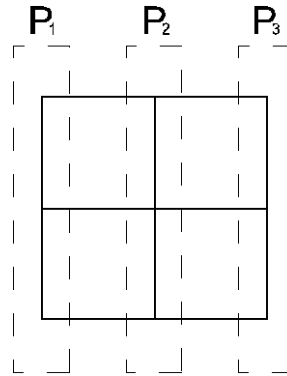


Figure 17-(1) Simple mesh composed of 3 parts

The stiffness matrix corresponding to the mesh shown in Fig. 17-(1) can be divided into three parts,

$$\mathbf{K} = \begin{bmatrix} \mathbf{K}_{11} & \mathbf{K}_{21}^T & \mathbf{0} \\ \mathbf{K}_{21} & \mathbf{K}_{22} & \mathbf{K}_{32}^T \\ \mathbf{0} & \mathbf{K}_{32} & \mathbf{K}_{33} \end{bmatrix}. \quad (17.4)$$

Assuming that \mathbf{K} is decomposed in the order of $P_1 \rightarrow P_2 \rightarrow P_3$, the decomposition of P_1 and the renewal of P_2 as a result are as follows:

$$\begin{aligned} \mathbf{K}_{11} &= \mathbf{L}_{11} \mathbf{L}_{11}^T \\ \mathbf{L}_{21} \mathbf{L}_{11}^T &= \mathbf{K}_{21} \\ \mathbf{K}_{22} - \mathbf{L}_{21} \mathbf{L}_{21}^T &= \mathbf{K}_{22}^* (= \mathbf{L}_{22} \mathbf{L}_{22}^T). \end{aligned} \quad (17.5)$$

In the same way, P_2 can be decomposed and P_3 can be renewed and decomposed. Note that the efficiency of calculation in sequential matrix decomposition with a single front matrix significantly depends on renumbering of the degrees of freedom. Fig. 17-(2) schematically shows

an efficient calculation sequence in a rectangular mesh. The algorithm for renumbering the degrees of freedom is based on the wavefront reduction method proposed by Sloan¹. Forward substitution takes place in the same sequence as the matrix decomposition, while backward substitution is carried out in the reverse order.

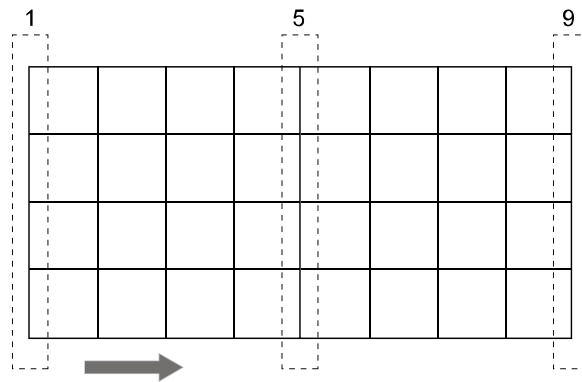


Figure 17-(2) Typical decomposition sequence of Skyline solver

17-2-2 Multi-frontal Solver

Multi-frontal solver is based on the matrix decomposition method² in which multiple front matrices are simultaneously considered and calculated by saving the matrices by element units. Unlike the order of the matrix used in the Skyline solver for the mesh shown in Fig. 17-(1), it is arranged as Eq. (17.6).

$$\mathbf{K} = \begin{bmatrix} \mathbf{K}_{11} & \mathbf{0} & \mathbf{K}_{21}^T \\ \mathbf{0} & \mathbf{K}_{33} & \mathbf{K}_{23}^T \\ \mathbf{K}_{21} & \mathbf{K}_{23} & \mathbf{K}_{22} \end{bmatrix}. \quad (17.6)$$

When \mathbf{K} is decomposed in the order of $(P_1, P_3) \rightarrow P_2$, it can be expressed as the Eq. (17.7) and

1 S.W.Sloan, *An Algorithm for Profile and WaveFront Reduction of Sparse Matrices*, International Journal For Numerical Methods In Engineering, Vol. 23, 239-251, 1986

2 J.H. Kim and S.J. Kim, *A Multifrontal Solver Combined with Graph Partitioners*, AIAA Journal, Vol. 38, 964-970, 1999

17-3 Iterative Method

The iterative method is used to find a value close to the exact solution to Eq. (17.1) by using the solution at the current step, \mathbf{u}_i and the residual value, ($\mathbf{r}_i = \mathbf{p} - \mathbf{K}\mathbf{u}_i$).

Calculation of \mathbf{u}_{i+1} is simply expressed as,

$$\mathbf{u}_{i+1} = \mathbf{u}_i + \mathbf{\Gamma}_i \mathbf{Q}(\mathbf{p} - \mathbf{K}\mathbf{u}_i) \quad (17.9)$$

where, $\mathbf{\Gamma}_i$ is a matrix operator determined by the type of iterative method, and \mathbf{Q} is a preconditioner, which affects the convergence speed. The iterative process continues until the number of iterations reaches the maximum number of iteration or the convergence tolerance of a residual value $\mathbf{r}_i (= \mathbf{p} - \mathbf{K}\mathbf{u}_i)$ is satisfied. MIDAS allows the user to set these parameters whose default values are as follows:

Maximum number of iterations

$N/4$ (if $N/4 > 1000$), 1000 (if $N/4 < 1000$)

Convergence tolerance

$$\|\mathbf{r}_i\| < 10^{-6} \|\mathbf{f}\| \quad (17.10)$$

17-3-1 CG and GMRES

MIDAS provides the CG³ (Conjugate Gradient) method for a symmetric matrix having positive signs and the GMRES⁴ (General Minimal Residual) method suitable for a general matrix. Both

3 H.R. Hestenes and E. Stiefel, *Methods of Conjugate Gradients for Solving Linear Systems*, J. Res. Nat. Bur. Standards Vol. 49 409-436, 1952

4 Y. Saad and M.H. Schultz, *GMRES: A Generalized Minimal Residual Algorithm for Solving Nonsymmetric Linear Systems*, SIAM J. Sci. Stat. Comput. Vol. 7, 856-869, 1986

the CG method and the GMRES method set the solution searching direction, \mathbf{d}_i so that the residual value, \mathbf{r}_i crosses at a right angle in the Krylov subspace $span\{\mathbf{r}_0, \mathbf{K}\mathbf{r}_0, \mathbf{K}^2\mathbf{r}_0, \dots\}$. Accordingly, if the result is obtained without any numerical errors, the exact solution can be theoretically obtained after N iterations (the number of degrees of freedom of a structure).

CG is a method, which finds a solution by setting the conjugated direction ($\mathbf{d}_i = \mathbf{r}_i + \beta_i \mathbf{d}_{i-1}$) as the search direction. CG has a characteristic to easily obtain the orthogonality of residual values using the symmetry of the stiffness matrix, \mathbf{K} . GMRES is a method, which executes the Gram-Schmidt orthogonalization at each step of the iterative calculation to make the residual value, \mathbf{r}_i retain orthogonality in the Krylov subspace $span\{\mathbf{r}_0, \mathbf{K}\mathbf{r}_0, \mathbf{K}^2\mathbf{r}_0, \dots\}$. As the amount of calculation increases with an increase in the number of iterations in the Gram-Schmidt orthogonalization, it incorporates a method, which restarts the Krylov subspace after an appropriate number of iterative calculations.

17-3-2 Pre-conditioner

Pre-conditioner plays an important role in increasing the convergence speed by obtaining \mathbf{K}^{-1} and a similar matrix ($\mathbf{Q} \approx \mathbf{K}^{-1}$) with a small amount of calculations. This is similar to finding the exact solution through one iterative calculation using \mathbf{K}^{-1} in place of \mathbf{Q} in Eq. (17.9). In MIDAS, the ILUT⁵ (Incomplete LU decomposition with threshold) pre-conditioner and the Jacobi pre-conditioner can be used. The ILUT pre-conditioner uses the Incomplete LU decomposition in which the drop-tolerance has been applied to the fill-in generated from the matrix decomposition process. The Jacobi pre-conditioner method uses $\mathbf{Q} = \text{diag}(\mathbf{K})^{-1}$ considering only the diagonal terms of the matrix \mathbf{K} .

⁵ Y. Saad, *ILUT: a Dual Threshold Incomplete ILU Factorization*, Numerical Linear Algebra with Applications Vol. 1, 387-402. 1994

17-4 Solver Characteristics

There are cases where the solution to linear simultaneous equations is automatically determined by MIDAS depending on the type of analysis problems.

Buckling analysis or dynamic analysis using the Lanczos' method: Use multi-frontal solver.

Dynamic analysis using the iterative method: Changed to multi-frontal solver.

In case where constraint equations are included: Use multi-frontal solver.

In case where the CG method is used, and non-symmetry stiffness occurs: Changed to GMRES method.

The performance levels of different solution methods for solving linear simultaneous equations vary considerably depending on the types of analysis. It is thus important to select an appropriate solution method for each case. The characteristics and the performance level of each solution method are noted below.

Direct method: It is stable irrespective of the matrix condition but requires a large memory space.

If the system memory is insufficient, the program automatically uses the disk storage.

- Skyline: Suitable to analyze one-dimensional structures

- Multi-frontal: Suitable to analyze two- or three-dimensional structures

Iterative method: Although a less memory is required, the calculation time can vary significantly depending on the matrix condition. It is appropriate if a structure contains many solid elements.

- ILUT pre-conditioner: The number of iterations is small.

- Jacobi pre-conditioner: Pre-conditioning is fast, and a less memory is required.

Chapter 18. Contact

18-1 Introduction

Let us consider two objects A and B in space. They can touch each other, but cannot physically penetrate into each other (i.e., they cannot exist in a common space). This is a basic condition for contact/impact analysis. The following equation conceptually expresses the relationship of the domains in which contact occurs.

$$\Omega^A \cap \Omega^B = \emptyset \quad (18.1)$$

where, Ω^A and Ω^B represent the domains of the objects A and B respectively.

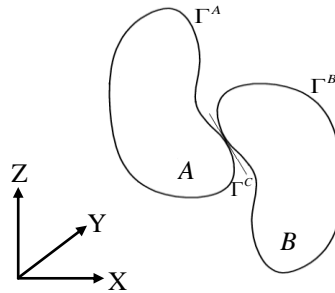


Figure 18-(1) Schematic representation of contact

The relationship between the boundary surfaces of the domains in contact is as follows:

$$\Gamma^C = \Gamma^A \cap \Gamma^B \neq \emptyset \quad (18.2)$$

where,

Γ^A, Γ^B : Boundary domains of the objects, A and B

Γ^C : Boundary surface on which the objects, A and B are in contact

When we assign a master and a slave to two objects, A and B , it does not matter if the master and

the slave are switched in the algorithm. However, we can achieve better convergence practically in numerical analysis if we assign the master to an object, which is rigid or dense, or its mesh is relatively coarse.

A slave node and a master surface become a basis of the algorithm for contact/impact analysis. MIDAS uses the penalty method for contact/impact analysis. Conceptually, this method pertains to inserting a spring between a contact surface and a node, which numerically penetrates into the surface. This method is advantageous in that it is easy to implement, and in case of dynamic analysis, it does not affect the time increments.

18-2 Contact search

MIDAS follows the steps below for contact search.

- (1) Global Search: For each slave node, a nearest master node is searched. For global search, a Bucket sort algorithm is used.
- (2) Local Search: Among the segments connected to a master node, a segment nearest to the slave node is searched.
- (3) Contact Search: A contact point on a master segment is calculated.

18-2-1 Global Search

In order to find the nearest node among N nodes, calculation for the following equation is performed $N-1$ times:

$$l^2 = (x_i - x_j)^2 + (y_i - y_j)^2 + (z_i - z_j)^2 \quad (18.3)$$

Since the above equation is solved for every node, the calculation takes place $N(N-1)$ times. This search may result in consuming the majority of the analysis time. For effective search, MIDAS uses a Bucket sort algorithm.

The basic concept of the Bucket sort algorithm pertains to dividing nodes into a number of groups (buckets) and calculating nodal distances only between the nearest buckets. In case of one-dimensional analysis, the number of buckets, which need to be searched, is 3 buckets in total, which are the left and right adjacent buckets and itself. Similarly, search for a total of 9 buckets and 27 buckets are required for two and three dimensional analyses respectively. The amount of calculations required here is expressed by,

$$N \left(\frac{3N}{NB_x} - 1 \right), \quad N \left(\frac{9N}{NB_x \cdot NB_y} - 1 \right), \quad N \left(\frac{27N}{NB_x \cdot NB_y \cdot NB_z} - 1 \right) \quad (18.4)$$

where, NB_x , NB_y & NB_z are the numbers of buckets in x, y and z directions respectively.

18-2-2 Local Search

This searches a master segment nearest to each slave node.

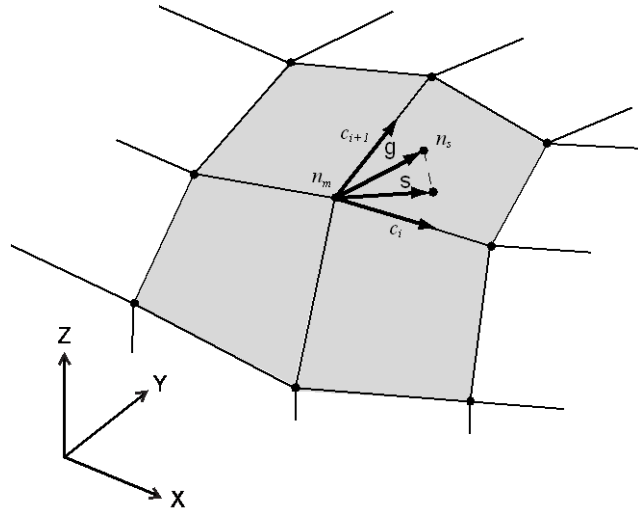


Figure 18-(2) Local search

Let us consider that n_m is a master node nearest to the slave node, n_s . We then define \mathbf{g} , which is a vector from n_m to n_s . The vector \mathbf{s} is the vector \mathbf{g} projected onto the master segment.

$$\mathbf{s} = \mathbf{g} - (\mathbf{g} \cdot \mathbf{m})\mathbf{m} \quad (18.5)$$

where,

$$\mathbf{m} = \frac{\mathbf{c}_i \times \mathbf{c}_{i+1}}{|\mathbf{c}_i \times \mathbf{c}_{i+1}|}$$

\mathbf{c}_i and \mathbf{c}_{i+1} are the frame vectors of the master segment. We then find s_i using Eq. (18.6), which is a segment on which the node, n_s is located, among the segments adjacent to the master node, n_m .

$$\begin{aligned} (\mathbf{c}_i \times \mathbf{s}) \cdot (\mathbf{c}_i \times \mathbf{c}_{i+1}) &> 0 \\ (\mathbf{c}_i \times \mathbf{s}) \cdot (\mathbf{s} \times \mathbf{c}_{i+1}) &> 0 \end{aligned} \quad (18.6)$$

18-2-3 Contact Search

In this part, the procedure for calculating the contact point on the master segment nearest to the slave node, n_s is introduced. Let us suppose that \mathbf{r} is a position vector from the origin to the contact point, and that \mathbf{t} is a position vector from the origin to the slave node, n_s .

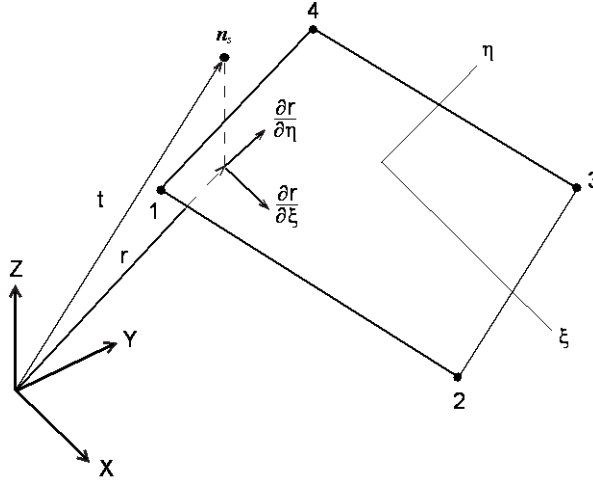


Figure 18-(3) Location of contact point

The line component drawn from the slave node, n_s to the nearest point on the master surface will be perpendicular to the master segment. Thus the contact point, (ξ_c, η_c) on the master segment, s_i can be found by using the following equations:

$$\begin{aligned} \frac{\partial \mathbf{r}}{\partial \xi}(\xi_c, \eta_c) \cdot [\mathbf{t} - \mathbf{r}(\xi_c, \eta_c)] &= 0 \\ \frac{\partial \mathbf{r}}{\partial \eta}(\xi_c, \eta_c) \cdot [\mathbf{t} - \mathbf{r}(\xi_c, \eta_c)] &= 0 \end{aligned} \quad (18.7)$$

Eq. (18.7) can be rewritten as Eq. (18.8), which can be numerically solved by using the Newton-Raphson method.

$$\begin{aligned} \begin{bmatrix} \frac{\partial \mathbf{r}}{\partial \xi} \\ \frac{\partial \mathbf{r}}{\partial \eta} \end{bmatrix} \begin{bmatrix} \frac{\partial \mathbf{r}}{\partial \xi} & \frac{\partial \mathbf{r}}{\partial \eta} \end{bmatrix} \begin{Bmatrix} \Delta \xi \\ \Delta \eta \end{Bmatrix} &= \begin{bmatrix} \frac{\partial \mathbf{r}}{\partial \xi} \\ \frac{\partial \mathbf{r}}{\partial \eta} \end{bmatrix} \left\{ \mathbf{r}(\xi_c, \eta_c) - \mathbf{t} \right\} \\ \xi_{i+1} &= \xi_i + \Delta \xi \\ \eta_{i+1} &= \eta_i + \Delta \eta \end{aligned} \quad (18.8)$$

Using the initial condition, $\xi_0 = 0$ and $\eta_0 = 0$, Eq. (18.8) is solved iteratively. In general, the solution can be converged within 4 iterations.

Now each slave node is checked whether or not the slave node has numerically penetrated into the master surface. If the slave node has not numerically penetrated into the master surface, nothing happens. If it has, the contact force is applied between the slave node and its contact point on the master segment. The applied force at this time is proportional to the degree of numerical penetration. The degree of penetration, l is defined by,

$$l = \mathbf{n}_i \cdot [\mathbf{t} - \mathbf{r}(\xi_c, \eta_c)] \quad (18.9)$$

where,

(ξ_c, η_c) : Contact point

$\mathbf{n}_i = \mathbf{n}_i(\xi_c, \eta_c)$: Vector perpendicular to the master segment, s_i at the contact point

If the slave node, n_s has numerically penetrated into the master segment, s_i , the force expressed in Eq. (18.10) is added to the slave node and the master segment, s_i .

$$\mathbf{f}_s = -lk_i \mathbf{n}_i \quad (18.10)$$

where, $k_i = f_{si} \frac{K_i A_i^2}{V_i}$: Stiffness factor of the master segment, s_i

K_i : Bulk modulus

A_i : Area of the master segment, s_i

V_i : Volume

f_{si} : Proportional coefficient (default value is 0.1)

The Eq. (18.10) can be directly applied to the slave node. However, in the master segment, the force is distributed to nodes of the master segment.

$$\mathbf{f}_m^j = h_j(\xi_c, \eta_c) \mathbf{f}_s \quad (18.11)$$

where, $j = 1, 2, 3, 4$: Nodes of the master segment, s_i

18-3 Function

18-3-1 Friction

Friction can be considered when contact/impact analysis is performed in MIDAS. The coulomb friction is used, and the friction coefficient is determined by,

$$\mu = \mu_k + (\mu_s - \mu_k) e^{-\beta|v|} \quad (18.12)$$

where,

μ_s : Static friction coefficient

μ_k : Dynamic friction coefficient

β : Damping coefficient

v : Relative velocity between a slave node and a master segment

18-3-2 Nodes to surfaces

This function is used for contact/impact analysis of slave nodes and master surfaces. It is required to specify a node as a slave and a surface as a master. Radius of a node can be specified to consider the physical size effect. When the distance between the node and the surface is less than the specified radius of the node, contact is considered to have taken place.

18-3-3 Surfaces to Surfaces

This function is used for contact analysis between surfaces. The user is free to set the master/slave surfaces in this function.

18-3-4 Single surface

This function defines only slave surfaces. It is useful for analyzing two separate surfaces of an object coming in contact with each other. Currently it can be used only in explicit dynamic analysis.

18-3-5 Tied

This function is used when master/slave surfaces are in contact with each other from the initial stage. And the two surfaces are not permitted to separate during the progress of analysis. Especially, this is useful when master/slave nodes do not coincide with each other. This function is based on the nodal constraint method as opposed to the penalty method. As such, a slave is set to the densely meshed side, and a master is set to the other side. If the master/slave is inversely set, the master surface can numerically penetrate through the slave surface.

Chapter 19. Fatigue Analysis

19-1 Introduction

The term for fatigue failure represents the phenomenon in which structural members fail under a repeatedly applied load, which by a single application does not exceed the yield strength. Two common methods exist for fatigue analysis, which are a stress-based (stress-life) method using the S-N curve and a strain-based (strain-life) method using the E-N curve. While the method based on the S-N curve is developed to purely execute the fatigue analysis, the method based on the E-N is developed for the crack propagation analysis, which includes fatigue analysis. This section will focus on the stress based method.

The S-N curve is a line graph, which shows the relationship of the stress amplitude (S) and the cycle to failure (N). S is caused by a reverse loading of constant amplitude, which is repeatedly applied to the structure until failure.

For fatigue analysis, static analysis is performed first. Then the stress amplitude is found by selecting one component among the maximum absolute stress, minimum absolute stress and von Mises stress. Applying this to the S-N curve, we can find the number of cycles of the repeated load at which fatigue failure takes place.

All structures have their own inherent S-N curves. But it is not practical to undertake fatigue testing for all structures. For such cases, the S-N curves, which are obtained from the standard reduced fatigue testing, are modified by certain factors. Also in general, structures are subjected to repeated loads of variable amplitudes. In order to use the S-N curve in such cases, the Rainflow-Counting technique is used. In this technique, the stress of unit amplitude and the number of cycles are extracted from the repeated stresses of variable amplitudes, which are then applied to the S-N curves.

19-2 Load Cycles

In case uniform amplitude of stresses is regularly acting like Fig. 19-(1), the stress amplitude, σ_a and the mean stress, σ_m can be calculated as,

$$\sigma_a = \frac{\sigma_{\max} - \sigma_{\min}}{2} \quad (19.1)$$

$$\sigma_m = \frac{\sigma_{\max} + \sigma_{\min}}{2} \quad (19.2)$$

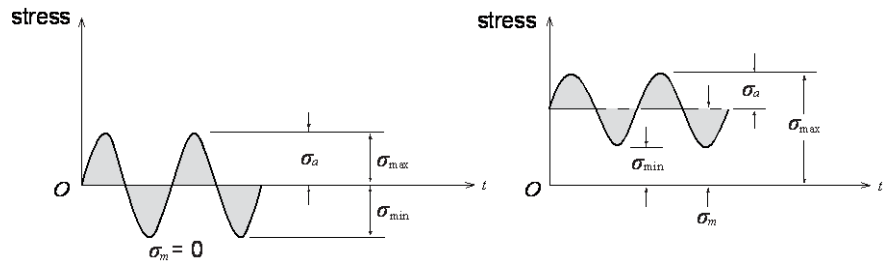


Figure 19-(1) Fully reverse loading and mean stress

In the stress-life method, if uniform amplitude of stresses is regularly repeated at the state of the mean stress being zero, the S-N curve in Fig. 19-(2) is used.

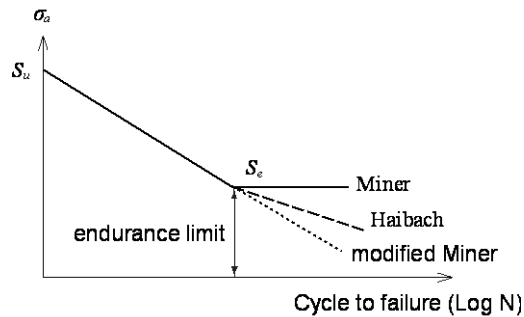


Figure 19-(2) S-N curve

S_u and S_e in Fig. 19-(2) represent the maximum amplitude stress and endurance limit amplitude stress respectively. The Miner's S-N curve in Fig. 19-(2) shows that repeated stresses under the endurance limit do not affect the fatigue life. And the modified Miner curve shows the relationship of accumulated fatigue damage even stresses less than the endurance limit are accumulated. However, the stress-life based fatigue analysis can not be used if fatigue failure occurs under a repeated load of 1,000 cycles.

Generally if an S-N curve for a material is not separately defined, an S-N curve like Fig. 19-(3) is used. This curve shows a line connecting from the point at which the stress in the magnitude of 90% of the maximum amplitude stress (S_u) is repeated 1,000 times and to a point at which the endurance limit amplitude stress ($S_e = 0.5S_u$) is repeated 10^6 times.

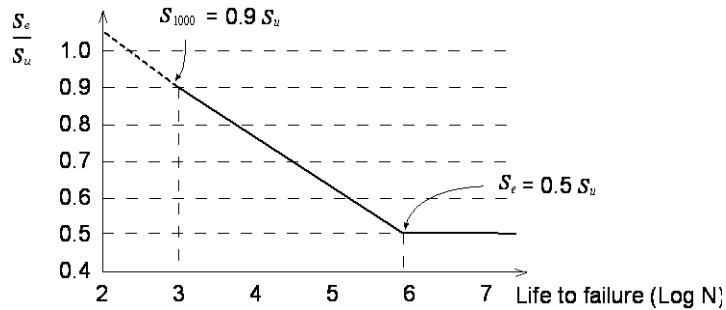


Figure 19-(3) Basic S-N curve shape

If we define b to represent the slope of the S-N curve as in Fig. 19-(3), the number of stress cycles (N), which leads to fatigue failure under the repeated action of a specific stress amplitude (S), can be calculated as,

$$b = -\frac{(\log S - \log S_e)}{\log N_e - \log N} \quad (19.3)$$

$$N = N_e \left(\frac{S}{S_e} \right)^{\frac{1}{b}} \quad (19.4)$$

The advantages and shortcomings of the stress-life method are as follows:

- Fatigue analysis can be performed through a relatively simple algorithm.
- Calculation is simple, and the analysis time is short.
- True plastic stress-strain curve is ignored, and all the strains are treated elastically. As such, it is not effective if plastic strains are significant.
- This is effective for a long life with small cyclical plastic strain components.

19-3 Mean Stress Effects

Even if the stress amplitude, σ_a , exerted onto a structure is the same, if the mean stress, σ_m is different, the fatigue life also changes as shown in Fig. 19-(4). As the mean stress, σ_m increases, the maximum stress, S_u and the endurance limit stress, S_e decrease. Haigh obtained such relationship first. The left diagram in Fig. 19-(4) shows the relationship between the mean stresses and maximum stresses under the same stress amplitude. The diagram on the right shows the effect of average stresses on the maximum stress factors and the endurance limit factors.

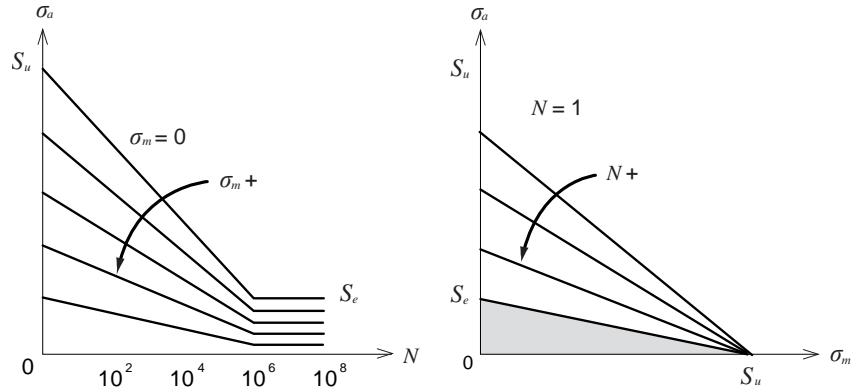


Figure 19-(4) Mean stress effects

Goodman and Gerber proposed expressions below to reflect the effect of average stresses, which can be represented as Fig. 19-(5),

$$\text{Goodman (England, 1899)} \quad \frac{\sigma_a}{S_e} + \frac{\sigma_m}{S_u} = 1 \quad (19.5)$$

$$\text{Gerber (Germany, 1874)} \quad \frac{\sigma_a}{S_e} + \left(\frac{\sigma_m}{S_u} \right)^2 = 1 \quad (19.6)$$

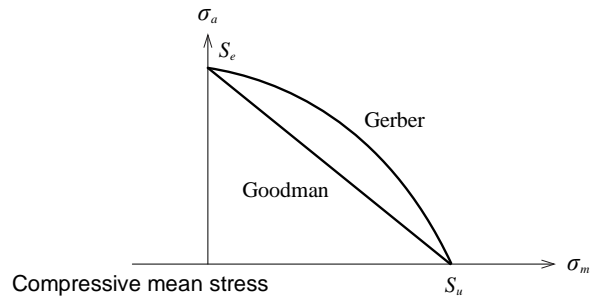


Figure 19-(5) Relationship of stress amplitude and mean stress

For example, if $\sigma_{\max} = 758.42\text{MPa}$, $\sigma_{\min} = 68.95\text{MPa}$ and $S_u = 1034.21\text{MPa}$, $\sigma_a = 344.74\text{MPa}$ and $\sigma_m = 413.69\text{MPa}$. Using the Goodman's equation, we find $S_e = 574.57\text{MPa}$. Note that S_e is a modified value based on the mean stress.

19-4 Modifying Factors

Generally, using a standard rotating bend test such as R.R Moore test, a baseline for the S-N curve is determined for a specimen loaded under the condition of fully reversed bending. At this point, if the endurance limit is S'_e , then the value of S_e in a real situation must be obtained through modifications. For steels, a number of empirical relationships have been developed, which can be simply used to arrive at appropriate S-N curves reflecting real situations. The following factors can be considered:

- Component size and shape
- Loading type
- Surface finish
- Surface treatment
- Temperature
- Environment

The following equation shows the true endurance limit using modification factors.

$$S_e = S'_e C_{size} C_{sur} \dots \quad (19.7)$$

The fatigue strength reduction factor is defined by,

$$K_f = \frac{1}{(C_{size} C_{load} C_{sur} \dots)} \quad (19.8)$$

The modification factor usually affects defining the endurance limit, and the modifications required for the rest of the S-N curve are not well defined. The modification factor is used to better reflect accurate safety factors for loading. The loading affects the endurance limit at one million cycles, and it can sometimes affect the fatigue strength at 1000 cycles. In such a case, the S-N curve can be modified as Fig 19-(6).

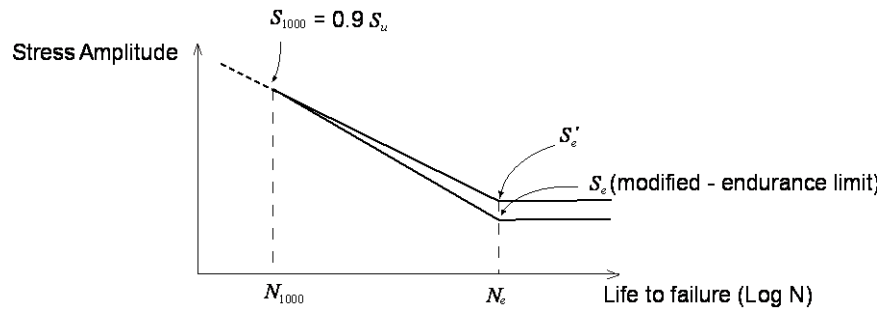


Figure 19-(6) Modifying factor effect

19-4-1 Component size and shape

When various diameters (for shaft) are used in fatigue tests, the endurance limit of a material can be modified by the following equations:

$$C_{size} = 1.0 (d \leq 8mm) \quad (19.9)$$

$$C_{size} = 1.189d^{-0.097} (8mm \leq d \leq 250mm) \quad (19.10)$$

If a specimen is not a circular section, but is a rectangular section, an equivalent diameter, d_{eq} can be calculated as follows:

$$d_{eq}^2 = 0.65wt \quad (19.11)$$

where, w stands for width, and t stands for thickness.

19-4-2 Types of loading

Fatigue analysis data are obtained through reversed bending load and axial load testing of specimens. Modification factors for loading types can be used to relate fatigue testing data to fatigue testing for other loads. The influence of loading type can alter the values of S_{1000} and S_e . The modification factors for the loading types of S_{1000} are as follows:

Measured Loading	Target Loading	C_{load}
Axial to	Bending	1.25
Axial to	Torsion	0.725
Bending to	Torsion	0.58
Bending to	Axial	0.8
Torsion to	Axial	1.38
Torsion to	Bending	1.72

Table 19-(1) modification factors for the loading types of S_{1000}

The modification factors for the loading types of the endurance limit, S_e at 1000 cycles are as follows:

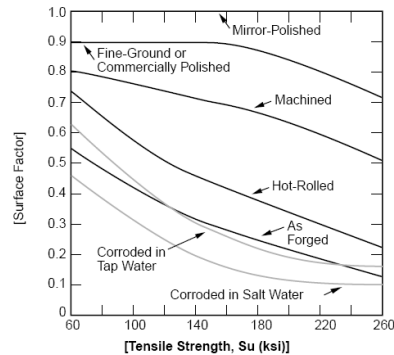
Measured Loading	Target Loading	C_{load}
Axial to	Torsion	0.82
Bending to	Torsion	0.82
Torsion to	Axial	1.22
Torsion to	Bending	1.22

Table 19-(2) modification factors for the loading types of S_e

19-4-3 Surface finish

Marks, grooves and machined traces on a material surface are the geometrical properties of the material, which add stress concentration to the existing stress. A material composed of uniform

and fine crystals such as high strength steel is more prone to rough surface finishes than to a material composed of coarse crystals such as cast iron. The surface finish modification factor is often presented in qualitative terms such as polished, machined or forged.



The diagram below presents a graph related to surface roughness. Qualitative surface roughness can be represented by such measures as the root mean square (R_A) and arithmetic average (AA). The surface roughness caused by mechanical fabrication can be found in the mechanical and manufacturing handbooks. Fig. 19-(7) presents the relationship between the surface factors, C_{sur} and tensile strength, S_u with respect to surface roughness.

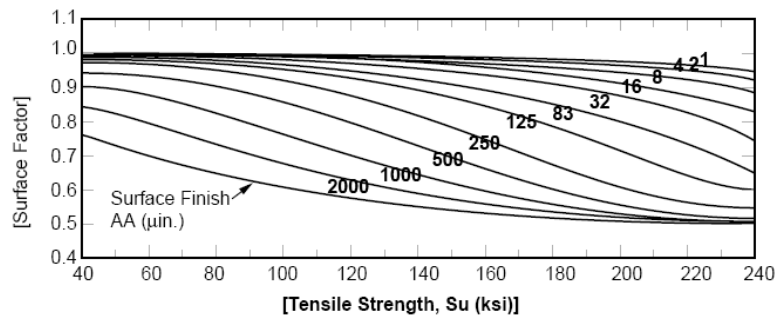


Figure 19-(7) Surface finish effect

Surface finish is more important for high strength steel. Local irregularities on surfaces adversely affect fatigue due to stress concentration.

19-4-4 Surface treatment

In addition to surface roughness, surface treatment also affects the fatigue life, especially the endurance limit. The surface treatment can be broadly classified into mechanical, thermal and plating processes, which can create residual stresses on the surfaces. When a structural component undergoes deformation due to external forces while being subjected to residual stresses, the residual stresses affect the tensile stresses on the surfaces, which in turn affect the fatigue life.

Mechanical treatment

Typical surface treatments commercially, which induce residual stresses, are cold forming and shot peening. Such surface treatments induce compressive residual stresses resulting in improvements in fatigue life.

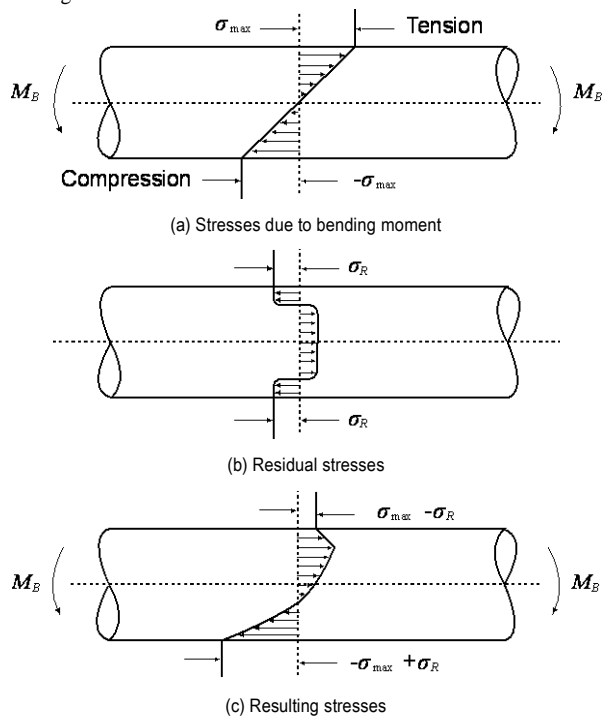


Figure 19-(8) Mechanical treatment effect

Fig. 19-(8) shows flexural stress becoming reduced at the top surface. Cold rolled bolts are thus more resistant to fatigue due to the residual stress. Cold forming or short peening affects fatigue life only when it is a long life. Neither affects too much if it is a short life. Appropriate modification factors for peening are between 1.5 and 2.0.

Plating treatment

Plating with such materials as chrome or nickel improves the endurance limit. However, plating may weaken the resistance to fatigue if a material is plated after mechanical treatment, as a result of reduction in compressive residual stresses on the surface.

Thermal effect

The endurance limit of steel tends to increase at low temperatures. At high temperatures, such endurance limit for steel does not appear due to the shift of electric potential. Creep becomes important at a temperature over approximately half the fusing point. In this range, the stress based fatigue life method is no longer valid. At high temperatures, the advantage of compressive residual stresses due to annealing may disappear.

19-4-5 Environment

A fatigue load in a corrosive environment leads to more harmful results than the case where fatigue and corrosion take place independently. Interaction between fatigue and corrosion, termed as corrosion-fatigue, exhibits a very complicated fracture mechanism. Research in this phenomenon is not matured, and little quantitative data or useful theoretical methods are available.

19-5 Rainflow-Counting Algorithm

The S-N curve shows the number of cycles of repeated stresses until fatigue failure is reached under the repeated stresses of a constant amplitude. But in reality, a load hysteresis loop exhibits the characteristics of variable amplitudes. In order to define fatigue damage under variable amplitude stresses, such variable amplitude is converted into a number of uniform amplitude stresses, which will utilize appropriate S-N curves. MIDAS uses the Rainflow-Counting method to sum up the cycles. The Rainflow-Counting method first reads in the local maximum and minimum points as follows:

$$A(i-1) \leq A(i+1) \leq A(i) \leq A(i+2) \quad (19.12)$$

$$A(i-1) \geq A(i+1) \geq A(i) \geq A(i+2) \quad (19.13)$$

It calculates the cycle of a period, and its amplitude is said to be S . All the amplitudes, each having a period at each cycle, are summed up. Eq. (19.12) has the shape of the left figure in Fig 19-(9), and Eq. (19.13) has the shape of the right figure in Fig 19-(9).

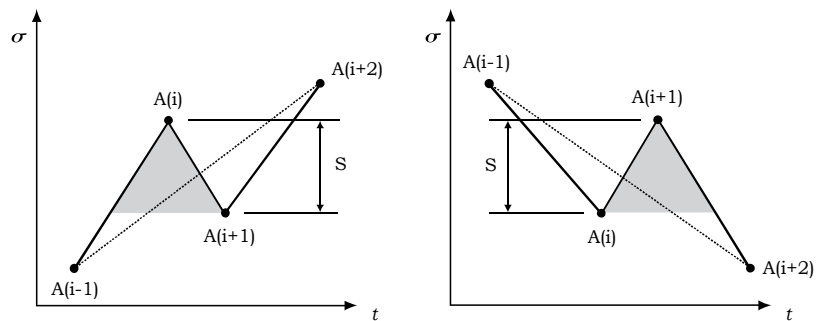


Figure 19-(9) Counting of one cycle

Next, Rainflow-Counting is performed, and the load cycle waning or waxing is finally drawn as Fig. 19-(10). Each S_1 , S_2 or S_3 is said to be a period of one cycle. Applying the Miner's rule to the unit alternating stress amplitudes thus obtained, the damage rate, which considers damage caused by the accumulated fatigue, can be obtained.

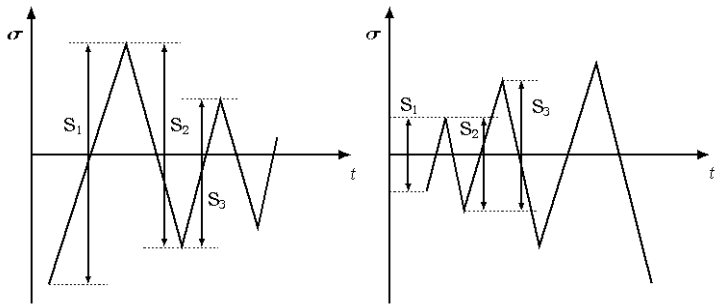


Figure 19-(10) Counting of load cycle amplitude

Stress spectrum is arranged as Fig. 19-(11).

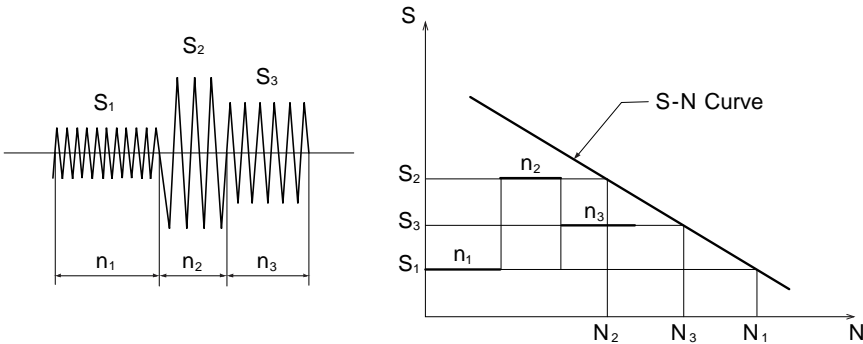


Figure 19-(11) Counting load cycle amplitude

The damage rate at the i-th repeated load is expressed as,

$$D_i = \frac{n_i}{N_i} \quad (19.15)$$

where, n_i represents the number of repetitions of the corresponding stress amplitude, and N_i represents the number of repetitions up to the point of fatigue failure. The final sum of damage is expressed as,

$$D_{total} = \sum_{i=1}^n D_i = \sum_{i=1}^n \frac{n_i}{N_i} \quad (19.14)$$

19-6 Fatigue Analysis Procedure

MIDAS follows the following procedure for fatigue analysis:

1. Read in the elastic stress data from the analysis results.
2. Obtain the absolute values of principal stresses under a critical load case.
3. Scale the acquired elastic stress using the stress concentration coefficient.
4. Analyze the load-time hysteresis graph through Rainflow-Counting.
5. Modify the stress amplitude value of S-N curve using the modification factor.
6. Calculate the damage considering the influence of mean stress.
7. Linearly sum the damage associated with each cycle using the Miner's rule.
8. Find the fatigue life or the safety coefficient at all nodes.

Chapter 20. CFD Analysis

20-1 Introduction

CFD (Computational Fluid Dynamics) analysis investigates fluid flows and predicts fluid loads acting on a structure subjected to winds. Wind loads acting on a civil structure is generally obtained from the design codes. But detail distribution of wind loads or wind effects on alternate designs can be predicted through CFD analysis. Especially when a structure retains a generally uniform cross section such as in bridge structures, flow information can be sufficiently found through 2-dimensional analysis.

Midas FEA analyzes 2-dimensional flow in a structured grid. The RANS (Reynolds averaged Navier-Stokes) equation is obtained from Favre averaging of the Navier-Stokes equation, which is based on 2-dimensional compressible viscous flow. The Favre average used here is the density weighted average. Also, the two-equation turbulence model can be applied, and analysis can be performed for both steady state and unsteady state. The computational fluid technique adopts spatial discretization using the density based time marching method and the finite volume method. The boundary conditions and turbulence models of computational fluid analysis in midas FEA are indicated below.

Boundary condition	Far-field boundary condition
	Solid wall boundary condition
	Symmetric boundary condition
Turbulence model	$q - \omega$ model: Wall function can be used
	$k - \omega$ SST (Shear Stress Transport) model
	$k - \omega$ BSL (Base Line) model

20-2 RANS equation and turbulence model

The RANS equation, which is a governing equation for turbulent compressible flow, and the turbulence model, can be expressed by a single equation.

$$\frac{\partial \mathbf{W}}{\partial t} + \frac{\partial \mathbf{E}}{\partial x} + \frac{\partial \mathbf{F}}{\partial y} = \frac{\partial \mathbf{E}_v}{\partial x} + \frac{\partial \mathbf{F}_v}{\partial y} + \mathbf{S} \quad (20.1)$$

where,

$$\mathbf{W} \quad \text{Conservative flow variable vector} \quad \{\rho, \rho u, \rho v, e, \rho s_1, \rho s_2\}^T$$

Each of \mathbf{E} and \mathbf{F} represents inviscid flux vector in the x direction and y direction respectively. \mathbf{E}_v and \mathbf{F}_v represent viscous flux vectors.

$$\mathbf{E} = \{\rho u, \rho u^2 + p, \rho uv, (e + p)u, \rho u s_1, \rho u s_2\}^T \quad (20.2)$$

$$\mathbf{F} = \{\rho v, \rho uv, \rho v^2 + p, (e + p)v, \rho v s_1, \rho v s_2\}^T \quad (20.3)$$

$$\mathbf{E}_v = \left\{ 0, \tau_{xx}, \tau_{xy}, \Omega_x, (\mu_m + \sigma_{s1}\mu_t) \frac{\partial s_1}{\partial x}, (\mu_m + \sigma_{s2}\mu_t) \frac{\partial s_2}{\partial x} \right\}^T \quad (20.4)$$

$$\mathbf{F}_v = \left\{ 0, \tau_{yx}, \tau_{yy}, \Omega_y, (\mu_m + \sigma_{s1}\mu_t) \frac{\partial s_1}{\partial y}, (\mu_m + \sigma_{s2}\mu_t) \frac{\partial s_2}{\partial y} \right\}^T \quad (20.5)$$

where,

ρ	Density
p	Pressure
e	Total energy
τ_{ij} , Ω_i	Viscous stress, Total energy flux
μ_m , μ_t	Molecular viscosity coefficient, Turbulence viscosity coefficient

s_1 and s_2 are variables for the 2-equation turbulence model equation. Their definitions change depending on the turbulence model. \mathbf{S} is the source term of the turbulence model, and its definition also changes depending on the turbulence model. midas FEA provides turbulence models, which are the $q-\omega$ model of Coakley¹ and the $k-\omega$ BSL/SST model of Menter². The $q-\omega$ model predicts a turbulence viscosity coefficient using the transport equation about turbulent velocity scale, q and specific dissipation rate, ω . Here ω retains the following relationship with turbulence kinetic energy, k and turbulent dissipation rate, ε .

$$s_1 = q = \sqrt{k}, \quad s_2 = \omega = \frac{\varepsilon}{k} \quad (20.6)$$

The $k-\omega$ BSL/SST model developed by Menter combines the advantages of the $k-\varepsilon$ and $k-\omega$ models. This is a turbulence model, which uses the $k-\omega$ model near the wall and the $k-\varepsilon$ model in other ranges. The variables in the $k-\omega$ BSL/SST model are as follows.

$$s_1 = k, \quad s_2 = \omega = \frac{\varepsilon}{k} \quad (20.7)$$

Although the $k-\omega$ BSL model exhibits similar characteristics as the $k-\omega$ model, the effect of free stream is little and the $k-\omega$ SST model exhibits superior performance in adverse pressure gradient as it includes the transfer of turbulent shear stress.

The turbulent compressible flow Eq (20.1) is known to cause numerical problems of obtaining converged solutions when a low velocity flow is analyzed. In order to overcome such problems, a local preconditioning method can be used. This method resolves such inflexibility of convergence by expressing the time term of Equation (20.1) in terms of the product of a primitive variable and a preconditioning matrix. Midas FEA uses the technique of Weiss and Smith³. The locally

¹ Coakley, T.J., "Turbulence Modeling Methods for the Compressible Navier-Stokes Equations," AIAA paper 83-1693, 1983

² Menter, F.R., "Two-Equation Eddy-Viscosity Turbulence Models for Engineering Applications," AIAA Journal, Vol. 32, 1994

³ Weiss, J.M and Smith, W.A., "Preconditioning Applied to Variable and Constant Density

preconditioned equation is expressed as,

$$\mathbf{\Gamma} \frac{\partial \mathbf{Q}}{\partial t} + \frac{\partial \mathbf{E}}{\partial x} + \frac{\partial \mathbf{F}}{\partial y} = \frac{\partial \mathbf{E}_v}{\partial x} + \frac{\partial \mathbf{F}_v}{\partial y} + \mathbf{S} \quad (20.8)$$

where,

\mathbf{Q} Primitive variable vector $\{p, u, v, T, s_1, s_2\}^T$

$\mathbf{\Gamma}$ Preconditioning matrix

In case of steady solution, if Equation (20.8) converges, $\partial \mathbf{Q} / \partial t = \mathbf{0}$, and as such there is no influence of the preconditioning matrix in a steady solution. midas FEA finds a solution by non-dimensionalizing the RANS equation and the turbulence equation. Non-dimensionalization is done on the basis of a free stream condition, and the non-dimensionalized equation retains a form identical to that of Equation (20.1).

Flows,” AIAA Journal, Vol. 33, 1995

20-3 Spatial discretization

The locally preconditioned Equation (20.8) can be simply expressed as,

$$\Gamma \frac{\partial \mathbf{Q}}{\partial t} + \nabla \cdot \bar{\mathbf{F}} = \nabla \cdot \bar{\mathbf{F}}_v + \mathbf{S} \quad (20.9)$$

If the above equation is integrated with respect to computational cells as shown in Fig. 20-(1) and a divergence theorem is applied, it is transformed into the following.

$$\Gamma \frac{d}{dt} \int_V \mathbf{Q} dV + \int_{\Omega} \bar{\mathbf{F}} \cdot \mathbf{n} d\Omega = \int_{\Omega} \bar{\mathbf{F}}_v \cdot \mathbf{n} d\Omega + \int_V \mathbf{S} dV \quad (20.10)$$

Since midas FEA uses a structured grid, it is cautioned that the cell placement is as shown in Fig. 20-(1). Assuming that each cell size is small enough and integrating with respect to the volume of cells and interface, the following semi-discretized equation, which has been spatially discretized, is arrived by the finite volume method.

$$\Gamma \frac{d\mathbf{Q}_{(i,j)}}{dt} + \mathbf{R} = \mathbf{0} \quad (20.11)$$

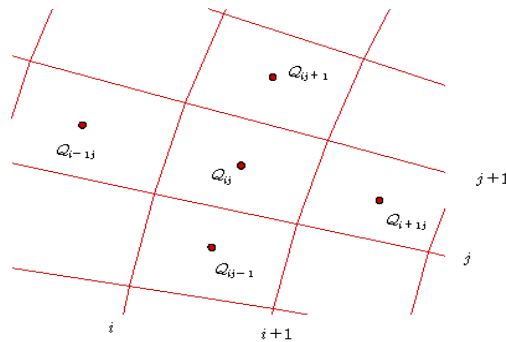


Fig. 20-(1). Placement of computational cells and index

The residual, \mathbf{R} can be expressed in terms of total flux, $\tilde{\mathbf{F}}_c$.

$$\mathbf{R} = \frac{1}{V_{(i,j)}} \left(\sum \tilde{\mathbf{F}}_c \cdot \mathbf{n} \Delta\Omega \right) + \mathbf{S}_{(i,j)} \quad (20.12)$$

For stable numerical analysis, the inviscid term in the flux vector, $\tilde{\mathbf{F}}_c$, is replaced with the numerical flux vector of Roe⁴, and wiggle is prevented by applying the entropy correction method. If upwind difference is simply used in calculating the numerical flux, only the first order accuracy can be obtained. In order to obtain more accurate solutions, higher order spatial discretization can be achieved while maintaining monotone, by applying van Leer's⁵ MUSCL extrapolation technique and limiter.

⁴ Roe, R.L., "Approximate Riemann Solvers, Parameter Vectors and Difference Schemes," J. of Comp. Physics, Vol. 43, 1981

⁵ van Leer, B., "Towards the Ultimate Conservative Difference Scheme. V. A Second Order Sequel to Godunov's Method," J. of Comp. Physics, Vol. 32, 1976

20-4 Steady flow

In steady flow analysis, we find \mathbf{Q}_p for which the time term becomes zero in the unsteady flow equation. Expressing Equation (20.1) using the time difference coefficient, θ ,

$$\Gamma \frac{\Delta \mathbf{Q}}{\Delta \tau} + \theta \mathbf{R}^{n+1} + (1 - \theta) \mathbf{R}^n = \mathbf{0} \quad (20.13)$$

midas FEA uses $\theta = 1$. If \mathbf{R}^{n+1} in the above equation is linearized and rearranged, the following simultaneous equations are obtained.

$$[\mathbf{D} + \frac{\Delta \tau}{V} (\mathbf{A} + \mathbf{B})] \Delta \mathbf{Q} = -\Delta \tau \mathbf{R}^n \quad (20.14)$$

The diagonal matrix, \mathbf{D} is as follows.

$$\mathbf{D} = \Gamma - \Delta \tau \mathbf{K} \quad (20.15)$$

where,

\mathbf{K}	Jacobian matrix of turbulence source term
\mathbf{A}	$\tilde{\mathbf{F}}_c$ Jacobian matrix at the cell boundary $i \pm 1/2$
\mathbf{B}	$\tilde{\mathbf{F}}_c$ Jacobian matrix at the cell boundary $j \pm 1/2$

The Jacobian matrix \mathbf{K} of the source term takes different forms depending on the turbulence model. In order to maintain stable numerical analysis, midas FEA only includes the dissipation term in the source term.

The solution for Equation (20.14) is calculated by the AF-ADI (Approximate Factorization-Alternative Direction Implicit) method.

$$[\mathbf{D} + \frac{\Delta \tau}{V} \mathbf{A}] \mathbf{D}^{-1} [\mathbf{D} + \frac{\Delta \tau}{V} \mathbf{B}] \Delta \mathbf{Q} = -\Delta \tau \mathbf{R}^n \quad (20.16)$$

Since the above equation is a block tri-diagonal matrix, the solution can be effectively calculated.

20-5 Unsteady flow

In unsteady flow analysis, dual time stepping is used, which has been developed to reduce errors resulting from applying the AF-ADI method. The time discretization equation derived by a stable “2-parameter family” integration scheme, while maintaining the second order accuracy in the time term, is as follows.

$$\left(1 + \frac{\phi}{2}\right) \frac{\Delta \mathbf{W}^n}{\Delta t} - \frac{\phi}{2} \frac{\Delta \mathbf{W}^{n-1}}{\Delta t} + \theta \mathbf{R}^{n+1} + (1 - \theta) \mathbf{R}^n = \mathbf{0} \quad (20.17)$$

Midas FEA uses $\phi = 1$ and $\theta = 1$. Adding the pseudo time term multiplied by the preconditioning matrix to the above equation and applying the dual time stepping, the next equations are obtained.

$$\frac{3}{2} \frac{\Delta \bar{\mathbf{W}}}{\Delta t} - \frac{1}{2} \frac{\Delta \mathbf{W}^{n-1}}{\Delta t} + \Gamma \frac{\Delta \mathbf{Q}^l}{\Delta \tau} + \mathbf{R}^{l+1} = \mathbf{0} \quad (20.18)$$

$$\Delta \bar{\mathbf{W}} = \mathbf{W}^{l+1} - \mathbf{W}^l \quad (20.19)$$

where,

l Index for dual time iteration

n Index for time increment

If \mathbf{R}^{l+1} in the above equation is linearized and rearranged, the following simultaneous equations are obtained.

$$\left[\mathbf{D} + \frac{\Delta \tau}{V} (\mathbf{A} + \mathbf{B})\right] \Delta \mathbf{Q} = -\Delta \tau \tilde{\mathbf{R}} \quad (20.20)$$

The diagonal matrix, \mathbf{D} is as follows.

$$\mathbf{D} = \frac{3}{2} \mathbf{M} \frac{\Delta \tau}{\Delta t} + \Gamma - \Delta \tau \mathbf{K} \quad (20.21)$$

$$\tilde{\mathbf{R}} = \frac{3}{2} \frac{\mathbf{W}^l - \mathbf{W}^n}{\Delta t} - \frac{1}{2} \frac{\mathbf{W}^n - \mathbf{W}^{n-1}}{\Delta t} + \mathbf{R}^l \quad (20.22)$$

where,

$\tilde{\mathbf{R}}$ Modified residual

\mathbf{M} Transformation matrix from \mathbf{Q} to \mathbf{W}

If the dual time stepping becomes converged, $\tilde{\mathbf{R}} = \mathbf{0}$, and the following relationship is satisfied.

$$\mathbf{W}^{l+1} = \mathbf{W}^l = \mathbf{W}^{n+1} \quad (20.23)$$

Similar to the steady flow analysis, solution for Equation (20.20) is calculated by the AF-ADI (Approximate Factorization-Alternative Direction Implicit) method.

20-6 Numerical stability

Since the Navier-Stokes equation retains the properties of both convection and diffusion, pseudo time increment $\Delta\tau$ is calculated as,

$$\frac{1}{\Delta\tau} = \frac{1}{\Delta\tau_h} + \frac{1}{\Delta\tau_p} \quad (20.24)$$

The time increment for convection, $\Delta\tau_h$ is controlled by the CFL number, and the time increment for diffusion, $\Delta\tau_p$ is controlled by the von Neumann number. The basic values of the CFL number and the von Neumann number are 10.0 and 5.0 respectively.

Since the approximate Riemann solver of Roe used to calculate the inviscid term of numerical flux can cause numerical wiggle, midas FEA uses the entropy correction. If we define the property of numerical viscosity used in the numerical flux vector of Roe as λ , λ is replaced by the following values.

$$\begin{aligned} |\lambda| &= |\lambda|, \text{ if } |\lambda| \geq \varepsilon_1 \\ |\lambda| &= \frac{1}{2} \left\{ \frac{|\lambda|^2}{\varepsilon_1} + \varepsilon_1 \right\}, \text{ if } |\lambda| < \varepsilon_1 \end{aligned} \quad (20.25)$$

Generally values in the range of $\varepsilon_1 = 0.0 - 0.25$ are used. The higher the value, the more dissipative property is retained in the solution. Its basic values for steady flow analysis and unsteady flow analysis are 0.05 and 0.0 respectively.

Considering numerical stability, midas FEA carries out turbulent steady analysis assuming laminar flow over the number of iterations defined by the user. Also, the initial flow field is obtained from the steady analysis results for stable analysis of unsteady flow.

20-7 Computational fluid analysis results

Computational fluid analysis results from midas FEA present velocity, pressure, etc. on the computational cells and aerodynamic coefficients.

Results on cells

Velocity u, v $[m/sec]$

Pressure p $[N/m^2]$

Turbulent kinetic
energy $k (= q^2)$ $[m^2/sec^2]$

Aerodynamic coefficients

Lift coefficient C_L

Drag coefficient C_D

Moment
coefficient C_M

The amount of results for velocity, pressure and turbulent kinetic energy is substantially large. So the results are produced at the time steps specified by the user. Aerodynamic coefficients on the other hand are produced at every time step.
